Etudes expérimentales et modélisation du comportement de phase et des propriétés de transport des mélanges liés à la capture et au stockage du carbone

Alfonso Gonzalez Perez

THÈSE DE DOCTORAT

de l'Université de recherche Paris Sciences et Lettres
PSL Research University

Préparée à MINES ParisTech

Etudes expérimentales et modélisation du comportement de phase et des propriétésde transport des mélangeslies à la capture et au stockage du carbone

Ecole doctorale n°432

SCIENCES DES MÉTIERS DE L'INGÉNIEUR

Spécialité ENERGÉTIQUE ET PROCÈDES

COMPOSITION DU JURY :

M. Jean Philippe PASSARELLO
Université Paris 13 Nord, Président

M. Jean Luc DARIDON
Université de Pau, Rapporteur

M. Richard GRAHAM
University of Nottingham, Rapporteur

M. Manuel MARTÍNEZ PIÑEIRO
Universidade de Vigo, Examinateur

M. Francois MONTEL
TOTAL, Examinateur

M. Patrice PARICAUD
Ensta-ParisTech, Examinateur

M. Antonin CHAPOY
Heriot-Watt University, Examinateur

M. Christophe COQUELET
Mines-ParisTech, Examinateur

Soutenue par
Alfonso **GONZALEZ PEREZ**
le 30 Novembre 2016

Dirigée par **Christophe COQUELET**
et **Antonin CHAPOY**

PREFACE

The work presented in this manuscript has been developed as part of my PhD studies at PSL-Mines ParisTech and Heriot-Watt University under the supervision of Prof. Christophe Coquelet, Dr. Patrice Paricaud and Dr. Antonin Chapoy, between October 2013 and October 2016. Phase behaviour models implemented in the in-house PVT software of the research group were used throughout this work. Part of the material in this manuscript has been presented or published elsewhere before; the list of publications concerning the studies described in this manuscript is given in LIST OF PUBLICATIONS BY THE CANDIDATE.

Alfonso González Pérez

October 2016

ABSTRACT

It is now widely accepted that anthropogenic CO_2 emissions produced from the burning of fossil fuels are responsible for the apparent rapid rise in global temperatures recorded over the past century. Worldwide concerns over the threat of global warming have motivated the majority of industrialised countries into working to reduce carbon emissions. CO_2 storage in depleted reservoirs and its application in Enhanced Oil/Gas Recovery (EOR) are among techniques being suggested for reducing the emission of this greenhouse gas. The main aim of this research is to develop a thermodynamic model from an accurate equation of state (EoS) for typical components of reservoir fluids and flue gases. The SAFT-VR Mie EoS was selected to study the phase behaviour and transport properties of mixtures related to carbon capture and storage (CCS). Four EoSs have been compared (PR, SRK, PC-SAFT and SAFT-VR Mie) by modelling density and vapour-liquid equilibria (VLE) data from the literature of 22 pure components and 108 binary systems of gases (CO_2, H_2S, N_2, O_2, Ar, CO and SO_2), *n*-alkanes and aromatics.

Isothermal vapour-liquid equilibrium of H_2S - Ar binary system was determined experimentally at three temperatures from 273 to 323 K. Densities of five H_2S binary systems (three CH_4-H_2S systems with 13, 18 and 28 % of acid gas, C_2H_6 - 34% H_2S and C_3H_8 - 13% H_2S) were measured continuously at 3 temperatures (253, 273 and 293 K) and at pressures up to 30MPa, using a vibrating tube densitometer, Anton Paar DMA 512. Following the same technique, the density of the ternary system 42% CO_2, 40% CH_4 and 18% H_2S was measured at pressures ranging from 0.2 to 31.5 MPa and at 6 temperatures between 253 and 353 K.

Three transport properties were modelled with SAFT-VR Mie and two models based on density predictions from the EoS. Density, viscosity and interfacial tension (IFT) of CO_2-rich systems were calculated by the SAFT-EoS (density), TRAPP model (viscosity) and DGT (IFT), for system of interest to CCS. Densities and viscosities of a multicomponent mixture of 50% CO_2, 40% CH_4 and 10% of other impurities were measured at 5 temperatures between 283 and 423 K and at 2.5-150 MPa pressure range, using an Anton Paar densitometer and the capillary tube technique for viscosity measurements. These experimental data continued studying the impact of impurities on the viscosity and density of CO_2-rich systems.

TABLE OF CONTENTS

LIST OF PUBLICATIONS BY THE CANDIDATE

A. Gonzalez, A. Valtz, P. Paricaud, C. Coquelet, A. Chapoy, *Experimental and modelling study of the densities of the hydrogen sulphide + methane mixtures at 253, 273 and 293 K and pressures up to 30 MPa,* Fluid Phase Equilib. **427**, 371–383 (2016).

A. Gonzalez, P. Paricaud, C. Coquelet, A. Chapoy, *Comparative study of vapour-liquid equilibrium and density modelling of mixtures related to carbon capture and storage with the SRK, PR, PC-SAFT and SAFT-VR Mie equations of state for industrial uses*, (in preparation).

A. Gonzalez, A. Valtz, P. Paricaud, C. Coquelet, A. Chapoy, *Vapour–liquid equilibrium data for the argon (Ar) + hydrogen sulphide (H_2S) system at 273, 298 to 323 K*, (in preparation).

A. Gonzalez, A. Valtz, P. Paricaud, A. Chapoy, C. Coquelet, *Experimental and modelling study of the density of one mixture of ethane + hydrogen sulphide and one mixture of propane + hydrogen sulphide at 253, 273 and 293 K and pressures up to 30 MPa*.

A. Gonzalez Perez, L. Pereira, P. Paricaud, C. Coquelet, A. Chapoy, *Modeling of transport properties using the SAFT-VR Mie equation of state*, published and presented (oral) in SPE Annual Technical Conference and Exhibition (Paper # SPE-175051-MS), Houston, Texas, USA (2015).

A. Gonzalez Perez, P. Paricaud, C. Coquelet, A. Chapoy, *Vapour-liquid equilibria and density modelling of CO_2-rich systems with PC-SAFT and SAFT-VR Mie*, presented (poster) in 13th International Conference on Properties and Phase Equilibria for Products and Process Design (PPEPPD), Porto, Portugal (2016).

C. Coquelet, P. Stringari, M. Hajiw, A. Gonzalez Perez, L. Pereira, M. Nazeri, R. Burgass, A. Chapoy, *Transport of CO_2: Presentation of New Thermophysical Property Measurements and Phase Diagrams*, presented (poster) in 13th International Conference on Greenhouse Gas Control Technologies (GHGT), Lausanne, Switzerland (2016).

LISTS OF TABLES

LISTS OF FIGURES

NOMENCLATURE

List of main symbols

a	Densitometer parameter calibration / Reduced Helmholtz free energy / Parameter second virial coefficient calculation / Parameter cubic EoS
A	Helmholtz free energy
AAD	Average absolute deviation
Ar	Argon
b	Densitometer parameter calibration / Parameter second virial coefficient calculation / Parameter cubic EoS
B	Second virial coefficient
BIP	Binary interaction parameter
C	unit conversion factor
c	Critical / IFT influence parameter / Parameter second virial coefficient calculation
C_2H_6	Ethane
C_3H_8	Propane
CCS	Carbon Capture and Storage
CEoS	Cubic Equation of State
CH_4	Methane
CO	Carbon monoxide
CO_2	Carbon dioxide
Comp	Component
CP	Critical point
c_p	Heat capacity
CPA	Cubic Plus Association
d	Temperature-dependent diameter / Parameter second virial coefficient calculation
DGT	Density Gradient Theory
EOR	Enhanced Oil Recovery
EoS	Equation of State
f	Fugacity
FPMC	Forced path mechanical calibration
G	Gibbs free energy / Single phase gas / mBWR coefficients

g	Radial distribution function
GC	Gas cromatograph / Group contribution
Gt	Gigaton
H	Enthalpy
h	Plank constant
H_2S	Hydrogen sulphide
HS	Hard-sphere
H-V	Huron-Vidal mixing rules
IFT	Interfacial tension
IG	Ideal gas
K	Natural transversal stiffness
k	Binary interaction parameter
k_b	Boltzmann
L	Length capillary tube / Single phase liquid
LJ	Lennard-Jones
M	Density vibrating mass
m	number of segments
MAD	Maximum average deviation
mBWR	Modified Benedict-Webb-Rubin
MIX	Multicomponent mixture
MPa	MegaPascal
M_w	Molecular weight
n	number of moles
N	number of molecules
N_2	Nitrogen
N_c	Number of components
n-C_i	*n*-alkane with *i* number of carbon atoms
NG	Natural gas
N_G	Number of groups
NO_x	Nitrogen oxides
O_2	Oxigen
OOIP	Origin oil in place

P	Pressure / Poise (viscosity unit)
PC	Perturbed chain
PR	Peng-Robinson
r	Radial distance
R	Ideal gas constant
RDF	Radial distribution function
SAFT	Statistical Associating Fluid Theory
SC	Supercritical
SLE	Solid-liquid equilibrium
SLVE	Solid-liquid-vapour equilibrium
SO_2	Sulphur dioxide
SRK	Soave-Redlich-Kwong
ST	SUPERTRAPP
SVE	Solid-vapour equilibrium
SW	Square-well
T	Temperature
TCD	Thermal conductivity detector
TPT	Thermodynamic perturbation theory
TRAPP	Transport Property Predictions
u	Pair potential / Uncertainty
U	Internal energy
V	Volume
v	Molar volume
VC	Volume correction
vdW	van der Waals
VLE	Vapour-Liquid equilibrium
VR	Variable range
VTD	Vibrating tube densitometer
W-S	Wong-Sandler mixing rules
x	Liquid mole fraction
y	Vapour mole fraction
Z	Compressibility factor

Greek letters

α	Relative volatility / parameter W-S mixing rules
β	Inverse of temperature
ε	Segment energy
ζ_n	Number density
η	Viscosity / Reduced density
λ	Mie exponentials
μ	Chemical potential
ρ	Density
σ	Variance / Segment diameter
Λ	Broglie wavelength
φ	Fugacity coefficient
τ	Period of oscillation / Parameter W-S mixing rules
ω	Variance / acentric factor
Ω	Grand thermodynamic potential
Δ	Difference / Variation

List of Main Subscripts and Superscripts

0	Corresponded state / Property evaluated at local density
c	Critical
calc	Calculated
calib	Calibration
E	Excess
exp	Experimental
i,j,k	Components i,j and k
k, l	Functional groups k and l
Liq	Liquid phase
r	Reduced
ref	Reference
rep	Repeatability
res	Residual
sat	Saturated
sys	System
t	Triple point
v	Vaporisation
Vap	Vapour phase

CHAPTER 1: INTRODUCTION

1.1 Scope

It is now widely accepted that anthropogenic CO_2 emissions produced from the burning of fossil fuels are responsible for the apparent rapid rise in global temperatures recorded over the past century. Despite a slowdown in the trend during the last two years, global CO_2 emissions increased on average around 4% per year in the last decade, reaching 37.5 Gt of CO_2 in 2014 (Figure 1.1) [1]. More than 60% of these carbon emissions are from large stationary emission sources and come directly from industry [2]. Large scale emission sources can be essentially attributed to the burning of fossil fuels for power generation, but also to cement manufacturing, petrochemical processes and metal production. Worldwide concerns over the threat of global warming have led the majority of industrialised countries to develop strategies to reduce carbon emissions [3]. To meet these goals, nations must increase their investment in 'clean' renewable sources of energy and develop solutions for reducing CO_2 emissions.

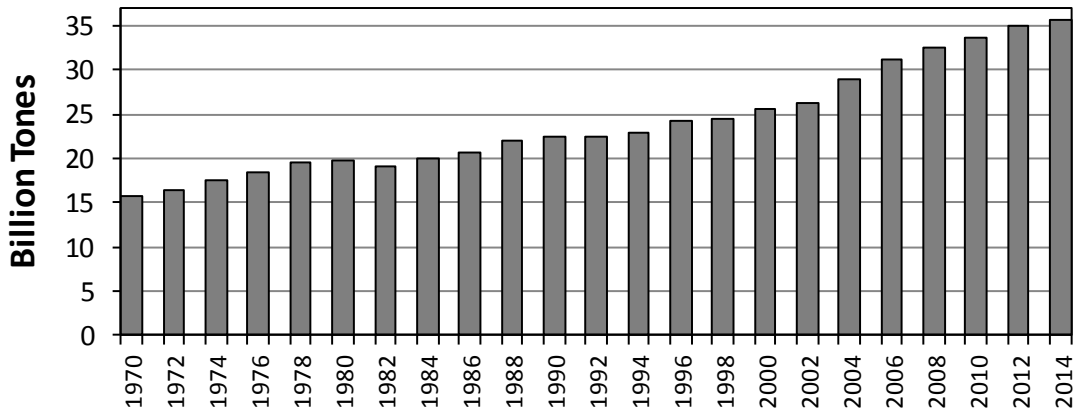

Figure 1.1. Trend in global CO_2 emissions [1]**.**

CO_2 storage in depleted reservoirs and its application in Enhanced Oil/Gas Recovery (EOR) are among the techniques being suggested for reducing the emission of this greenhouse gas. The industry has a long experience with injection of CO_2 for EOR processes. However, the main source of CO_2 are now industrial plants (i.e. power plants, chemical processes etc.) and these CO_2 sources contain different impurities (e.g. N_2, CO, H_2 etc.). Challenging fluid behaviour can occur, close to the critical point of

CO_2, such as multiphase behaviour. This may alter the conditions of CO_2 transport or EOR operations in the exploitation of hydrocarbons. The objective here is to develop a model for investigating the effect of CO_2 (and impurities) on the phase behaviour and physical properties (density, viscosity, IFT, etc.) of CO_2-oil systems.

The purpose of this research is to study the phase behaviour of reservoir fluids within the framework of CO_2 capture, transport and storage (CCS) especially in hydrocarbon reservoirs. Although the approach of this research is purely thermodynamic, throughout the following subsection the key principles to understand CCS chain are provided.

1.2 Carbon Capture and storage

In recent years, Carbon Capture and Storage (CCS) has been presented as one of the most promising methods to counterbalance CO_2 emissions from the combustion of fossil fuels. CCS is defined as a chain of process consisting in the separation of carbon dioxide from large scale industrial sources of emissions, the transport of the captured CO_2 to a storage location and the preservation of the isolated from the atmosphere [4].

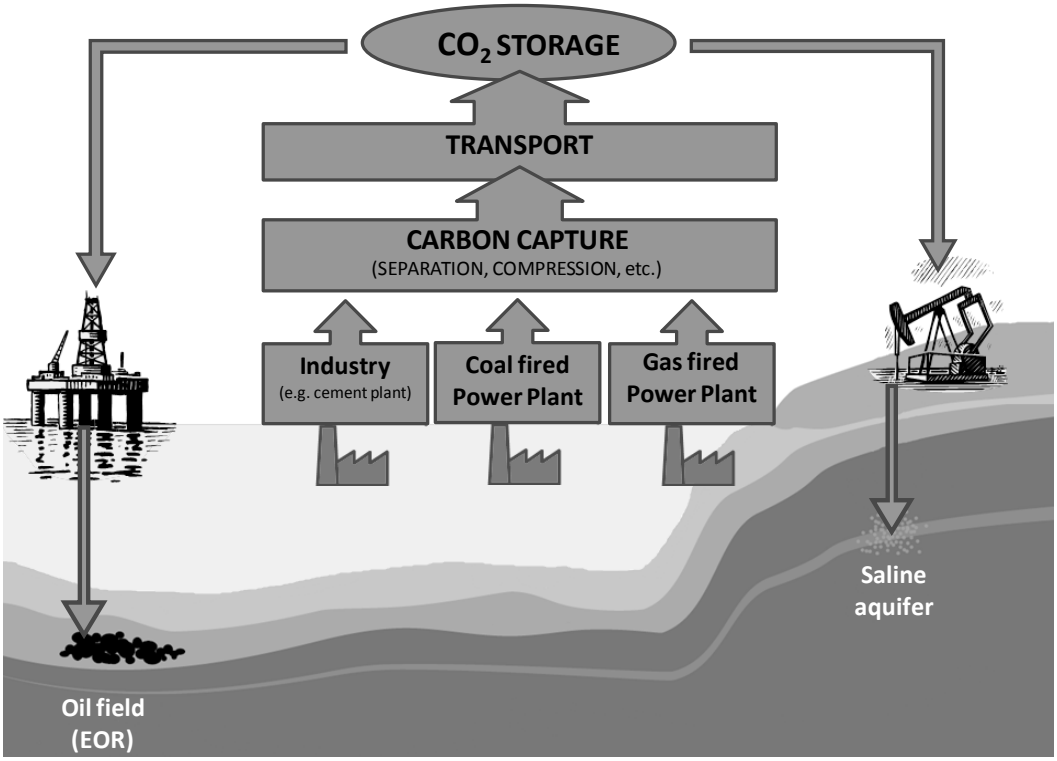

Figure 1.2. Sketch of Carbon Capture and Storage (CCS).

1.2.1 Carbon Capture

The aim of CO_2 capture is to produce a high-purity stream of CO_2 in order to remove all the CO_2 present in natural gases and power plant flue gases. CO_2 has been typically removed to purify other gas streams. Large industrial plants, such as natural gas processing plants and ammonia production facilities, have developed different technologies to remove CO_2 from gas steams. Applications of CO_2 removal from flue gas steams are the target of CCS technologies. There are three main approaches to capture the CO_2 from burning fossil fuels depending on the process or the power plant [2]:

- *Pre-combustion capture process*. The primary fuel is processed in a reactor with water steam and oxygen to produce a gas mixture named "synthesis gas" (syngas) which mainly consists of CO and H_2. In a second reactor, the carbon monoxide can be reacted with more steam in order to produce additional hydrogen, together with CO_2. The hydrogen can be separated and then used as a carbon-free fuel. The relatively high pressure (between 2-7 MPa) and high concentrations of CO_2 (generally from 15 up to 60% in volume on dry basis) are more favourable for CO_2 separation [2,5].

- *Post-combustion capture process*. CO_2 from the flue gases produced by the conventional combustion of the primary fuel in air is captured using a liquid solvent, e.g. amines. The typical flue gases have a composition between 10-15% in volume of CO_2 [6].

- *Oxyfuel combustion capture process*. In this capture system, oxygen instead of air is used for the combustion of the primary fuel [5]. A purity of 95-99% of oxygen is required in oxyfuel combustion; therefore, the resulting flue gas is composed mainly of water and carbon dioxide, with high contents of CO_2 (higher than 80% in volume on dry basis). After the combustion of the fuel (coal or hydrocarbons) and before the transport of CO_2, it is necessary to remove air pollutants (NO_x and SO_x) and non-condensed gases (such as nitrogen) [2]. The purification of the CO_2 steams can be accomplished by different means according to the requested level of purity (solvents, membranes, solid sorbents or by cryogenic separation).

1.2.2 Transport of CO_2

Carbon dioxide must be transported from the capture point to the storage location. The most common method to transport carbon dioxide is the use of pipelines, although CO_2 can also be transported by ship, road or railway in insulated tanks [2]. The first long distance pipeline dates from the 70's, built for delivering CO_2 for enhanced oil recovery (EOR) to oil fields in the Permian Basin of West Texas and eastern New Mexico. To date (2016), there are around 50 CO_2 transportation pipelines in the U.S. with a combined length of over 7250 km [7], even though only 20% are supplied from industrial sources (carbon capture), since natural sources of CO_2 have been typical used for EOR operations. Thus, it can be said that CO_2 transport by pipelines is a mature technology, even though, except for the U.S., most countries have little or no experience with CO_2 pipelines [8].

In many aspects, CO_2 pipelines could be compared to natural gas pipelines, but the design parameters are different in terms of the thermophysical properties of carbon dioxide [7]. For this reason, the standards and regulations of CO_2 pipelines are based on natural gas regulations. In fact, the European Directive 2099/31/EC about geological CO_2 storage states that the framework used for natural gas pipelines is adequate to regulate CO_2 as well [8]. There are already specific standards and regulations for CO_2 pipelines published in diverse countries, such as those listed below [8]:

- Europe: DNV-RP-J202.
- Unites States: CFR 49 part 195.
- Canada: CSA Z662.

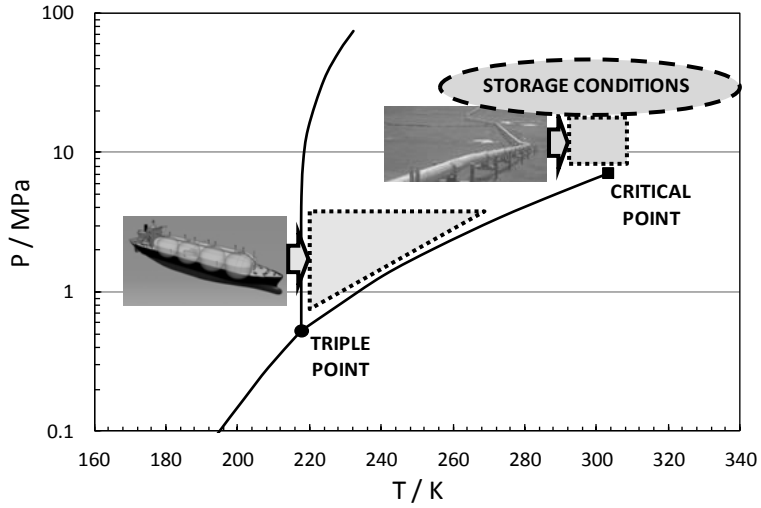

Figure 1.3. Potential pressure and temperature windows of CO_2 transport and storage [9]**.**

CO_2 transport in the liquid-dense (vessels) and supercritical (pipelines) phases is more advantageous than in the gaseous state due to the relatively high density with a relatively low viscosity of CO_2 steams above the critical pressure (Figure 1.3). Generally, captured gaseous CO_2 is compressed to a pressure up to 8 MPa in order to avoid two-phase regime during the transportation [2]. The reason behind is that the critical pressure of CO_2 is 7.38 MPa [10]. Therefore, above this pressure it is guaranteed that there will be no phase change with temperature variation along the pipeline. However, the presence of impurities will affect the critical pressure of the CO_2-rich steam (Figure 1.4), leading to the coexistence of liquid and vapour phases. Thus, the specification for composition of CO_2 steam is an important requirement in the design of pipelines (Table 1.1).

Table 1.1. Example of composition specifications [11]**.**

Component	**Contain**	**Limitation**
Carbon dioxide	> 95% of CO_2	
Water	< 500 ppm*	Solubility limit of water in CO_2
Oxygen	< 4 vol % (< 1000 ppm* EOR applications)	Total content of non-condensable gases (O_2, CH_4, N_2, Ar and H_2) should not exceed 4 vol%
Nitrogen	< 4 vol %	
Hydrocarbons	< 4 vol %	
Hydrogen	< 4 vol %	
Argon	< 4 vol %	
Hydrogen sulphide	< 200 ppm*	Health and safety considerations
Carbon monoxide	< 2000 ppm*	
Sulphur oxides	< 100 ppm*	
Nitrogen oxides	< 100 ppm*	

* Parts per million by weigh

Elevated water and hydrogen sulphide contents cause much higher corrosion rates, and in the case of water might also form hydrates [2]. The range of pressures of a CO_2 steam to ensure a safe and cost-effective transport is defined by the ambient temperature range, the impurities and the condition of single dense phase operation. For example, the operating pressure range of the existing CO_2 pipelines in the U.S. goes from 8.6 to 20 MPa and the temperature range can be set between 277 and 311K [12].

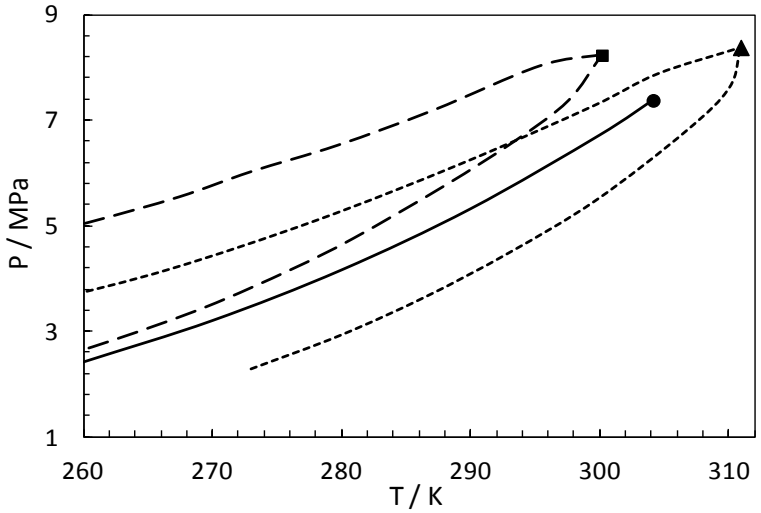

Figure 1.4. CO_2 saturation line (solid line) and predicted P-T envelop of two CO_2-rich mixtures (dashed lines). Symbols: experimental critical points of (●) pure CO_2, (■) mixture 1 (94% CO_2, 3% O_2 and 3% Ar) and (▲) mixture 2 (92% CO_2, 3% O_2 and 5% SO_2) [13]**.**

1.2.3 Storage

In the context of depleted hydrocarbon reservoirs, CO_2 geological storage is associated with enhanced oil recovery (CO_2 EOR). The oil and gas industry has come to call the phases of the production as Primary, Secondary and Tertiary. During the Primary Production Phase, oil and gas are produced by the pent-up energy of the confined fluids in the reservoir and when the pore pressure is depleted, "artificial lift" is used to increase the flow from the production well. At the end of this phase, sometimes up to 80-90% of the original oil in place (OOIP) is still in the reservoir. The Secondary Production Phase consists of water injection in order to repressurise the formation; therefore, new injection wells are drilled. Fresh water is not used and the produced water is recirculated into the ground again. It is often that, even after the second phase, 50-70% of OOIP remains in the reservoir. The CO_2 enhanced oil recovery (EOR) is used during the Tertiary Production Phase. Injecting almost pure CO_2 (<5% of impurities), oil viscosity and surface tension between the fluid and the reservoir rock are reduced, leading to the CO_2 sweeping up the oil from the injector to the producer well [14].

Mineral sediments (*e.g.* sand, clay) and other particles (*e.g.* crushed shells, precipitated carbonates) were deposited over millions of years, and then they were pressurized and cemented as more materials have been piled on, forming the called sedimentary rocks.

The CO_2 is injected in these rocks at depths of around 1000 meters or more, to ensure that it does not escape and also to have enough pressure (due to the overburden) to maintain CO_2 as critical fluid. These sedimentary rocks (*e.g.* sandstone and limestone) are permeable, with porosities between 10% and 30%, which allows fluid to flow through them. The void-spaces are full of water or oil and gas, depending on if it is a reservoir or an aquifer. Both reservoir and aquifer need to be confined by a cap rock, an impermeable rock which prevents upwards fluid migration as a result of structural or stratigraphic trapping.

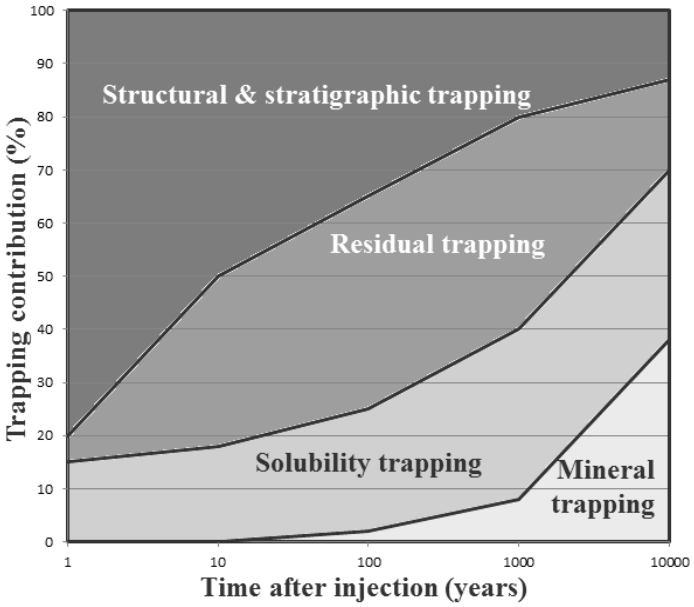

Figure 1.5: CO_2 trapping mechanism [2].

CO_2 storage follows four different trapping mechanisms. These trapping processes take place over many years at different rates from days to years to thousands of years, but, in general, the storage security increases with time since the end of the injection, due to the appearance of a more stable mechanism (Figure 1.5). According to a chronology succession, the geological storage mechanisms are [15]:

- *Structural/stratigraphic trapping*. CO_2 is confined by impermeable rocks (*e.g.* shales). Once CO_2-rich phase is injected, it percolates through the porous rock until the top of the formation where is trapped. This is the most dominant of the trapping mechanisms.

- *Residual/capillary trapping*. CO_2 is kept in pores. When the CO_2 moves through the porous rock, an amount of the fluid remains in the pore due to the differences in

surface tension between injected CO_2-rich phase and the other phases contained in the pores. This is often the mechanism which holds oil for millions of years.

- *Solubility trapping*. CO_2 is dissolved in underground water. This phase of the trapping process involves the CO_2 dissolution into the salt water (or brines) already present in the porous rock. This phenomenon can be probably attributed to the fact that water containing CO_2 is denser and sinks to the bottom of the formation over time.
- *Mineral trapping*. CO_2 crystallizes into carbonate rock. Dissolved CO_2 forms weak carbonic acid, which can react with the minerals present in the surrounding rock to form carbonate minerals. This is the most secure and final phase of trapping.

This research will, however, be focussed on neither stratigraphic nor mineral trapping, since the former just depends on the geology and morphology of the surrounding rock and the latter is a chemical process. From a thermodynamic point of view, capillarity and solubility trapping are processes which require predictive phase equilibria calculations of reservoir and rich-CO_2 fluids. In this sense, the presence of impurities will change the thermophysical properties, such as interfacial tension (IFT), capillary pressure and solubility.

1.3 Goals

Leaving aside the CCS aspects previously presented, which have been studied, there are still unanswered questions about carbon capture, transport and storage. The cost of investment and the cost of energy for capture, purification and storage of CO_2-rich gas flows, among others, are key engineering challenges that still require further investigation [16]. For example, from the technological point of view, a very important element is the transportation, mainly by pipelines, as the CO_2 stream could contain other gases like CH_4, N_2, O_2, H_2S, SO_2, NO_x and Ar. These impurities can change the thermodynamic behaviour of the stream and cause a breakdown in the pipeline [17]. This implies that to economically optimize the process, CCS technology requires increasing the energy efficiency. From the approach of this work, it means describing with the highest precision the thermodynamic properties in order to define accurately the energy required for any process involved in CCS [18].

The main objective of the work developed in this thesis has been to study the phase equilibria of reservoir fluids and typical compounds of flue gases. To this end, it has been necessary to develop a thermodynamic model from an accurate equation of state (EoS) for CO_2, hydrocarbons and other gases, such as N_2, O_2, H_2S, Ar, etc. Several EoSs are assessed to achieve this goal, by analysing the accuracy in their thermodynamic representation.

Besides studying phase equilibria, the second goal of this thesis has been to model the transport properties of CO_2-rich systems, such as density, viscosity and interfacial tension.

Another objective of this research has been to contribute with reliable experimental work: to study the vapour-liquid equilibria of one system relevant for the CCS projects which has not been investigated, to measure the density of hydrogen sulphide systems and to investigate the density and viscosity of a synthetic mixture of CO_2 with high level of impurities.

1.4 Thesis overview

In Chapter 2, the experimental work and procedure used in this research are explained and the measured data are presented. In Chapter 3, a description of the molecular forces and the definition of phase behaviour are presented. The concept of Equation of State (EoS) and the Statistical Associating Fluid Theory (SAFT) are also introduced in Chapter 3. A complete description of the model which is primarily used in this research, the SAFT-VR Mie EoS, is presented in Chapter 4. Additionally, in this chapter, a comparative study of vapour-liquid equilibria and density modelling with four different EoSs is presented. In Chapter 5 about transport properties, the viscosity and interfacial tension models are then described, as well as the results of modelling CO_2-rich systems concerning the transport properties. In Chapter 6, the experimental measurements presented in the Chapter 2 are then modelled and discussed. Finally, in Chapter 7, the main conclusions that can be extracted from the studies developed in this thesis are summarised and recommendations for future works are proposed.

CHAPTER 2: EXPERIMENTAL STUDY

This chapter aims to provide data interesting for the CCS. It is divided into two parts: first a literature review, where existing experimental data are analysed and systems showing a lack of experimental data (VLE and densities) are identified, then the experimental work done (experimental procedures, measurements and their uncertainties) during this thesis. Phase equilibrium data, density and viscosity of CO_2 or H_2S systems have been measured. Data presented in this chapter will be used in the following chapters to validate the investigated models.

2.1 Introduction

In the context of the Carbon Capture and Storage, the compounds of interest are the one present in reservoir fluids and typical flue gas. Seven gases (CO_2, N_2, O_2, Ar, H_2S, CO and SO_2), twenty alkanes (between methane and nC_{32}) and two aromatics (benzene and toluene) have been chosen to validate the model. A summary of the VLE and density data available in the literature for the studied binary mixtures is presented in Table 2.1.

Systems studied experimentally have been chosen because of one of these criteria: lack of experimental data, extension of the conditions range and continuity in the work of our research centres. First, vapour-liquid equilibrium (VLE) of the Ar- H_2S binary system has been studied. No data have been found in the literature for this system and both H_2S and Ar are components present in reservoirs (traces of Ar in natural gases) and flue gas steams. Second, densities of three systems of CH_4 + H_2S have been measured in order to extend the range of data to lower temperatures (253K). Densities of a C_2H_6 + H_2S and a C_3H_8 + H_2S systems have also been measured complementing the work of Rivollet [20,21,22] at the laboratories of the CTP Mines-ParisTech. Third, in the framework of the joint industrial project (JIP) entitled “Impact of Common Impurities on Carbon Dioxide Capture, Transport and Storage” [23], the densities of a ternary system of CO_2-CH_4-H_2S have been measured. Also as part of this JIP and continuing the work of Nazeri [24] at the labs of the IPE in the Heriot-Watt university, the density and viscosity of a multicomponent CO_2-rich synthetic mixture have been studied.

Table 2.1. Vapour-liquid equilibrium (■) and density (□) data available in the literature for the binary systems studied in this work (NIST Databases [42,171]).

		CO_2	H_2S	N_2	Methane	Ethane
Gases	CO_2					
	H_2S	■ □				
	N_2	■ □	■ □			
	O_2	■ □		■ □		
	Ar	■ □		■ □	■ □	■
	SO_2	■		■	■	
	CO	■	■	■ □	■ □	■ □
Alkanes	C_1	■ □	■ □	■ □		
	C_2	■ □	■ □	■ □	■ □	
	C_3	■ □	■ □	■ □	■ □	■ □
	i-C_4	■ □	■	■	■ □	■ □
	n-C_4	■ □	■	■ □	■ □	■ □
	i-C_5	■	■	■	■	
	n-C_5	■ □	■	■	■ □	■ □
	n-C_6	■ □	■	■	■	■
	n-C_7	■ □	■	■	■ □	■ □
	n-C_8	■ □		■ □	■	■
	n-C_9	■	■	■	■	
	n-C_{10}	■ □	■ □	■	■ □	■ □
	n-C_{12}	■		■	■	■
	n-C_{14}	■ □		■	■ □	■
	n-C_{15}		■			
	n-C_{16}	■ □		■	■	■ □
	n-C_{18}	■			■ □	■
	n-C_{20}	■ □	■	■	■ □	■ □
	n-C_{24}	■			■	■
	n-C_{32}	■			■	
A.	Benzene	■	■	■	■	■
	Toluene	■ □	■ □	■	■ □	■

Besides experimental measurements, high-quality experimental data require well-defined uncertainty levels [19]. All the aspects regarding the definition and calculation of the uncertainty in our measurements are provided in Appendix A.

2.2 Vapour-liquid equilibria of H_2S - Ar

Many sour natural gases (NG) reservoirs and sour gas condensates fields have been discovered in the last thirty years. This kind of natural hydrocarbon gas reservoirs represents about half of the known total worldwide resources (270 trillion m^3) [25]. Acid natural gases contain significant amounts of carbon dioxide (CO_2) and hydrogen sulphide (H_2S), with compositions between of 0-80% moles for CO_2 and 0-30% for H_2S [26].

Acid gases need to be removed from the NG by a gas sweetening process. One of the most commonly used technology for sour gas sweetening process is absorption by alkanolamine. After the regeneration of the alkanolamine and the separation of the removed gases, acid gases are sent and injected into a depleted gas/oil reservoir or a secure geological formation for disposal.

To better design the injection process of acid gases or CO_2 captured streams, accurate phase equilibrium data as well as robust thermodynamic models are indispensable. However, impurities contained in flue gases may modify CO_2 phase behaviour. Thus, in the context of CCS, H_2S and, to a lesser degree, Ar could be significant impurities in the CO_2-rich stream [27]. VLE data of the Ar+H_2S system have been measured, because, to our knowledge, no data were found in the literature.

2.2.1 Materials

Hydrogen sulphide (H_2S) and Argon (Ar) were supplied by Air Liquide with a certified purity higher than 99.5 vol% and 99.999 vol% respectively. No additional purification was performed before use, except for careful degassing.

2.2.2 Equipment description

The apparatus was designed based on a "static-analytic method". Two capillary ROLSI™ samplers [28,29] (Armines' Patent) are used to sample liquid and vapour phases (see Figure 2.1). The cell volume is about 20 ml and it can be operated up to 473 K. The equilibrium cell is made of a Hastelloy tube which allows to work up to 23 MPa. This tube replaces the sapphire tube which lets visual observations inside the cell, but it limited the pressure to 10 MPa. A magnetic Teflon-coated stirrer driven by an

adjustable speed external system is placed inside the cell in order to achieve a fast thermodynamic equilibrium and to provide a good mixing of the fluids between measurements [27].

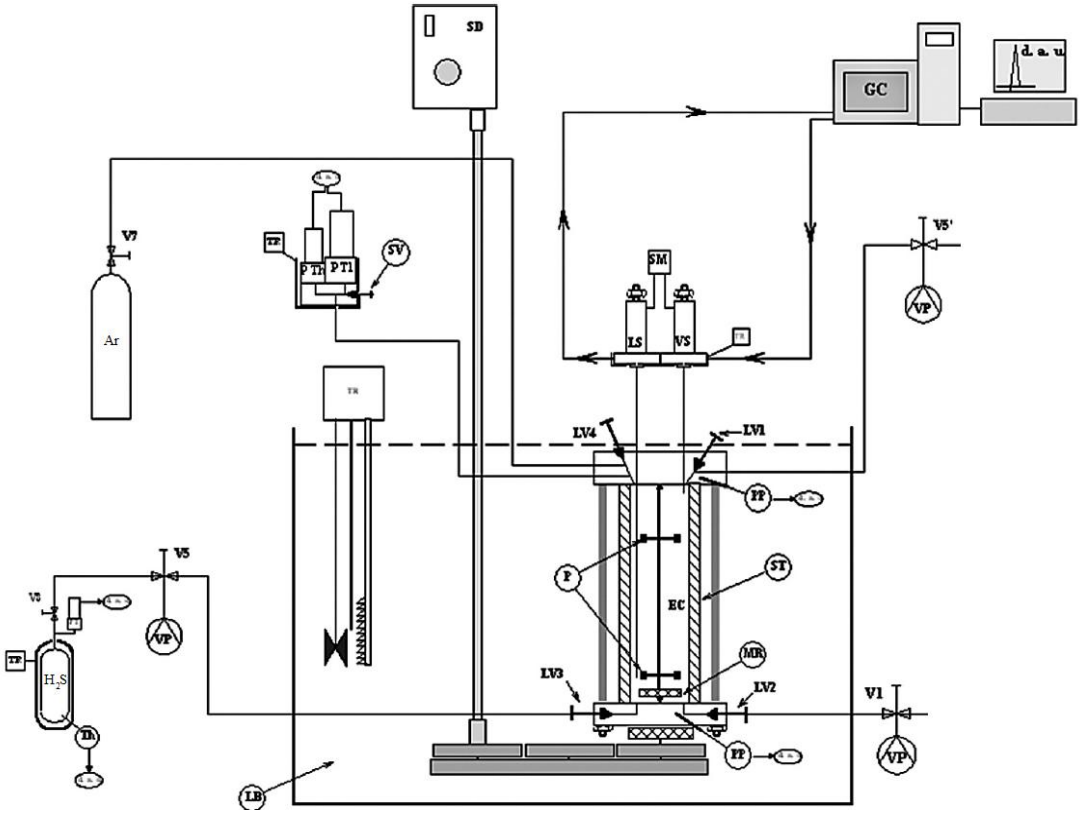

Figure 2.1. Schematic diagram of the VLE equipment [27]**: EC, equilibrium cell; LB, liquid bath; LS, liquid sampler; PP, platinum resistance probe; PT, pressure transducer; TR temperature regulator, VS, vapour sampler; VP, vacuum pump.**

The equilibrium cell is totally immersed in a liquid bath which keeps the temperature stable to ±0.1 K. The equilibrium cell is equipped with two probes, mounted in the upper and lower level of the cell, in order to obtain a precise measure of the temperature. The pressure in the cell is tracked by a pressure transducer. The pressure transducer and temperature probes are connected to a HP data acquisition unit (HP34970A). The HP data acquisition unit is connected to a computer through a RS232 interface. From the computer, real-time temperature and pressure readings during experiments are accessible. Two capillary tubes of 0.1 internal diameters connect the equilibrium cell with the vapour and liquid samplers. Then, the sampling is effectuated using two ROLSI^{TM} capillary samplers. The sample is swept to the gas chromatograph (GC) for compositional analysis. The GC used was the Shimadzu GC-2014 equipped

with a thermal conductivity detector (TCD), which was calibrated for the studied compounds.

2.2.3 Calibration procedure and uncertainty

Temperatures are measured with two *Pt*100 (100Ω platinum resistance) probes. The probes have been calibrated against a 25 Ω reference thermometer (Tinsley Precision Instrument). From the calibrations, the expanded uncertainty in temperatures measurements was estimated to be $u(T, k=2)= 0.02$ K. The calibration of the pressure transducers was done using a dead weight balance (Desgranges & Huot, model 5202S). The expanded uncertainty of pressure measurements is estimated to be less than $u(P, k=2)= 0.002$ MPa.

The thermal conductivity detector (TCD) of the gas chromatograph (GC) Shimadzu was calibrated for both H_2S and Ar. The TCD calibration consists in the injection and analysis of fixed volumes between 50 and 500 µL of one compound into the GC with an automatic syringe. The expanded uncertainty from the calibration of the GC is estimated to be less than 1.7% for H_2S mole numbers and 0.7% for Ar mole numbers. The maximum uncertainty on composition takes into account standard uncertainties from calibration and repeatability (see Appendix A). It is estimated to be $u(x)= 0.0030$ and $u(y)= 0.0062$, for the liquid and vapour phases respectively.

2.2.4 Experimental procedure

After the equilibrium cell and loading lines are vacuumed and the desired temperature is set, the cell is first loaded with hydrogen sulphide. Visual observations of the liquid level inside the cell have not been possible. Thus the volume of H_2S loaded was roughly estimated from the internal volume of the line that linked the equilibrium cell and the bottle of pure H_2S. When the temperature equilibrium is reached, i.e. when the upper and lower temperature probes give equivalent temperatures, the vapour pressure of the H_2S is recorded and starting the injection of the lighter component (argon). Ar is introduced step by step, increasing the pressure and leading to successive equilibrium mixtures of increasing overall Ar composition [27]. For each equilibrium condition, at least six samples of both vapour and liquid phases are analysed in order to check the repeatability of the measurements [27].

2.2.5 Results

Vapour-liquid equilibrium (VLE) data of the Ar-H_2S system have been measured at 273.01, 298.00 and 322.96 K. There are no previous studies of this system, the VLE were predicted using an EoS. The temperature range desired was initially between 258 and 298 K. However, taking into consideration the predictions from the model and the maximum operational pressure of the set-up (23 MPa), the temperature range was increased in order to study the phase equilibrium close to the critical region for at least one of the studied isotherms (323 K).

Table 2.2. Vapour–liquid equilibrium pressures, phase compositions for Ar ($_1$) - H_2S ($_2$) mixtures and uncertainties of measurements (N: number of samples; and σ: Standard deviation). Uncertainty on temperature $u(T)$ = 0.02 K and uncertainty on pressure $u(P)$= 0.002 MPa.

Pressure [MPa]	x_1	N_x	u_{rep} [σ_x]	u_{calib}	$u(x_1)$	y_1	N_y	u_{rep} [σ_y]	u_{calib}	$u(y_1)$
T=273.01K										
2.114	0.0068	6	0.0003	0.0001	0.0003	0.4755	7	0.0041	0.0039	0.0057
4.064	0.0205	7	0.0011	0.0002	0.0011	0.6923	7	0.0013	0.0052	0.0054
6.083	-					0.7657	6	0.0003	0.0056	0.0056
9.399	0.0577	6	0.0001	0.0006	0.0007	0.8045	6	0.0014	0.0058	0.0060
12.710	0.0812	6	0.0001	0.0007	0.0008	0.8195	6	0.0003	0.0060	0.0060
15.956	0.1046	6	0.0002	0.0011	0.0012	0.8223	6	0.0008	0.0061	0.0061
19.679	0.1315	6	0.0001	0.0012	0.0012	0.8091	6	0.0006	0.0059	0.0059
22.855	0.1545	6	0.0003	0.0015	0.0016	0.7966	6	0.0006	0.0058	0.0058
T=298.00K										
3.045	0.0081	6	0.0001	0.0001	0.0002	0.2812	9	0.0016	0.0035	0.0038
5.202	0.0257	7	0.0001	0.0003	0.0004	0.5244	7	0.0016	0.0044	0.0046
7.516	0.0454	7	0.0001	0.0005	0.0006	0.6239	8	0.0015	0.0051	0.0054
10.089	0.0685	6	0.0002	0.0007	0.0008	0.6738	7	0.0020	0.0057	0.0060
14.194	0.1087	6	0.0004	0.0011	0.0012	0.7010	6	0.0019	0.0059	0.0062
18.396	0.1557	7	0.0001	0.0014	0.0014	0.6925	6	0.0017	0.0058	0.0060
22.257	0.2084	7	0.0007	0.0018	0.0019	0.6593	10	0.0025	0.0057	0.0062
T=322.96K										
4.279	0.0069	11	0.0001	0.0002	0.0003	0.1224	9	0.0007	0.0017	0.0018
5.006	-					0.2134	8	0.0019	0.0028	0.0034
6.149	0.0248	10	0.0001	0.0003	0.0004	0.3119	8	0.0019	0.0038	0.0043
7.440	0.0382	8	0.0001	0.0004	0.0006	0.3859	9	0.0024	0.0045	0.0051
8.945	0.0546	9	0.0002	0.0006	0.0007	0.4459	9	0.0015	0.0046	0.0049
10.522	0.0728	8	0.0001	0.0008	0.0008	0.4858	9	0.0018	0.0049	0.0052
11.932	0.0897	10	0.0004	0.0009	0.0010	0.5053	10	0.0019	0.0049	0.0053
13.710	0.1139	9	0.0003	0.0010	0.0011	0.5188	9	0.0017	0.0047	0.0051
16.773	0.1651	6	0.0001	0.0014	0.0014	0.5168	7	0.0011	0.0044	0.0045
18.790	0.2111	6	0.0005	0.0015	0.0016	0.4890	8	0.0024	0.0043	0.0049
20.373	0.2729	7	0.0021	0.0022	0.0030	0.4269	8	0.0027	0.0040	0.0048

The experimental VLE data for the Ar-H_2S system as well as their uncertainties are presented in Table 2.2. The modelling and discussion of the measured data will be done in Chapter 6.

2.3 Density measurements of C_1-C_3 and H_2S binary systems

Natural gas (NG) is progressively considered as the fossil energy source of choice [27]. The exploration and production of NG fields have been focused during the past twenty years on sour or acid gas reservoirs with higher content of acid gases due to the continuous increase in the energy demand [27,30]. For these natural gases with high H_2S and/or CO_2 content, carbon capture storage (CCS) technologies, such as oxy-fuel combustion, have the potential to become economically competitive with other zero-carbon and renewal sources of energy [31]. There are limited references available in the literature concerning single phase density ($PT\rho x$) of binary systems of hydrogen sulphide with methane, ethane and propane (Table 2.3).

Table 2.3. Available experimental $PT\rho x$ data in the literature with their uncertainties for the C_1-C_3 and hydrogen sulphide binary systems.

System	Reference	H_2S mol fraction		Pressure		Temperature		Density	
		Range (%)	u(x_{H2S}) (%)	Range (MPa)	u(P) (MPa)	Range (K)	u(T) (K)	Range (kg·m^{-3})	u(ρ) (%)
CH_4-H_2S	Reamer et al. [32]	10-90	0.3	1-69	0.001	277 411	0.01	1-69	0.5
	Bailey et al. [33]	50.7	0.01	0.2-38	0.003	299 501	0.01	1-230	1
C_2H_6-H_2S	Robinson et al. [34]	53	-	6.6-14	-	344	-	121-398	-
	Rivollet et al. [20]	4-14	0.02	0.1-20	0.002	254 363	0.02	1-506	0.05
C_3H_8-H_2S	Rambosek [35]	10	-	0.7-5.9	-	273 357	-	555-786	-
	Robinson et al. [34]	57	-	5.4-13	-	366	-	134-444	-
	Jarne et al. [22]	22-27	0.02	0.1-40	0.002	263 363	0.01	1-506	0.05

In 1951, Reamer et al [32] did a thorough study of the H_2S + CH_4 binary mixture. They measured vapour-liquid equilibria (VLE) and densities of nine systems [36]. Reamer's density measurements cover a wide range of compositions (0.1-0.9 mol fraction H_2S), temperatures (277-411 K) and pressures (up to 69 MPa) with 1140 data. Bailey et al. [33] studied the system 49% mol of CH_4 and 51% mol of H_2S at higher temperature

(501 K). The main goal of the new measurements presented for the H_2S + CH_4 is to complete the literature data at low temperature.

Regarding the ethane and propane systems, few works have been found with *PTρx* data. Rambosek's thesis (1950) [35] and Robinson Jr. et al. work (1965) [34] can be mentioned. The more complete research for these systems has been found in Rivollet's thesis [21] which data were later published by Rivollet et al. [20] and Jarne et al. [22]. The objective of our measurements is to produce new density data by extending the range of composition. The studied mixture of C_2H_6-H_2S contains higher amount of hydrogen sulphide than those mixtures measured by Rivollet, while the C_3H_8-H_2S mixture has lower composition in acid gas.

2.3.1 Sample preparation

The specification and sources of the chemicals used in this work are summarized in Table 2.4. Three mixtures of CH_4 + H_2S, one of C_2H_6 + H_2S and one of C_3H_8 + H_2S were prepared volumetrically at laboratory temperature in 300 cm^3 cylinder with its own pressure transducer to track the pressure of the sample. The final pressure target of the mixtures in the vessel was approximately 40 MPa in order to avoid any phase change and possible variations of composition during the injection of mixture into the densitometer set-up.

Table 2.4. Details of the chemicals, suppliers and purities of the components used in this study.

Chemical Name	Source	Initial Purity [a]	Certification	Analysis Method [b]
Hydrogen sulphide	Air Liquide	0.995 vol	Air Liquide Certified	SM
Methane	Air Liquide	0.99995 vol	Air Liquide Certified	SM
Ethane	MESSER	0.9995 vol	MESSER Cetified	SM
Propane	MESSER	0.9995 vol	MESSER Cetified	SM
Carbon Dioxide	Air Liquide	0.99995 vol	Air Liquide Certified	SM

[a] No additional purification is carried out.
[b] SM: Supplier method

To prepare the mixture, a volume of H_2S is first injected into the cylinder; thereby the injected volume will contain the number of moles calculated by an equation of state to

reach the expected final composition. Second, the methane is pumped in the cylinder until the desired pressure is reached. In the case of the ethane and propane, the compressor could not be used because of the possibility of two coexistent phases during the compression. In consequence, the final pressure was reached by heating a secondary cylinder filled with ethane or propane and then the pressurised gas was transferred to the sample cylinder with H_2S until the target pressure in the vessel is reached at ambient temperature. Finally, the composition of each mixture was validated by gas chromatography analysis (Varian model CP-3800). The resulting compositions of the prepared mixtures are reported in Table 2.5.

Table 2.5. Resulting compositions of the studied mixture of methane, ethane and propane with hydrogen sulphide.

Mixture	Component	x_{H2S}	$u(x_{H2S})$
1	Methane	0.1315	0.0006
2	Methane	0.1803	0.0008
3	Methane	0.2860	0.0011
4	Ethane	0.3390	0.0013
5	Propane	0.1326	0.0010

2.3.2 Equipment description

The density of the studied mixture have been measured by a Vibrating Tube Densitometer (VTD), Anton Paar model DMA 512, using the one fluid reference calibration method [37]. It is a synthetic method where the composition of the mixture is known a priori. A schematic sight of the apparatus is presented in Figure 2.2. A full description and validation of the experimental set-up and procedures are available in Bouchot and Richon [38], Coquelet et al. [39] and Nazeri et al. [40].

The main part of the set-up is the Anton Paar densitometer (1) which consists in a U-shape vibrating tube made of Hastelloy. The densitometer temperature is set by a liquid bath (4) which maintains the temperature stable to ±0.01 K. The circuit between the valves V2 and V4 is immersed in a second liquid bath (4) which ensures a constant temperature of the fluid during the test. The period of oscillation, the pressure from the transducers (6) and the temperature from the probes (7) are recorded with a HP53131A

data acquisition unit (9). The parts of the set-up are connected by a circuit of lines with a diameter of 1/16 inches.

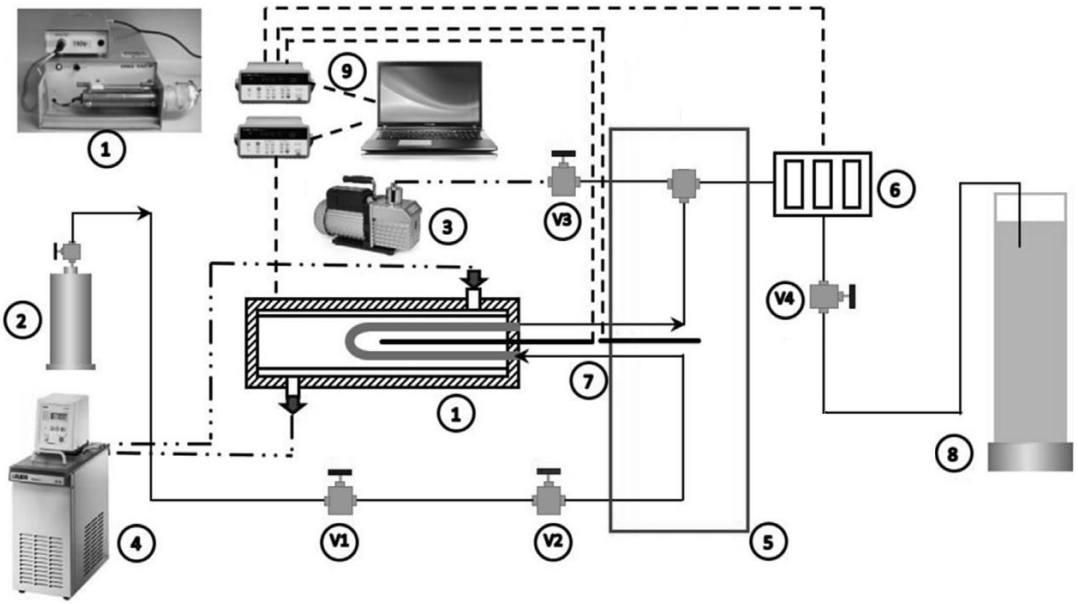

Figure 2.2. Schematic diagram of the equipment [40]**: (1) Anton Paar DMA 512 densitometer, (2) 300cc sample vessel, (3) Vacuum pump, (4) Lauda RE206 liquid bath, (5) Liquid bath of circuit, (6) Pressure transducers, (7) Temperature probes, (8) Neutralisation column and (9) Data acquisition unit. Circuit: (V1) Inlet circuit valve, (V2) Flow controlling ball valve, (V3) Vacuum valve, (V4) and (V5) Neutralisation valve.**

2.3.3 Calibration procedure and uncertainty

The temperature of the system in the set-up is regulated by two liquid baths. Temperatures are measured with two *Pt*100 (100Ω platinum resistance) probes. The probes calibration has been done with a 25 Ω reference thermometer. From calibrations, the expanded uncertainty in temperature measurements was estimated to be 0.03 K.

The pressure was measured by two pressure transducers at two complementary ranges, one between 0 and 5 MPa and another from 5 up to 30 MPa. The calibration of the transducers was done using a dead weight balance. The expanded uncertainties of the pressure measurements from the calibration are estimated to be less than 0.003 MPa for low pressure (up to 5 MPa) and 0.005 MPa for higher pressures than 5 MPa (up to 30 MPa).

The calibration of the densitometer has been done using the one fluid reference calibration method [37]. Despite hydrogen sulphide is the fluid in common between the

studied mixtures, ethane is the pure fluid chosen to calibrate the densitometer in order to avoid working with pure H_2S due to its toxicity [41]. The density of the injected system is linked to the acquired period of oscillation by a first-order polynomial calibration:

$$\rho = a\tau^2 + b \tag{2.1}$$

where ρ is the density of the fluid, τ the vibrating period and '*a*' and '*b*' are the calibration parameters. These two unknown parameters ('*a*' and '*b*') were optimised using the density data of pure C_2H_6 from NIST ThermoData Engine [42] at three temperatures (253, 273 and 293 K) and pressures up to 30 MPa,

From manufacturer's specifications, the standard uncertainty on the period of oscillation is 10^{-8} s. Uncertainty on the parameters of the calibration has been estimated to be 0.5% over the investigated range of pressures; however, it is worth highlighting that, due to the used technique, average uncertainty at low pressure (below 0.5 MPa) was 6.1%.

The standard and combined uncertainties reported herein have been calculated according to the procedure presented in Appendix A.

2.3.4 Experimental procedure

Three isotherms of each binary system were measured at 253, 273 and 293 K. The mixture was gradually charged from the cylinder in the experimental set-up while the vibrating period, the temperature and the pressure were recorded continuously during the slow-increasing pressure up to 30 MPa and the slow decompression (the pressure in the vessel containing the mixture was maintained at pressure higher than 30 MPa during all the measurements). During the depressurisation, the acid outlet gas was neutralised by bubbling it through a column with a basic solution of sodium hydroxide.

2.3.5 Results

Densities of three binary mixtures of CH_4 and H_2S with 0.1315, 0.1803 and 0.2860 mol fractions of hydrogen sulphide, one mixture of 0.661 mol C_2H_6 + 0.339 mol H_2S and one mixture of 0.1326 mol C_3H_8 + 0.8674 H_2S have been measured continuously using a high temperature and high pressure VTD Anton Paar. Before the measurements, the

phase envelopes of these binary systems have been studied in order to forecast at which pressure the two phases behaviour is found.

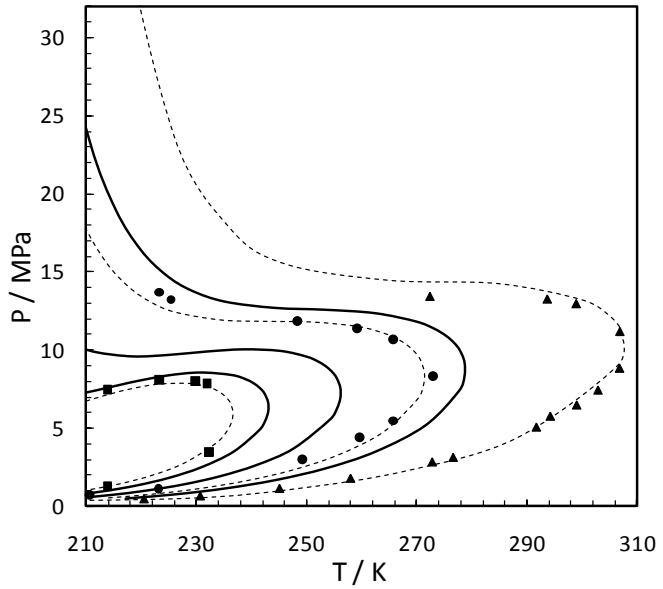

Figure 2.3. Predicted phases envelopes with the PR EoS of the methane + hydrogen sulphide systems with 0.1101, 0.1315, 0.1803, 0.248, 0.286 and 0.458 mol fractions of H_2S. The solid lines are the compositions studied in this work and the dashed lines are other phase diagrams compared against Kohn and Kurata data [43]**: (■) 0.1101, (●) 0.248 and (▲) 0.458 mol fractions of H_2S.**

Phase diagrams of our measured CH_4 + H_2S systems calculated by a thermodynamic model (the PR EoS) and other three systems comparing calculations against literature data [43] are shown in the Figure 2.3. According to Scott and van Konynenburg [44], the phase diagram of CH_4 + H_2S system is classified as type III [45]. This means that the curves presented in the phase envelops of Figure 2.3 are dew lines, therefore no density was measured in the liquid region. The studied binary mixtures of CH_4 + H_2S are systems with no critical point [46,47], thus all our *PTρx* measurements have been done in the gas phase. In the P-T envelopes presented, there is no phase change for any of the studied isotherms for the 0.1315 mol fraction of H_2S system. However, it is possible to enter the two phase region at 253 K for the 0.1803 mol fraction of H_2S system and at 253 and 273 K in the 0.2860 mol fraction of H_2S system.

Regarding the systems C_2H_6 + H_2S and C_3H_8 + H_2S, the phase diagram of this systems is classified as type I due to the existence of a continuous critical locus between the critical point of both compounds, according to the works of Kay et al. [48] and Brewer et al. [49] (Figure 2.4). Predictions for these systems show that there is a phase change for both mixtures at the three isotherms.

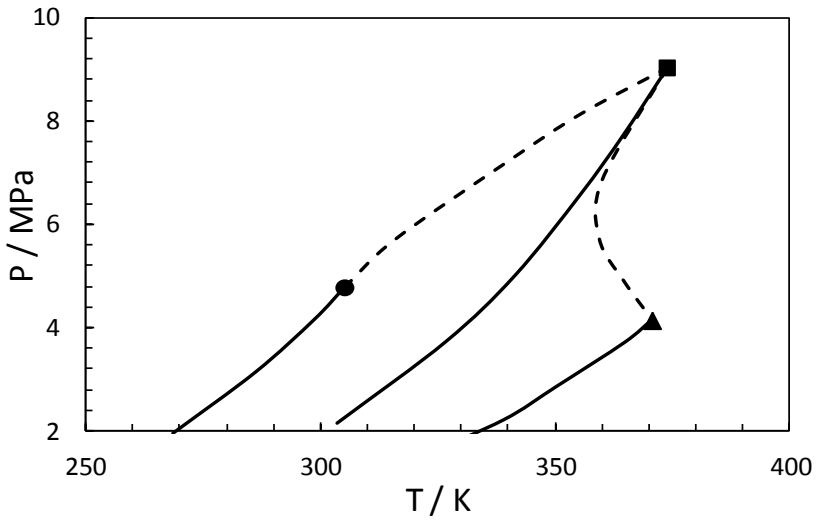

Figure 2.4. Critical loci (dashed lines) of the C_2H_6 + H_2S and C_3H_8 + H_2S systems [48,49]. Data: critical point of ethane (●), hydrogen sulphide (■) and propane (▲) [50].

Experimental density data for the measured systems are presented in Appendix B, in Tables B.1 to B.15. The compressibility factors derived from the measured temperature, pressure and density data, as well as their uncertainty, are also reported in Tables B.1-B.15. Modelling and discussion of the measured data will be done in Chapter 6 after the introduction of the investigated equations of state.

2.4 Density measurements of the CO_2–CH_4–H_2S ternary system

The main components of sour natural gases reservoirs and sour gas condensates fields are methane, carbon dioxide and hydrogen sulphide. Thus, following the same reasoning as for the previous density measurements of methane and hydrogen sulphide systems, the study of the CO_2–CH_4–H_2S ternary system is interesting for CCS and the oil and gas industry. These measurements were done in the context of the Joint Industrial Project titled "Impact of Common Impurities on Carbon Dioxide Capture, Transport and Storage" [23]. Phase equilibrium of this system has been studied in several works [51,52,53], however, to our knowledge, there is no measurements of the volumetric behaviour.

Density measurements have been done using the same equipment and following the same experimental procedure presented in section 2.3. These measurements have been performed for six isotherms from 253 to 353, and pressures up to 30 MPa.

2.4.1 Sample preparation

The specifications of the used chemicals can be found in Table 2.4. The mixture of CO_2+CH_4+H_2S was prepared gravimetrically at laboratory temperature. The target pressure was 40 MPa and the pressure of the mixture in the vessel was tracked by the transducer installed in the cylinder. The expected composition of the CO_2–CH_4–H_2S was forty-forty-twenty respectively. H_2S is first injected into the vessel due its lower saturation pressure at room temperature, followed by CO_2. Both masses of H_2S and CO_2 were measured with a balance with a precision of ±0.1g. Then, the methane was pumped in the cylinder until the target pressure is reached. Afterwards, the composition of mixture was validated by gas chromatography analysis (Varian model CP-3800). The resulting composition of the prepared mixtures was 0.4212 mol of CO_2, 0.4053 mol of CH_4 and 0.1735 mol of H_2S.

2.4.2 Calibration procedure

For this mixture, the method used to calibrate the vibrating tube densitometer was the forced path mechanical calibration (FPMC) model [38]. The VTD Anton Paar cell can be modelled by means of a linear hollow vibrating system whose internal volume is $V_i=V_i\,(T,P)$ and total vibrating mass is $M=(M_0+\rho V_i)$, where M_0 is the proper mass of the tube under vacuum and ρ the density of the inner fluid to be determined [40]. The relation between them can be presented by the following equation:

$$\rho = \left(\frac{M_0}{V_i}\right)\left[\left(\frac{K}{K_0}\right)\left(\frac{\tau^2}{\tau_0^2}\right)-1\right] \tag{2.2}$$

where K is the natural transversal stiffness $K=K(T, P)$ and τ the oscillation period under the mechanical effect of a fluid. The subscript '0' refers to the evaluation of the stiffness and period of the vibrating tube at vacuum condition.

The FPMC calibration method were well-described by Bouchot and Richon [38]. After evaluating the terms from the Eq. 2.2, the complete FPMC model can be written as:

$$\rho(T,P)=\left(\frac{M_0}{L_{00}}\right)\left(\frac{1}{\pi\, r_i^2(T,P)\,\delta\, L(T,P)}\right)\left[\left(\frac{\Delta r^4(T,P)}{\Delta r_0^4(T)}\exp(-3\gamma_T P)\right)\left(\frac{\tau^2(T,P)}{\tau_0^2(T)}\right)-1\right] \tag{2.3}$$

where (M_0/L_{00}) and γ_T are the two unknown parameters that need to be estimated during the calibration with this method.

In this case, carbon dioxide was the fluid used for calibrating the densitometer. Thus, both parameters, (M_0/L_{00}) and γ_T, have been optimised using density data of pure CO_2 from the NIST ThermoData Engine [42] at six temperatures (253, 273, 293, 313, 333 and 353 K) and pressures up to 30 MPa.

Despite the FPMC calibration model is more sophisticated than the one fluid reference method used for the previous measurement, the uncertainty of the gas densities measured at low pressure is still higher than the uncertainty of the measurements over the whole range of pressures. Therefore, this is not because of the calibration method used, it is the limitation of the apparatus for measuring densities at low pressure due to the inertia of the vibrating tube [54]. The average relative uncertainty in the calibration procedure has been estimated to be 0.4%, although it is worth noting the uncertainty of the gas phases at pressures (below 5MPa) is 5.4%.

2.4.3 Results

Densities of the ternary mixtures of 0.4212 mol CO_2 + 0.4053 mol CH_4 + 0.1735 mol H_2S have been measured continuously using a VTD Anton Paar at 253.10, 273.74, 293.37, 313.82, 333.98 and 353.63K. Before density measurements, the phase envelop of the ternary system has been studied in order to predict at which pressure the two phase region is found. As seen in Figure 2.5, there is phase change at 253 and 273K.

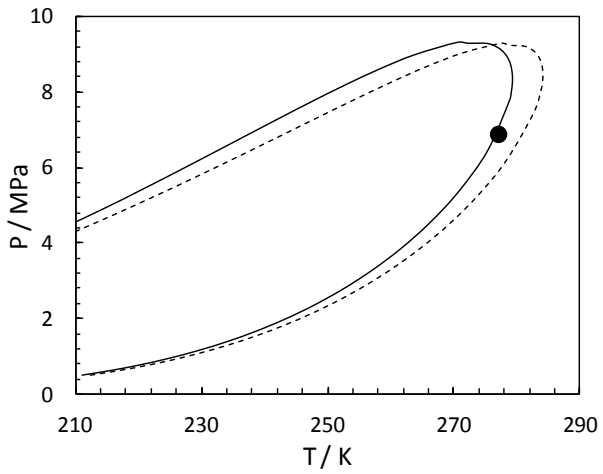

Figure 2.5. Phases envelopes predicted with the PR EoS. Solid line: our mixture. Dashed line: 0.471 mol CO_2 + 0.350 mol CH_4 + 0.179 mol H_2S [52]**. Dew point literature mixture (●)** [52]**.**

Experimental density data of the ternary systems well as compressibility factors are presented in Appendix B, in Table B.16 to Table B.21. Modelling and discussion will be presented in Chapter 6.

2.5 Density and viscosity measurements of a multicomponent CO_2–rich mixture

Carbon dioxide pipelines play a key role by linking the capture and storage sites. Thus, the study of transport properties is essential for a safe and economic transport of CO_2-rich steams. In pipeline systems, density and viscosity are two of the most important transport properties.

In this part of the work, the density and viscosity measurements of a multicomponent CO_2-rich mixture with 50% of impurities are presented. Transport properties were measured in the laboratories of the Institute of Petroleum Engineering in the Heriot-Watt University (UK) as part of the JIP titled "Impact of Common Impurities on Carbon Dioxide Capture, Transport and Storage" [23] and continuing Nazeri's work [24].

2.5.1 Materials

The system studied was a commercial multicomponent mixture containing CO_2, nitrogen and hydrocarbons. The mixture was supplied by BOC with a certification on the gravimetrical basis in accordance with ISO 6142. The multicomponent mixture was named MIX4, in order to differentiate this mixture from others studied previously in the laboratory. The composition of the MIX4 is given in Table 2.6.

Table 2.6. Composition of MIX4.

Components	**MIX4**
Carbon Dioxide	Balance
Methane	39.99 (±0.200) %
Ethane	3.510 (±0.018) %
Propane	1.530 (±0.008) %
n-Butane	0.501 (±0.006) %
i-Butane	0.499 (±0.005) %
n-Pentane	0.513 (±0.006) %
Nitrogen	3.524 (±0.018) %

2.5.2 Equipment description

Densities and viscosities were measured using an in-house designed and constructed setup. The experimental system was designed to reach a maximum operational pressure of 200 MPa and a maximum operational temperature of 523 K. The temperature range of work is between 203 and 473 K.

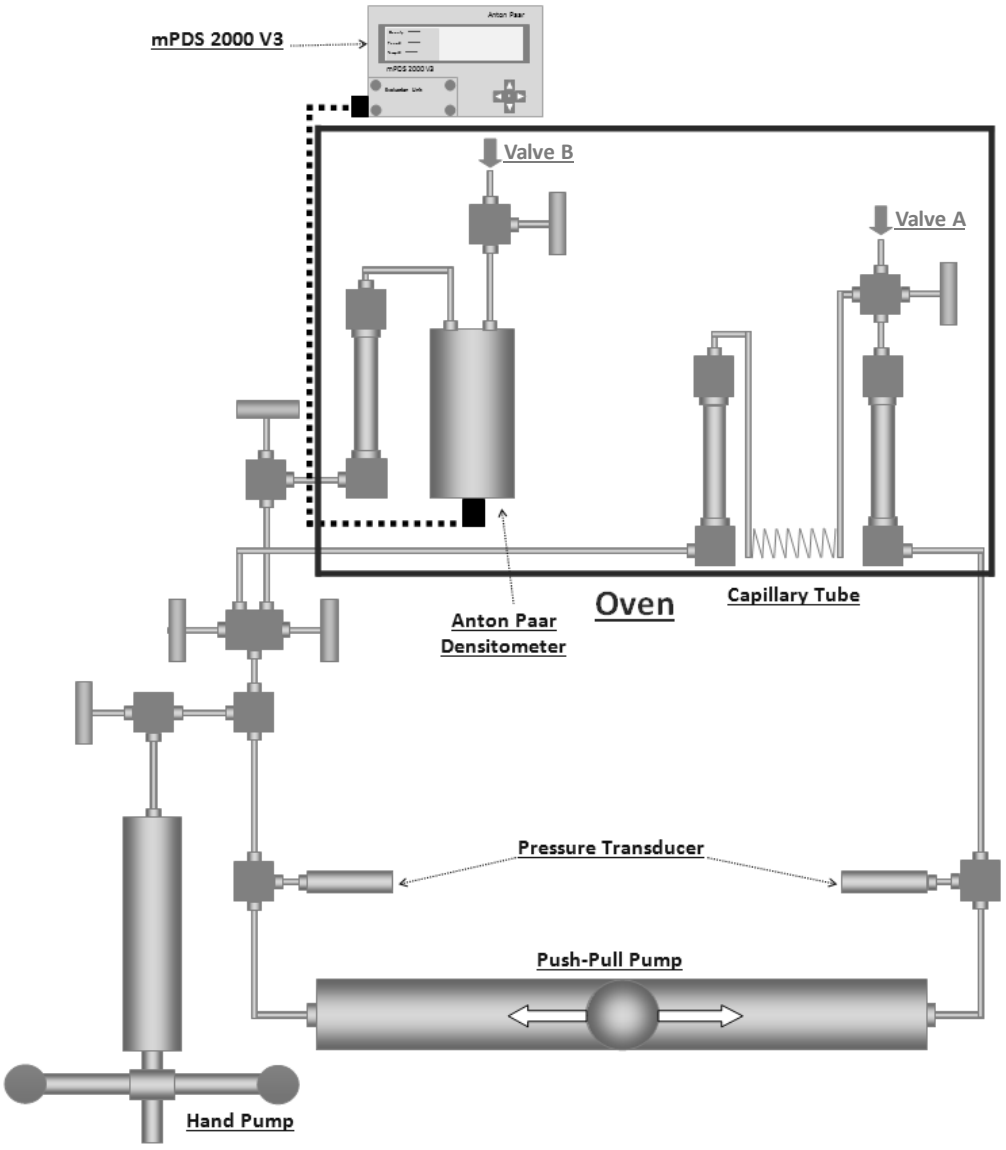

Figure 2.6. Schematic view of the viscosity experimental setup [55]**.**

A schematic view of the experimental setup is shown in Figure 2.6. The setup is essentially formed by a capillary tube with a (measured) length of 14.781 meters and a (calculated) internal diameter of 0.29478 millimetres. This tube connects two long cylinders of 25 cm^3. A three-way valve (valve A) is installed on the top of one of the

cylinders to inject the sample inside the capillarity tube and both cylinders. An oscillating U densitometer Anton Paar DMA-HPM is connected to the setup and a second three-way valve (valve B) is installed to inject sample to the system through the densitometer. This part of the experimental system is installed inside an oven, manufactured by BINDER GmbH. Outside the oven, the main equipment is a push-pull mercury pump driven by a motor. The base side of both cylinders are connected to the opposite sides of this pump, which can move the sample fluid forwards and backwards between the two cylinders. The pressure of the complete fluid system is controlled by a hand pump which is connected to a mercury reservoir in order to increase or decrease the amount of mercury in the system. Both the opposed piston pump and the hand pump are fitted with a Mitutoyo linear transducers readable to 0.005 mm on Mitutoyo SD-D1E readouts. As a 1 mm movement represents 0.151 cm^3 displacement in both pumps, the readability is 0.000755 cm^3. The opposed piston pump has a variable control with which the speed can be adjusted to a maximum of 5 cm^3/s. The rate can be set with a margin of error of ±0.00003 cm^3/s.

2.5.3 Calibration procedure and uncertainty

The period of oscillation of the vibrating tube during the measurements are linked to the density of the fluid by the calibration. Here again the one fluid reference calibration method [37] has been used (Eq. 2.1). Carbon dioxide has been used as the reference fluid. The calibration parameters have been fitted for each isotherm using density correlations of pure CO_2 from the NIST ThermoData Engine [42]. Due to the large range of pressures (up to 125 MPa), three sets of A and B parameters were regressed at each temperature for each phase state (gas, liquid and supercritical).

For viscosity measurements, the calibration parameter is the internal diameter of the capillary tube. The calibration of the diameter of this tube was done using correlations of viscosity data of pure CO_2 from NIST ThermoData Engine [42]. The pressure drop at the desired pressures and temperatures is measured. Then, the viscosity is estimated employing the Hagen-Poiseuille equation (Eq. 2.5) and assuming an initial diameter of 0.29653 mm, based on previous experiments [56]. The diameter is optimised by minimising the deviations between the experimental measurement and the viscosity data from the literature [24].

2.5.4 Experimental procedure

The capillary tube viscosity measurement method has been employed to measure the viscosity [55]. For each test, the setup was loaded with the mixture through the injection point on top of the densitometer after vacuuming the system. Then after disconnecting the sample cylinder from the system, the sample fluid was pushed through the capillary tube into the other cylinder using the push-pull mercury pump. The temperature of the system was set to the desired condition using the oven and the desired pressure was set using the hand pump. Once conditions are stabilized the period of oscillation is recorded and; after isolating the densitometer by closing the related valve (Valve B), the sample is pumped through the capillary tube at a number of flow rates. To ensure the consistency of the measurements, at each pressure, viscosities were determined at three flow rates and pressure drops were recorded three times at each flow rate. Then, each viscosity point is the average of nine separate readings [24].

To pump the sample fluid through the capillary tube using the piston pump results in a dynamic differential pressure that is monitored and recorded until stabilisation. Then, the pump was stopped to record the static differential pressure. The difference between total and static differential pressure was used as the pressure drop across the tube. To ensure laminar flow conditions, Reynolds numbers were checked for the flow rates in which the measurements were performed. Poiseuille equation (equation 2.5) can relate the pressure drop across the capillary tube to the viscosity, tube characteristics and also flow rate for laminar flow:

$$\Delta P = \frac{128 L Q \eta}{C \pi D^4} \tag{2.5}$$

where, ΔP is differential pressure across the capillary tube viscometer in psi, Q represents the flow rate in cm^3/sec, L is the length of the capillary tube in cm, D refers to the internal diameter of the capillary tube in cm, η is the viscosity of the flown fluid in cP and C is a unit conversion factor (C= 6894757 if the above units are used).

The tube length changes with temperature but it has no noticeable influence on the obtained viscosity. The set flow rate has no effect on the accuracy of the viscosity measurement. Only differential pressure as a variable in the above formulation can cause error in viscosity measurement. The usual variation in differential pressure measurements is ±0.01 psi ($7 \cdot 10^{-5}$ MPa) and this leads to an error of 1% in the

calculated viscosity. Taking into consideration the uncertainty in the pressure drop, the flow rate, the calibration of the tube diameter, the measure of the tube length and the standard deviation, the average uncertainty of the viscosity measurements is 2% (Appendix A).

2.5.5 Results

Density and viscosity of the multicomponent mixture of CO_2 with 50% impurities have been measured using the described capillary tube technique. A total of 55 viscosity data points for MIX4 have been measured at 5 temperatures (283.3, 298.3, 323.4, 373.5 and 423.4 K) and at 11 pressures, up to 125 MPa for density and up to 150 MPa for viscosity.

Viscosity and density measurements as well as their uncertainties are reported in Table 2.7. The presented measurements will be discussed and modelled in Chapter 6, after the presentation of the viscosity model (TRAPP [57]).

Table 2.7. Experimental results of the density and viscosity of MIX4.

T	P	ρ	u(ρ)		η	u(η)	
[K]	[MPa]	[kg·m^{-3}]	[kg·m^{-3}]	[%]	[μPa·s]	[μPa·s]	[%]
283.32	2.358	35.02	0.67	1.90	13.86	0.25	1.79
283.32	3.599	57.06	0.69	1.20	14.24	0.27	1.88
283.28	5.109	89.52	0.80	0.89	14.99	0.30	2.00
283.31	10.659	292.83	1.02	0.35	25.59	0.52	2.02
283.32	22.098	527.73	2.04	0.39	45.74	0.94	2.05
283.34	35.405	605.55	1.36	0.22	59.43	1.22	2.06
283.34	51.394	656.44	0.81	0.12	72.38	1.51	2.08
283.32	79.028	719.56	0.61	0.09	90.35	1.72	1.91
283.33	105.697	760.87	0.50	0.07	105.53	1.87	1.77
283.34	118.307	776.28	0.44	0.06	111.89	2.02	1.80
283.34	151.361	-			129.83	2.17	1.67
298.36	2.489	35.95	0.66	1.82	14.43	0.24	1.64
298.36	3.537	53.52	0.85	1.59	14.78	0.24	1.60
298.38	5.233	85.87	1.11	1.29	15.49	0.30	1.91
298.40	10.508	231.24	1.50	0.65	21	0.49	2.35
298.29	20.974	461.63	1.18	0.25	38.5	0.89	2.31
298.30	34.825	571.52	0.85	0.15	53.08	1.16	2.19
298.29	51.869	636.75	0.87	0.14	66.58	1.43	2.15
298.30	75.932	691.06	0.50	0.07	81.61	1.64	2.01
298.36	104.263	736.68	0.39	0.05	99.45	1.78	1.79
298.36	125.698	767.30	0.38	0.05	110.58	1.92	1.74
298.38	151.995	-			122.92	2.06	1.68
323.44	2.682	34.96	0.57	1.64	14.79	0.23	1.55
323.45	3.509	47.02	0.68	1.44	15.16	0.23	1.51
323.44	5.247	74.15	0.86	1.16	16.16	0.29	1.78
323.47	10.639	180.61	0.83	0.46	19.87	0.48	2.41
323.49	20.988	375.84	0.61	0.16	31.69	0.87	2.73
323.41	34.508	500.16	0.51	0.10	46.25	1.13	2.44
323.43	51.918	588.21	0.38	0.06	58.54	1.39	2.38
323.44	75.753	655.44	0.32	0.05	72.69	1.59	2.19
323.45	103.628	707.73	0.28	0.04	87.45	1.73	1.98
323.44	122.665	735.59	0.26	0.03	99.3	1.87	1.88
323.43	151.623	-			112.49	2.00	1.78
373.56	1.999	21.88	0.47	2.15	16.57	0.22	1.33
373.57	3.482	39.08	0.51	1.31	16.87	0.22	1.31
373.53	5.185	60.00	0.59	0.99	17.54	0.28	1.57
373.54	10.639	132.33	0.60	0.46	19.87	0.46	2.32
373.55	22.408	290.80	0.53	0.18	29.54	0.83	2.82
373.55	34.550	405.67	0.46	0.11	36.12	1.07	2.95
373.56	50.876	503.16	0.42	0.08	46.76	1.34	2.86
373.55	77.014	589.51	0.34	0.06	60.64	1.53	2.52
373.54	101.980	646.82	0.30	0.05	75.03	1.66	2.22
373.55	125.609	680.36	0.26	0.04	83.46	1.79	2.15
373.54	149.658	-			92.77	1.93	2.08
423.43	2.124	19.22	0.40	2.08	18.6	0.22	1.20
423.43	3.537	32.31	0.41	1.27	18.88	0.22	1.18
423.43	5.171	50.09	0.42	0.84	19.26	0.28	1.45
423.44	10.639	103.82	0.44	0.42	19.87	0.47	2.34
423.45	24.221	250.54	0.45	0.18	28.11	0.84	2.99
423.45	35.212	337.92	0.43	0.13	32.75	1.01	3.08
423.46	51.352	430.54	0.39	0.09	41.22	1.28	3.09
423.47	76.125	518.05	0.36	0.07	52.43	1.45	2.76
423.45	104.021	588.50	0.35	0.06	65.04	1.68	2.58
423.45	128.084	647.30	0.34	0.05	73.41	1.81	2.47
423.44	144.549	-			78.54	1.95	2.48

CHAPTER 3: THERMODYNAMIC BACKGROUND

The physical properties of every fluid depend directly on the nature of the molecules of the substance and the surrounding conditions. Therefore, in this third chapter the intermolecular forces which govern the molecular behaviour and influence the prediction of thermophysical properties are discussed.

Equations of state (EoSs) are mathematical expressions that describe the state of matter and relate the physical conditions of pressure, temperature and molar volume. EoSs are developed from a molecular description of compounds and they are employed to calculate the thermodynamic properties which describe the phase equilibrium. Then, the evolution and the wide variety of EoSs are presented in this chapter.

3.1 Intermolecular forces

The behaviour of fluids is driven by the interaction between molecules; therefore, a good description of the thermodynamic properties is relied on a good representation of intermolecular forces. The main classes of interactions between two point particles are dispersion forces (London), Coulombic interaction (charge-charge force), Keesom interaction (angle-average dipole-dipole interaction) and angle-average quadrudipole-quadrudipole interaction [58]. Hence, within the framework of an Equation of State (EoS), it is necessary to obtain an accurate analytical expression for the Helmholtz free energy that can take each of these interactions into account. Therefore, effective intermolecular potential is developed in order to facilitate the analysis of the interactions between two molecules.

Whereas the interactions described previously are attractive in nature, there is also repulsion between the molecules. In this way, a repulsive contribution is taken in account by most of intermolecular-potential models. For this reason, many of these potentials are based on a combination of an attractive and a repulsive parts. Indeed, these parts have common features, the repulsive term tends to infinity at short intermolecular distances, and the attractive tends to zero when the distance is infinite. Below, five of the most-common pair potentials are introduced [59]:

- Hard-sphere potential (HS):

$$u(r)=\begin{cases}\infty & r<\sigma\\ 0 & r\geq\sigma\end{cases} \tag{3.1}$$

- Square-well potential (SW)[60]:

$$u(r)=\begin{cases}\infty & r<\sigma\\ -\varepsilon & \sigma\leq r<\lambda\sigma\\ 0 & r\geq\lambda\sigma\end{cases} \tag{3.2}$$

- Sutherland potential [61]–[63]:

$$u(r)=\begin{cases}\infty & r<\sigma\\ -\varepsilon\left(\dfrac{\sigma}{r}\right)^{\lambda} & r\geq\sigma\end{cases} \tag{3.3}$$

- Yukawa potential [64]:

$$u(r)=\begin{cases}\infty & r<\sigma\\ -\varepsilon\dfrac{\exp\left[-\lambda\left(\dfrac{\sigma}{r}-1\right)\right]}{\sigma/r} & r\geq\sigma\end{cases} \tag{3.4}$$

- Lennard-Jones potential (LJ) [65]–[67]:

$$u(r)=4\varepsilon\left(\left(\frac{\sigma}{r}\right)^{12}-\left(\frac{\sigma}{r}\right)^{6}\right) \tag{3.5}$$

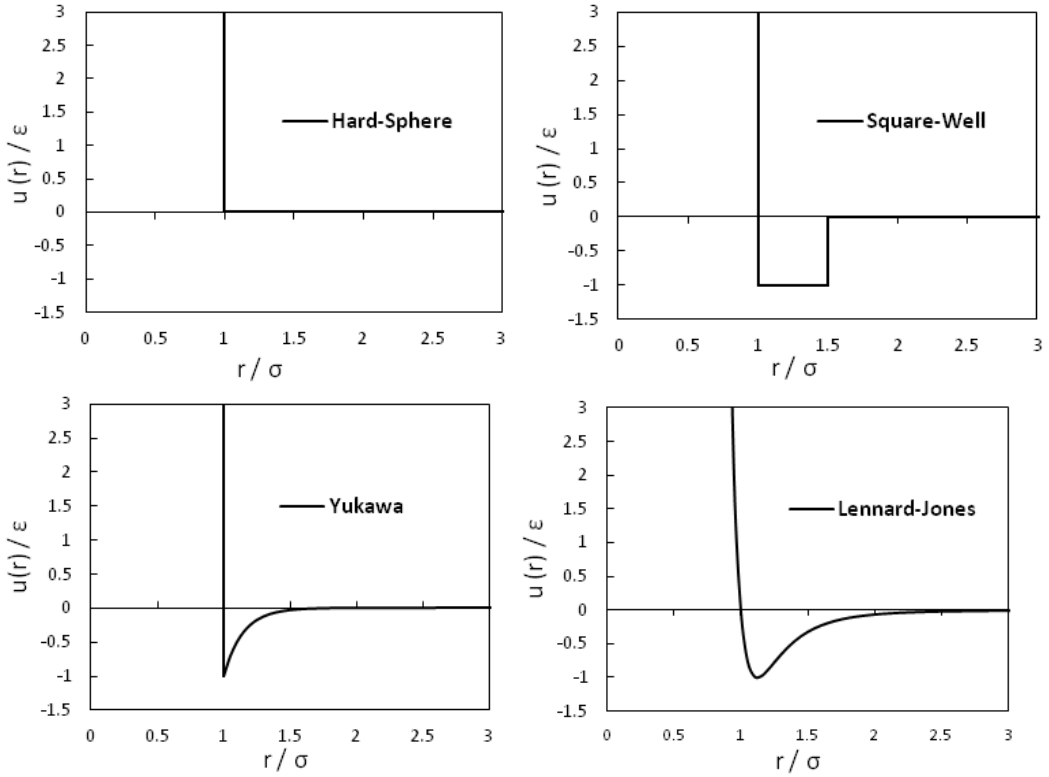

Figure 3.1. Hard-Sphere, Square-Well, Yukawa and Lennard-Jones Potentials [68].

In Figure 3.1, some intermolecular pair potentials are presented graphically. According to the equations and analysing the chart, it can be seen that the hard-sphere potential contains only a repulsive contribution, the square-well potential consists of a HS repulsive term and a constant attractive for a certain radial distance and Lennard-Jones potential is a continuous potential that depends on the repulsive-attractive exponents.

Despite the equations of state are described in further details in next sections, the intermolecular potential models employed by two of the models studied in this work are defined below. First, the PC-SAFT EoS [69,70] is one of the equations of state that has been evaluated in this thesis. In this model molecules are presented as hard-chains composed of spherical segments and the segment-interaction potential is a modified square-well potential:

$$u(r) = \begin{cases} \infty & r < (\sigma - s_1) \\ 3\varepsilon & (\sigma - s_1) \le r < \sigma \\ -\varepsilon & \sigma \le r < \alpha\sigma \\ 0 & r \ge \alpha\sigma \end{cases} \tag{3.6}$$

where, *u(r)* is the pair potential dependent of the radial distance *r* between two segments, σ the temperature-independent segment diameter, ε the potential depth, λ the reduced width and s_1 is assumed as $s_1 = 0.12\sigma$. This modified SW potential was suggested by Chen and Kreglewski [71] and, in contrast with their work, there is no additional temperature correction for ε [69]. In Figure 3.2, the modified SW potential is depicted the difference with the original SW is the soft repulsion between σ and σ-s_1.

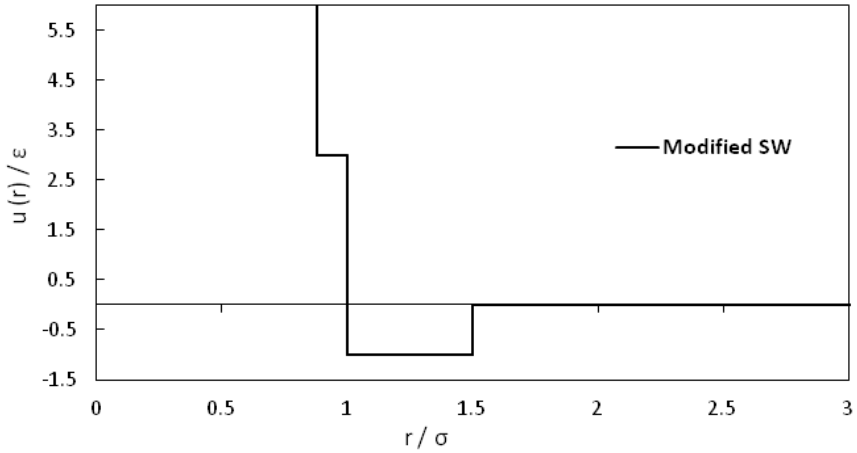

Figure 3.2. Chen and Kreglewski modified Square-Well intermolecular potential.

The other EoS pair potential is described using the Mie potential [72], a variable range family of potentials, named after Gustav Mie in 1903 [73]. Mie represented the pair potential in terms of power law, function of the inverse of radial distance between segments, and characterizing the nature of the repulsion and attractive monomer-monomer interactions with the λ_r and λ_a exponents. Thereby, the Mie potential is defined as [74]:

$$u^{Mie}(r) = C\varepsilon\left(\left(\frac{\sigma}{r}\right)^{\lambda_r} - \left(\frac{\sigma}{r}\right)^{\lambda_a}\right) \tag{3.7}$$

with

$$C = \frac{\lambda_r}{\lambda_r - \lambda_a}\left(\frac{\lambda_r}{\lambda_a}\right)^{\frac{\lambda_a}{\lambda_r - \lambda_a}} \tag{3.8}$$

where, r is the radial distance, ε the potential depth and λ_r and λ_a are the repulsive and attractive parameters, respectively. As it can be seen in the Figures 3.3, the Mie potentials provide a higher flexibility to describe the segment interactions, however both exponents are not completely independent due to the connection between the repulsive and attractive interactions. In this sense, changing λ_r not only affect the part of the repulsion, but also the attraction part, and vice-versa, because of λ_r and λ_a dependence on the C parameter (Eq. 3.8).

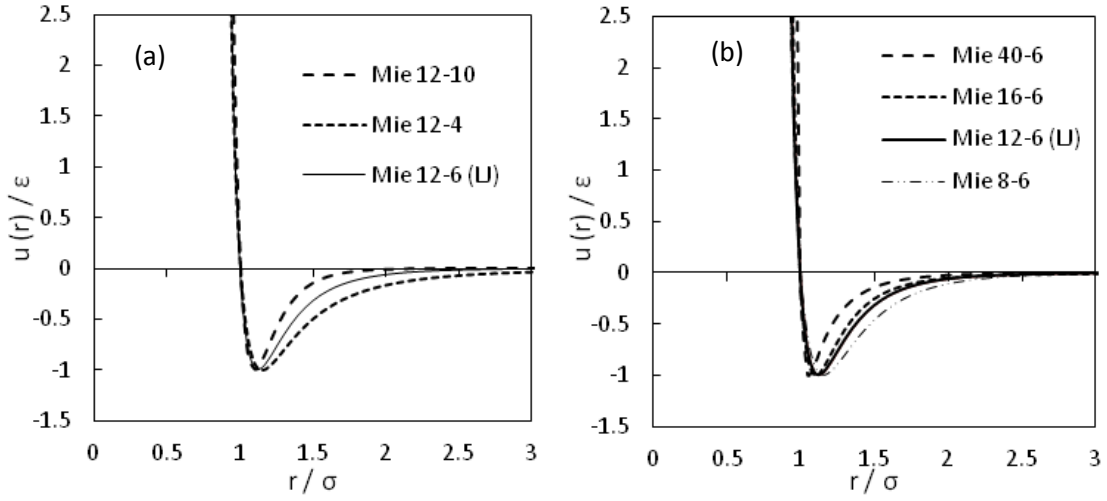

Figure 3.3. Mie intermolecular potentials with fixed $\lambda_r = 12$ and varying λ_a from 4 to 10 (a), and Mie potential with $\lambda_a = 6$ and varying λ_r from 8 to 40 (b) [75].

Frequently, these Mie potentials are named according to their repulsion-attractive exponents, *e.g.* a Mie 12-6 is the potential with λ_r = 12 and λ_a= 6. Particularly, the Mie 12-6 is one of the pair potentials presented previously, the Lennard-Jones potential. The generic Mie potential is more flexible than the LJ potential, since two more parameters can be adjusted. Due to its soft-core variable range, the advantage of the Mie potential is the versatility of a potential model with a variable repulsive exponent (as well as a variable attractive exponent), in contrast with other pair potentials model with hard-core repulsion.

3.2 Phase behaviour

A phase can be defined as any homogeneous and physically distinct region that is separated by a boundary from another different homogeneous region. Phase behaviour defines the phase or the phases in which a fluid exists at given conditions of pressure, molar volume and temperature (*PVT* conditions) [76]. Then, changing the *PVT* conditions, mass and thermal transfer may take place between the coexisting phases until reached the equilibrium. Phase equilibrium occurs when more than one phase is present in equilibrium; the study and understanding of this phenomenon is a central problem of thermodynamics. Phase equilibrium is characterized by the uniformity of pressure and temperature between the phases in the system, *i.e.* mechanical and thermal equilibria. Besides these thermal and mechanical equilibria, the third thermodynamic requirement for phase equilibrium is chemical equilibrium, expressed as [50]

$$\mu_i^{phase1}(T,P,\bar{x}) = \mu_i^{phase2}(T,P,\bar{y}) \tag{3.9}$$

where μ_i is the chemical potential of each component *i*, defined as [77]:

$$\mu_i = \left(\frac{\partial U}{\partial n_i}\right)_{S,V,n_{j\neq i}} = \left(\frac{\partial H}{\partial n_i}\right)_{S,\mathrm{P},n_{j\neq i}} = \left(\frac{\partial G}{\partial n_i}\right)_{\mathrm{P,T},n_{j\neq i}} = \left(\frac{\partial A}{\partial n_i}\right)_{\mathrm{T},V,n_{j\neq i}} \tag{3.10}$$

where, *U* is the internal energy, *S* the entropy, *V* the volume, *n* the number of moles of each component, *H* the enthalpy, *G* the Gibbs free energy and A the Helmholtz free energy.

The maximum possible number of coexisting phase in equilibrium with no chemical reaction is defined by the Gibbs phase rule [78]:

$$F = 2 + N_C - N_P \tag{3.11}$$

where N_C is the number of components, N_P is the number of phase and F is the degree of freedom, *i.e.* the number of independent intensive variables in the system.

According to the Gibbs phase rule, in a single-component system (N_C=1), the maximum number of coexisting phases (F=0) is three (N_P=3). If the different phases of a single-component are represented through a pressure-temperature diagram, as F=0 none of intensive variable can be independent. Therefore, the result is a point in the P-T diagram (triple point). The other characteristic lines in the P-T phase diagram are the Solid-Liquid (SLE), Solid-Vapour (SVE) and Vapour-Liquid (VLE) equilibria, which are the equilibrium curves of Figures 3.4. SLE, SVE and VLE represent two phases (N_P=2) in equilibrium with one degree of freedom (F=1), which means that one of the intensive variables is independent.

Knowledge of phase equilibria is fundamental in chemical and petroleum engineering and the main tool to predict the phase diagrams and thermodynamic properties are the equations of state (EoS). EoSs have become indispensable for the correlation and prediction of vapour-liquid equilibria [79]. In the following sections, the evolution and the features of the equations of state are presented.

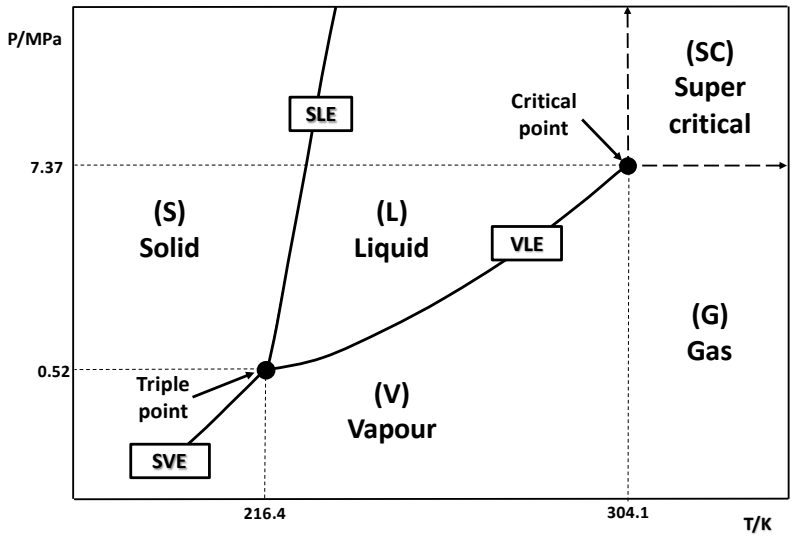

Figure 3.4. P-T simplified phase diagram of CO_2 [80]**.**

3.3 Equations of state

An Equation of State (EoS) is an analytical expression describing the state of matter and relating pressure (P), temperature (T) and molar volume (V). The result of this equation is a proper description of the PVT relationship, leading to the EoSs estimate the thermodynamics properties of gases and liquids necessary for the study of phase equilibria of fluids and mixtures of fluids. Countless equations of state have been proposed in the literature. Among all of these EoSs proposed by different authors, just a few are based on a fundamental theories, and most of EoS are based on empirical or semi-empirical basis, as a result of the mathematical processing of experimental data [81]. Next, the EoS evolution from the Ideal Gas to recently advanced EoSs will be described.

3.3.1 Evolution of EoSs

In 1834, Boyle's and Charles' laws were combined by Clapeyron [82] into the origin of the Ideal Gas (IG) law. Although, initially the IG law was not formulated in this way, nowadays the equation of ideal gases is expressed in molar units as:

$$Pv = RT \tag{3.12}$$

where v is the molar volume and R is the ideal gas constant in the same units of the PVT properties. The Helmholtz free energy of a mixture of ideal gas is given by [83]:

$$\frac{A^{IDEAL}}{Nk_BT} = \left(\sum_{i=1}^{n} x_i \ln \rho_i \Lambda_i^3 \right) - 1 \tag{3.13}$$

where N is the number of molecules, k_b the Boltzmann constant, $x_i=N_i/N$ the mole fraction, $\rho_i = N_i/V$ the molecular number density and Λ_i is the thermal de Broglie wavelength of species i which is given for spherical molecules by:

$$\Lambda = \frac{h}{\sqrt{2\pi m k_B T}} \tag{3.14}$$

where h is the Planck constant and m the mass of the particle.

Next milestone in the history of the EoSs is the van der Waals (vdW) equation of state (1873) which is the first cubic equation of state (CEoS) [84]. Although the vdW equation of state was the first EoS that considered a pairwise attractive inter-molecular force, there has not been any significant improvement of CEoS until Redlich and Kwong revised the van der Waals EoS in 1949 [85]. Carnahan and Starling developed an EoS for hard sphere fluids in 1969 [86] and later presented a reformulation of the vdW EoS using their hard-sphere term [87]. In the 1970's, Soave proposed a modification known as Soave-Redlich-Kwong (SRK) EoS [88] which allowed better descriptions of pure component vapour pressure, while later Peng and Robinson (PR) [89] developed a new EoS based on the semi-empirical vdW equation that improved the poor saturated liquid density description of the SRK EoS for hydrocarbons [90]. These two equations combined simplicity and reasonable accuracy, and gave accurate results for mixture of non-polar fluids; for this reason the SRK and PR EoSs had rapidly gained acceptance by the hydrocarbon industry.

The cubic EoSs are expressed as the sum of two terms, first the repulsion pressure, which is the same for both EoS, and second the attraction pressure. Then, the SRK and PR EoSs can be expressed as

$$SRK: \quad P = \frac{RT}{v-b} - \frac{a\alpha(T)}{v(v-b)} \tag{3.15}$$

$$PR: \quad P = \frac{RT}{v-b} - \frac{a\alpha(T)}{v^2+2bv-b^2} \tag{3.16}$$

where R is the ideal gas constant, P the pressure, v the molar volume and T the temperature. $\alpha(T)$ is a function of temperature, acentric factor and critical temperature (T_c) and pressure (P_c). a and b are the adjustable parameters of the CEoS calculated using the T_c and P_c of each component.

CEoS are probably the most-widely employed EoSs for engineering applications [91] and, because of this, many modifications have been proposed. Thus, for the purpose of improving the cubic EoSs, different functional terms or additional parameters were proposed, *e.g.* the Peneloux volume translation [92] which provides better liquid densities calculations [93]. However, despite the success of cubic EoSs, the accuracy of these equations decreases when predicting the behaviour of substances that form strong

associations between molecules, such as hydrogen bonding (Figure 3.5), as classical EoSs were developed by considering only the dispersion-attractive forces [94].

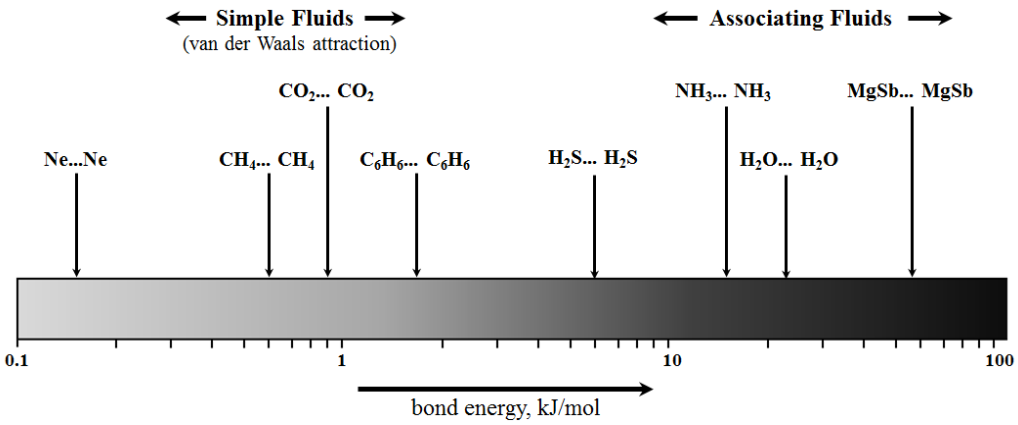

Figure 3.5. Continuous distribution of bond strengths [95].

Therefore, in order to improve the CEoS for associative fluids, it was necessary to add some contributions to the perturbation expansion of the free energy according to the thermodynamic perturbation theory (TPT) of Wertheim [96]–[99]. Hence, by combining the simplicity of a cubic equation of state (SRK) and the TPT employed for the association part, the Cubic Plus Association EoS (CPA) [100] was developed. Also by applying Wertheim's TPT and extending it to mixtures, Chapman et al. [101] derived the Statistical Associating Fluid Theory (SAFT) equation of state. Many modifications of the SAFT-based EoSs were suggested over the years, such as CK-SAFT [102], Lennard-Jones SAFT (LJ-SAFT) [103], variable range potential SAFT (SAFT-VR) [104], soft-SAFT [105] and perturbed-chain SAFT (PC-SAFT) [69,106]. According to perturbation theories, the idea behind the statistical theory is to split the Helmholtz free energy in several contributions. Each SAFT version is different depending on the approach used to calculate the contributions (hard sphere, chain, association, etc.) and the interaction pair potential between the segments (square-well, Lennard-Jones, Mie, etc.).

Leaving aside the SAFT EoS, in the last 25 years, as a result of advances in thermodynamic statistical mechanics and computer power, another EoS based on perturbation theories have been developed. Among these equations are the Perturbed Hard Chain Theory (PHCT) [107,108] and its derivatives the Perturbed Soft Chain Theory (PSCT) [109,110], the Perturbed Anisotropic Chain Theory (PACT) [111,112] and the Associated Perturbed Anisotropic Chain Theory (APACT) [113,114].

3.3.2 SAFT Equations of State

The Statistical Associating Fluid Theory (SAFT) EoS is based on Wertheim's thermodynamic perturbation theory (TPT) [96]–[99]. The SAFT-EoS was proposed by Chapman et al. [101], [115], [116] and by Huang and Radosz [102], [117], being often referred to as original SAFT EoS and they converted it in a very useful engineering equation.

The SAFT-EoS was developed by considering the fluid as monomers which form chains and have association sites. Due to this consideration, size asymmetries (*i.e.* non-sphericity of molecules) and interactive anisotropies (*e.g.* hydrogen bonding) are analysed by the chain and association contribution respectively, whereas cubic EoSs consider spherical molecules dominated by van der Waals forces. The general equation for the SAFT EoS can be expressed in terms of the Helmholtz free energy, as a sum of different contributions:

$$\frac{A^{TOTAL}}{Nk_bT} = \frac{A^{IDEAL}}{Nk_bT} + \frac{A^{SEGMENT}}{Nk_bT} + \frac{A^{CHAIN}}{Nk_bT} + \frac{A^{ASSOCIATION}}{Nk_bT} \tag{3.17}$$

A schematic representation of the contributions generally taken in account in the SAFT EoSs is depicted in Figure 3.6. Firstly, the ideal contribution considers the fluid as ideal gas of punctual non-interacting particles and is given in Equation 3.13. Then, the Segment contribution is often composed of a hard-sphere contribution and a dispersion contribution, which describe the interaction between the spherical segments that form the fluid. Thanks to the chain contribution, the asymmetry of the molecules is taken into account by representing as chains of spherical segments. Finally, the association contribution takes into account the hydrogen bonds, regarded as a short-ranged, directional, and strongly attractive interaction between molecules in polar fluids [118].

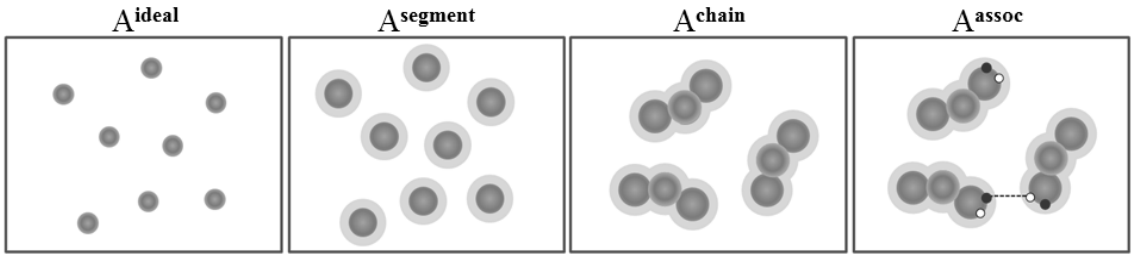

Figure 3.6. Schematic representation of the physical basis of the SAFT [68]**.**

Nowadays, there are many different embodiments of the generic SAFT approach, differing mainly in the interaction potential used to model the reference fluid [72], because different monomeric fluids are considered and diverse simplifications are proposed. Due to this, monomer contribution is generally the only one that shows big differences amongst the SAFT versions, so that, it can be said that the contributions of the chain and the association terms are quite similar among the SAFT versions.

In the SAFT equations of state, the molecules of non-polar pure components are generally characterized by three parameters: the number of segments *m*, a size parameter σ (*i.e.* diameter of segment) and an energy parameter ε (*i.e.* depth of pair potential). Furthermore, if the molecules of the fluid are associative compounds, there are two more parameters which characterise the geometry (K^{AB}) and the energy (ε^{AB}) of the association.

As almost all the SAFT variants use the same chain and association terms [119], these contributions are presented next. On the one hand, the association term in the SAFT-like EoSs is derived from Wertheim's first-order TPT [96]–[99]. The association contribution extended to multicomponent mixtures is given by the equation:

$$\frac{A^{ASSOCIATION}}{Nk_BT} = \sum_i^n x_i \left[\sum_{A=1}^{s} (\ln X^{A_i} - \frac{X^{A_i}}{2}) + \frac{s}{2} \right] \tag{3.18}$$

where *s* is the number of sites of type *A* on the molecule of species *i*, and X^A is the fraction of molecules not bonded at site *A*, defined as:

$$X^{A_i} = \frac{1}{1 + \sum_j^n x_j \sum_{B=1}^{s} \rho X^{B_j} \Delta^{A_i B_j}} \tag{3.19}$$

where ρ is the molecular density and Δ^{AB} is the association strength between sites *A* and *B*. This last parameter depends on the geometry and the energy of the associative sites. The expression of the association strength Δ^{AB} calculation may vary depending on the version of SAFT equations of state.

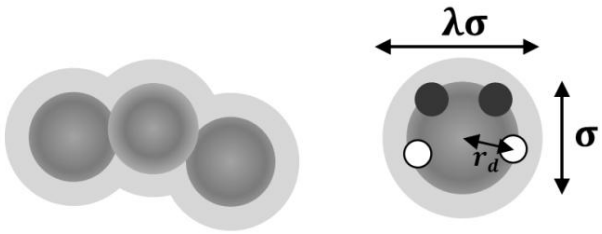

Figure 3.7. Two examples of molecular models in the SAFT representation: a molecule formed by a three segment chain (m=3) and a spherical molecule (m=1) with 4 associative sites (*e.g.* water), where r_d is the distance between centre of a site and the centre of the segment; and $\lambda\sigma$ is the width of the interaction potential ($u(\lambda\sigma)=0$) [120]**.**

On the other hand, the chain term in the SAFT-EoSs is derived from the associating fluid theory which states that association bonds are replaced by covalent (chain forming) bonds [121]. Hence, the chain contribution is obtained by considering that there is a complete bounding between the spherical segments which form the chain, and consequently it is calculated as the limit of the fraction of non-bonded particles when it approaches to zero. After some mathematical development, the chain contribution is given by the equation:

$$\frac{A^{CHAIN}}{Nk_BT} = \sum_i^n x_i(1-m_i)\ln(g_{ii}(d_{ii})^{HS}) \tag{3.20}$$

where g_{ii} is the radial distribution function (RDF) for the interaction of two hard spheres i, which is a function of the temperature-dependent diameter d. This expression of g_{ii} depends on the specific SAFT version developed.

The radial distribution function (RDF) plays a very important role in molecular thermodynamics. The RDF $g(r)$ is the probability of one particle to find another particle at the distance r [122]. The RDF is related to the local density, $\rho g(r)$ [123]. It is also related to the pair potential: at a shorter distance than the core diameter, the RDF has to be zero, due to the very high repulsive forces. Similarly, the probability of finding another particle is the highest at the distance where the attractive forces are stronger. Generally, the limit of the RDF when the distance tends to infinite approaches to one [124], in order to match the local density with the macroscopic density. To illustrate this, the RDF and LJ potential of argon are plotted in Figure 3.8.

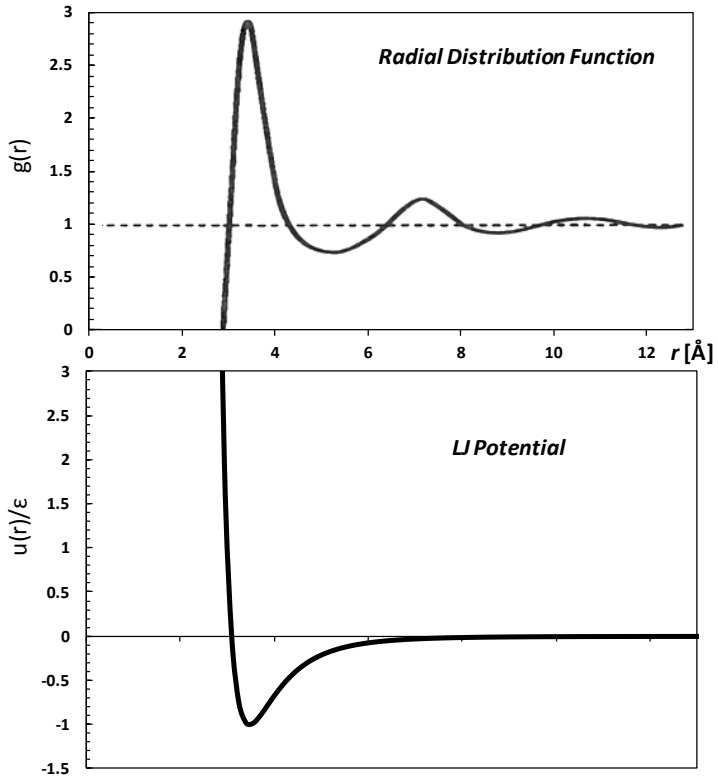

Figure 3.8. The upper plot is a smooth curve drawn from the RDF of Argon at 133K and 1,11 g/cm3 [124] **and the lower plot is the Lennard-Jones potential calculated for the same molecule.**

Table 3.1. References of some of the most well-known SAFT versions (from Thermodynamic models for industrial applications) [119]

SAFT variant	Reference	Comments
Original SAFT	Chapman *et al.* [101], [121]	Mostly comparisons against simulation data. Parameters for six hydrocarbons and two associating fluids are given.
CK-SAFT	Huang and Radosz [102], [117]	Parameters for 100 different fluids.
Simplified SAFT	Fu and Sandler [118]	Parameters for ten non-associating and eight associative compounds.
LJ-SAFT	Kraska and Gubbins [125], [103]	Alkanes, alkanols, water (pure components). Mixtures of alkanes, alkanols, water.
SAFT-VR	Gil-Villegas *et al.* [104] McCabe *et al.* [126]	Alkanes, perfluoroalkanes (pure components). Comparisons against simulation data.
Soft SAFT	Blas and Vega [105]	Parameters for six alkanes and five alkanols.
PC-SAFT	Gross and Sadowski [69]	The Gross and Sadowski article contains parameters for 100 compounds.
Simplified PC-SAFT	Von Solms *et al.* [127] Tihic *et al.* [128]	Tihic *et al.* article contains parameters 100 compounds..

In 1989, Chapman and co-workers developed the first SAFT equation of state. In the following 25 years, several versions of SAFT have been developed: the original SAFT, Huang-Radosz (CK) SAFT, simplified SAFT, SAFT-LJ (Lennard-Jones), SAFT-HS (Hard Sphere), SAFT-VR (Variable Range), Soft SAFT, PC-SAFT (Perturbed Chain) and simplified PC-SAFT EoSs. These are the well-known SAFT variants and more information about them is detailed in the Table 3.1.

3.3.2.1 Perturbed Chain - SAFT EoS

The PC-SAFT EoS [69], [106] is a modified SAFT equation of state developed by applying the perturbation theory of Barker and Henderson (BH) [129], [130] to a hard-chain reference fluid. This equation of state is based on a molecular model which assumes non-spherical molecules to be chains of freely jointed spherical segments. The perturbed hard-chain theory (PCHT) developed by Prausnitz [107], [108] was the first EoS based on this molecular model and it revealed its potential for future works.

Within the framework of BH's perturbation theory, taking into account the modified square-well pair potential suggested by Chen and Kreglewski [71] presented in section 3.1, a reference fluid can be used to describe the repulsion in two ways, first with a hard repulsion (hard-sphere) and with a soft repulsion with a temperature-dependent segment diameter. After integrating the modified square-well, this effective collision diameter is given by [69]:

$$d_i(T) = \sigma_i \left[1 - 0.12 \exp\left(-\frac{3\varepsilon_i}{k_b T} \right) \right] \tag{3.21}$$

The PC-SAFT EoS is expressed in terms of the Helmholtz free energy as

$$\frac{A^{RESIDUAL}}{Nk_bT} = \frac{A^{HARD-CHAIN}}{Nk_bT} + \frac{A^{DISPERSION}}{Nk_bT} + \frac{A^{ASSOCIATION}}{Nk_bT} \tag{3.22}$$

where $A^{RESIDUAL}$ is the difference between the Total and the Ideal contributions of Helmholtz free energy. It is worth highlighting that in the equation above, the hard-chain reference contribution is calculated as the sum of hard-sphere (HS) and chain contributions. As mentioned in previous subsection, the Chain and Association contributions are defined identically to the *original* SAFT EoS. For calculating the hard-

sphere contribution in terms of Helmholtz free energy and the average radial distribution function of the HS fluid, the equations used are based on the expressions of Boublik [131] and Mansoori *et al.* [132].

Special attention is given to the interaction between hard-chains by the dispersion contribution. To this end, the perturbation theory of Barker and Henderson is used to calculate the attractive part of the chain interactions, where the Helmholtz free energy is given as a sum of first and second order contributions. These equations were developed based on the expression of the site pair distribution function of hard chains given by Chiew [133].

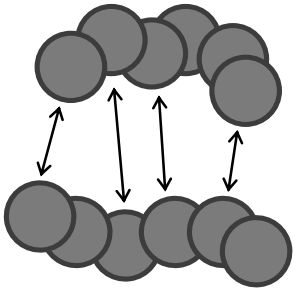

Figure 3.9. The Attractive interactions between the connected segments in the PC-SAFT EoS [134]**.**

For solving the integrals which get involved in the mathematical development of A^{disp}, the universal parameters necessary to calculate the equations proposed by Liu and Hu [135] were determined by assuming first a Lennard-Jones potential to the hard chains and regressed subsequently to experimental pure-component data. Gross and Sadowski proposed the series of n-alkanes, as the most fitted molecules to a chainlike shape, for adjusting the universal model constantans for the dispersion contribution.

3.3.2.2 Variable Range SAFT EoSs

Gil-Villegas *et al.* [104] developed a version of the statistical associating fluid theory for chain molecules of hard-core monomers with attractive potentials of variable range (SAFT-VR). When evaluating the different contributions to the Helmholtz free energy according to the Wertheim's TPT, where the concept of segment is replaced by the concept of monomer, the general form of the SAFT-VR EoSs can be written as:

$$\frac{A^{RESIDUAL}}{Nk_bT} = \frac{A^{MONO}}{Nk_bT} + \frac{A^{CHAIN}}{Nk_bT} + \frac{A^{ASSOCIATION}}{Nk_bT} \tag{3.23}$$

where, as was discussed above, the equations to calculate the contribution due to chain and association interactions are the same as the *original* SAFT. The A^{MONO} is the contribution energy due to the monomer interactions [104] and it is given by:

$$\frac{A^{MONO}}{Nk_bT} = \left(\sum_i^N x_i m_i\right)\frac{A^M}{N_s k_b T} = \left(\sum_i^N x_i m_i\right) a^M \tag{3.24}$$

with,

$$a^M = a^{HS} + \beta a_1 + \beta^2 a_2 \tag{3.25}$$

where m_i is the number of spherical segments of chain i, N_s is the total number of spherical monomers and β is the inverse of the temperature ($\beta = 1/k_bT$). As it can be seen in the equations, the monomer Helmholtz free energy is developed as a series expansion in β, according to the perturbation theory of Barker and Henderson [77,78]. The BH theory is based on the high-temperature expansion (HTE) approach of Zwanzig [136] and considers a hard-sphere system as a reference fluid, while the attractive term acts as a perturbation. Accordingly, $a^{HS}=A^{HS}/(N_s k_b T)$ is obtained from the of Boublik [131] and Mansoori *et al.* [132] equation, a_1 correspond to the average of the monomer-monomer potential energy calculated with the hard-sphere structure at first order in expansion and the second order term a_2 describes the fluctuation of the attractive energy as a consequence of the compression of the fluid due to the action of the attractive well [104]. Therefore, all the calculation necessary of a^M depend on the interactions between monomers, defined by the intermolecular potentials.

In the Section 3.1, the most common intermolecular pair potentials were introduced and the SAFT-VR EoSs are based on those potentials. The fundamental concept was to take into account the differences in the range of the interactions between monomers. Different modifications and extensions of SAFT variable range have been proposed, since the first SAFT-VR EoS developed by Gil-Villegas *et al.* [104] developed, until the last variant of Lafitte *et al.* [72], the SAFT-VR Mie EoS.

In the first variable range version, analytical expressions of the a_1 and a_2 for square-well fluids, Sutherland fluids and Yukawa fluids were developed. Following, a further extension of the SAFT-VR EoS was developed to account for chain molecules which are formed from soft-core monomers with variable repulsive and attractive ranges [137]. Basically it was focused on providing a simple compact equation of state for Lennard

and Jones core (LJC), using a specific case (m=6 and n=12) of the Mie m-n family of potentials [138]. Later, Patel *et al.* [139] and Dos Ramos *et al.* [120] extended SAFT-VR Square-Well to both short-range ($1.1 \leq \lambda \leq 1.8$) and long-range ($1.2 \leq \lambda \leq 3.0$). In 2006, to extend further the predictive capabilities of the SAFT-VR treatment for the more-general case of Mie potentials, a description of the free energy and structure via the radial distribution function (RDF) at contact of the monomer Mie reference fluid was then proposed [74], and this version is known as SAFT-VR Mie 2006 [72] to avoid confusing this EoS with SAFT-VR Mie described below. To conclude this short SAFT-VR review, Lafitte *et al.* [72] presented a highly accurate equation of state (EoS) for chain molecules formed from spherical segments interacting through Mie potentials. Essentially, the difference between the SAFT-VR Mie 2006 and this last SAFT-VR Mie is the possibility to adjust one additional parameter (the attractive range, λ_a) and the application of the Barker and Henderson [129], [130] perturbation expansion up to third order, which leads to a better description of critical points.

Table 3.2. Summary of the SAFT-VR versions

SAFT-VR variant	Potential [*u(r)*]	Parameters	Monomer Contribution (A^{MONO})
SAFT-VR [104] (1997)	Square-Well (short-range)	• m, σ, ε • λ: range of interaction ($1.1 \leq \lambda \leq 1.8$)	
SAFT-VR SW [139] (2005)	Square-Well (large-range)	• m, σ, ε • λ: range of interaction ($1.1 \leq \lambda \leq 3.0$)	• BH high-temperature perturbation expansion of second order.
SAFT-VR Mie [74] (2006)	Mie potential (m-n)	• m_s, σ, ε • λ: range of repulsion	
SAFT-VR Mie [72] (2013)	Mie potential (λ_r - λ_a)	• m, σ, ε • λ_r: range of repulsion • λ_a: range of attraction	• BH high-temperature perturbation expansion of third order.

Leaving aside the intermolecular potential, the SW and the Mie versions of the SAFT-VR EoS obtain the monomer contribution through a BH high-temperature perturbation expansion, but the former as a second order expression and the latter as a third order expression, being the third-order term treated empirically. Furthermore, the SAFT-VR SW EoS uses a linear expansion to first order to calculate the radial distance function (RDF) of the monomeric fluid, whereas the SAFT-VR Mie EoS develops an expansion

in exponential form to the second order to represent the RDF. A much better description of the RDF at contact is given with this second-order expansion; therefore, a more accurate chain term is obtained, resulting in a better description of non-spherical molecules.

3.3.2.3 Group Contribution Methods

An important aspect in the development of thermodynamic methodologies is the predictive capability, which is commonly perceived as the ability to provide predictions of phase behaviour and other properties without the need for experimental data for the determination of molecular model parameters [140]. The Group Contribution (GC) approaches are included between the thermodynamic methodologies with high predictive power. GC methods are developed based on the assumption that the properties of a given compound can be determined through the chemically distinct functional groups which form that compound [141]. These estimation methods work well for the classes of mixtures for which the parameters have been developed and are extremely popular in the chemical industry due to their simplicity and ease of use [140]. Basically, the main applications of GC could be divided in:

- Prediction of pure component properties: GC methods based on correlations of experimental critical properties, acentric factor, etc. For example, Lydersen developed one of the first successful GC methods for estimating critical properties [142].
- Calculation of activity coefficients: all the versions of UNIFAC and the ASOG method are the most successful GC approach to calculate the activity coefficient in the liquid phase of multicomponent mixtures [143].
- Treatment the liquid and vapour phase in EoS: most equations of state require component-specific and/or mixture parameters which can be estimated through a GC approach based on contributions of functional groups (Figure 3.10), as *e.g.* the PSRK EoS [144], Jaubert's PPR78 EoS [145], the chain-of-rotators GC EoS [146], GC-PR-CPA [147] and the GC approaches of SAFT-based EoSs [148]–[155].

UNIFAC and its modifications are widely used and it is considered one of the best illustrations of GC methods. However, UNIFAC can show higher deviations in certain temperature and pressure ranges and also inconsistencies in the description of the critical region [156], depending on the utilization and the mixing rules and the EoS

used. Besides, the use of activity coefficient methods is limited to the calculation of other properties (such as densities, heat capacities, etc.). In contrast, EoS approach has no limits in their range of application, because EoSs can treat liquid and vapour phases and can be used to estimate other thermophysical properties through thermodynamic relations.

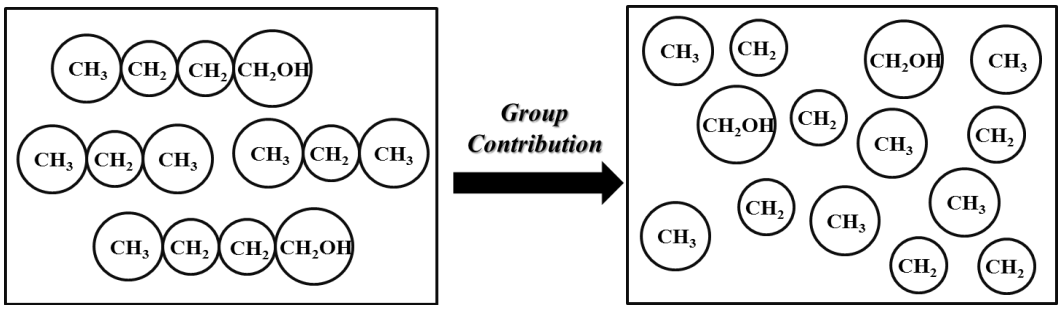

Figure 3.10. The Attractive Representation GC approach of binary system 1-butanol + n-propane [157]**, from molecules to functional groups.**

On the other hand, modern equations of state are generally less predictive due to the need for adjusted parameters to every compound for their successful application and EoSs can also require combining rules and adjustable mixture parameters. Hence, EoSs can be combined with group contribution approaches in an effort to use equations of state in a more predictive way.

Therefore, group contribution approaches have also been developed within the framework of SAFT incorporating heteronuclear molecular models (Figure 3.11) which represent molecules as chains of segments [148]. Consequently, from the point of view of Wertheim's TPT, it is possible to develop an equation of state maintaining a link between the nature of the different segments making up the molecules and the corresponding parameters. Numerous SAFT versions have been reformulated based on a heteronuclear tangent molecular model according to a GC approach (Table 3.3).

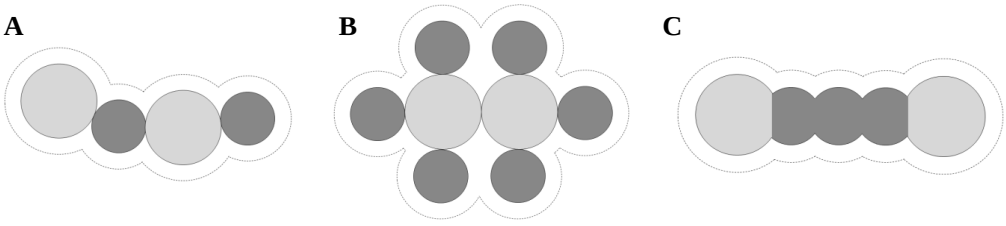

Figure 3.11. Heteronuclear models within the framework of SAFT-VR:
(A) United-atom tangent model; (B) all-atom tangent model; and (C) united-atom *fused* model.

According to all the aspects about the SAFT-like EoSs and the group contribution methodology described previously, a GC approach applied to the SAFT-VR Mie EoS has been developed. This generalization (SAFT-γ Mie) proposed by Papaioannou, is a group contribution based on a fused heteronuclear molecular model (represented by C in Figure 3.11), where the attractive-repulsive interaction are described by variable range Mie potential [141]. [158]

Table 3.3. Summary of published works of several SAFT + Group Contribution approach EoSs (from *Thermodynamic models for industrial applications*) [119]

SAFT variant	Reference	Application
Original SAFT **SAFT-VR**	Tamouza *et al.* [148], [149]	Alkanes, aromatics, olefins, alcohols.
Original SAFT **SAFT-VR** **PC-SAFT**	Thi *et al.* [150]	Alkanes, esters.
SAFT **PC-SAFT**	Emami *et al.* [151]	General.
PC-SAFT **SAFT-VR**	Le Thi *et al.* [152]	H_2, CO_2 + Alkanes (including a GC method for the k_{ij}).
Original SAFT **SAFT-VR** **PC-SAFT**	Huynh *et al.* [153]	Polycyclic aromatic hydrocarbons.
SAFT-VR	Tihic *et al.* [154]	General (non-associative compounds).
SAFT-VR SW	Lymperiadis *et al.* [155]	Hydrocarbons, alcohols.
SAFT-VR Mie	Papaioannou *et al.* [141]	n-Alkanes, n-Alkyl esters.

CHAPTER 4: MODELLING PHASE AND VOLUMETRIC BEHAVIOURS

This chapter is focused on modelling the phase and volumetric behaviours of binary mixtures. It is organized in three parts. The first section presents the main features, expressions and molecular parameters of the SAFT-VR Mie EoS. A comparison between this novel SAFT-VR Mie EoS and other common models (PR, SRK and PC-SAFT EoSs) in the evaluation of thermodynamic properties is presented in the second section. This quantitative comparison has been made with respect to experimental density and phase equilibrium data of 108 binary mixtures of five main gaseous compounds (CO_2, CH_4, C_2H_6, N_2 and H_2S). In the third part of this chapter, a group contribution approach, the SAFT-γ Mie EoS, is presented as development of the SAFT-VR Mie EoS aiming at increasing its predictive aspect.

4.1 SAFT-VR Mie

The SAFT-VR Mie EoS is one of the latest updates of the SAFT variable range family of equations of state. As a consequence, at the moment only few works presenting applications and results involving this EoS have been published. According to Lafitte *et al.* [72], validity and accuracy of the EoS have been assessed with Monte Carlo simulation and compared against experimental data of pure components and two binary mixtures (CO_2+*n*-decane and ethane+*n*-decane). In the following subsections, the modelling approach, description of the EoS and Mie molecular parameters are detailed.

4.1.1 Modelling aspects and approaches

In section 3.2, phase equilibrium has been defined as the simultaneous thermal ($T^{phase1} = T^{phase2}$), mechanical ($P^{phase1} = P^{phase2}$) and chemical equilibria ($\mu^{phase1} = \mu^{phase2}$). This work is focused on the representation of vapour-liquid equilibria (VLE), and a symmetric approach has been adopted for solving the phase equilibrium condition, which means that the chemical potentials have been evaluated in terms of fugacity coefficients for both vapour and liquid phases. Fugacity characterizes the escaping tendency of a component from one phase to the other and is a common property used

for evaluating the deviation from the ideal behaviour. The thermodynamic equilibrium is reached when, at constant temperature and pressure, same amount of molecules passes from the liquid phase to the vapour phase and vice-versa. The mathematical equation which represents this condition of equilibrium in a multicomponent system is the equality of the partial molar fugacities at the system pressure and temperature, namely [77]:

$$f_i^{Liq}(P,T,\bar{x}) = f_i^{Vap}(P,T,\bar{y}) \tag{4.1}$$

where *Liq* is the liquid phase index, *Vap* the vapour phase index, *i* the compound index, $\overline{x}$ the vector of compositions of the liquid phase and $\overline{y}$ the vector of compositions of the vapour phase.

According to the phi-phi (φ-φ) approach for the vapour and liquid phases, the equilibrium is rewritten in the following form:

$$P\,x_i\varphi_i^{Liq}(P,T,\bar{x}) = P\,y_i\varphi_i^{Vap}(P,T,\bar{y}) \tag{4.2}$$

where φ_i is the partial molar fugacity coefficient, strictly related to the residual chemical potential:

$$\ln(\phi_i) = \frac{\mu_i^{RES}}{kT} - \ln Z \tag{4.3}$$

At this point, an equation of state is required to calculate the residual chemical potential (μ_i^{res}) and the compressibility factor (Z). According to the SAFT approach, both Z and μ_i^{res} are calculated from first-order partial derivatives of the Helmholtz free energy.

Firstly, within the framework of the SAFT-VR Mie EoS, the compressibility factor is calculated by re-arranging the equation $PV=ZnRT$.

$$Z = \frac{P}{\rho kT} \tag{4.4}$$

where P is calculated by means of Eq. 4.5. This equation defines the pressure as a first-order partial derivative of the Helmholtz free energy with respect to the volume. However, using a variable change, the pressure is calculated by deriving with respect to the density [72].

$$P = -\left(\frac{\partial A}{\partial V}\right)_{N,T} = \left(\frac{\partial A}{\partial \rho_s}\right)_{N,T}\left(\frac{\partial \rho_s}{\partial V}\right) \tag{4.5}$$

where ρ_s is the total number density of spherical segments, which is related to the density of the mixture ρ through:

$$\rho_s = \rho \sum_i^n x_i m_i \tag{4.6}$$

where m_i is the number of spherical segments forming the molecules of compound *i*.

At a given temperature, pressure is function of density and compressibility factor which is also function of the density. Therefore, an iterative process (Newton-Raphson method) is necessary to estimate the density and *Z* at the system conditions (*P*-*T*). A modification of the algorithm developed by Michelsen [159] has been used.

The iterative process to calculate the density is presented in Figure 4.1. η is the packing fraction, also defined as the reduced density. The density at a given system pressure (P^{sys}), along with the T and the molar fractions (x_i), must be iteratively determined by adjusting the reduced density η until $P^{calc}=P^{sys}$. In order to converge to a right solution, the suitable starting values of the reduced density for a liquid and a vapour phases are respectively η=0.5 and η=10^{-10} [69]. It is worth mentioning that the values of η>0.7405 [=$\pi/(3\sqrt{2})$] are higher than the closest packing of segments, thereby having no physical relevance. The starting value chosen for η depends whether a liquid or vapour phase density is required, and this choice is indicated in the first step of the flowchart [160].

Secondly, once the density has been estimated, the residual chemical potential (μ_i^{res}) is calculated as the partial derivative of Helmholtz free energy with respect to the moles of each compound in the mixture (n_i), as described in the following equation:

$$\frac{\mu_i^{RES}}{kT} = a^{RES} + n_i\left(\frac{\partial a^{RES}}{\partial n_i}\right)_{T,\mathrm{v},n_{k\neq i}} \tag{4.7}$$

where a^{RES} is the reduced residual Helmholtz free energy.

A certain number of partial derivatives of thermodynamic properties are needed for developing an algorithm for the phase equilibrium calculation involving the equations related to a model such as the SAFT-VR Mie EoS. Analytical derivatives of all the density and composition dependent variables within the EoS have been obtained and

implemented in the algorithm since numerical derivatives demonstrated to lead to wrong calculations in Newton-Raphson iterative processes. All the equations necessary to calculate the a^{RES} contribution for the SAFT-VR Mie EoS are presented in the following subsection.

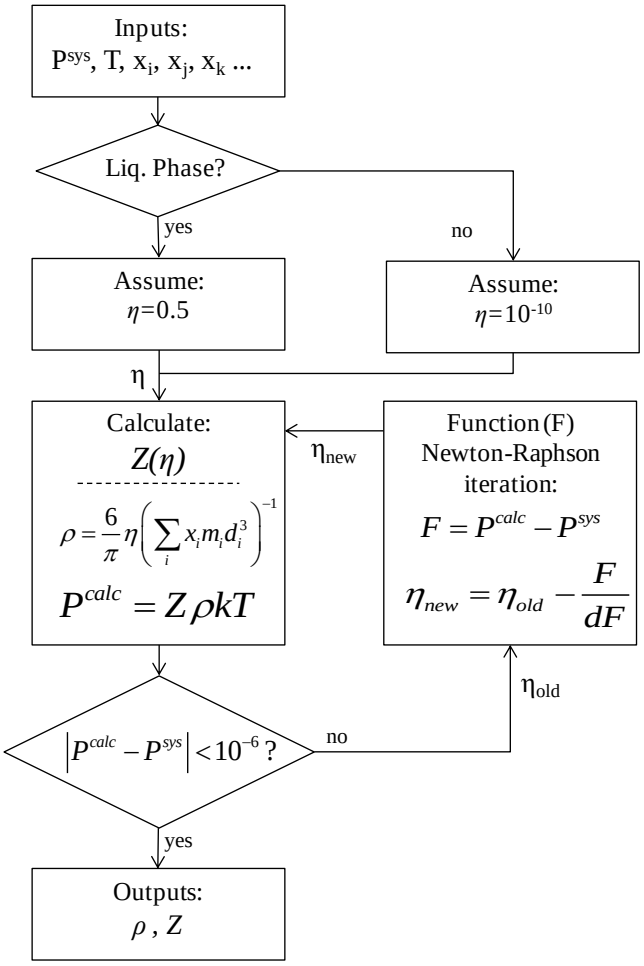

Figure 4.1. Flow chart of iterative process to calculate the density (ρ).

4.1.2 Description and formulation

The SAFT-VR Mie EoS is expressed in terms of the reduced Helmholtz free energy as the sum of several contributions:

$$a = \frac{A}{Nk_bT} = a^{IDEAL} + a^{RESIDUAL} = a^{IDEAL} + a^{MONO} + a^{CHAIN} + a^{ASSOC} \tag{4.8}$$

where A is the Helmholtz energy, a the reduced Helmholtz energy and superscripts define the different contributions.

The Ideal contribution has been presented in Chapter 3 (Eq. 3.13) and is not taken into account on the phase behaviour calculations. However the contribution of the ideal-gas Helmholtz free energy is reconsidered in Chapter 5 for interfacial tension calculations. With respect to the remaining terms in Eq. 4.8, the association contribution has been neglected, seeing that only non-associative compounds have been considered in this work.

4.1.2.1 Monomer Contribution

The interaction between the monomers are defined by the Mie potential (see section 3.1) as follows [72,75,90]:

$$u_{ij}^{Mie} = C_{ij}\varepsilon_{ij}\left(\left(\frac{\sigma_{ij}}{r_{ij}}\right)^{\lambda_{r,ij}} - \left(\frac{\sigma_{ij}}{r_{ij}}\right)^{\lambda_{a,ij}}\right) \tag{4.9}$$

where,

$$C_{ij} = \frac{\lambda_{r,ij}}{\lambda_{r,ij} - \lambda_{a,ij}}\left(\frac{\lambda_{r,ij}}{\lambda_{a,ij}}\right)^{\frac{\lambda_{a,ij}}{\lambda_{r,ij} - \lambda_{a,ij}}} \tag{4.10}$$

The "mono" contribution is the Helmholtz free energy for the reference monomeric fluid and can be expressed as:

$$a^{MONO} = \left(\sum_{i=1}^{n} x_i m_i\right) a^{M} \tag{4.11}$$

where a^M is the corresponding energy per monomer [72] expressed as a third order high-temperature expansion in the inverse of temperature ($\beta = 1/k_b T$):

$$a^{M} = a^{HS} + \beta a_1 + \beta^2 a_2 + \beta^3 a_3 \tag{4.12}$$

In Eq. 4.12, a^{HS} is the hard-sphere contribution and a_1, a_2 and a_3 are the first, second and third order perturbation terms respectively.

The hard-sphere term is given by the expression of Boublik [131] and Mansoori et al. [132] for multicomponent mixtures of hard-spheres:

$$a^{hs} = \frac{6}{\pi\rho_s}\left[\left(\frac{\zeta_2^{\,3}}{\zeta_3^{\,2}} - \zeta_0\right)\ln\left(1-\zeta_3\right) + \frac{3\zeta_1\zeta_2}{\left(1-\zeta_3\right)} + \frac{\zeta_2^{\,3}}{\zeta_3\left(1-\zeta_3\right)^2}\right] \tag{4.13}$$

where ξ_1 , ξ_2 and ξ_3 are the moments of the number density and are defined as:

$$\zeta_l = \frac{\pi\rho_s}{6}\left(\sum_{i=1}^{n} x_{s,i} d_{ii}^{\,l}\right) \quad l \in \{0,1,2,3\} \tag{4.14}$$

where $x_{s,i}$ is the mole fraction of segments of component i:

$$x_{s,i} = \frac{m_i x_i}{\sum_{k=1}^{n} m_k x_k} \tag{4.15}$$

and d_{ii} is the effective for the segment of each component and is obtained from

$$d_{ii} = \int_0^{\sigma_{ii}} \left[1 - \exp\left(-\beta u_{ii}^{Mie}(r)\right)\right] dr \tag{4.16}$$

Table 4.1. Reduced abscissas and weights of the ten-point Gauss-Legendre quadrature [161,162]

x_i^{GL}	w_i^{GL}
0.97390653	0.06667134
0.86506337	0.14945135
0.67940957	0.21908636
0.43339539	0.26926672
0.14887434	0.29552422

To compute this integral, Paricaud [161] proposed the efficient Gauss-Legendre quadrature integration technique. Then, by applying the ten-point Gauss-Legendre quadrature [162], the diameter d is estimated as [161]:

$$\frac{d}{\sigma} \approx 1 - \left(\frac{1-x_\infty}{2}\right)\sum_{i=1}^{5} w_i^{GL}\left(\exp\left(-\frac{u^*(x_{1i})}{T^*}\right)\right) + \exp\left(-\frac{u^*(x_{2i})}{T^*}\right) \tag{4.17}$$

with

$$x_{1i} = 0.5\left(1 + x_\infty + x_i^{GL}(1-x_\infty)\right) \tag{4.18}$$

$$x_{2i} = 0.5\left(1 + x_\infty - x_i^{GL}(1-x_\infty)\right) \tag{4.19}$$

The constants w_i^{GL} and x_i^{GL} are given in Table 4.1. u^* is the reduced potential (u/ε), T^* the reduced temperature (k_bT/ε) an x_∞ the reduced distance below which the potential is considered as infinite. However, Mie potentials as well as LJ potential do not exhibit any unfeasible maximum [161], therefore the infinite reduced distance is x_∞=0.

Considering the thermal expansion of the monomer contribution, the first order mean-attractive is calculated by [72]:

$$a_1 = \sum_{i=1}^{n}\sum_{j=1}^{n} x_{s,i}x_{s,j}a_{1,ij} \tag{4.20}$$

where,

$$a_{1,ij} = C_{ij}\left[x_{0,ij}^{\lambda_{a,ij}}\left(a_{1,ij}^{S}\left(\rho_s;\lambda_{a,ij}\right)+B_{ij}\left(\rho_s;\lambda_{a,ij}\right)\right)-x_{0,ij}^{\lambda_{r,ij}}\left(a_{1,ij}^{S}\left(\rho_s;\lambda_{r,ij}\right)+B_{ij}\left(\rho_s;\lambda_{r,ij}\right)\right)\right] \tag{4.21}$$

with $x_{0,ij} = \sigma_{ij}/d_{ij}$ and where the following expressions are used to estimate B_{ij}:

$$B_{ij}\left(\rho_s;\lambda_{ij}\right) = 2\pi\rho_s d_{ij}^3\varepsilon_{ij}\left[\frac{1-\zeta_x/2}{\left(1-\zeta_x\right)^3}I_{\lambda,ij} - \frac{9\zeta_x(1+\zeta_x)}{2\left(1-\zeta_x\right)^3}J_{\lambda,ij}\right] \tag{4.22}$$

with,

$$\zeta_x = \frac{\pi\rho_s}{6}\left(\sum_{i=1}^{n}\sum_{j=1}^{n} x_{s,i}x_{s,j}d_{ij}^3\right) \tag{4.23}$$

and the values of I_λ and J_λ are obtained by

$$I_{\lambda,ij} = -\frac{x_{0,ij}^{3-\lambda_{ij}}-1}{\lambda_{ij}-3} \tag{4.24}$$

$$J_{\lambda,ij} = -\frac{\left(x_{0,ij}\right)^{4-\lambda_{ij}}\left(\lambda_{ij}-3\right)-\left(x_{0,ij}\right)^{3-\lambda_{ij}}\left(\lambda_{ij}-4\right)-1}{\left(\lambda_{ij}-3\right)\left(\lambda_{ij}-4\right)} \tag{4.25}$$

and the perturbation term a_1^S is calculated from

$$a_{1,ij}^{S}\left(\rho_s;\lambda_{ij}\right) = -2\rho_s\left(\frac{\pi\varepsilon_{ij}d_{ij}^3}{\lambda_{ij}-3}\right)\frac{1-\zeta_x^{eff}\left(\lambda_{ij}\right)/2}{\left(1-\zeta_x^{eff}\left(\lambda_{ij}\right)\right)^3} \tag{4.26}$$

where the effective packing is obtained by:

$$\zeta_x^{eff}\left(\lambda_{ij}\right)=c_1\left(\lambda_{ij}\right)\zeta_x+c_2\left(\lambda_{ij}\right)\zeta_x^2+c_3\left(\lambda_{ij}\right)\zeta_x^3+c_4\left(\lambda_{ij}\right)\zeta_x^4 \tag{4.27}$$

where the coefficients c_1, c_2, c_3 and c_4 are calculated by the λ parameters of the pure fluid [72]:

$$\begin{pmatrix} c_1 \\ c_2 \\ c_3 \\ c_4 \end{pmatrix} = \begin{pmatrix} 0.81096 & 1.7888 & -37.578 & 92.284 \\ 1.0205 & -19.341 & 151.26 & -463.50 \\ -1.9057 & 22.845 & -228.14 & 973.92 \\ 1.0885 & -6.1962 & 106.98 & -677.64 \end{pmatrix} \cdot \begin{pmatrix} 1 \\ 1/\lambda_{ij} \\ 1/\lambda_{ij}^2 \\ 1/\lambda_{ij}^3 \end{pmatrix} \tag{4.28}$$

The second-order fluctuation term is treated similarly:

$$a_2=\sum_{i=1}^{n}\sum_{j=1}^{n}x_{s,i}x_{s,j}a_{2,ij} \tag{4.29}$$

where,

$$\begin{aligned} a_{2,ij}=\frac{1}{2}K^{HS}\left(1+\chi_{ij}\right)\varepsilon_{ij}C_{ij}^2\Big[& x_{0,ij}^{2\lambda_{a,ij}}\left(a_{1,ij}^{S}\left(\rho_s;2\lambda_{a,ij}\right)+B_{ij}\left(\rho_s;2\lambda_{a,ij}\right)\right) \\ & -2x_{0,ij}^{\lambda_{a,ij}+\lambda_{r,ij}}\left(a_{1,ij}^{S}\left(\rho_s;\lambda_{a,ij}+\lambda_{r,ij}\right)+B_{ij}\left(\rho_s;\lambda_{a,ij}+\lambda_{r,ij}\right)\right) \\ & +x_{0,ij}^{2\lambda_{r,ij}}\left(a_{1,ij}^{S}\left(\rho_s;2\lambda_{r,ij}\right)+B_{ij}\left(\rho_s;2\lambda_{r,ij}\right)\right)\Big] \end{aligned} \tag{4.30}$$

with the Carnahan-Starling compressibility expression is given by

$$K^{HS}=\frac{\left(1-\zeta_x\right)^4}{1+4\zeta_x+4\zeta_x^2-4\zeta_x^3+\zeta_x^4} \tag{4.31}$$

and with

$$\chi_{ij}=f_1\left(\alpha_{ij}\right)\bar{\zeta}_x+f_2\left(\alpha_{ij}\right)\bar{\zeta}_x^5+f_3\left(\alpha_{ij}\right)\bar{\zeta}_x^8 \tag{4.32}$$

where

$$\bar{\zeta}_x=\frac{\pi\rho_s}{6}\left(\sum_{i=1}^{n}\sum_{j=1}^{n}x_{s,i}x_{s,j}\,\sigma_{ij}^3\right) \tag{4.33}$$

$$\alpha_{ij} = C_{ij}\left(\frac{1}{\lambda_{a,ij}-3} - \frac{1}{\lambda_{r,ij}-3}\right) \tag{4.34}$$

Finally, the third order expansion is again obtained by

$$a_3 = \sum_{i=1}^{n}\sum_{j=1}^{n} x_{s,i}x_{s,j}a_{3,ij} \tag{4.35}$$

where $a_{3,ij}$ is calculated by the following simple expression [72]:

$$a_{3,ij} = -\varepsilon_{ij}^3 f_4\left(\alpha_{ij}\right)\bar{\zeta}_x \exp\left(f_5\left(\alpha_{ij}\right)\bar{\zeta}_x + f_6\left(\alpha_{ij}\right)\bar{\zeta}_x^2\right) \tag{4.36}$$

$$\alpha_{ij} = C_{ij}\left(\frac{1}{\lambda_{a,ij}-3} - \frac{1}{\lambda_{r,ij}-3}\right) \tag{4.37}$$

The f_k functions used in Eq.4.32 (k=1,2,3) and Eq.4.36 (k=4,5,6) are obtained by the following generalized expression (Eq.4.38) and the ϕ coefficients presented in Table 4.2.

$$f_k\left(\alpha_{ij}\right) = \left(\sum_{n=0}^{n=3}\phi_{k,n}\alpha_{ij}^n\right) \Big/ \left(1 + \sum_{n=4}^{n=6}\phi_{k,n}\alpha_{ij}^{n-3}\right) \tag{4.38}$$

Table 4.2. Coefficients $\phi_{i,n}$ for Eq.4.38 and 4.49

n	$\phi_{1,n}$	$\phi_{1,n}$	$\phi_{1,n}$	$\phi_{1,n}$	$\phi_{1,n}$	$\phi_{1,n}$	$\phi_{1,n}$
0	7.536556	−359.44	1550.9	−1.19932	−1911.28	9236.9	10
1	−37.60463	1825.6	−5070.1	9.063632	21390.18	−129430	10
2	71.74595	−3168.0	6534.6	−17.9482	−51320.7	357230	0.57
3	−46.83552	1884.2	−3288.7	11.34027	37064.54	−315530	−6.7
4	−2.467982	−0.82376	−2.7171	20.52142	1103.742	1390.2	−8
5	−0.50272	−3.1935	2.0883	−56.6377	−3264.61	−4518.2	-
6	8.095688	3.709	0	40.53683	2556.181	4241.6	-

4.1.2.2 Chain Contribution

The Chain contribution is calculated assuming that the monomers are completely bonded and chains are formed by *m* segments tangentially fused at $r=\sigma$ [72]. Then, the chain contribution can be expressed as:

$$a^{CHAIN} = -\sum_i x_i (m_i - 1) \ln g_{ii}^{Mie}\left(\sigma_{ii}\right) \tag{4.39}$$

where the Mie radial distribution function (RDF) is obtained by

$$g_{ij}^{Mie}\left(\sigma_{ij}\right) = g_{d,ij}^{HS}\left(\sigma_{ij}\right)\exp\left[\beta\varepsilon_{ij}\, g_{1,ij}\left(\sigma_{ij}\right)\Big/ g_{d,ij}^{HS}\left(\sigma_{ij}\right) + \left(\beta\varepsilon_{ij}\right)^2 g_{2,ij}\left(\sigma_{ij}\right)\Big/ g_{d,ij}^{HS}\left(\sigma_{ij}\right)\right] \tag{4.40}$$

First, the expression for g_d^{HS} is presented as

$$g_{d,ij}^{HS}\left(\sigma_{ij}\right) = \exp\left(k_0 + k_1 x_{0,ij} + k_2 x_{0,ij}^2 + k_3 x_{0,ij}^3\right) \tag{4.41}$$

where the density dependent coefficients are calculated from

$$k_0 = -\ln\left(1-\zeta_x\right) + \frac{42\zeta_x - 39\zeta_x^2 + 9\zeta_x^3 - 2\zeta_x^4}{6\left(1-\zeta_x\right)^3} \tag{4.42}$$

$$k_1 = \frac{-12\zeta_x + 6\zeta_x^2 + \zeta_x^4}{2\left(1-\zeta_x\right)^3} \tag{4.43}$$

$$k_2 = \frac{-3\zeta_x^2}{8\left(1-\zeta_x\right)^2} \tag{4.44}$$

$$k_3 = \frac{3\zeta_x + 3\zeta_x^2 - \zeta_x^4}{6\left(1-\zeta_x\right)^3} \tag{4.45}$$

Second, the first order perturbation term to the RDF is obtained by

$$g_{1,ij}\left(\sigma_{ij}\right) = \frac{1}{2\pi\varepsilon_{ij} d_{ij}^3}\left[3\frac{\partial a_{1,ij}}{\partial\rho_s} - C_{ij}\lambda_{a,ij} x_{0,ij}^{\lambda_{a,ij}} \frac{a_{1,ij}^S\left(\rho_s;\lambda_{a,ij}\right) + B_{ij}\left(\rho_s;\lambda_{a,ij}\right)}{\rho_s} + C_{ij}\lambda_{r,ij} x_{0,ij}^{\lambda_{r,ij}} \frac{a_{1,ij}^S\left(\rho_s;\lambda_{r,ij}\right) + B_{ij}\left(\rho_s;\lambda_{r,ij}\right)}{\rho_s}\right] \tag{4.46}$$

and the second-order RDF is given by

$$g_{2,ij}\left(\sigma_{ij}\right) = \left(1+\gamma_{c,ij}\right) g_{2,ij}^{MCA}\left(\sigma_{ij}\right) \tag{4.47}$$

where

$$g_{2,ij}^{MCA}\left(\sigma_{ij}\right)=\frac{1}{2\pi\varepsilon_{ij}^{2}d_{ij}^{3}}\left[3\frac{\partial\left(a_{2,ij}/\left(1+\chi_{ij}\right)\right)}{\partial\rho_{s}}-\varepsilon_{ij}K^{HS}C_{ij}^{2}\lambda_{\mathrm{r},ij}x_{0,ij}^{2\lambda_{\mathrm{r},ij}}\frac{a_{1,ij}^{S}\left(\rho_{s};2\lambda_{\mathrm{r},ij}\right)+B_{ij}\left(\rho_{s};2\lambda_{\mathrm{r},ij}\right)}{\rho_{s}}\right.$$
$$+\varepsilon_{ij}K^{HS}C_{ij}^{2}\left(\lambda_{\mathrm{r},ij}+\lambda_{\mathrm{a},ij}\right)x_{0,ij}^{\left(\lambda_{\mathrm{r},ij}+\lambda_{\mathrm{a},ij}\right)}\frac{a_{1,ij}^{S}\left(\rho_{s};\lambda_{\mathrm{r},ij}+\lambda_{\mathrm{a},ij}\right)+B_{ij}\left(\rho_{s};\lambda_{\mathrm{r},ij}+\lambda_{\mathrm{a},ij}\right)}{\rho_{s}}$$
$$\left.-\varepsilon_{ij}K^{HS}C_{ij}^{2}\lambda_{\mathrm{a},ij}x_{0,ij}^{2\lambda_{a,ij}}\frac{a_{1,ij}^{S}\left(\rho_{s};2\lambda_{a,ij}\right)+B_{ij}\left(\rho_{s};2\lambda_{a,ij}\right)}{\rho_{s}}\right] \tag{4.48}$$

and where γ_c is a correction factor function of the temperature and density:

$$\gamma_{c,ij}=\phi_{7,0}\left(-\tanh\left(\phi_{7,1}\left(\phi_{7,2}-\alpha_{ij}\right)+1\right)\bar{\zeta}_{x}\theta_{ij}\exp\left(\phi_{7,3}\bar{\zeta}_{x}+\phi_{7,4}\bar{\zeta}_{x}^{2}\right)\right) \tag{4.49}$$

with

$$\theta_{ij}=\exp\left(\beta\varepsilon_{ij}\right)-1 \tag{4.50}$$

4.1.3 Mie molecular parameters

Five physical parameters are required to describe each non-associating compound with the SAFT-VR Mie equation of state. The Mie molecular parameters are the number of spherical segments (m_s), the diameter of segment (σ), the strength of the interaction between the segments (ε) and the Mie potential repulsive and attractive exponents (λ_r - λ_a). An important feature and requirement of SAFT-like EoSs is that the pure component parameters are fitted to experimental data.

Thus, the Mie pure-component parameters {m_s, σ, ε, λ_r, λ_a} reported by Lafitte et al. [72] and Dufal et al. [90] were adjusted using vapour pressure, saturated-liquid density, condensed-liquid density and speed of sound data points. The regression was carried out by minimizing the following objective function F:

$$\min_{\theta}F=\frac{w_1}{N_{P_{sat}}}\sum_{i=1}^{N_{P_{sat}}}\left[\frac{P_{sat,i}^{\exp}(T_i)-P_{sat,i}^{calc}(T_i;\theta)}{P_{sat,i}^{\exp}(T_i)}\right]^2+\frac{w_2}{N_{\rho_{sat}}}\sum_{i=1}^{N_{\rho_{sat}}}\left[\frac{\rho_{sat,i}^{\exp}(T_i)-\rho_{sat,i}^{calc}(T_i;\theta)}{\rho_{sat,i}^{\exp}(T_i)}\right]^2$$
$$+\frac{w_3}{N_{\rho}}\sum_{i=1}^{N_{\rho}}\left[\frac{\rho_{i}^{\exp}(T_i,P_i)-\rho_{i}^{calc}(T_i,P_i;\theta)}{\rho_{i}^{\exp}(T_i,P_i)}\right]^2+\frac{w_4}{N_{u}}\sum_{i=1}^{N_{u}}\left[\frac{u_{i}^{\exp}(T_i,P_i)-u_{i}^{calc}(T_i,P_i;\theta)}{u_{i}^{\exp}(T_i,P_i)}\right]^2 \tag{4.51}$$

where w_1, w_2, w_3 and w_4 are the weights of each property in the objective function and are generally set to w_1=w_2= w_3 =1 and w_4=1/4, N_{Psat}, $N_{\rho sat}$, N_ρ and N_u are respectively

the number of vapour pressure (P_{sat}), saturated liquid density (ρ_{sat}), condensed liquid density (ρ) and speed of sound (u) data points, the superscripts *exp* and *calc* refer to experimental data and calculated values, and θ is the vector of parameters which will be adjusted by the minimization. The reduced temperature range ($T_r=T/T_c$) imposed to fit the parameters is between 0.4 and 0.9.

Table 4.3. SAFT-VR Mie pure-component parameters from the literature [72,90]**.**

Compound	m	σ [Å]	ε/k_B [K]	λ_r	λ_a
CO_2	1.500	3.192	231.88	27.557	5.1646
Methane	1.000	3.741	153.36	12.650	6
Ethane	1.437	3.726	206.12	12.400	6
Propane	1.685	3.906	239.89	13.006	6
i-Butane	1.719	4.218	281.12	14.612	6
n-Butane	1.851	4.089	273.64	13.650	6
i-Pentane	1.746	4.471	339.95	16.688	6
n-Pentane	1.961	4.293	321.94	15.847	6
n-Hexane	2.110	4.423	354.38	17.203	6
n-Heptane	2.241	4.543	381.42	18.252	6
n-Octane	2.625	4.470	369.18	17.378	6
n-Nonane	2.810	4.533	387.55	18.324	6
n-Decane	2.998	4.589	400.79	18.885	6
n-Dodecane	3.252	4.748	437.72	20.862	6
n-Pentadecane	3.933	4.774	444.51	20.822	6
n-Eicosane	4.879	4.878	475.76	22.926	6
N_2	1.421	3.176	72.438	9.8749	6
O_2	1.428	2.967	81.476	8.9218	6
CO	1.556	3.093	72.110	9.7420	6
SO_2	2.460	2.851	225.73	11.865	6
Argon	1.000	3.404	117.84	12.085	6
Benzene	2.278	3.781	297.53	11.594	6
Toluene	1.711	4.5487	474.13	19.125	6

According to previous literature works [72,90], the following criteria can be considered in the regression procedure in order to reject parameters with no physical sense and to respect some constraints:

- The number of segments (m_s) should increase with the degree of asymmetry of the molecule, *i.e.* for n-alkanes, *m* increase with the size of the chain.

- The parameter σ should be larger than 3 Å. However, there can be exceptions below 3Å, *e.g.* sulphur dioxide (SO_2) or oxygen (O_2).
- Acceptable values of the ε/k_b parameter are between 90 (low deep interaction between gases as CO, N_2 or Ar) and 500 K.
- The range of λ_r is wide, from values lower than 12 for short alcohol chains to values that are three times the Lennard-Jones repulsive exponent. Similarly to the number of segments, λ_r increases with number of carbons of *n*-alkane chains.
- Generally, the attractive exponent is held constant as about λ_a=6, although it can be also adjusted if it is necessary, *e.g.* carbon dioxide and the perfluoro-alkanes.

The Mie molecular parameters used in this work are from the literature and are reported in Table 4.3.

Mie parameters for H_2S

The only available set of parameters for the hydrogen sulphide, H_2S was performed considering it as an associating compound [163]. Therefore, a new set of parameters for the H_2S has been regressed from experimental data. The resulting SAFT-VR Mie parameters for pure hydrogen sulphide are reported in Table 4.4, as well as the average absolute deviation (AAD) between the results from the correlation with EoS and the experimental vapour pressure P_{sat}, saturated-liquid densities ρ_{sat} (Fig. 4.2) and enthalpy of vaporization ΔH_v [42].

Table 4.4. Mie molecular parameters for hydrogen sulphide, and average absolute deviation (%AAD) from experimental correlations [42] **for the vapour pressure (P_{sat}), the saturated-liquid density (ρ_{sat}) and the enthalpy of vaporization (ΔH_v).**

Compound	m_s	σ/Å	(ε/k)/K	λ_r	λ_a	AAD (%) [(a)]		
						P_{sat}	ρ_{sat}	ΔH_v
H_2S	1	3.7783	387.28	22.451	6	2.2	0.4	3.7

[(a)] $$AAD(\%) = \frac{1}{N}\sum_{i=1}^{N}\left(\left|X_{\exp} - X_{EoS}\right| / X_{\exp}\right)\cdot 100$$

H_2S densities in the gas, liquid and supercritical regions have been calculated for 13 temperatures between 200 to 500 K and pressures up to 100 MPa, reporting an %AAD of 2.3%. However, considering the H_2S single phase densities at the pressure and temperature ranges of our measurements, the average absolute deviation is 0.9% (Fig. 4.3).

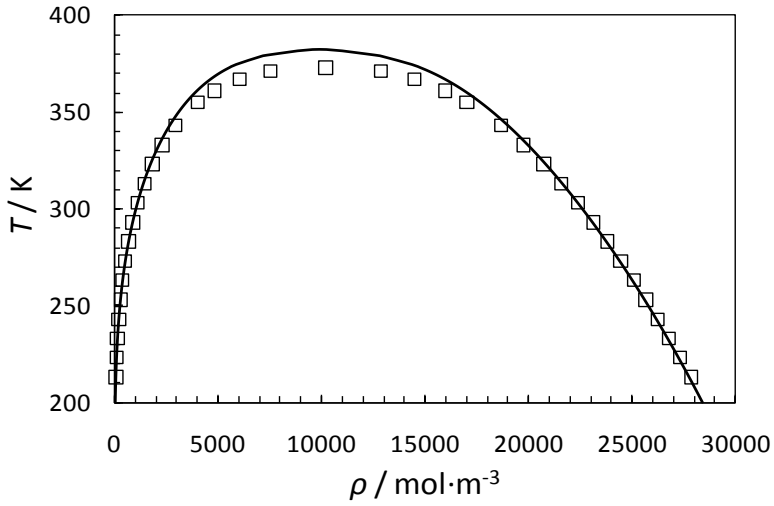

Figure 4.2. Temperature-density coexistence envelop for pure H_2S. Comparison between experimental data (□) [42] **and SAFT-VR Mie calculation.**

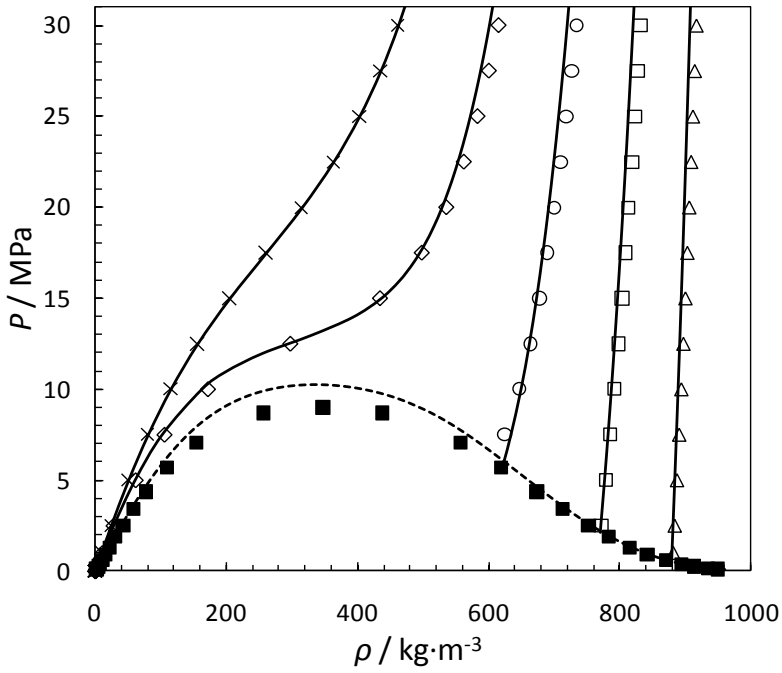

Figure 4.3. Correlated and experimental densities of pure H_2S. The solid lines are isotherms calculated with the SAFT-VR Mie and the dashed line is the calculated coexistence curve. The symbols denote experimental data: from the literature [42] **at T=250K (Δ), T=300K (□), T=350K (○), T=400K (◇) and T=450K (×) and at saturation (■).**

Mie parameters for long alkanes

Long-alkanes parameters have not been found in the literature. Hence, in order to avoid fitting the parameters for each compound, the molecular parameters for the series of *n*-alkanes have been correlated with respect to the molecular weight (M_w) following a

similar procedure as Pedersen *et al.* for PC-SAFT [164]. It has been found that the number of segments m increases linearly with molecular weight M_w for long-chain alkanes. Thus, from a least squares analysis, m and M_w can be related using Eq. 4.52. However, to correlate the diameter and energy of the segment, as well as the Mie repulsion exponent, the linear dependence is considered between the products $m\sigma$, $m\varepsilon$ and $m\lambda_r$ and M_w (Equations 4.53-4.55). In Figure 4.4, these correlations are plotted together with the coefficients of determination (R^2) from the least squares analysis.

$$m = 0.01357\ \mathrm{M_W} + 1.0324 \tag{4.52}$$

$$m\sigma = 0.07278\ \mathrm{M_W} + 3.2699 \tag{4.53}$$

$$m\varepsilon/\mathrm{k_b} = 8.0315\ \mathrm{M_W} + 52.044 \tag{4.54}$$

$$m\lambda_r = 0.3723\ \mathrm{M_W} + 4.3413 \tag{4.55}$$

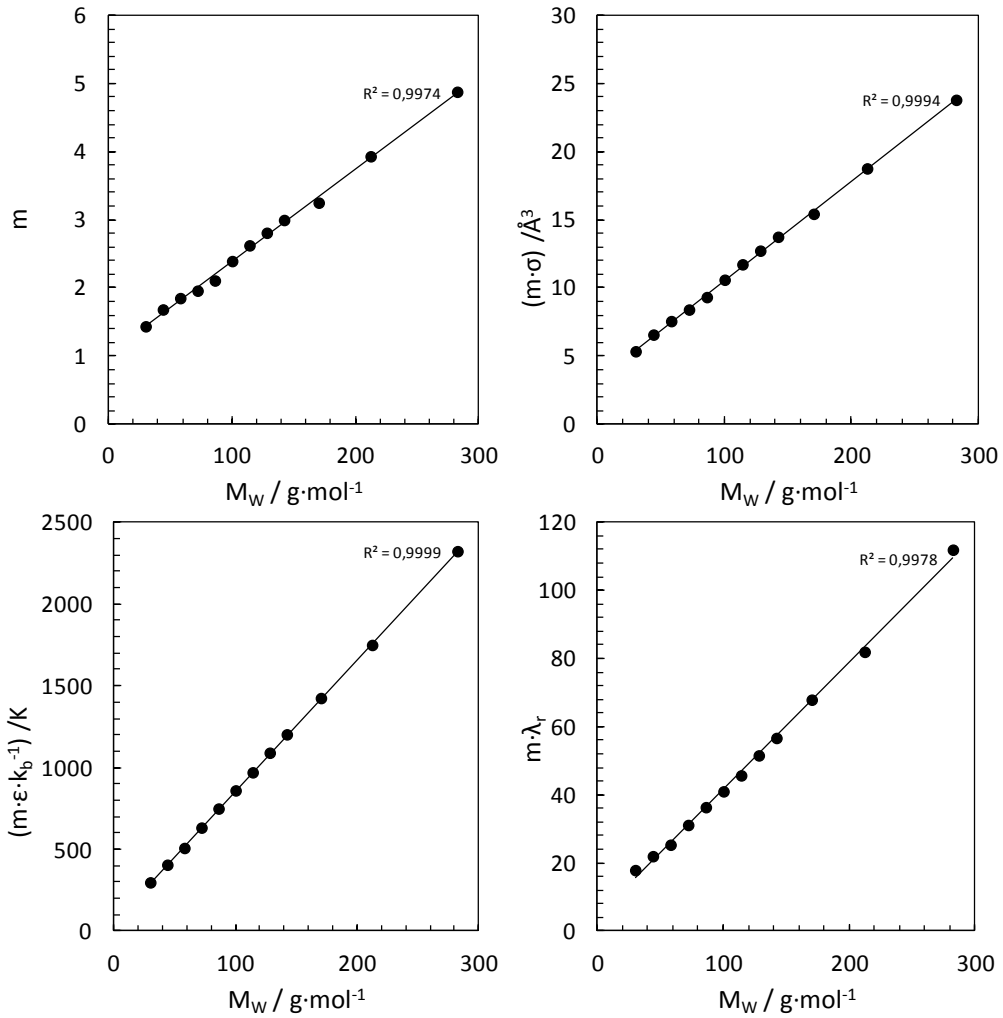

Figure 4.4. Correlations of the SAFT-VR Mie molecular parameters for the series of *n*-alkanes.

4.2 Comparative study of EoSs

This part of the work is focused at comparing the capability of four equations of state (EoSs) in modelling vapour-liquid equilibria (VLE) and density of binary mixtures of interest in the field of CCS. The assessed models are the classical PR and SRK EoS, the well-known PC-SAFT EoS and the previous presented SAFT-VR Mie EoS.

4.2.1 Cubic EoSs

The Soave-Redlich-Kwong (SRK) [88] and Peng-Robinson (PR) [89] EoSs are the two studied cubic EoSs (CEoS). Most of the CEoS are pressure-explicit equations and once they are solved for volume (or density), other properties, such as fugacity or chemical potential, can be obtained by thermodynamic relations [16,165]. The cubic family of EoSs are based on a cubic dependence on the volume with two or more adjustable parameters which are fitted to experimental data. CEoS can be expressed by this general formula [166]:

$$P = \frac{RT}{v-b} - \frac{a\alpha(T)}{v^2 + u\,v\,b + wb^2} \tag{4.56}$$

where a and b are the parameters of the CEoS calculated using the critical temperature (T_c) and pressure (P_c) of each component; $\alpha(T)$ (α function)is a function of temperature, acentric factor, T_c and P_c. SRK and PR are the CEoS considered in this work, u and w are constants, and their values are u= 1 and w= 0 for SRK and u= 2 and w= -1 for PR. In this work, the original expression for the α function were used, proposed by Soave [88] for the SRK EoS and by Peng and Robinson [167] for the PR EoS. A description of the equations to calculate the $\alpha(T)$ and the a and b parameters is presented in Appendix C.

No pure component parameters are adjusted for the CEoS. The critical properties and acentric factor values for the studied compounds are presented in Table C.1.

In order to extend the CEoS to multicomponent systems, the standard van der Waals mixing rules were used, i.e.:

$$b = \sum_i x_i b_i \tag{4.57}$$

$$a = \sum_i \sum_j x_i x_j \sqrt{a_i a_j} \left(1 - k_{ij}\right) \tag{4.58}$$

where x_i and x_j are the composition of pure components i and j, and k_{ij} is the binary interaction parameter (BIP). The BIPs are coefficients introduced to better describe the experimental phase behaviour of binary mixtures.

In general, liquid densities tend to be underestimated by the SRK and PR CEoS [168]. To improve the density predictions of dense fluid phases, volume translations can be used. The Peneloux volume correction (VC) [92] has been implemented herein (Equation 4.59) and the results with and without Peneloux shift parameters are discussed in the Subsection 4.2.3.

$$V = V^{EoS} + \sum_i^{N_C} x_i V_i^c \tag{4.59}$$

where V^{EoS} is the molar volume calculated by the SRK and PR EoSs and $V^c{}_i$ the volume correction parameter. The volume translation parameters have been treated as temperature independent [92] and the values of the parameters for each CEoS are also reported in Table C.1. The liquid density calculations are improved by the use of temperature-dependent parameters for the volume corrections; however more calculated thermophysical properties are affected by using temperature-dependent parameters, such as heat capacities (c_v and c_p) [169].

4.2.2 SAFT-like EoSs

The PC-SAFT and SAFT-VR Mie EoSs are the SAFT–like EoSs that have been compared in this study. As it was presented in Chapter 3, these EoSs are expressed in terms of the reduced Helmholtz energy and as a sum of several contributions corresponding to the free energy of the reference fluid and the various perturbation terms (Eqs. 3.22 and 3.23).

One of the most important differences between the SAFT-VR Mie and PC-SAFT EoSs is the pair potential considered (Figure 4.5). Regarding the PC-SAFT EoS, the modified square well pair potential (Eq. 3.6), suggested by Chen and Kreglewski [71] is applied to compute the effective hard sphere diameter, while the Lennard-Jones (LJ) potential

was used for the dispersion term. Concerning the SAFT-VR Mie EoS, the pair potential is the Mie potential that is a generalized version of the LJ potential (Eq. 3.7).

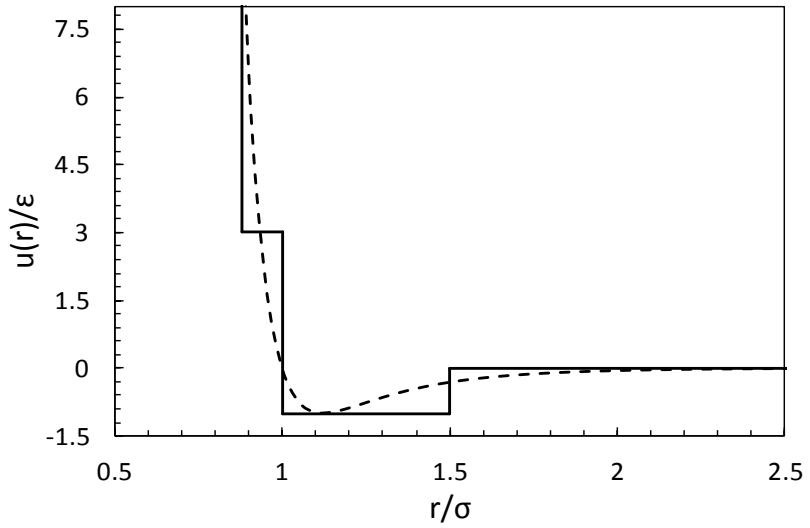

Figure 4.5. Molecular pair potentials. Continuous line: modified SW pair potential. Dashed line: 12-6 Mie potential (LJ).

Another difference between these EoSs is the number of parameters regressed by fitting pure component data. For non-associating components, the PC-SAFT EoS requires three parameters: the segment number (m), the segment diameter (σ) and the segment energy (ε). For the SAFT-VR Mie EoS, besides the traditional SAFT parameters m, σ and ε, two extra parameters are required to describe the Mie potentials (λ_r and λ_a). The PC-SAFT parameters are fitted to vapour pressure and saturated liquid density, while the SAFT-VR Mie parameters are regressed using in addition condensed-liquid density and speed of sound data points [170].

A summary of the expressions necessary to calculate the residual Helmholtz free energy using the PC-SAFT EoS is presented in Appendix D. The phase equilibria calculations were performed following the approach presented in Subsection 4.1.1 for the SAFT-VR Mie. The PC-SAFT pure-component parameters from the literature used in this work are reported in Table D.2.

This study focuses on non-associative compounds. Here a non-associating model for H_2S with the PC-SAFT and SAFT-VR Mie EoSs has been considered, despite H_2S has been described by Dufal et al. [163] using a 4C association model with the SAFT-VR Mie EoS. Note also that Diamantonis et al. found that considering H_2S as an

associating-compound is slightly less accurate using the PC-SAFT EoS for describing the VLE of systems such as CO_2-H_2S [16].

Besides pure molecular parameters, binary interaction parameters (BIPs) can be adjusted against vapour-liquid equilibrium data. The BIPs are coefficients introduced to correct the unlike attractive dispersive energy (ε_{ij}) [119]. The conventional Berthelot-Lorentz combining rule (Eq.4.60) [69] is used in the PC-SAFT EoS, while the SAFT-VR Mie model uses a specific geometric relation defined by Eq.4.61 [72].

$$\varepsilon_{ij} = (1 - k_{ij})\sqrt{\varepsilon_i \varepsilon_j} \tag{4.60}$$

$$\varepsilon_{ij} = (1 - k_{ij})\frac{\sqrt{\sigma_i^3 \sigma_j^3}}{\sigma_{ij}^3}\sqrt{\varepsilon_i \varepsilon_j} \tag{4.61}$$

where σ_i is the segment diameter of compound *i*; the mixing rule used to calculate σ_{ij} is given by

$$\sigma_{ij} = \frac{\sigma_i + \sigma_j}{2} \tag{4.62}$$

4.2.3 Results and discussion

108 binary systems of 29 typical components in flue gases and reservoir fluids were considered in this study. The selected components are 7 gases (CO_2, N_2, O_2, Ar, H_2S, CO and SO_2), 20 alkanes and 2 aromatics (benzene and toluene). A summary of the VLE and density data available in the literature for the studied binary mixtures has been presented in Table 2.1. This comparative analysis has included an enormous amount of experimental data collected from the literature. All data sets collected are included in the NIST Databases [42,171]. However, many of the PVT data collected have not been used in order to avoid wrong calculations (*i.e.* VLE points close to the critical point) or because they were not consistent (*i.e.* data points not following the trend of the isotherm and data sets with lack of consistency between isotherms or other authors). In total, 22904 VLE and 26479 density experimental data points of binary mixtures have been used in this work. In addition, 31928 single phase densities of pure components have been obtained from correlations and EoSs.

The comparative study is divided into two parts: phase equilibrium and density calculations. For the phase equilibrium, bubble point pressures and vapour phase

compositions are predicted with zero binary interaction parameters (k_{ij}=0). Binary interaction parameters are then regressed on the VLE data for each binary mixture. In order to do a fair comparison between EoSs, the regression was done by treating the k_{ij}'s as temperature independent. The BIPs have been regressed by minimizing the objective function given in Eq.4.63, which is the sum of the deviations between the calculated bubble point pressures and the experimental VLE data. Subsequently, the deviations in the bubble point calculations were again determined for each model using the regressed k_{ij}'s.

$$\min F = \frac{100}{N}\sum_{1}^{N}\left(\frac{\left|P_{bubble}^{\exp} - P_{bubble}^{cal}\right|}{P_{bubble}^{\exp}}\right) \tag{4.63}$$

The second part of the study is focused on density calculations. Firstly, the densities of pure components are predicted and compared against the correlated data from the literature. Secondly, the densities of binary systems are calculated and also compared against the compiled experimental density data. The k_{ij} values regressed on bubble points were used for predicting densities and the volume-translation concept within the framework of CEoS was also considered.

The modelling results are assessed by comparing the average deviations between the models and the experimental data. The AAD is the average absolute deviation and is defined as

$$AAD(\%) = \frac{1}{N}\sum_{i=1}^{N}\left(\left|X^{\exp} - X^{EoS}\right| / X^{\exp}\right)\cdot 100 \tag{4.64}$$

where X is the evaluated property (bubble pressure, vapour mol fraction or density), N is the number of data, the *exp* and *EoS* exponents denote the experimental data and the calculations from the equation of state, respectively.

4.2.3.1 VLE calculations

The Mie molecular parameters of the *n*-alkanes series were correlated to the molecular weights. Then, before introducing the VLE results, the vapour pressure of nC$_{14}$, nC$_{16}$, nC$_{18}$, nC$_{24}$ and nC$_{32}$ were studied using the correlated parameters (Figure 4.6). At reduced temperatures ($T_r = T/T_c$) between of $0.5 < T_r < 0.9$, the average absolute

deviation of the calculated vapour-pressure is 5.8%. However, the VLE calculations for the systems containing long n-alkanes are performed at temperatures that can be considered around 0.7 T_r. Therefore, the average deviation in the saturation pressure of the long-chain alkanes is 1.95%, and is similar to the %AAD of the description of saturation pressure of the *n*-eicosane using fitted parameters from the literature, 1.83%.

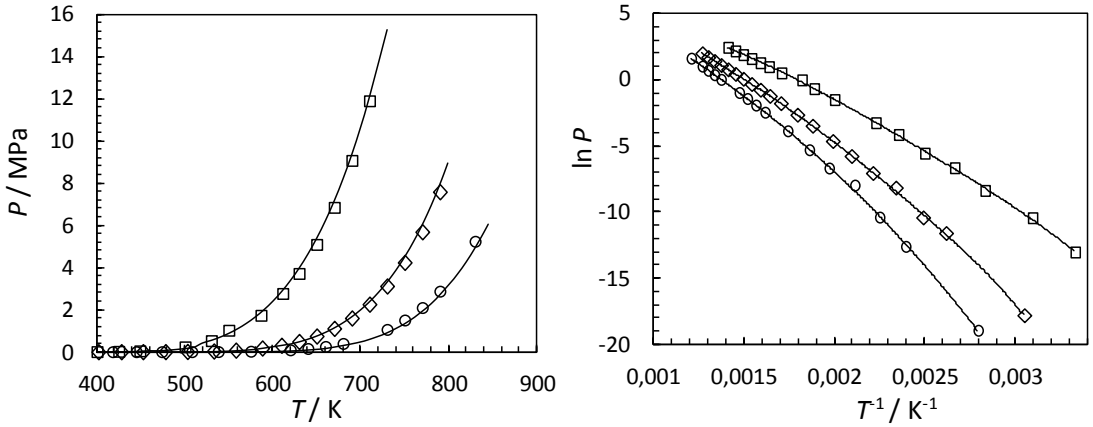

Figure 4.6. Vapour-pressure curves of *n*-C_{16} (□), *n*-C_{24} (◇) and *n*-C_{32} (○) calculated using the correlated SAFT-VR Mie molecular parameters.

The phase equilibrium study is divided in five parts, according to the main five gaseous components considered in this work: CO_2, CH_4, C_2H_6, N_2 and H_2S. Due to the large number of considered systems, several types of phase diagrams have been found.

According to the Scott and van Konynenburg classification [44], the phase diagrams of the studied systems are classified as type I (*e.g.* CH_4– CO_2, C_2H_6– H_2S, CO_2– O_2 [172]), type II (*e.g.* CO_2–*n*-octane, CO_2–*n*-decane [173]), type III (*e.g.* CO_2 + longer *n*-alkanes than C_{14} [174] or CH_4–H_2S [47]) and type V (*e.g.* CH_4–*n*-hexane [175]). Despite the different temperature ranges and number of experimental data available, all the studied systems were treated equally, *i.e.* special treatments in favour of a particular model was avoided in order to do a relevant comprehensive evaluation of the four models.

The VLE results of modelling the CO_2 binary systems are firstly presented in Table 4.5. The experimental VLE data for 27 mixtures of CO_2 over a broad range of temperatures were modelled using the SRK, PR, PC-SAFT and SAFT-VR Mie EoSs. In general, the four studied models lead to similar results for the phase equilibrium predictions (k_{ij}=0) and calculations ($k_{ij}\neq0$), with %AAD averaging approximately 15% and 4.3% respectively. It has been observed that the deviations of the SRK model are similar to

those reported for the PR EoS, as well as the BIPs regressed for each studied system. However, comparing both SAFT EoSs, a slight difference can be seen between the regressed k_{ij} values. The k_{ij} values for the CO_2 + n-alkanes systems and their trend are plotted in Figure 4.7

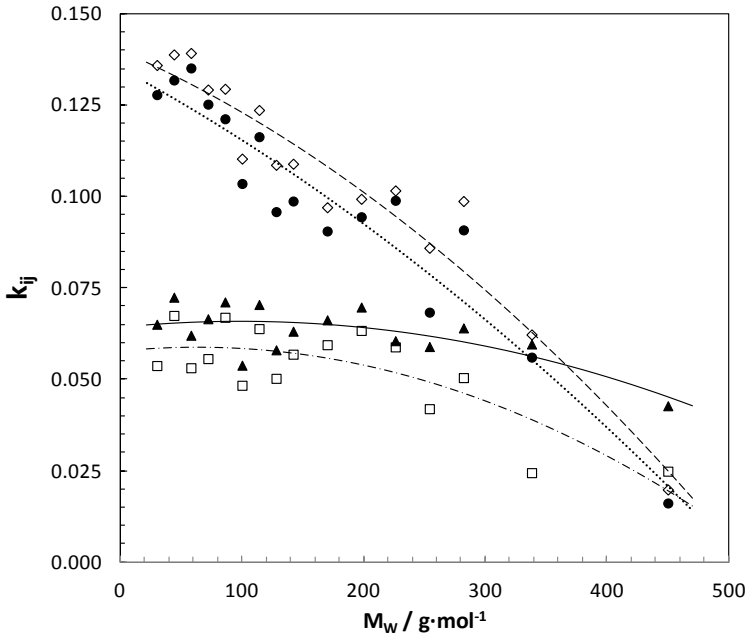

Figure 4.7. Binary interaction parameters of n-alkanes + CO_2 binary system and their trend curves for the SRK (◇, dashed lines), PR (●, dotted line), PC-SAFT (▲, continuous line) and SAFT-VR Mie (□, dot-dashed line) EoS.

The SAFT-VR Mie EoS is on average the model which predicts the VLE of CO_2 systems with the lowest %AADs to experimental data. Both CEoS models better describe the phase equilibrium of the mixtures of CO_2 with gases (N_2, O_2, Ar, H_2S, CO and SO_2) and aromatic compounds (benzene and toluene); while the SAFT-based EoSs better performed for the CO_2 + alkanes systems.

Special mention is made in Figure 4.8 about the CO_2 + N_2 system. We focus our attention on this binary system because of the very poor predictions done by the CEoS and SAFT-VR Mie. In Figure 4.8a, it can be observed that the PC-SAFT EoS predicts (k_{ij}=0) with reasonable accuracy this system. The SRK and PR models underestimate the bubble point pressure, while it is overestimated by the SAFT-VR Mie EoS. In Figure 4.8b, the four models similarly describe the phase equilibria by using the fitted BIPs.

Table 4.5. Average absolute deviations (%AAD) in predictions (k_{ij}=0) and calculations (using regressed k_{ij}'s) of bubble pressure (ΔP^{bubble}) and vapour phase composition (Δy_1) of CO_2 + Comp2 binary systems with the SRK, PR, PC-SAFT and SAFT-VR Mie EoS.

Comp2	T_{range} [K]	SRK			PR			PCSAFT			SAFT-VR Mie		
		k_{ij}	ΔP	Δy_1	k_{ij}	ΔP	Δy_1	k_{ij}	ΔP	Δy_1	k_{ij}	ΔP	Δy_1
CH_4	143	0	13.49	3.88	0	13.35	3.99	0	10.22	3.26	0	2.76	3.01
	301	0.0956	2.83	2.12	0.0951	2.41	1.83	0.0856	3.82	2.41	0.0042	2.28	2.82
C_2	207	0	15.39	6.42	0	15.76	6.36	0	14.61	6.88	0	13.22	7.56
	298	0.1359	3.24	2.19	0.1278	3.19	2.27	0.0650	2.93	2.74	0.0537	2.12	2.32
C_3	210	0	15.66	6.14	0	15.44	5.98	0	15.68	7.03	0	15.35	6.61
	366	0.1388	3.28	1.06	0.1318	3.27	1.09	0.0724	3.07	0.61	0.0674	2.30	0.58
nC_4	227	0	14.76	4.66	0	14.57	4.73	0	14.83	6.2	0	12.62	7.03
	418	0.1392	3.11	1.31	0.1351	2.95	1.33	0.0620	3.26	1.01	0.0531	1.81	0.94
iC_4	250	0	13.88	4.88	0	13.74	4.82	0	12.79	4.63	0	11.45	4.71
	398	0.131	3.74	1.84	0.1256	3.48	1.91	0.0646	3.38	1.77	0.0549	3.13	1.80
nC_5	252	0	12.43	3.91	0	12.47	3.96	0	11.74	3.40	0	10.86	3.71
	463	0.1292	5.05	1.95	0.1252	4.69	1.82	0.0665	4.31	1.18	0.0556	4.02	1.22
iC_5	253	0	16	3.78	0	16.04	3.69	0	14.64	3.09	0	13.95	3.14
	453	0.1221	3.91	1.77	0.1158	3.63	1.78	0.0649	3.5	1.65	0.0550	3.37	1.70
nC_6	238	0	15.73	2.71	0	15.62	2.63	0	16.95	2.97	0	16.21	3.04
	393	0.1294	4.61	0.99	0.1212	4.40	1.04	0.0711	3.71	0.82	0.0669	3.88	0.92
nC_7	238	0	17.3	3.21	0	17.44	3.08	0	15.84	3.13	0	15.60	3.18
	501	0.1103	5	1.70	0.1035	5.06	1.81	0.0538	5.89	1.77	0.0483	5.26	1.57
nC_8	238	0	15.54	1.75	0	15.50	1.72	0	15.04	1.79	0	14.79	1.85
	531	0.1236	6.05	1.30	0.1163	6.12	1.25	0.0704	6.26	1.25	0.0638	5.47	1.24
nC_9	315	0	20.05	1.11	0	19.21	1.03	0	17.74	1.53	0	17.42	1.46
	418	0.1086	2.72	0.57	0.0958	2.58	0.50	0.0580	2.63	0.55	0.0502	2.55	0.58
nC_{10}	277	0	19.61	2.51	0	18.95	2.43	0	16.63	3.76	0	15.92	3.13
	583	0.1089	4.94	0.89	0.0987	4.15	0.83	0.0631	4.33	0.89	0.0568	2.08	1.11
nC_{12}	313	0	10.67	-	0	10.75	-	0	7.81	-	0	7.96	-
	417	0.0970	1.69	-	0.0905	1.27	-	0.0662	0.89	-	0.0594	1.03	-
nC_{14}	290	0	12.9	-	0	14.32	-	0	14.96	-	0	15.45	-
	373	0.0993	1.78	-	0.0944	1.59	-	0.0697	3.34	-	0.0633	3.42	-
nC_{16}	283	0	16.52	-	0	15.87	-	0	16.50	-	0	17.76	-
	573	0.1016	4.35	-	0.0989	4.46	-	0.0605	5.21	-	0.0588	5.40	-
nC_{18}	323	0	16.73	-	0	14.57	-	0	17.10	-	0	19.43	-
	673	0.0859	7.31	-	0.0683	7.72	-	0.0589	7.36	-	0.0419	7.55	-
nC_{20}	300	0	20.9	-	0	21.19	-	0	16.33	-	0	22.19	-
	573	0.0987	5.77	-	0.0908	5.86	-	0.0640	4.17	-	0.0504	5.27	-
nC_{24}	353	0	11.21	-	0	9.88	-	0	15.82	-	0	18.78	-
	573	0.0622	5.36	-	0.0560	6.20	-	0.0596	5.06	-	0.0244	6.60	-
nC_{32}	335	0	10.37	-	0	11.92	-	0	19.60	-	0	10.93	-
	573	0.0198	5.79	-	0.0161	6.04	-	0.0427	5.14	-	0.0248	5.37	-
H_2S	224	0	12.31	4.91	0	12.95	4.96	0	14.13	5.36	0	13.86	5.23
	366	0.0984	1.46	1.09	0.0966	1.44	1.46	0.0618	1.68	0.95	0.0621	1.12	1.89
N_2	218	0	5.50	3.56	0	3.86	2.92	0	6.02	2.27	0	22.35	8.28
	301	-0.0245	2.88	3.63	-0.0192	3.05	3.10	-0.0079	4.89	1.91	-0.1083	6.31	2.85
O_2	218	0	21.78	11.09	0	22.82	12.11	0	20.80	11.09	0	19.21	10.02
	298	0.1072	5.54	4.04	0.1188	6.31	3.69	0.0475	7.63	6.47	-0.0291	5.01	3.68
Ar	233	0	23.03	7.85	0	17.53	7.88	0	15.80	8.06	0	14.17	8.12
	299	0.123	5.82	4.31	0.1211	6.86	2.93	0.0213	5.51	3.96	-0.0163	6.25	2.66
SO_2	313	0	11.98	-	0	12.88	-	0	17.00	-	0	6.19	-
	403	0.0676	5.46	-	0.0671	5.55	-	0.0424	7.85	-	0.0078	4.83	-
CO	223	0	12.29	3.91	0	10.28	2.83	0	9.65	5.59	0	8.03	4.95
	283	-0.0710	5.50	5.05	-0.0573	5.70	4.38	-0.0103	6.89	4.85	-0.0078	6.18	5.49
Benzene	273	0	20.25	1.77	0	21.50	1.85	0	27.82	3.75	0	21.66	1.80
	413	0.0987	7.07	1.20	0.0992	6.23	1.24	0.0433	8.91	6.04	0.0776	7.08	1.87
Toluene	230	0	27.27	6.54	0	28.49	6.57	0	45.99	9.85	0	19.70	6.31
	572	0.1012	6.56	6.00	0.0995	6.40	5.84	0.0965	13.87	7.13	0.0481	10.45	5.55

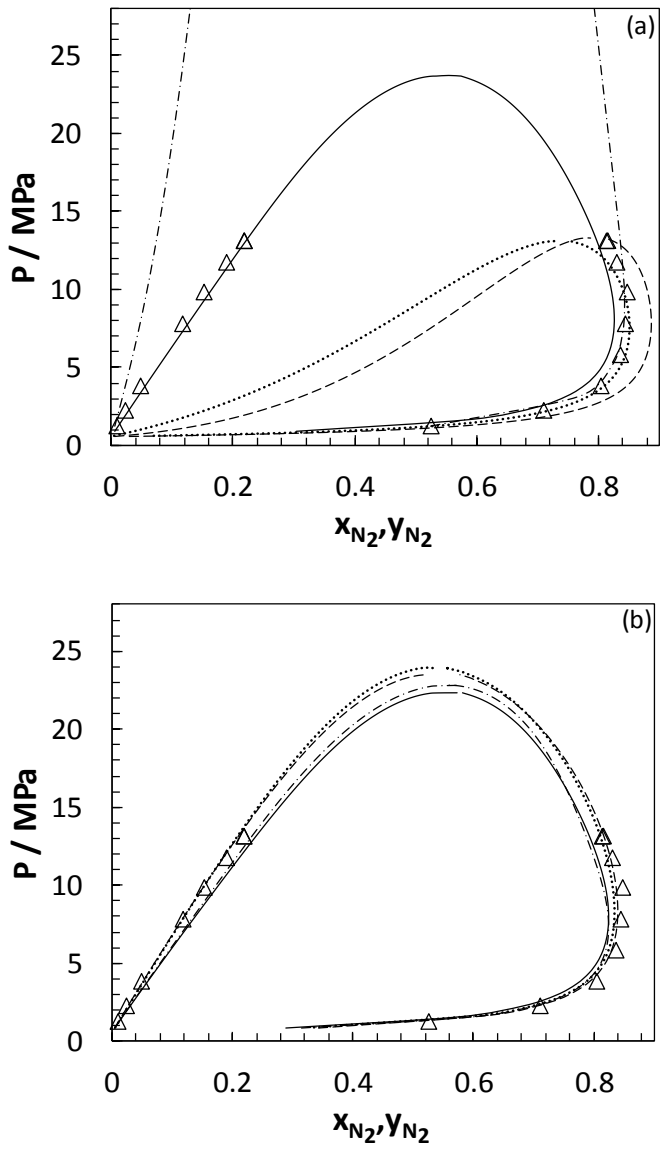

Figure 4.8. Pressure–composition diagrams of the CO_2 + N_2 system at 218K. Experimental data (△) [176]**. The SRK (dashed lines), PR (dotted line), PC-SAFT (continuous line) and SAFT-VR Mie (dot-dashed line) EoS with k_{ij} =0 (a) and with regressed k_{ij} (b).**

The average absolute deviation in the bubble point pressures and vapour-phase compositions for the CH_4 + Comp2 binary systems predicted by the four studied models are presented in Table 4.6, as well as the regressed k_{ij} values and model deviations in the VLE calculations. The SAFT-VR Mie model presents the best predictive capability (9.9% in ΔP^{bubble} against the 12.8% of PR EoS), the four studied models report comparable AADs around 4.5% using the fitted independent temperature BIP. In Figure 4.9, the phase diagram of the CH_4 + CO_2 system is performed as an example of the good agreement between the CEoS and VLE data for such type of systems.

Table 4.6. Average absolute deviation (%AAD) in prediction (k_{ij}=0) and calculations (using regressed k_{ij}'s) of bubble pressure (ΔP^{bubble}) and vapour phase composition (Δy_1) of CH_4 + Comp2 binary systems with the SRK, PR, PC-SAFT and SAFT-VR Mie EoS.

Comp2	T_{range} [K]	SRK			PR			PCSAFT			SAFT-VR Mie		
		k_{ij}	ΔP	Δy_1	k_{ij}	ΔP	Δy_1	k_{ij}	ΔP	Δy_1	k_{ij}	ΔP	Δy_1
CO_2	143	0	13.45	3.85	0	13.40	4.00	0	10.13	3.25	0	2.72	2.99
	301	0.0956	2.78	2.10	0.0951	2.56	1.84	0.0356	3.42	2.39	0.0042	2.24	2.79
C_2	130	0	1.76	1.26	0	1.73	1.20	0	6.04	3.79	0	3.58	1.99
	283	-0.0029	1.72	1.24	0.0012	1.67	1.17	0.0131	3.18	3.33	0.0007	3.36	1.94
C_3	90	0	4.95	1.64	0	5.51	1.80	0	3.63	0.89	0	3.84	0.97
	360	0.0088	3.61	1.51	0.0149	2.53	1.52	0.0117	2.01	0.99	-0.0028	3.50	0.96
nC_4	144	0	5.18	0.97	0	6.57	0.94	0	5.62	0.90	0	5.27	0.51
	411	0.0111	4.41	0.85	0.0190	4.24	0.75	-0.0044	5.06	0.87	-0.0063	4.72	0.55
iC_4	151	0	6.39	2.11	0	6.42	2.16	0	5.66	1.77	0	5.19	1.85
	377	0.0239	3.20	1.78	0.0250	3.33	1.86	0.0194	2.84	1.82	0.0094	3.17	1.74
nC_5	173	0	5.21	2.25	0	6.86	2.43	0	7.77	2.46	0	5.91	1.33
	449	0.0171	2.35	1.97	0.0241	2.24	1.62	0.0099	5.32	1.96	-0.0116	4.41	1.13
iC_5	344	0	6.43	6.77	0	6.80	7.14	0	6.55	6.69	0	6.05	6.32
	410	-0.0078	5.39	6.65	-0.0056	6.30	7.01	0.0089	5.22	6.57	0.0058	5.37	6.20
nC_6	138	0	11.42	0.89	0	13.69	0.80	0	12.46	0.58	0	10.83	0.65
	444	0.0233	5.43	0.82	0.0302	5.33	0.71	0.0121	6.52	0.47	0.0095	5.39	0.52
nC_7	183	0	11.45	1.24	0	12.02	1.17	0	9.49	1.08	0	8.59	0.65
	511	0.0303	7.58	0.68	0.0371	7.65	0.64	0.0184	5.61	0.81	-0.0068	5.20	0.71
nC_8	223	0	13.68	0.79	0	14.45	0.79	0	11.87	0.74	0	10.63	0.74
	423	0.0441	4.09	0.47	0.0489	4.26	0.47	0.0143	4.827	0.41	0.0086	4.69	0.42
nC_9	223	0	14.57	0.44	0	16.82	0.45	0	12.34	0.43	0	9.69	0.45
	423	0.0421	3.14	0.34	0.046	3.26	0.35	0.0141	4.017	0.29	0.0083	3.92	0.30
nC_{10}	244	0	8.64	1.11	0	9.44	0.97	0	8.84	1.04	0	8.52	0.86
	583	0.0358	4.42	1.03	0.0406	4.25	0.94	0.0186	3.927	0.85	-0.0284	3.90	0.89
nC_{12}	323	0	15.05	-	0	15.59	-	0	10.19	-	0	9.12	-
	373	0.0223	7.09	-	0.0255	6.94	-	0.0208	5.467	-	-0.0303	5.09	-
nC_{14}	295	0	15.48	-	0	15.72	-	0	13.717	-	0	15.15	-
	448	0.0312	3.47	-	0.0333	3.45	-	0.0223	4.027	-	-0.0340	5.44	-
nC_{16}	270	0	14.65	-	0	14.99	-	0	14.367	-	0	16.28	-
	623	0.0423	5.81	-	0.0487	5.77	-	0.0195	4.237	-	-0.0414	5.80	-
nC_{18}	323	0	6.97	-	0	7.14	-	0	7.737	-	0	8.13	-
	448	-0.0076	5.64	-	-0.0088	5.69	-	0.0196	4.157	-	-0.0341	4.92	-
nC_{20}	313	0	14.45	-	0	14.61	-	0	11.27	-	0	18.37	-
	573	-0.0281	7.40	-	-0.0303	7.16	-	0.0180	4.777	-	-0.0373	5.46	-
nC_{24}	318	0	27.65	-	0	27.69	-	0	27.01	-	0	29.39	-
	455	0.0612	9.86	-	0.0593	10.47	-	0.0369	5.20	-	-0.0613	8.14	-
nC_{32}	343	0	6.89	-	0	6.59	-	0	8.57	-	0	19.944	-
	343	-0.0290	2.91	-	-0.0318	2.78	-	0.0255	2.69	-	-0.0509	2.694	-
H_2S	188	0	15.39	5.86	0	15.98	5.96	0	14.02	4.94	0	13.67	5.41
	367	0.0769	4.96	2.34	0.0841	4.82	2.30	0.0386	4.63	2.08	0.0314	4.83	2.28
N_2	100	0	8.19	1.85	0	8.44	1.82	0	8.48	1.92	0	10.604	3.17
	199	0.0293	2.56	1.42	0.0305	2.38	1.17	0.0263	2.16	1.25	0.0457	3.57	2.53
Ar	105	0	6.08	8.74	0	5.69	8.48	0	8.04	9.14	0	4.68	8.85
	178	0.0277	2.32	5.36	0.0268	2.60	4.49	0.0263	5.92	6.71	-0.0063	3.27	5.90
SO_2	241	0	50.82	7.12	0	54.89	8.46	0	30.45	6.13	0	5.82	1.95
	301	0.1282	5.74	0.77	0.136586	5.16	0.79	0.058617	8.65	3.21	0.0026	5.29	1.73
CO	105	0	5.71	3.82	0	6.08	4.19	0	9.23	4.54	0	5.49	6.34
	186	0.0211	2.35	3.76	0.0232	2.33	3.44	0.0318	3.86	4.25	0.0083	3.09	4.41
Benzene	270	0	9.34	4.45	0	12.95	4.14	0	14.57	2.99	0	9.09	3.09
	501	0.0284	5.35	4.15	0.0409	5.37	3.67	0.0160	8.50	3.10	-0.0249	5.00	3.33
Toluene	233	0	21.62	5.18	0	25.16	5.28	0	17.57	5.63	0	21.41	1.72
	543	0.0511	8.84	4.61	0.059	9.65	4.37	0.0344	8.45	4.19	-0.0435	8.82	2.61

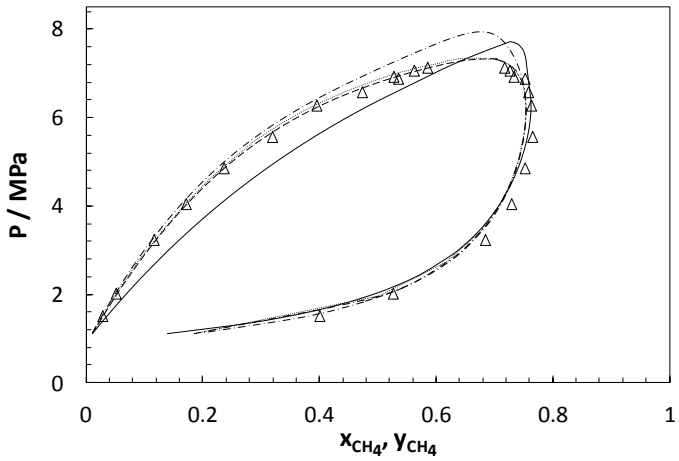

Figure 4.9. Pressure–composition diagram of the CH_4 + CO_2 system at 230K. Comparison between experimental data (△) [177] **and phase equilibrium calculated by SRK (dashed lines), PR (dotted line), PC-SAFT (continuous line) and SAFT-VR Mie (dot-dashed line) EoS using regressed k_{ij}.**

In Table 4.7, the results for the C_2H_6 + Comp2 systems are reported. One can observe that the lowest deviations between predicted (k_{ij} =0) and experimental VLE data of these binary systems containing ethane were obtained in general with CEoS. It is worth noting the high deviation in the vapour-phase composition for ethane + gases binary systems reported by all the models, with AADs around 21% for predicted and 12% for calculated Δy_1. Such high deviations in the vapour composition may be explained by the low miscibility of ethane in the vapour phases which leads to high relative errors, as depicted for example for the C_2H_6 + Ar system in Figure 4.10.

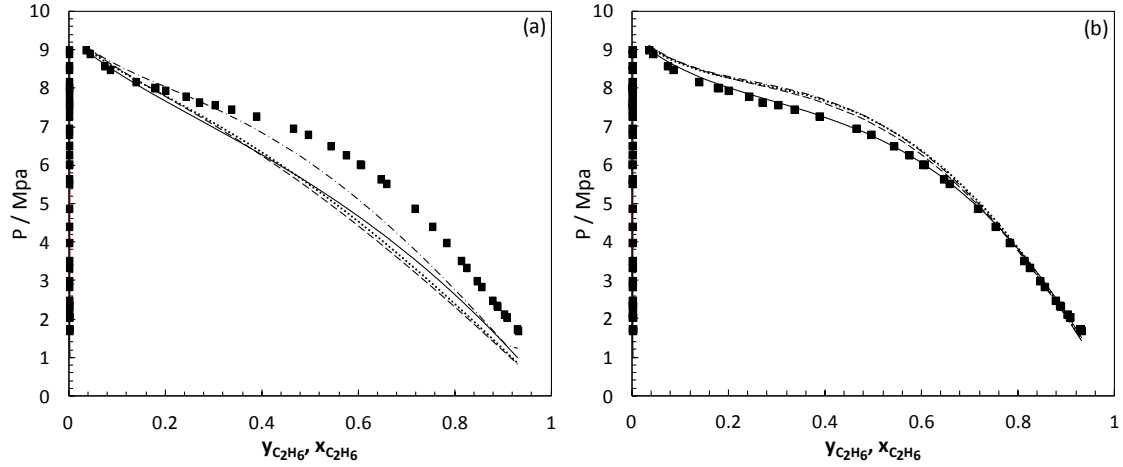

Figure 4.10. Pressure–composition diagrams of the C_2H_6 + Ar system at 116K. Experimental data (■) [178]**. The SRK (dashed lines), PR (dotted line), PC-SAFT (continuous line) and SAFT-VR Mie (dot-dashed line) EoS with k_{ij} =0 (a) and with regressed k_{ij} (b).**

Table 4.7. Average absolute deviations (%AAD) in predictions (k_{ij}=0) and calculations (using regressed k_{ij}'s) of bubble pressure (ΔP^{bubble}) and vapour phase composition (Δy_1) of C_2H_6 + Comp2 binary systems with the SRK, PR, PC-SAFT and SAFT-VR Mie EoS.

Comp2	T_{range} [K]	SRK			PR			PCSAFT			SAFT-VR Mie		
		k_{ij}	ΔP	Δy_1	k_{ij}	ΔP	Δy_1	k_{ij}	ΔP	Δy_1	k_{ij}	ΔP	Δy_1
CO_2	207	0	15.31	6.39	0	15.75	6.35	0	14.61	6.88	0	13.22	7.56
	298	0.1359	3.16	2.16	0.1278	3.18	2.26	0.0650	2.93	2.74	0.0537	2.12	2.32
C_1	130	0	1.73	1.26	0	1.67	1.17	0	6.13	3.81	0	3.62	2.01
	283	-0.0029	1.69	1.24	0.0012	1.54	1.14	0.0121	3.28	3.35	0.0007	3.40	1.96
C_3	127	0	4.09	2.64	0	2.65	2.76	0	3.34	3.01	0	2.64	2.71
	370	-0.0059	2.65	2.80	-0.0055	2.52	2.78	-0.0046	3.04	2.76	-0.0018	2.50	2.72
nC_4	235	0	8.29	1.96	0	3.39	1.97	0	3.63	1.96	0	3.33	3.07
	416	0.0077	4.22	2.06	0.0079	2.94	2.18	-0.0064	3.27	1.98	-0.0049	2.98	2.76
iC_4	203	0	3.61	5.62	0	2.87	5.59	0	2.37	3.23	0	2.71	3.03
	394	-0.0079	2.95	5.00	-0.0065	2.32	5.27	-0.0010	2.19	3.16	-0.0038	3.02	3.13
nC_5	278	0	2.70	2.79	0	3.00	2.63	0	2.93	2.61	0	2.87	2.53
	450	0.0086	2.24	2.52	0.0094	2.16	2.38	-0.0049	2.18	1.93	-0.0036	2.10	1.88
nC_6	298	0	6.40	3.35	0	6.31	3.33	0	7.47	3.85	0	9.74	3.43
	450	-0.0091	5.65	3.39	-0.0062	5.55	3.37	-0.0108	5.62	3.13	-0.0183	5.34	2.56
nC_7	235	0	2.67	1.01	0	2.76	1.24	0	3.18	1.11	0	4.70	1.15
	500	0.0058	2.69	0.99	0.0065	2.58	1.18	0.0035	2.89	0.95	-0.0158	2.55	0.74
nC_8	273	0	4.76	0.59	0	5.40	0.56	0	3.65	0.63	0	2.31	0.62
	373	-0.0170	1.88	0.60	-0.0184	1.78	0.59	-0.0041	2.84	0.60	-0.0016	1.92	0.62
nC_{10}	277	0	3.96	0.96	0	3.88	1.11	0	9.61	1.90	0	8.17	1.14
	511	0.0159	3.36	0.92	0.0143	3.27	1.08	0.0213	3.32	1.01	-0.0134	3.16	0.92
nC_{12}	298	0	4.41	-	0	4.50	-	0	17.26	-	0	19.67	-
	373	0.0058	3.87	-	0.0059	3.91	-	0.0176	3.90	-	-0.0228	3.74	-
nC_{14}	323	0	2.29	-	0	2.14	-	0	15.20	-	0	13.33	-
	423	0.0044	1.98	-	0.0025	1.99	-	0.0228	2.31	-	-0.0182	1.89	-
nC_{16}	262	0	5.76	-	0	7.77	-	0	18.65	-	0	20.66	-
	514	0.0059	5.50	-	0.0049	7.35	-	0.0194	5.47	-	-0.0275	5.28	-
nC_{18}	323	0	4.43	-	0	4.97	-	0	16.84	-	0	35.94	-
	423	0.0010	4.40	-	0.0052	4.63	-	0.0243	3.29	-	-0.0361	3.39	-
nC_{20}	308	0	9.11	-	0	10.16	-	0	13.36	-	0	36.15	-
	572	-0.0164	7.87	-	-0.0200	7.90	-	0.0137	5.42	-	-0.0478	3.29	-
nC_{24}	300	0	12.76	-	0	13.21	-	0	11.69	-	0	29.63	-
	368	-0.0313	5.75	-	-0.0337	5.73	-	-0.0068	7.26	-	-0.0626	8.86	-
H_2S	188	0	14.67	5.90	0	14.72	6.13	0	14.50	5.92	0	13.97	4.78
	358	0.0871	4.73	3.27	0.0838	4.76	3.23	0.0645	4.49	3.67	0.0506	4.72	3.84
N_2	110	0	7.08	11.20	0	8.71	11.74	0	8.48	9.78	0	3.29	9.45
	297	0.0345	3.10	8.17	0.0386	3.49	6.49	0.0412	3.31	6.07	0.0086	3.15	6.95
Ar	103	0	23.73	44.65	0	25.41	68.07	0	20.38	44.77	0	16.07	37.76
	116	0.0512	4.67	12.33	0.0547	4.31	27.82	0.0304	1.99	18.63	0.0253	5.04	16.77
CO	100	0	6.82	32.54	0	8.05	28.04	0	13.36	36.39	0	10.61	33.52
	248	0.0063	6.63	31.84	0.0178	6.44	25.17	0.0124	9.35	30.26	0.0086	6.67	26.36
Benzene	273	0	6.94	2.96	0	8.32	2.98	0	9.78	5.15	0	3.85	1.88
	553	0.0423	3.60	2.59	0.0321	2.08	2.22	0.0198	2.44	2.26	-0.0011	3.84	1.87
Toluene	373	0	7.55	3.67	0	8.35	3.46	0	8.73	3.78	0	8.01	2.61
	473	0.0088	6.92	3.46	0.0292	7.70	2.73	-0.0007	7.33	3.31	-0.0109	5.69	3.46

The SAFT-VR Mie EoS is the best model for predicting the VLE of nitrogen + Comp2 binary mixtures; however, these mixtures are the only systems which, on average, are better predicted by the cubic equations of state using the regressed BIP (Table 4.8). An example which illustrates this is the phase equilibria of the N_2 + H_2S system performed in Figure 4.11, where it can be seen that the SAFT-VR Mie model better predicts the VLE data, although, by using regressed k_{ij} values, the PR EoS describes this system slightly better than the SAFT-like EoS.

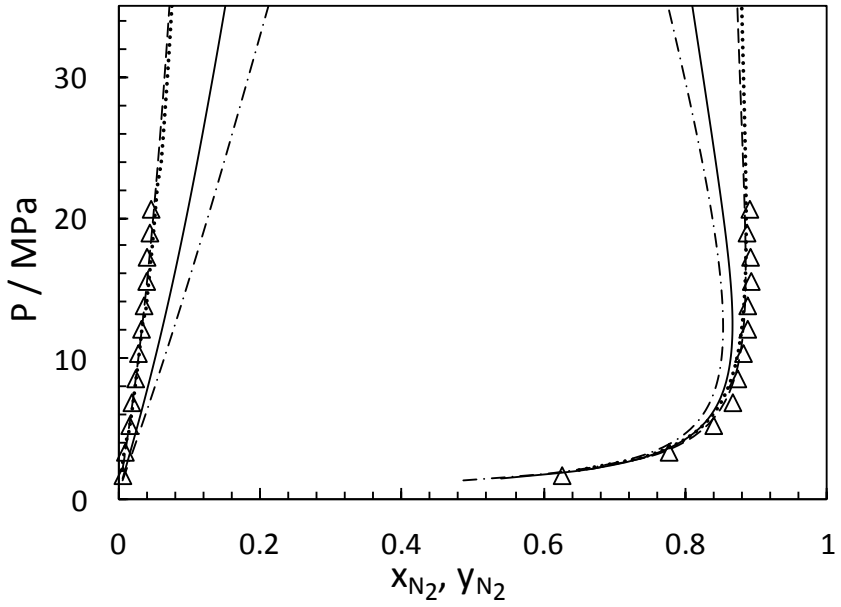

Figure 4.11. Pressure–composition diagram of the N_2 + H_2S system at 256K. Comparison between experimental data (△) [179]**, the SAFT-VR Mie EoS with k_{ij} =0 (continuous line) and with regressed k_{ij} (dashed lines) and the PR EoS with k_{ij} =0 (dot-dashed line) and with regressed k_{ij} (dotted line).**

Finally, the VLE results of modelling the H_2S + Comp2 binary systems are reported in Table 4.9. The PC-SAFT EoS reports higher deviations than the other EoSs for the systems that contain H_2S. As with the previously presented CO_2, methane and ethane mixtures, the model that better performs for hydrogen sulphide binary systems is the SAFT-VR Mie EoS. Hydrogen sulphide was modelled as a non-associating molecule and the results from the SAFT-based EoSs are in agreement with VLE data of the H_2S + Comp2 systems, although better results are expected when modelling the H_2S as an associating compound.

Table 4.8. Average absolute deviations (%AAD) in predictions (k_{ij}=0) and calculations (using regressed k_{ij}'s) of bubble pressure (ΔP^{bubble}) and vapour phase composition (Δy_1) of N_2 + Comp2 binary systems with the SRK, PR, PC-SAFT and SAFT-VR Mie EoS.

Comp2	T_{range} [K]	SRK			PR			PCSAFT			SAFT-VR Mie		
		k_{ij}	ΔP	Δy_1	k_{ij}	ΔP	Δy_1	k_{ij}	ΔP	Δy_1	k_{ij}	ΔP	Δy_1
CO_2	218	0	5.47	3.56	0	3.86	2.92	0	6.02	2.27	0	22.26	8.28
	301	-0.0245	2.86	3.63	-0.0192	3.05	3.10	-0.0079	4.89	1.91	-0.1083	6.22	2.85
C_1	100	0	8.16	1.85	0	8.38	1.80	0	8.57	1.94	0	10.55	3.19
	199	0.0293	2.53	1.42	0.0305	2.32	1.15	0.0263	2.25	1.27	0.0457	3.52	2.55
C_2	110	0	7.08	11.20	0	8.71	11.74	0	8.48	9.78	0	3.21	9.45
	297	0.0345	3.10	8.17	0.0386	3.49	6.49	0.0412	3.31	6.07	0.0086	3.06	6.95
C_3	114	0	13.61	3.62	0	14.03	3.57	0	13.18	3.68	0	12.29	4.12
	353	0.0766	7.88	1.36	0.0790	7.76	1.29	0.0588	7.59	1.11	0.0205	7.53	2.27
nC_4	239	0	16.41	3.54	0	16.65	3.49	0	17.26	3.28	0	16.25	4.86
	421	0.0858	7.05	2.98	0.0813	6.84	2.75	0.0657	7.90	2.76	-0.0093	9.40	3.10
iC_4	120	0	17.22	3.87	0	18.76	4.08	0	16.92	4.36	0	10.04	6.45
	394	0.0956	6.19	1.96	0.0971	6.10	1.93	0.0696	6.09	1.89	0.0197	5.79	6.56
nC_5	277	0	14.85	2.51	0	16.43	2.87	0	18.50	3.43	0	12.62	2.90
	447	0.0912	5.94	1.33	0.0964	5.92	1.26	0.0650	6.35	1.87	-0.0074	6.13	1.85
iC_5	277	0	15.60	3.06	0	17.14	3.24	0	21.09	5.88	0	19.99	6.02
	377	0.0944	5.76	1.94	0.0967	5.62	1.91	0.0706	5.58	2.06	0.0132	7.85	2.17
nC_6	233	0	23.50	1.54	0	26.36	1.34	0	28.60	2.24	0	8.21	1.93
	498	0.118	8.36	1.73	0.1295	7.21	1.35	0.0894	6.83	1.58	-0.0125	5.34	1.00
nC_7	251	0	25.22	4.86	0	25.80	5.33	0	22.69	5.98	0	11.65	5.13
	523	0.1311	8.47	2.71	0.1356	7.92	2.59	0.0841	6.89	2.32	-0.0150	6.97	2.10
nC_8	233	0	27.09	5.10	0	27.36	5.25	0	25.63	6.18	0	25.64	6.24
	543	0.1893	5.37	3.74	0.1888	5.24	3.27	0.0893	5.30	4.85	-0.0186	7.46	4.61
nC_9	261	0	23.39	4.01	0	25.63	2.82	0	29.06	3.86	0	7.92	4.25
	543	0.1829	7.61	5.00	0.1854	6.07	3.76	0.1344	6.48	3.74	-0.01455	4.96	4.09
nC_{10}	263	0	18.21	0.18	0	21.79	0.19	0	30.15	0.22	0	29.33	0.42
	563	0.1006	4.92	0.17	0.1118	4.66	0.16	0.1034	5.78	0.26	-0.0497	4.21	0.44
nC_{12}	298	0	18.68	-	0	19.20	-	0	31.05	-	0	24.99	-
	593	0.2106	5.24	-	0.196	3.59	-	0.1103	5.61	-	-0.0597	4.61	-
nC_{14}	298	0	36.04	-	0	38.21	-	0	41.46	-	0	13.56	-
	434	0.2079	8.73	-	0.1975	8.92	-	0.1543	8.14	-	-0.0209	6.83	-
nC_{16}	298	0	38.66	-	0	39.42	-	0	41.06	-	0	30.31	-
	703	0.2056	7.20	-	0.2002	7.45	-	0.1382	9.13	-	-0.0835	8.07	-
nC_{20}	323	0	26.58	-	0	27.87	-	0	33.07	-	0	31.44	-
	423	0.2226	3.99	-	0.2051	4.53	-	0.1634	7.64	-	-0.0967	8.32	-
H_2S	200	0	34.56	11.90	0	37.55	14.25	0	31.72	12.18	0	24.14	10.88
	344	0.1565	7.85	3.22	0.1738	5.49	2.80	0.1294	5.48	3.97	0.0708	5.28	2.97
O_2	100	0	4.46	2.68	0	4.21	2.20	0	3.61	1.86	0	3.65	3.09
	136	-0.0142	2.43	1.27	-0.0129	2.23	0.93	-0.0122	2.91	1.10	0.0025	1.80	2.28
Ar	100	0	2.53	1.10	0	2.32	0.89	0	1.96	1.87	0	3.56	2.86
	134	-0.0079	1.71	0.55	-0.0073	1.49	0.48	0.0028	1.74	1.76	-0.004	3.26	2.80
SO_2	241	0	14.95	9.99	0	18.14	11.47	0	12.23	12.67	0	11.78	15.07
	413	0.1156	5.95	6.34	0.1305	5.48	5.75	0.0237	6.90	6.33	0.0104	7.14	6.66
CO	100	0	1.58	10.90	0	1.61	10.82	0	2.27	11.75	0	2.32	11.42
	122	0.0059	1.77	11.15	0.0058	1.60	11.06	0.0064	1.97	10.86	0.0032	1.94	10.75
Benzene	288	0	36.63	0.73	0	43.00	0.62	0	44.04	0.79	0	26.16	0.55
	398	0.1721	6.36	1.09	0.1721	7.67	0.82	0.1302	6.36	1.09	0.0499	11.88	0.38
Toluene	313	0	12.39	9.25	0	14.34	10.26	0	12.39	9.25	0	11.41	4.83
	548	0.1632	10.37	7.49	0.1785	9.79	7.39	0.0965	11.37	7.49	0.0113	8.95	4.50

Table 4.9. Average absolute deviations (%AAD) in predictions (k_{ij}=0) and calculations (using regressed k_{ij}'s) of bubble pressure (ΔP^{bubble}) and vapour phase composition (Δy_1) of H_2S+ Comp2 binary systems with the SRK, PR, PC-SAFT and SAFT-VR Mie EoS.

Comp2	T_{range} [K]	SRK			PR			PCSAFT			SAFT-VR Mie		
		k_{ij}	ΔP	Δy_1	k_{ij}	ΔP	Δy_1	k_{ij}	ΔP	Δy_1	k_{ij}	ΔP	Δy_1
CO_2	218 301	0	12.23	4.88	0	12.94	4.95	0	14.13	5.36	0	13.86	5.23
		0.0984	1.38	1.06	0.0966	1.43	1.35	0.0618	1.68	0.95	0.0621	1.12	1.89
CH_4	100 199	0	15.36	5.86	0	15.92	5.94	0	14.03	4.96	0	13.71	5.43
		0.0769	4.93	2.34	0.0841	4.76	2.28	0.0386	4.64	2.10	0.0314	4.87	2.30
C_2	110 297	0	14.67	5.90	0	14.72	6.13	0	14.42	5.92	0	13.97	4.78
		0.0871	4.73	3.27	0.0838	4.76	3.23	0.0620	4.41	3.67	0.0506	4.72	3.84
C_3	114 353	0	15.67	4.73	0	15.80	4.69	0	15.07	4.53	0	12.54	4.61
		0.0866	4.49	1.98	0.0819	4.55	2.02	0.0576	4.70	1.77	0.0524	3.23	2.10
nC_4	239 421	0	16.20	4.61	0	16.07	4.72	0	14.08	4.59	0	11.38	4.36
		0.1046	2.52	2.05	0.0891	2.55	2.09	0.0538	2.23	1.83	0.0504	2.10	2.52
iC_4	120 394	0	8.86	3.13	0	8.77	3.04	0	8.62	2.94	0	9.11	3.49
		0.0631	2.39	1.84	0.0625	2.42	1.86	0.0513	2.27	1.81	0.0348	2.33	2.02
nC_5	277 447	0	13.83	4.28	0	13.61	4.32	0	13.29	4.16	0	14.54	4.79
		0.0700	3.74	2.86	0.0654	3.50	2.93	0.0464	2.85	2.58	0.0455	3.10	3.13
iC_5	277 377	0	9.74	4.23	0	9.83	4.10	0	9.68	4.17	0	9.67	4.36
		0.0763	4.23	2.13	0.0708	4.27	2.19	0.0480	3.86	1.94	0.0459	4.00	2.07
nC_6	233 498	0	12.40	1.76	0	11.58	1.71	0	11.73	1.60	0	10.77	1.59
		0.0690	2.20	0.69	0.0575	2.09	0.83	0.0407	2.88	0.57	0.0386	2.35	0.76
nC_7	251 523	0	16.31	2.20	0	15.96	2.05	0	14.23	1.64	0	14.50	1.95
		0.0736	5.84	1.38	0.0641	5.40	1.43	0.0482	5.28	1.21	0.0440	5.41	1.35
nC_9	233 543	0	16.45	1.39	0	13.47	1.17	0	9.30	1.20	0	3.47	1.27
		0.0517	2.49	0.89	0.0402	2.18	0.80	0.0193	4.12	0.76	0.0082	2.03	0.89
nC_{10}	261 543	0	15.85	0.22	0	13.14	0.32	0	18.53	0.39	0	19.59	0.45
		0.0496	5.30	0.25	0.0371	5.53	0.37	0.0390	4.79	0.22	0.0557	4.29	0.14
nC_{12}	263 563	0	5.28	-	0	4.77	-	0	24.75	-	0	20.92	-
		0.0244	4.13	-	0.0106	4.15	-	0.0358	6.76	-	0.0446	6.13	-
nC_{15}	298 593	0	8.45	-	0	8.31	-	0	14.66	-	0	15.06	-
		0.0097	7.86	-	-0.0094	7.92	-	0.0323	3.32	-	0.0376	1.63	-
nC_{20}	298 434	0	10.47	-	0	13.31	-	0	28.05	-	0	18.36	-
		-0.0201	5.47	-	-0.0373	5.88	-	0.0712	6.14	-	0.0429	5.78	-
N_2	200 344	0	34.56	11.90	0	37.55	14.25	0	31.72	12.18	0	24.14	10.88
		0.1565	7.85	3.22	0.1738	5.49	2.80	0.1294	5.48	3.97	0.0708	5.28	2.97
CO	100 136	0	24.51	25.50	0	30.03	36.62	0	18.57	32.96	0	19.36	20.29
		0.0664	8.80	11.36	0.0825	9.16	12.65	0.07648	8.71	15.85	0.0258	5.01	9.53
Benzene	288 398	0	2.93	0.58	0	2.81	0.33	0	9.85	1.02	0	3.46	0.30
		0.0038	2.38	0.45	0.0041	2.13	0.22	0.0107	7.06	1.11	0.0042	3.11	0.50
Toluene	313 548	0	4.47	1.59	0	4.15	1.63	0	10.25	0.99	0	7.01	1.67
		0.0047	4.39	1.50	0.0032	4.11	1.57	0.0121	7.60	1.01	0.0080	6.46	1.37

A summary of the VLE results is reported in Table 4.10. The deviation of each collection of mixtures is presented, divided into four groups: gases, alkanes, aromatics and average. The overall deviations of the four models are also provided in this table. It can be first concluded that the cubic equations of state and the SAFT models have comparable predictive capabilities (%AAD around 14% in ΔP^{bubble} and 5% in Δy_1) and similar results in VLE calculations using the regressed BIPs (approximately 4.8% in ΔP^{bubble} and 3.1% in Δy_1) were obtained for all models. Nevertheless, in general, the SAFT-VR Mie predicts (k_{ij}=0) and describes (using the fitted BIPs) the phase equilibria of the 108 binary systems slightly better than the other three studied EoSs. Focusing our attention on the groups of compounds, it can be highlighted that the SAFT-based EoSs allow for the lowest deviations on the description of systems containing alkanes, while both CEoS perform better for mixtures containing gaseous components as well as the aromatic compounds. If the two cubic models are compared, despite the high level of similarity, it can be concluded that, on average, the SRK EoS better predicts the phase behaviour of the studied systems with (k_{ij}=0)., while the PR EoS reports lower deviations on the VLE calculations, when $k_{ij}\neq 0$. In general, the PC-SAFT EoS leads to higher average deviations, especially for the mixtures with gases and aromatics. Nonetheless, as previously mentioned, the PC-SAFT model outperformed the CEoS for the systems containing alkanes. This is because the PC-SAFT EoS is a hard-chain reference fluid and the dispersive contribution to the Helmholtz free energy is fitted to the series of n-alkanes.

VLE calculations using the BIPs fitted to the literature data present substantial improvement, decreasing, on average, by around 65% the deviation on bubble point pressures and 40% on the vapour-phase composition. In order to continue comparing the equations of state, the BIPs have been used for studying statistically the results of the four models.

The average k_{ij}'s for the four EoSs have been calculated by averaging the regressed BIPs for all the binary systems. The CEoS present similar average k_{ij} around 0.068, while the SAFT-like EoSs give smaller values, around 0.045 for the PC-SAFT EoS and 0.031 for the SAFT-VR Mie EoS. The average k_{ij} can be an indicator of the predictive capability of the model for multicomponent systems. A small average k_{ij} implies that a smaller adjustment is necessary to tune it from the default state (k_{ij}=0) to the optimal value [180].

Table 4.10. Summary of the average absolute deviations (%AAD) in bubble pressure (ΔP^{bubble}) and vapour phase composition (Δy_1) predicted (k_{ij}=0) and calculated ($k_{ij}\neq0$) by the SRK, PR, PC-SAFT and SAFT-VR Mie EoS.

			SRK		PR		PC-SAFT		SAFT-VR Mie	
Comp1	Comp2		ΔP	Δy_1	ΔP	Δy_1	ΔP	Δy_1	ΔP	Δy_1
CO_2	Gases	$k_{ij}=0$	14.92	6.60	13.47	6.43	13.85	6.75	13.99	7.84
		$k_{ij}\neq0$	5.04	4.26	5.49	3.52	6.55	4.30	5.72	3.67
	Alkanes	$k_{ij}=0$	14.35	3.56	14.27	3.53	14.24	3.79	13.64	3.83
		$k_{ij}\neq0$	3.90	1.34	3.84	1.35	3.81	1.26	3.53	1.34
	Aromatics	$k_{ij}=0$	23.76	4.16	24.99	4.21	36.90	6.80	20.68	4.06
		$k_{ij}\neq0$	6.82	3.60	6.32	3.54	11.39	6.58	8.77	3.71
	Average	$k_{ij}=0$	15.13	4.23	14.89	4.18	15.79	4.68	14.21	4.66
		$k_{ij}\neq0$	4.32	2.15	4.31	2.00	4.84	2.40	4.29	2.04
CH_4	Gases	$k_{ij}=0$	16.85	5.07	17.70	5.39	13.26	4.99	5.86	4.66
		$k_{ij}\neq0$	3.15	2.68	3.01	2.35	4.80	3.56	3.49	3.47
	Alkanes	$k_{ij}=0$	10.05	1.62	10.67	1.65	9.64	1.70	10.24	1.36
		$k_{ij}\neq0$	4.61	1.44	4.60	1.42	4.16	1.53	4.48	1.28
	Aromatics	$k_{ij}=0$	15.48	4.81	19.06	4.71	16.07	4.31	15.25	2.40
		$k_{ij}\neq0$	7.09	4.38	7.51	4.02	8.48	3.65	6.91	2.97
	Average	$k_{ij}=0$	11.91	3.02	12.79	3.11	10.95	2.95	9.93	2.49
		$k_{ij}\neq0$	4.54	2.09	4.53	1.96	4.62	2.28	4.49	2.05
C_2H_6	Gases	$k_{ij}=0$	13.52	20.13	14.53	24.07	14.27	20.75	11.43	18.61
		$k_{ij}\neq0$	4.46	11.55	4.44	12.99	4.42	12.27	4.34	11.25
	Alkanes	$k_{ij}=0$	4.81	2.02	4.67	2.04	8.46	2.21	12.22	1.97
		$k_{ij}\neq0$	3.54	1.95	3.51	2.00	3.52	1.89	3.34	1.73
	Aromatics	$k_{ij}=0$	7.25	3.31	8.33	3.22	9.26	4.47	5.93	2.25
		$k_{ij}\neq0$	5.26	3.03	4.89	2.47	4.88	2.78	4.77	2.66
	Average	$k_{ij}=0$	6.92	7.50	7.13	8.66	9.79	7.93	11.50	6.90
		$k_{ij}\neq0$	3.89	4.90	3.83	5.29	3.83	5.05	3.68	4.64
N_2	Gases	$k_{ij}=0$	12.88	6.69	13.65	7.09	12.98	7.10	14.16	8.60
		$k_{ij}\neq0$	3.79	4.36	3.41	4.02	4.50	4.32	4.85	4.72
	Alkanes	$k_{ij}=0$	19.43	3.49	20.69	3.52	22.75	3.91	15.77	4.23
		$k_{ij}\neq0$	5.79	2.50	5.51	2.15	5.93	2.29	5.89	2.90
	Aromatics	$k_{ij}=0$	24.51	4.99	28.67	5.44	28.21	5.02	18.79	2.69
		$k_{ij}\neq0$	8.36	4.29	8.73	4.10	8.86	4.29	10.41	2.44
	Average	$k_{ij}=0$	17.72	4.54	19.07	4.72	20.04	4.93	14.93	5.33
		$k_{ij}\neq0$	5.51	3.20	5.22	2.87	5.70	3.06	5.86	3.37
H_2S	Gases	$k_{ij}=0$	23.77	14.09	26.84	18.61	21.47	16.83	19.12	12.13
		$k_{ij}\neq0$	6.01	5.21	5.36	5.60	5.29	6.92	3.80	4.80
	Alkanes	$k_{ij}=0$	11.97	3.19	11.68	3.18	14.03	3.01	12.51	3.09
		$k_{ij}\neq0$	4.02	1.64	4.00	1.67	3.88	1.54	3.46	1.76
	Aromatics	$k_{ij}=0$	29.53	18.70	33.79	25.43	25.15	22.57	21.75	15.59
		$k_{ij}\neq0$	8.32	7.29	7.33	7.73	7.10	9.91	5.15	6.25
	Average	$k_{ij}=0$	12.91	4.87	13.14	5.65	14.75	5.21	12.77	4.44
		$k_{ij}\neq0$	4.26	2.19	4.11	2.27	4.44	2.43	3.65	2.20
Overall	Gases	$k_{ij}=0$	14.97	10.39	15.56	12.10	13.44	11.13	11.06	10.25
		$k_{ij}\neq0$	4.38	5.76	4.27	5.97	5.08	6.52	4.42	5.91
	Alkanes	$k_{ij}=0$	13.16	2.99	13.47	2.99	14.90	3.14	13.94	3.16
		$k_{ij}\neq0$	4.76	1.93	4.68	1.86	4.60	1.79	4.48	1.90
	Aromatics	$k_{ij}=0$	14.94	3.67	16.91	3.71	20.10	4.32	13.18	2.48
		$k_{ij}\neq0$	6.18	3.25	6.11	3.01	8.19	3.67	7.13	2.54
	Average	$k_{ij}=0$	13.68	4.92	14.19	5.36	15.10	5.29	13.31	4.85
		$k_{ij}\neq0$	4.82	3.05	4.73	3.03	5.03	3.21	4.71	2.98

A sensitivity analysis has been performed in order to understanding how much the %AAD decreases by the employment of the optimal k_{ij}. The sensitivities between predicted (*predic*) and calculated (*calc*) bubble pressure and vapour composition are calculated as

$$Sensitivity\ \Delta P^{bubble} = \frac{1}{N}\sum_{i=1}^{N}\left|\left(\Delta P_{calc} - \Delta P_{predic}\right)/k_{ij}\right| \tag{4.65}$$

$$Sensitivity\ \Delta y_1 = \frac{1}{N}\sum_{i=1}^{N}\left|\left(\Delta y_{calc} - \Delta y_{predic}\right)/k_{ij}\right| \tag{4.66}$$

The average sensitivities for the ΔP and Δy_1, as well as the average k_{ij}, are reported in Table 4.11. As it can be observed in this table, one can differentiate two levels of sensitivity between the CEoS and the SAFT-based EoS, being PC-SAFT and SAFT-VR Mie EoS twice more sensitive than PR and SRK models. For example, according to the average sensitivity, by modifying 0.1 the value of the k_{ij}, it changes the deviation on bubble point pressure in 1.4% for the CEoS, 2.7% for the PC-SAFT EoS and 2.9% for the SAFT-VR Mie EoS. It also important to note that there is no linear change between ΔP and k_{ij}, but in this work the sensitivity index is roughly well defined by our calculated average sensitivities [180].

Table 4.11. Average absolute binary interaction parameters and average sensitivities in the VLE calculations.

	SRK	PR	PC-SAFT	SAFT-VR Mie
$\left\|\overline{k_{ij}}\right\|$	0.0680	0.0677	0.0445	0.0313
Sensitivity in ΔP (%)	137.4	140	270.2	294.7
Sensitivity in Δy_1 (%)	24.5	28.7	52.1	76.9

4.2.3.2 Density calculations

The capabilities of the models to describe pure compound densities were first compared. 22 components from the 27 compounds that are presented in this work have been selected, dismissing the long-chain n-alkanes (longer than *n*-C_{12}) due to the unavailability of correlations of data for these compounds in the whole ranges of pressure and temperature. The pure compound density comparison is divided into saturated-liquid density and single-phase fluid density predictions ($PT\rho$).

First, the saturated-liquid densities of the studied compounds have been correlated by SRK, PR, PC-SAFT and SAFT-VR Mie EoS at 15 temperatures below $0.9T_r$. The deviations in the calculated liquid saturated densities are shown in Figure 4.12. On average, the SAFT-VR Mie EoS leads to AAD below 1%, slightly smaller than 1.4% for the PC-SAFT model and significantly smaller than the AAD of the CEoS, 6% for PR and 12% for SRK. The PR EoS better predicts the saturated-liquid density of CO_2, most alkanes and aromatic compounds than the SRK EoS, while the SRK EoS is more accurate for small molecules like CH_4, N_2, O_2, Ar and CO. The saturated density predictions of the CEoS are improved using the Peneloux volume correction, decreasing the AAD% to 4% for the PR+VC and 6% for the SRK+VC. The SAFT-based models require the use of experimental vapour pressure, saturated-liquid density and *PTρ* data to fit the molecular parameters; therefore it was evident that the SAFT-based EoS predicts saturated-liquid density better than the CEoS. Obviously, the SAFT-VR Mie EoS with 5 molecular parameters correlates the saturated properties with lower deviations than PC-SAFT with 3 parameters.

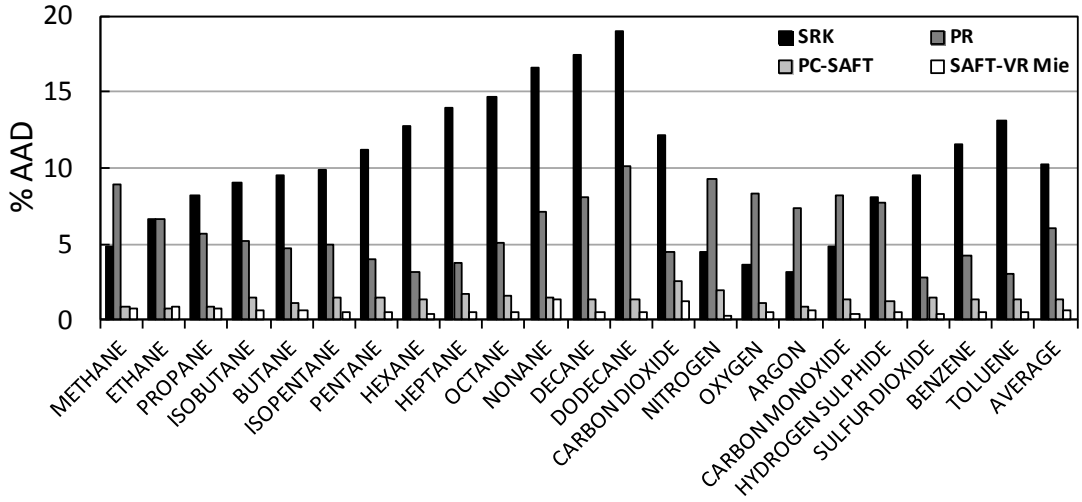

Figure 4.12. Deviations in the correlated saturated liquid density by SRK (black), PR (dark gray), PC-SAFT (light grey) and SAFT-VR Mie (white) EoS.

However, unlike the cubic models, the SAFT models do not reproduce well the critical point (CP), especially the critical pressure (P_c), and this leads to larger density deviations around the CP. Again, the SAFT-VR Mie EoS predicts comparatively better the critical point than the PC-SAFT model. An example of CP calculations is reported in Table 4.12 for CO_2. It can be observed that, as it is usual for SAFT-EoS, all the critical properties are overestimated by the PC-SAFT and SAFT-VR Mie EoS.

Table 4.12. Critical properties of CO_2 predicted with PC-SAFT and SAFT-VR Mie and comparison with experimental data.

Critical property	Exp [181]	PC-SAFT		SAFT-VR Mie	
		value	%AAD	Value	%AAD
T_c/K	304.1	309.4	1.73	307.2	0.99
P_c/MPa	7.38	7.92	7.32	7.81	5.43
ρ_c/kg·m^{-3}	467.6	482.5	3.19	473.1	1.18

For the single-phase densities (*PTρ*), 31928 densities of pure compounds from reliable correlations and multi-component EoSs [42] have been obtained. Thus, the *PTρ* data of the 22 components have been evaluated at 15 temperatures between 253 and 523K and pressures up to 150MPa, at gas, liquid or SC states depending on *P-T* conditions. The deviations of the density calculations are presented as %AAD, as well as the maximum average deviation (MAD%), i.e. the largest value in a set of absolute deviations. As it was mentioned, the use of volume corrections can improve density calculations of fluid dense phases.

In Table 4.13, the results of *PTρ* modelling with PC-SAFT, SAFT-VR Mie and the cubic EoSs with and without volume correction (VC) are reported. In general, the deviations are similar to the results of the correlated saturated-liquid densities; the SAFT-VR Mie EoS is the most accurate model for the predictions of *PTρ* (1.2% AAD), followed by the PC-SAFT (1.6% AAD), PR (6.7% AAD) and SRK (7.4% AAD) EoSs. By comparing the two cubic EoSs, it can be observed that the SRK EoS better predicts the densities of gas molecules and short-chain alkanes (until n-butane). However, the PR EoS provides better predictions for aromatics and longer alkanes. One can see a considerable improvement when cubic models are combined with the Peneloux volume translation, as expected, and deviations to experimental densities are reduced by more than 70%. The SRK+Peneloux and PR+Peneloux deviations are around 2% and these results are actually comparable to the deviations reported for SAFT-like EoS. However, it is worth mentioning that the maximum absolute deviation (%MAD) for the CEoS are much higher than the %MAD reported for the PC-SAFT and SAFT-VR Mie EoSs and, despite the use of the volume correction, gives better average results, in many cases the %MAD is slightly higher when applying the Peneloux-VC.

Table 4.13. Average (AAD%) and maximum (MAD%) absolute deviations in correlated single-phase fluid density by the SRK, SRK + Peneloux, PR, PR + Peneloux, PC-SAFT and SAFT-VR Mie models within 253-523 K and 0-150 MPa.

	SRK				PR				PC-SAFT		SAFT-VR Mie	
	without VC		with VC		without VC		with VC					
Components	AAD%	MAD%	AAD%	MAD%	AAD%	MAD%	AAD%	MAD%	AAD%	MAD%	AAD%	MAD%
C_1	1.28	6.08	1.26	6.17	7.09	11.90	0.92	3.79	1.45	2.48	0.95	1.94
C_2	2.37	15.13	1.71	15.90	7.82	11.64	2.54	10.72	1.98	4.05	0.41	6.26
C_3	4.19	20.17	2.33	18.06	7.54	12.42	3.07	14.40	1.88	13.77	0.53	6.69
iC_4	4.42	21.08	2.28	18.90	6.73	13.41	2.26	15.12	1.15	8.64	0.71	8.26
nC_4	5.66	15.59	2.12	16.30	6.37	10.46	2.15	11.72	1.71	5.70	0.95	6.85
iC_5	5.90	18.97	2.00	19.86	5.48	12.67	1.92	12.86	1.68	9.80	0.83	13.19
nC_5	7.85	20.61	2.18	20.79	4.73	14.60	2.17	15.47	1.36	15.31	0.96	14.02
nC_6	9.74	22.53	2.17	20.91	4.50	15.09	2.22	15.80	1.76	14.30	1.14	12.37
nC_7	11.66	20.94	2.14	16.52	4.81	11.97	2.16	12.39	1.93	8.31	1.38	9.80
nC_8	13.82	21.85	2.16	13.11	5.47	14.05	2.18	9.14	2.10	7.86	1.53	10.74
nC_9	15.95	24.02	2.20	10.37	7.16	16.63	2.15	7.57	2.45	8.19	1.66	9.31
nC_{10}	17.68	25.72	2.25	9.68	9.30	18.74	2.19	6.83	2.38	8.68	1.61	9.57
nC_{12}	19.83	27.96	2.37	7.90	12.89	21.38	2.28	5.65	2.44	9.63	1.74	10.09
CO_2	2.84	8.82	1.83	15.85	8.25	11.09	1.23	13.60	0.73	8.48	1.62	5.11
N_2	1.96	8.40	1.08	8.45	7.46	12.91	1.03	4.63	1.14	4.38	0.61	2.94
O_2	1.49	3.83	1.32	3.91	5.67	12.15	0.97	2.36	1.54	3.24	0.50	2.18
Ar	1.35	3.34	1.06	4.05	6.69	12.78	0.72	1.48	1.05	2.86	1.18	2.39
CO	2.05	3.93	1.11	4.82	7.27	13.21	0.99	1.90	1.90	4.31	0.84	1.77
H_2S	3.84	14.46	2.34	13.78	6.23	10.96	2.06	11.93	0.73	12.89	1.99	10.75
SO_2	8.01	21.27	3.86	17.05	1.63	13.53	2.62	14.65	1.99	10.81	1.71	8.60
Benzene	9.15	14.22	2.79	12.13	6.90	12.84	2.58	7.91	1.10	4.84	1.35	7.64
Toluene	11.72	15.70	2.83	10.41	6.75	11.57	2.47	8.28	0.97	2.96	1.26	8.11
Average	7.40	16.12	2.06	12.95	6.67	13.45	1.95	9.46	1.61	7.80	1.16	7.66

The second stage of the density calculations analysis is the modelling of binary systems. The experimental density data available for the studied mixtures are summarised in Table 2.1 and, as it can be seen, there are no data for many of the considered systems during the VLE analysis. Therefore, 26479 single phase density ($PT\rho x$) literature data were collected from NIST standard reference database [171], even though it is worth noting that the data used for the mixture with long-chain alkanes are saturated liquid density data points. The density data of 57 binary mixtures of CO_2, CH_4, C_2H_6, N_2 and H_2S with alkanes, gases and toluene were modelled with the SRK, PR, PC-SAFT and

SAFT-VR Mie equation of state, as well as using the Peneloux volume correction coupled with CEoS. The phase equilibria of all these binary systems were studied and are presented in the VLE section. Therefore, the previously reported BIP are used herein in order to avoid the wrong calculations of the two phase region during *PTρx* calculations.

The AAD in density calculations using the investigated EoS are reported in Tables 4.14-4.18. The number of data taken into consideration, the ranges of temperatures, pressures and compositions are presented in these tables, besides the average absolute deviations of the different investigated models.

Table 4.14. Deviation in calculated density of CO_2 + Comp2 systems by SRK, PR, PC-SAFT and SAFT-VR Mie with and without volume correction.

		Ranges						SRK		PR		PC-SAFT	SAFT-Mie
Comp2	No Data	T [K]		P [MPa]		x_{CO2}		no VC	VC	no VC	VC		
C_1	1312	219	673	0.1	100.0	0.10	0.90	3.76	2.67	4.11	2.62	3.08	2.57
C_2	1607	210	477	1.7	69.0	0.17	0.98	7.00	6.22	8.07	6.79	6.27	5.57
C_3	1269	294	510	2.5	70.6	0.03	0.98	4.57	4.12	7.31	3.51	4.12	2.93
iC_4	346	280	440	3	200.0	0.24	0.97	4.05	1.07	5.70	1.50	4.87	1.92
nC_4	345	280	440	0.4	200.0	0.01	0.97	3.88	2.25	5.14	1.10	2.87	2.17
nC_5	358	307	323	2.5	35.0	0.21	0.99	9.73	4.91	5.85	5.31	2.45	1.99
nC_6	176	308	313	6.3	12.5	0.05	0.98	8.17	5.10	6.74	5.39	3.18	2.83
nC_7	558	220	459	0.1	55.5	0.02	0.99	8.65	5.22	7.02	5.46	3.09	2.65
nC_8	24	308	308	12.0	35.0	0.93	0.97	3.91	1.63	3.33	1.95	3.80	2.43
nC_{10}	792	283	555	0.10	120.0	0.03	0.94	7.86	4.00	4.43	2.17	1.46	1.23
C_{14}*	40	323	344	1.0	6.0	0.10	0.99	12.00	5.01	12.51	2.60	1.63	1.90
C_{16}*	8	313	313	1.6	6.0	0.19	0.59	25.26	1.79	17.94	2.03	0.89	1.01
C_{20}*	60	310	373	0.5	7.6	0.04	0.68	21.48	8.64	19.42	6.32	0.92	1.10
H_2S	540	249	500	1.5	60.0	0.06	0.94	3.72	1.91	3.47	1.87	3.25	1.84
N_2	2034	225	673	4.0	800.0	0.10	0.99	9.34	3.67	10.67	3.58	3.50	2.98
O_2	230	273	383	4.0	20.0	0.85	0.95	5.37	3.92	6.16	3.84	3.14	2.28
CO	53	308	343	22.5	47.0	0.86	0.95	1.80	1.78	1.84	1.75	1.70	2.17
Ar	458	250	501	1	61.0	0.05	0.94	9.67	5.88	9.80	5.90	5.96	5.68
Toluene	360	291	423	1.1	67.1	0.12	0.90	8.08	5.76	7.91	6.32	8.12	7.17

* Only saturated-liquid density data

Table 4.15. Deviation in calculated density of CH_4 + Comp2 systems by SRK, PR, PC-SAFT and SAFT-VR Mie with and without volume correction.

Comp2	No Data	Ranges						SRK		PR		PC-SAFT	SAFT-Mie
		T [K]		P [MPa]		x_{CH4}		no VC	VC	no VC	VC		
C_2	833	100	394	0.1	35.8	0.10	0.92	4.90	4.09	4.98	3.81	3.42	2.60
C_3	2686	100	510	0.1	68.9	0.01	0.97	4.90	3.44	5.17	2.88	2.19	2.04
iC_4	136	100	256	0.1	16.5	0.18	0.94	5.86	1.75	5.68	2.96	0.76	0.64
nC_4	138	100	479	0.1	31.0	0.15	0.95	7.80	2.05	7.07	2.12	1.83	1.66
nC_5	580	310	511	2.7	34.5	0.03	0.93	6.94	2.61	7.36	2.53	2.24	2.00
nC_7	827	185	510	0.4	69.8	0.10	0.75	8.16	3.85	7.92	3.96	3.70	3.53
nC_{10}	922	293	444	0.1	140.0	0.09	0.96	7.91	3.69	7.33	3.73	3.66	3.60
C_{14}*	24	294	448	2.0	9.5	0.08	0.36	17.12	6.09	11.57	3.24	0.80	1.15
C_{18}*	24	323	448	1.9	8.7	0.08	0.36	21.37	7.36	16.3	6.52	0.87	1.15
C_{20}*	12	313	313	0.3	5.0	0.02	0.27	19.35	11.66	27.94	13.22	0.79	1.17
CO_2	1452	219	673	0.1	100	0.02	0.90	3.76	2.67	4.11	2.62	3.08	2.57
H_2S	1220	277	501	0.8	69.0	0.10	0.90	9.72	5.54	9.85	5.39	5.20	4.97
N_2	1868	100	673	0.1	138.0	0.01	0.99	2.32	1.85	2.97	1.27	2.14	0.90
CO	112	116	125	2.0	160.0	0.20	0.71	5.76	1.40	12.14	1.53	1.29	1.04
Ar	259	100	423	0.1	138	0.08	0.85	0.98	1.06	12.87	2.26	0.62	0.53
Toluene	392	185	373	0.1	140	0.04	0.95	5.80	3.27	5.90	3.12	1.84	1.27

* Only saturated-liquid density data

Table 4.16. Deviation in calculated density of C_2H_6 + Comp2 systems by SRK, PR, PC-SAFT and SAFT-VR Mie with and without volume correction.

Comp2	No Data	Ranges						SRK		PR		PC-SAFT	SAFT-Mie
		T [K]		P [MPa]		x_{C2H6}		no VC	VC	no VC	VC		
C_1	833	100	394	0.1	35.8	0.10	0.92	4.90	4.09	4.98	3.81	3.42	2.60
C_3	1462	102	400	1.5	34.6	0.01	0.95	7.27	4.31	5.13	3.66	0.80	0.64
iC_4*	6	115	130	0.0	0.0	0.69	0.72	6.09	3.58	5.31	5.22	0.45	1.06
nC_4	12	311	311	3.4	13.8	0.25	0.78	7.63	2.17	4.02	2.79	1.25	0.42
nC_5	57	309	309	3.1	7.1	0.68	0.99	13.39	9.05	10.51	7.30	2.13	2.62
nC_7	30	185	353	0.1	7.5	0.02	0.68	11.34	1.98	8.12	1.31	0.92	0.89
nC_{10}	1366	278	511	1.4	68.9	0.10	0.90	11.04	2.51	7.06	1.94	0.59	0.81
C_{16}*	29	313	353	4.7	10.4	0.88	0.99	24.60	18.44	19.90	18.10	11.74	12.14
C_{20}*	29	323	423	0.9	7.8	0.10	0.84	19.08	10.70	13.56	11.43	1.74	3.02
CO_2	1607	210	477	1.7	69.0	0.17	0.98	7.00	6.22	8.07	6.79	6.27	5.57
H_2S	357	254	363	1.6	21.5	0.02	0.96	6.09	3.05	5.08	3.35	2.93	1.96
N_2	373	113	477	2.0	62.0	0.25	0.99	3.49	2.17	2.82	1.69	1.47	0.58
CO	5	303	343	8.1	10.6	0.42	0.48	2.93	2.19	1.00	0.98	2.29	0.87

* Only saturated-liquid density data

Table 4.17. Deviation in calculated density of N_2 + Comp2 systems by SRK, PR, PC-SAFT and SAFT-VR Mie with and without volume correction.

Comp2	No Data	Ranges						SRK		PR		PC-SAFT	SAFT-Mie
		T [K]		P [MPa]		x_{N2}		no VC	VC	no VC	VC		
C_1	1868	100	673	0.1	138.0	0.01	0.99	2.32	1.85	2.97	1.27	2.14	0.90
C_2	373	113	477	2.0	62.0	0.01	0.75	3.49	2.17	2.82	1.69	1.47	0.58
C_3	23	399	422	8.6	42.1	0.01	0.83	8.89	7.92	12.35	8.72	7.79	6.72
nC_4	493	428	478	6.0	68.9	0.10	0.91	4.97	2.13	5.62	1.69	3.01	1.21
nC_8	144	293	373	25.0	100.0	0.79	0.79	10.12	3.66	2.37	1.12	0.83	0.66
nC_{10}	8	313	313	0.1	40.1	0.01	0.38	16.36	3.35	6.32	0.87	0.43	0.48
CO_2	2034	225	673	4.0	800.0	0.01	0.90	9.34	3.67	10.67	3.58	3.50	2.98
H_2S	47	293	373	10.3	24.1	0.78	0.91	1.45	0.92	2.62	0.65	2.06	0.78
O_2	2	100	100	0.1	0.1	0.68	0.82	3.31	1.10	9.53	2.02	1.81	0.98
Ar	565	100	423	2.7	800.0	0.16	0.80	1.37	1.00	3.43	0.96	1.18	0.92
CO	109	250	400	8.0	20.0	0.90	0.95	1.73	1.22	1.94	0.35	1.62	0.09

Table 4.18. Deviation in calculated density of H_2S + Comp2 systems by SRK, PR, PC-SAFT and SAFT-VR Mie with and without volume correction.

Comp2	No Data	Ranges						SRK		PR		PC-SAFT	SAFT-Mie
		T [K]		P [MPa]		x_{H2S}		no VC	VC	no VC	VC		
C_1	1220	277	501	0.8	69.0	0.10	0.90	9.72	5.54	9.85	5.39	5.20	4.97
C_2	357	254	363	1.6	21.5	0.04	0.98	6.09	3.15	5.08	3.35	2.93	1.96
C_3	135	263	363	4.354	34.7	0.27	0.90	9.15	6.24	7.31	6.00	8.33	5.35
nC_5	520	278	511	1.4	68.9	0.25	0.80	8.24	2.94	3.67	2.49	1.61	0.64
nC_{10}	481	278	444	1.40	69.0	0.23	0.81	19.66	3.65	10.01	5.54	3.30	3.08
CO_2	540	249	500	1.5	60.0	0.06	0.94	3.72	1.81	3.47	1.77	3.25	1.84
N_2	47	293	373	10.3	24.1	0.09	0.22	1.45	0.92	2.62	0.65	2.06	0.78
Toluene	116	373	501	9	65	0.92	0.92	7.93	6.71	7.13	7.02	8.21	8.42

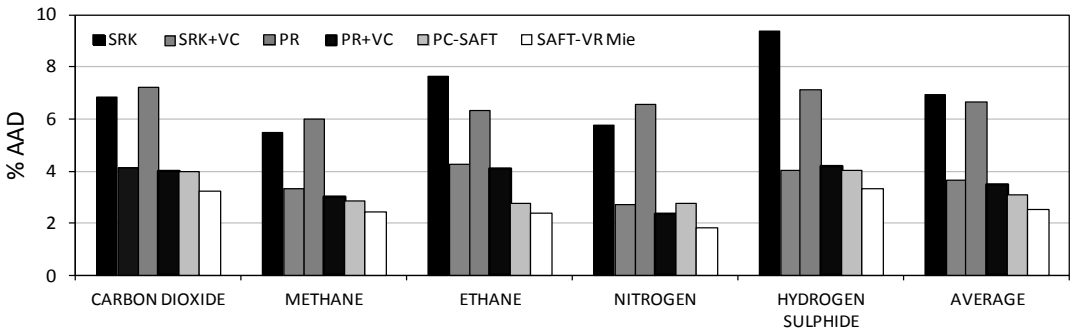

Figure 4.13. Deviations in the calculated density of binary systems of CO_2, CH_4, C_2H_6, N_2 and H_2S + Comp2 by SRK (black), SRK+Peneloux (diagonal grey lines), PR (dark gray), PR+Peneloux (vertical grey lines) PC-SAFT (light grey) and SAFT-VR Mie (white) EoS.

The average absolute deviations in density calculations of binary system are summarised in Figure 4.13. The models can be divided into three groups according to their level of agreement to the experimental data: SAFT-EoS (2.75% AAD), CEoS+VC (3.5% AAD) and CEoS without VC (6.75% AAD). In Figure 4.14 and 4.15, the densities of C_2H_6 + H_2S and CO_2 + H_2S systems are performed using one of each group of equations in order to illustrate the usual results comparing the density calculations from SAFT-EoS, CEoS+VC and CEoS.

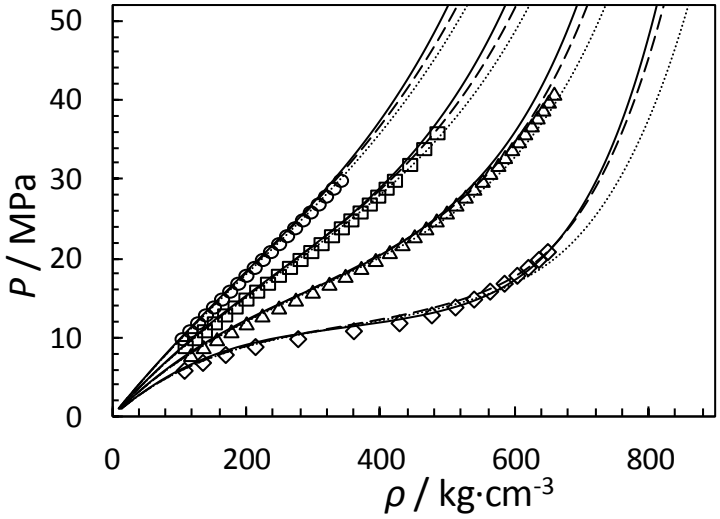

Figure 4.14. Experimental and calculated densities of the 0.514 mole CO_2 + 0.486 mole H_2S using SAFT-VR Mie (continuous lines), PR+Peneloux (dashed lines) and PR (dotted lines) EoS with the regressed k_{ij}. Symbols [182]**: (◇) 350K, (△) 400K, (□) 450K and (○) 500K.**

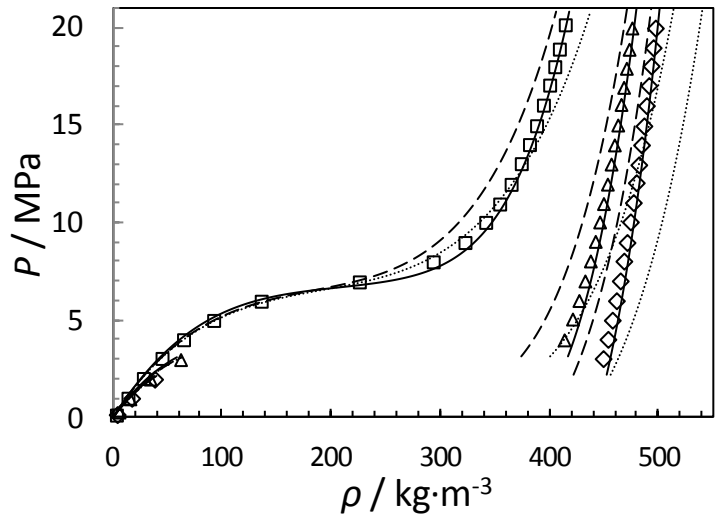

Figure 4.15. Experimental and calculated densities of the 0.857 mole C_2H_6 + 0.143 mole H_2S using SAFT-VR Mie (continuous lines), SRK+Peneloux (dashed lines) and SRK (dotted lines) EoS with the regressed k_{ij}. Symbols [20]**: (◇) 268K, (△) 283K and (□) 322K .**

The more precise models are the SAFT-based EoS; the SAFT-VR Mie EoS predicts densities with higher accuracy than the other investigated models for most of the studied systems. Nevertheless, the PC-SAFT model gives better density calculations for mixtures with long-chain alkanes, for example the saturated liquid density of the systems CO_2 + *n*-C_{20}, CH_4 + *n*-C_{20} and C_2H_6 + *n*-C_{20} are described with around 30% lower AAD than with the SAFT-VR Mie EoS. In a second level of accuracy, the CEoS coupled with the Peneloux volume translation report a little higher average deviation than the PC-SAFT model, indeed density calculations of the N_2 + Comp2 are better performed using the CEoS+VC than the PC-SAFT EoS (Figure 4.16).

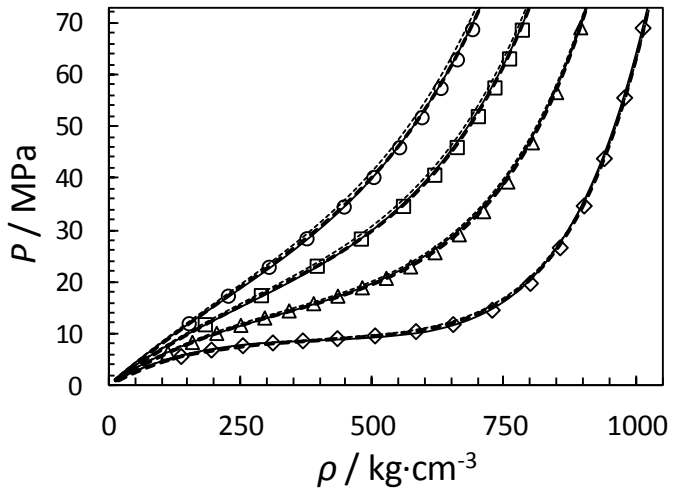

Figure 4.16. Experimental and calculated densities of the 0.9101 mole CO_2 + 0.0899 mole N_2 using PC-SAFT (continuous lines), SRK+Peneloux (dashed lines) and SRK EoS with the regressed k_{ij}. Symbols [183]**: (◇) 300K, (△) 350K, (□) 400K and (○) 450K.**

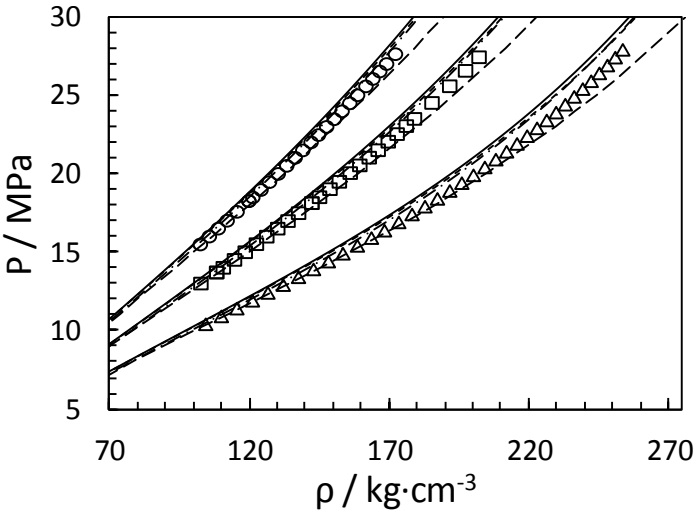

Figure 4.17. Experimental and calculated densities of the 0.8 mole CH_4 + 0.2 mole N_2 using SRK (continuous lines), SRK+Peneloux (dotted lines), PR (dashed lines) and PR+Peneloux (dot-dashed line) EoS with the regressed k_{ij}. Symbols [184]**: (△) 270K, (□) 313K and (○) 353K.**

Finally, the CEoS without the Peneloux volume translation (VC) present the lowest accuracy in density calculations; the AAD without VC almost doubles the deviations coupling the volume translation. Therefore, as obtained for pure compounds, the density calculations of binary mixtures with CEoS are significantly improved using the VC and both CEoS perform with similar accuracy. On the one hand, the PR EoS is on average slightly more accurate and it better predicts the densities of C_2H_6 and H_2S + Comp2 binary systems. On the other hand, the SRK EoS leads to better results for the CO_2, CH_4 and N_2 + Comp2 mixtures, as shown in Figure 4.17 for the CH_4 + N_2 system.

4.2.4 Remarks and conclusions

A comprehensible comparison has been made between the SRK, PR, PC-SAFT and SAFT-VR Mie EoSs in the scope of CCS. These models were used to describe both VLE and density data. The investigated equations of state have been used to predict the phase behaviour of 108 binary systems of typical components of flue gases and reservoir fluids. In general, the SAFT-VR Mie better predicts the VLE with an average deviation of 13.3% compared to the experimental data for equilibrium pressure, followed by the CEoS, with 13.7% for the SRK and 14.2% for the PR EoSs. Independent temperature binary interaction parameters (BIPs) have been regressed on the VLE data. Using fitted BIPs, the SAFT-VR Mie EoS is the most accurate model among the four, to correlate the phase equilibria of the investigated systems, with an AAD of 4.71%, slightly higher deviations are observed for PR (4.73%) and SRK (4.82%). The PC-SAFT EoS is the model which reports on average a little higher deviation (5.03%), however it is worth noting that the PC-SAFT model correlates the systems with alkanes better than CEoS. In addition, the SAFT-based EoSs are more sensitive to the variation of k_{ij} than the CEoS. Therefore, SAFT-like EoSs have better predictive capabilities as smaller k_{ij} are necessary. There is no big increase in accuracy between the correlations from CEoS and SAFT-EoS when the BIPs are used. Therefore, one may prefer to use a simpler and computationally faster CEoS when the BIPs can be optimized using available VLE data, or the more-complex SAFT-VR Mie EoS when we look for a high predictive capability, or when the predictions of derivative thermodynamic properties are important.

Both PC-SAFT and SAFT-VR Mie EoSs have shown higher accuracy than the SRK and PR models in density calculations of the 22 selected pure components. First, the

saturated-liquid density at temperatures below 0.9 T_r have been performed by the SAFT-VR Mie EoS with an average absolute deviation of 0.6%, while the PC-SAFT, PR and SRK models report, respectively, an AAD of 1.4%, 6.1% and 10.2%. Secondly, single-phase densities at 15 temperatures between 253 and 523 K and pressures up to 150 MPa were correlated by using the investigated models with different levels of agreement. Again, the SAFT-VR Mie EoS is the model that best correlates the *PTρ* data with an AAD of 1.2%. In order to improve the poor density predictions from the CEoS, the Peneloux volume translation were used with the SRK and PR models and the deviations in the density calculations were reduced by more than 70%.

Finally, the single-phase fluid densities of 57 binary systems were performed by the evaluated models using the temperature independent k_{ij} regressed in this work. In this part of the comparative study, the SAFT-VR Mie EoS leads to the lowest deviation in modelling the density of most of binary systems. On average, the deviations in the *PTρx* calculations of binary systems are AAD=2.7% for the SAFT-like EoSs, AAD=3.5% for the CEoS+VC and AAD=6.7% for the CEoS without VC.

In summary, the VLE and densities of the investigated systems were predicted with higher accuracy using the SAFT-VR Mie EoS, as it was expected. This is because of the higher complexity and flexibility (two extra parameters) of the model in comparison with CEoS and PC-SAFT. Although the computational time has not been evaluated quantitatively, it is remarkable to note that modelling with the SAFT-VR Mie model requires much longer computational time than the CEoS. Despite the differences between the SRK, PR, PC-SAFT and SAFT-VR Mie equations of state, it can be concluded that the investigated models are accurate enough for PVT modelling of fluids related to carbon capture. The comparison may be completed by further studies with associative compounds (*i.e.* water) also related to CCS, other associating models (for example CPA) and more thermophysical properties (c_p, speed of sound or IFT).

4.3 SAFT-γ Mie

A popular approach to increase the predictive capability of a thermodynamic methodology is its formulation within a group contribution (GC) approach [185]. The SAFT-γ Mie EoS is a GC approach of the SAFT-VR Mie EoS, therefore SAFT-γ model is also characterised by Mie interactions between the segments. This generalization was

formulated by Papaioannou et al. [141] and, basically, the GC approach represents the molecules as associating heteronuclear chains of fused spherical segments of various chemical groups [186].

4.3.1 Modelling aspects and approach

The GC approach is based on the decomposition of molecules into functional groups and the prediction of thermophysical properties from the properties attributable to the given groups [157]. For the SAFT-γ Mie EoS, each functional group (*k*) is represented by one segment or number of segments (v_k^*), and according to the Mie potential the adjusted parameters to each functional groups are the diameter of the segment (σ_k), the depth of the potential (ε_k) and the attractive (λ_k^a) and repulsive (λ_k^r) exponents. Besides, the size of the segment is defined by the shape factor S_k. This parameter reflects the proportional contribution from the functional group *k* to the total Helmholtz free energy [186].

In the SAFT-VR Mie EoS, each molecule *i* is directly represented by a number of segments m_i of size σ_i and energy ε_k. However, in the framework of the SAFT-γ approach, in addition to the segment parameters, the factor $v_{k,i}$ is the number of the same group *k* on compound *i*, necessary to build the molecule.

The SAFT- γ Mie formulation is analogous to the previously presented for the SAFT-VR Mie EoS. Nevertheless, there are significant differences in the general equations between both EoSs, basically because the number of segment m_s must be replaced by the $v_{k,i}$, v_k^* and S_k parameters. First, the segment number density ρ_s presented in Eq. 4.6 is reformulated as:

$$\rho_s = \rho\left(\sum_{i=1}^{N_C} x_i \sum_{k=1}^{N_G} v_{k,i} v_k^* S_k\right) \tag{4.67}$$

where N_C and N_G are the number of components and type of groups respectively.

Second, regarding the monomer contribution, the terms a_1, a_2 and a_3 of the thermal expansion are calculated by:

$$a_n = \sum_{k=1}^{N_G}\sum_{l=1}^{N_G} x_{s,k}\, x_{s,l}\, a_{n,kl} \qquad n = 1,2,3 \tag{4.68}$$

where $x_{s,k}$ and $x_{s,l}$ are the fractions of segments of a group of type k or l. These segment fractions are defined as:

$$x_{s,k} = \frac{\sum_{i=1}^{N_C} x_i \, v_{k,i} v_k^* S_k}{\sum_{j=1}^{N_C} x_j \sum_{l=1}^{N_G} v_{l,j} v_l^* S_l} \tag{4.69}$$

The segment fraction is also used to calculate the packing fraction ξ_x of a hypothetical pure fluid of diameter d_x [141]:

$$d_x^3 = \sum_{k=1}^{N_G} \sum_{l=1}^{N_G} x_{s,k} \, x_{s,l} \, d_{kl}^3 \tag{4.70}$$

$$\zeta_x = \frac{\pi \rho_s}{6} d_x^3 \tag{4.71}$$

Finally, in order to calculate the chain contribution, the concept of average molecular parameters is introduced. This is because the chain contribution is evaluated through the radial distribution function at distance between molecules. To calculate the average parameters, the molecular fraction $z_{k,i}$ of a given group k on a molecule i is first estimated by

$$z_{k,i} = \frac{v_{k,i} v_k^* S_k}{\sum_{l=1}^{N_G} v_{l,j} v_l^* S_l} \tag{4.72}$$

It is noteworthy that the molecular fraction $z_{k,i}$, quantity independent of the compositions of the mixture, must not be confused with the fraction $x_{s,k}$, which instead is composition-dependent [141].

Then, the effective diameter and the average molecular segment parameters of each component are obtained as

$$\overline{d}_{ii}^3 = \sum_{k=1}^{N_G} \sum_{l=1}^{N_G} z_{k,i} \, z_{l,i} \, d_{kl}^3 \tag{4.73}$$

$$\overline{\sigma}_{ii}^3 = \sum_{k=1}^{N_G} \sum_{l=1}^{N_G} z_{k,i} \, z_{l,i} \, \sigma_{kl}^3 \tag{4.74}$$

$$\bar{\varepsilon}_{kl} = \sum_{k=1}^{N_G} \sum_{l=1}^{N_G} z_{k,i}\, z_{l,i}\, \varepsilon_{kl} \tag{4.75}$$

$$\bar{\lambda}_{kl} = \sum_{k=1}^{N_G} \sum_{l=1}^{N_G} z_{k,i}\, z_{l,i}\, \lambda_{kl} \tag{4.76}$$

The chain contribution for the SAFT- γ Mie is calculated by reformulating the Eq. 4.39 as follows:

$$a^{CHAIN} = -\sum_{i=1}^{N_C} x_i \sum_{k=1}^{N_G} \left(\nu_{k,i} \nu_k^* S_k - 1\right) \ln g_{ii}^{Mie} \tag{4.77}$$

where g_{ii}^{Mie} is the RDF of the hypothetical one-fluid Mie system [141]. The value of the RDF is calculated using the average molecular parameters with the same equation used for the SAFT-VR Mie EoS (Eqs. 4.40-4.50).

Within SAFT-like EoS and group contribution methods, the parameters of the functional groups are typically estimated from experimental data [157]. Thus, SAFT- γ Mie parameters of the functional groups (*e.g.* methyl-CH_3, methylene-CH_2, etc) are fitted to the experimental data of a series of compounds that contain such groups [185]. Parameters for several chemical families have been fitted by Papaionau et al. [141] and Dufal et al. [186], linear and branched alkanes (CH_3, CH_2, CH, and C functional groups), linear and branched alkylbenzenes (aCH, aCCH_2, and aCCH groups), alkenes (CH_2,and CH groups), esters (COO group) and carboxylic acids (COOH group).

4.3.2 SAFT-γ Mie modelling results

In order to validate the developed code, pure-components have been first modelled using the parameters fitted by Papaioannou *et al.* [141]. Taking into account the compounds studied in the present work, the saturation properties of 10 *n*-alkanes, from ethane to dodecane have been predicted using the SAFT-γ Mie equation of state. For the chemical family of the *n*-alkanes, the SAFT-γ Mie EoS requires the parameters for only two functional groups: methyl (CH_3) and the methylene (CH_2).

Likewise, the SAFT-VR Mie EoS, five physical parameters are required: S_k (shape factor), σ, ε, λ_r and λ_a. These parameters are reported above in Table 4.19.

Table 4.19. Group parameters for the methyl and methylene functional groups [141]**.**

Functional group	S_k	λ^r_{kk}	λ^a_{kk}	σ_{kk}	ε_{kk}
Methyl (CH_3)	0.57255	15.050	6	4.0772	256.77
Methylene (CH_2)	0.22932	19.871	6	4.8801	473.39

In the SAFT- γ VR Mie EoS, the number of segments is defined by v_k^* and it is usually fixed to one, although molecular groups for individual species can be defined with longer number segments, as methanol (CH_3-OH) with v_k^*=2 and acetone (CH_3-CO-CH_3) with v_k^*=3.

In order to build the molecules, it is necessary to define the parameters $v_{k,i}$ which represent the number of times that each group *k* is contained in molecule *i*, *e.g. n*-decane is defined by $v_{CH3,decane}$=2 and $v_{CH2,decane}$=8.

In this approach, it is not enough with the group parameters. Crossed dispersive interaction parameters between the functional groups (ε_{kl}) are fitted to the experimental data of the series of components containing such groups (Table 4.20).

Table 4.20. Dispersion interaction ε_{kl} energies for the methyl and methylene functional groups [141]**.**

ε_{kl}/k_B [K]	CH_3	CH_2
CH_3	256.77	350.77
CH_2	350.77	473.39

The percentage average absolute deviations (%AAD) related to the predictions of saturation pressures and saturated-liquid densities are presented in the Table 4.21. The AAD% are referred to the experimental data obtained from the NIST ThermoData engine [42] in the reduced-temperature range of 0.4-0.9. The comparisons between data and predictions of bubble pressures and saturated densities of fluid phases (liquid and vapour) along the saturation line of the pure *n*-alkanes are depicted in Figure 4.18.

Having studied the pure components with the SAFT-γ Mie EoS, next the capability of the model in predicting properties of binary mixture of n-alkanes has been evaluated.

Two representative binary mixtures have been investigated using this GC approach. The modelling results of these systems are presented in Figures 4.19 and 4.20.

Table 4.21. Average absolute deviation of saturation pressures (P^{SAT}) and saturated-liquid densities (ρ^{SAT}) of alkanes series at reduced temperatures between 0.4 and 0.9

Substance	AAD% P^{SAT}	AAD% ρ^{SAT}
Ethane	2.27	1.67
Propane	2.13	0.83
***n*-Butane**	1.41	0.47
***n*-Pentane**	1.92	0.41
***n*-Hexane**	1.63	0.32
***n*-Heptane**	0.97	0.42
***n*-Octane**	1.17	0.51
***n*-Nonane**	0.78	0.64
***n*-Decane**	1.71	0.51
***n*-Dodecane**	1.68	0.58
Average	1.57	0.63

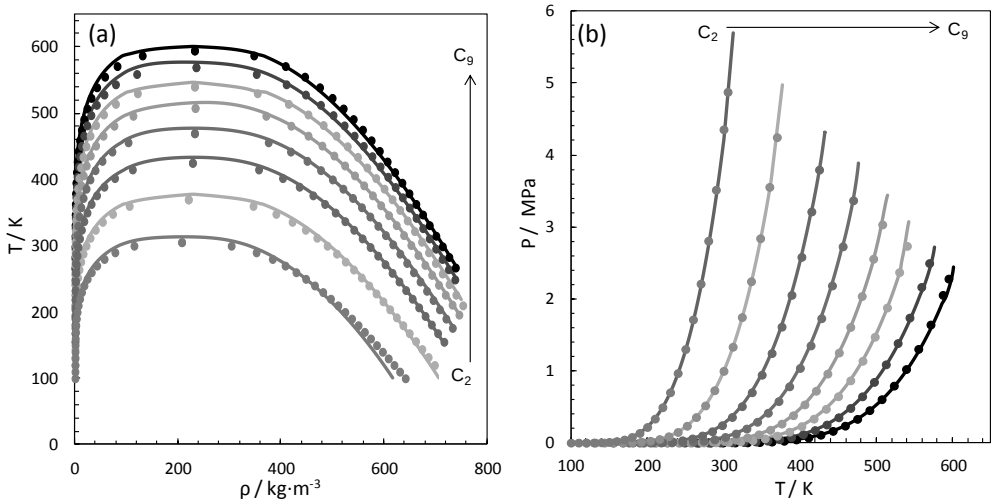

Figure 4.18. Comparison between the SAFT-γ Mie EoS and experimental data of saturated densities (a) and saturation pressures (b) for the C2-C9 n-alkanes series. The symbols represent the pure-component correlated data from NIST [42] **and curves represent SAFT-γ predictions.**

The first study concerned the VLE of the ethane + *n*-decane system in a wide range of temperature (298-449K). As it can be seen in Figure 4.19, the SAFT-γ Mie EoS does not describe the phase equilibrium (in particular for the vapour composition) with a very

good agreement with the experimental data [187,188]. After having calculated the bubble point for 94 experimental data points from the literature, a %AAD of 10.5% for the vapour pressure and 29% for the vapour mole composition (y_1) were reported. We already expected these high deviations because ethane is made up by two methyl (CH_3) groups which are only one type of the functional groups which form the *n*-alkanes series. Therefore, to better perform the VLE of these systems, ethane must be taken into consideration as one functional group itself. In comparison with SAFT-VR Mie, the modelling result of the same set of experimental data reports a %AAD of 3.5% for the vapour pressure and 2.9% for the vapour mole composition (y_1).

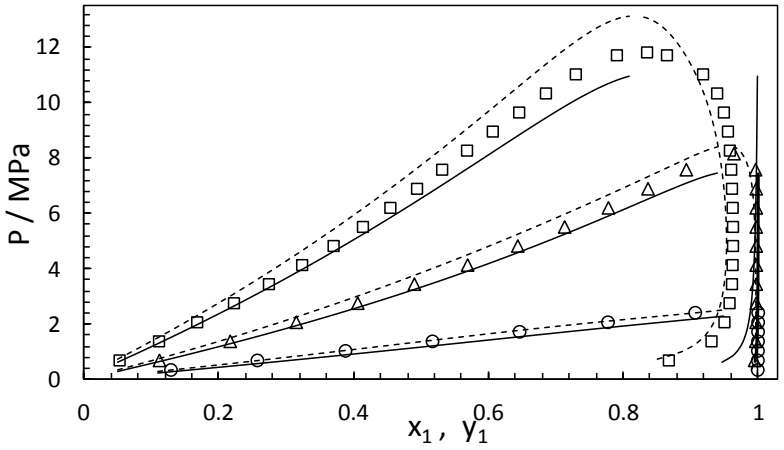

Figure 4.19. Pressure-composition representation of the VLE of the binary mixture of ethane (1) and n-decane (2). The continuous curves represent the prediction of SAFT-γ Mie estimation, the dashes curves the prediction of SAFT-VR Mie and the symbols the experimental data at (○) 277 K, (△) 344 K and (□) 444 K [187].

The second studied system has been the *n*-butane + *n*-decane binary mixture. A very good agreement between the predictions using the SAFT-γ Mie EoS and the VLE experimental data of this binary mixture can be seen in Figure 4.20. As it was previously described in the aspects of the model, the calculations of phase behaviour of mixtures of *n*-alkanes are purely predictive and, leaving aside the smallest molecules (methane and ethane), in a good agreement with experimental data from the literature.

The predictive capability of the SAFT-γ Mie EoS has also been evaluated in density calculations. The single-phase densities (*PTρx*) of binary mixtures of ethane and n-decane with other n-alkanes have been modelled and compared with experimental data from the literature. Again, all the reference for data used herein have been collected from the NIST Database [171].

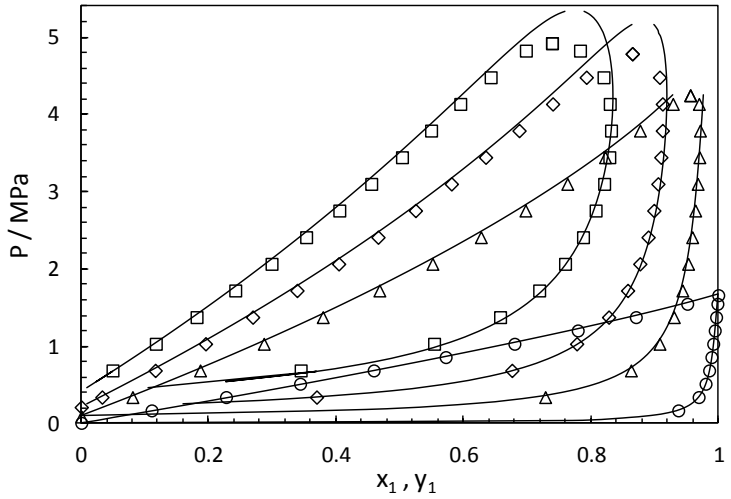

Figure 4.20. VLE of the binary mixture of *n*-butane (1) and *n*-decane (2). The continuous curves represent the prediction using the SAFT-γ Mie EoS and the symbols the experimental data at (○) 377 K, (△) 444 K, (◇) 477 K and (□) 511 [189].

Despite the possibility of using an individual group for ethane has been suggested, the *PTρx* of binary ethane mixtures has been performed using the SAFT-γ Mie EoS defining ethane as two methyl groups. Densities of some of the C_2H_6 binary mixtures studied in section 4.2 have been predicted using the SAFT- γ Mie and the modelling results are presented in Table 4.22. In order to compare the GC approach with the calculations from the original EoS, the results from the SAFT-VR Mie EoS are also reported. It can be observed in Table 4.22 that the SAFT-γ Mie EoS reports slightly higher deviations than the SAFT-VR Mie EoS. Nevertheless, the SAFT-γ Mie predictions are in good agreement with the literature data and present better results than the calculations obtained using the CEoS+VC reported in Table 4.16.

Similarly, the densities of *n*-decane + *n*-alkanes binary mixtures have been also studied using the SAFT- γ Mie EoS. The density calculations using the SAFT-γ Mie EoSs and SAFT-VR Mie are presented in Table 4.23. Again, both Mie EoSs are in good agreement with the literature data (Figure 4.21).

Table 4.22. Deviation in calculated density of C_2H_6 + *n*-alkanes systems by SAFT-VR Mie and SAFT- γ Mie.

Comp2	No Data	T_{min} [K]	T_{max} [K]	P_{min} [MPa]	P_{max} [MPa]	x_{C2H6} min	x_{C2H6} max	SAFT-VR Mie %AAD	SAFT-γ Mie %AAD
C_3	1462	102	400	1.5	34.6	0.01	0.95	0.64	1.35
C_4	12	311	311	3.4	13.8	0.25	0.78	0.42	0.47
C_5	57	309	309	3.1	7.1	0.68	0.99	2.62	2.93
C_7	30	185	353	0.1	7.5	0.02	0.68	0.89	0.92
C_{10}	1366	278	511	1.4	68.9	0.10	0.90	0.81	0.86

Table 4.23. Deviation in calculated density of *n*-decane + *n*-alkanes systems by SAFT-VR Mie and SAFT- γ Mie.

Comp2	No Data	T_{min} [K]	T_{max} [K]	P_{min} [MPa]	P_{max} [MPa]	x_{Decane} min	x_{Decane} max	SAFT-VR Mie %AAD	SAFT-γ Mie %AAD
C_4	574	311	511	1.4	68.9	0.16	0.82	0.55	0.54
C_6	750	313	363	1.0	25.0	0.10	0.95	0.40	0.43
C_8	750	313	363	1.0	25.0	0.04	0.94	0.42	0.44
C_{12}	14	298	289	1.0	1.0	0.10	0.90	0.49	0.55
C_{20}	15	313	343	1.0	1.0	0.20	0.80	0.71	0.78

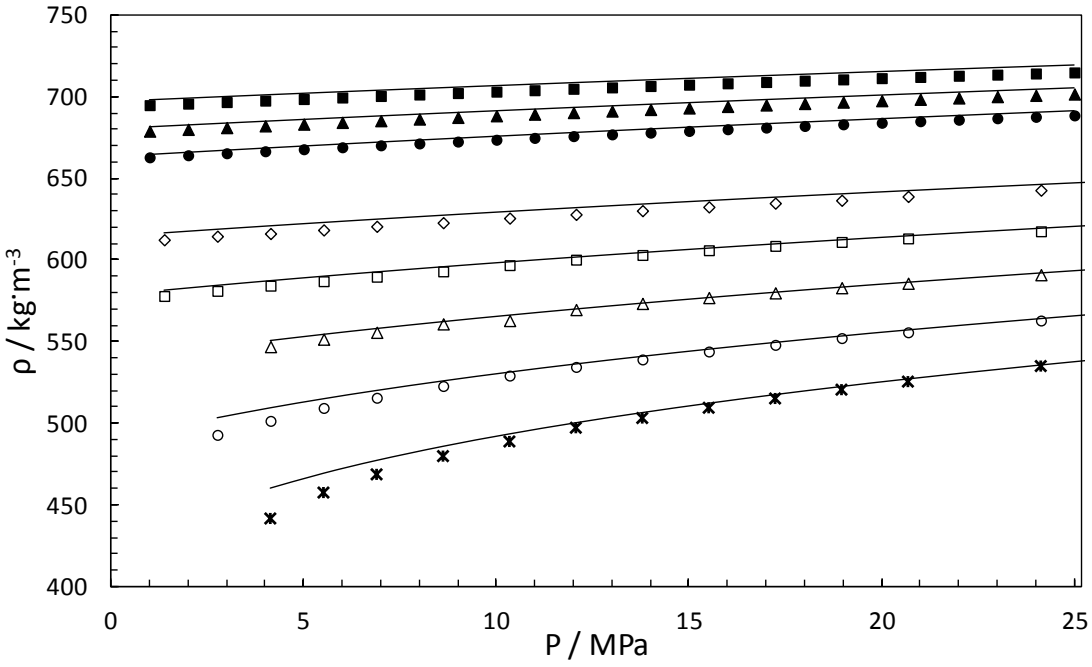

Figure 4.21. Single-phase density predictions using the SAFT-γ Mie. Symbols are data for the system 0.66 mol *n*-C_4 + 0.34 mol *n*-C_{10} at (◇) 344, (□) 377, (△) 410, (○) 444 and (⋆) 477 K [190] **and for the system 0.53 mol *n*-C_8 + 0.47 mol *n*-C_{10} at (■) 323 K, (▲) 343 K and (●) 363 K** [191]**.**

4.3.3 Conclusions SAFT-γ Mie modelling

The capabilities of the SAFT-γ Mie EoS have been assessed for the chemical family of the *n*-alkanes. The fluids used to evaluate the SAFT-γ Mie EoS are ten *n*-alkanes from ethane to *n*-dodecane. The pure-component properties of the aforementioned *n*-alkanes have been correlated by the SAFT-γ Mie EoS with average relative errors of 1.57% for the vapour pressure and 0.63% for the saturated liquid density.

The VLE of two binary systems have been performed using the SAFT-γ Mie EoS. First, the C_2H_6–*n*-decane has been studied and large deviations in the description of the vapour composition have been found (29% AAD). Second, the VLE of the *n*-butane and *n*-decane binary mixture has been modelled and the comparison with respect to experimental data revealed an AAD of 3.5% for the bubble pressure and 3% for vapour composition. Thus, it has been concluded that ethane cannot be defined as two methyl groups and it must be necessary to consider ethane as an individual species in order to improve the VLE description of these binary mixtures.

The single-phase densities of 10 binary mixtures of ethane and *n*-decane with other n-alkanes have been also studied using the SAFT-γ Mie EoS. The calculated densities are in good agreement with data from the literature.

CHAPTER 5: MODELLING TRANSPORT PROPERTIES WITH THE SAFT-VR MIE EOS

The SAFT-VR Mie EoS provides very good density predictions for pure component and binary systems according to the comparative study carried out in Chapter 4. Since most models for transport properties are functions of temperature and density, they can be combined with the SAFT-Mie EoS for an accurate prediction of those properties. In Chapter 5, two transport properties were modelled with SAFT-VR Mie and two models based on density predictions from the EoS. Thus, the viscosity (η) and interfacial tension (IFT) of CO_2-rich systems were calculated by coupling the SAFT-VR Mie EoS with the TRAPP method (η) and Density Gradient Theory (IFT), respectively, for mixtures related to carbon capture storage (CCS).

5.1 Viscosity

5.1.1 TRAPP method

TRAPP (TRAnsport Properties Prediction) is a predictive model based on the extended corresponding states theory (ECS) proposed by Hanley [57] and Mo and Gubbins [192], used to estimate the viscosity and thermal conductivity of pure fluids and their mixtures over the entire phase range. Methane was employed as reference fluid [193] in the original TRAPP, although in most recent version, propane is the reference fluid (SUPERTRAPP [194]). Other reference fluids can be selected such as CO_2 [24, 195] and refrigerants (R134a) [196].

The SUPERTRAPP (ST) model coupled with the SAFT-VR Mie EoS is the viscosity model used in this work. According to the ST model, the residual viscosity of the mixture at a corresponding state point (T_0 and ρ_0) is given by:

$$\Delta\eta(\rho,T) = \eta_m - \eta_m^0 = F_{\eta m}[\eta_R - \eta_R^0] + \Delta\eta^{ENSKOG} \tag{5.1}$$

where η_m^0 is the viscosity of the mixture at low pressure evaluated by the approximation of Herming and Zipperer [158]. The term η_R-η_R^0 is the residual viscosity of the reference fluid which is calculated as [197]:

$$\eta_R - \eta_R^0 = G_1 \exp[\rho_0^{0.1} G_2 + \rho_0^{0.5}(\rho_{r,R} - 1)G_3] - G_1 \tag{5.2}$$

where η_R is the real viscosity at T_0 and ρ_0 of the reference fluid, η_R^0 is the viscosity at low pressure and T_0, and $\rho_{r,R}$ is the reduced density calculated as $\rho_{r,R} = \rho_0 / \rho_{c,R}$. The corresponding state (T_0 and ρ_0) is calculated as $T_0 = T/f_m$ and $\rho_0 = \rho h_m$. G_1, G_2 and G_3 are parameters that can be calculated as:

$$G_1 = \exp\left(E_1 + E_2/T\right) \tag{5.3}$$

$$G_2 = E_3 + E_4/T^{1.5} \tag{5.4}$$

$$G_3 = E_5 + E_6/T + E_7/T^2 \tag{5.5}$$

where the E_i parameters have been correlated for propane as reference fluid and are presented in Table 5.1.

Table 5.1. E_i parameter SUPERTRAPP Model [50].

E_1	-14.113294896
E_2	968.22940153
E_3	13.686545032
E_4	-12511.628378
E_5	0.01168910864
E_6	43.527109444
E_7	7659.4543472

In order to calculate the terms $F_{\eta m}$ and $\Delta\eta^{ENSKOG}$, the following mixing rules were applied:

$$h_m = \sum_i \sum_j y_i y_j h_{ij} \tag{5.6}$$

$$f_m h_m = \sum_i \sum_j y_i y_j h_{ij} f_{ij} \tag{5.7}$$

$$h_{ij} = \frac{\left((h_i)^{1/3} + (h_j)^{1/3}\right)}{8} \tag{5.8}$$

$$f_{ij} = (f_i f_j)^{1/2} \tag{5.9}$$

where y_i is the mole fraction of component *i*; f_i and h_i are functions of the critical parameters and acentric factor defined as:

$$f_i = \frac{T_C}{T_C^R}[1 + (\omega - \omega^R)(0.05203 - 0.7498 \ln T_r)] \tag{5.10}$$

$$h_i = \frac{\rho_C^R}{\rho_C}\frac{Z_C^R}{Z_C}[1 + (\omega - \omega^R)(0.1436 - 0.2822 \ln T_r)] \tag{5.11}$$

The viscosity dimensional scaling factor can be calculated as:

$$F_{\eta m} = (M_R)^{-1/2}(h_m)^{-2}\sum_i\sum_j y_i y_j (f_{ij} M_{ij})^{1/2}(h_{ij})^{4/3} \tag{5.12}$$

with

$$M_{ij} = \frac{2M_i M_j}{M_i + M_j} \tag{5.13}$$

where M_i denotes the molecular weight.

The expression $\Delta\eta^{ENSKOG}$ is the residual viscosity which takes into account the differences in the molecules size based on the hard sphere assumption [50]:

$$\Delta\eta^{ENSKOG} = \eta_m^{ENSKOG} - \eta_x^{ENSKOG} \tag{5.14}$$

with

$$\eta_m^{ENSKOG} = \alpha\rho^2\sum_i\sum_j y_i y_j \sigma_{ij}^6 \eta_{ij}^0 g_{ij}^{hs} + \sum_i \beta_i Y_i \tag{5.15}$$

where the α parameter is α=9.725x10^{-7}, σ_i the hard-sphere diameter calculated as σ_i=4.771 $h_i^{1/3}$, and η_i^0 the non-attracting rigid sphere calculated from:

$$\eta_i^0 = 26.69\left[\frac{M_i T}{\sigma_i^4}\right]^{1/2} \tag{5.16}$$

And the mixing rules used are defined as

$$\sigma_{ij} = \frac{\sigma_i + \sigma_j}{2} \tag{5.17}$$

$$\eta_{ij}^0 = \frac{y_i \eta_i^0}{y_i + y_j \phi_{ij}} + \frac{y_j \eta_j^0}{y_j + y_i \phi_{ji}} \tag{5.18}$$

The radial distribution function of the hard-sphere fluid is given by the following equation [198]:

$$g_{ij}^{hs} = \frac{1}{(1-\xi)} + \frac{3\xi}{(1-\xi)^2} \Phi_{ij} + \frac{2\xi^2}{(1-\xi)^3} \Phi_{ij}^2 \tag{5.19}$$

where

$$\Phi_{ij} = \frac{\sigma_i \sigma_j}{2\sigma_{ij}} \frac{\sum_k y_k \sigma_k^2}{\sum_k y_k \sigma_k^3} \tag{5.20}$$

$$\xi = \frac{\pi}{6} \rho \sum_k y_k \sigma_k^3 \tag{5.21}$$

To obtain the values of β_i,, it is necessary to solve the linear system of equations of the form:

$$\sum_i B_{ij} \beta_i = Y_i \tag{5.22}$$

with

$$Y_i = y_i \left[1 + \frac{18\pi}{15} \rho \sum_j y_j \frac{M_j}{M_i + M_j} \sigma_{ij}^3 g_{ij}^{hs} \right] \tag{5.23}$$

$$B_{ij} = 2 \sum_k y_i y_k \frac{g_{ik}}{\eta_{ik}^0} \left(\frac{M_k}{M_i + M_k} \right)^2 \left[\left(1 + \frac{5M_i}{3M_k} \right) \delta_{ij} - \frac{2M_i}{3M_k} \delta_{jk} \right] \tag{5.24}$$

where δ_{ij} is the Kronecker function which is a delta function (*i.e.*, δ_{ij} =1 if i=j and δ_{ij} =0 in other cases).

In the ST method [194], the fluid reference is propane and its residual viscosity is calculated using the Eq. 5.2. As the studied mixtures are CO_2-rich streams, carbon dioxide has been used as the reference fluid, CO_2-SUPERTRAPP (CO_2-ST) [24, 195].

The residual viscosity of pure CO_2 has been calculated as a function of density and temperature using the following equation proposed by Fenghour et al. [195]:

$$\eta(\rho,T)=\eta_0(T)+\Delta\eta(\rho,T) \tag{5.25}$$

with

$$\eta_0(T)=\frac{1.00697\,T^{0.5}}{\Psi_\eta^*(T^*)} \tag{5.26}$$

where η_0 is the zero-density viscosity in units of μPa·s and Ψ_η^* the reduced effective cross section and it can be obtained from the empirical equation:

$$\ln\Psi_\eta^*(T^*)=\sum_{i=0}^{4}a_i(\ln T^*)^i \tag{5.27}$$

where a_i are the coefficients of the representation of the zero-density viscosity of CO_2 presented in Table 5.2 [195]. T^* is the reduced temperature calculated as follows:

$$T^*=\frac{k}{\varepsilon}T \tag{5.28}$$

where ε is the energy parameter (ε/k=251.196 K).

Table 5.2. Coefficientes a_i of the Ψ_η^* for CO_2. [195].

a_0	0.235156
a_1	-0.491266
a_2	$5.211155\cdot10^{-2}$
a_3	$5.347906\cdot10^{-2}$
a_4	$-1.537102\cdot10^{-2}$

In the second term of the Eq. 5.25, $\Delta\eta(\rho,T)$ is the excess viscosity and can be correlated by the following expression:

$$\Delta\eta(\rho,T)=d_{11}\rho+d_{21}\rho^2+\frac{d_{64}\rho^6}{T^{*3}}+d_{81}\rho^8+\frac{d_{82}\rho^8}{T^*} \tag{5.29}$$

where ρ is the density of CO_2 in kg/m^3 and d_{ij} are the coefficients reported in Table 5.3. The densities have been obtained from a modified Benedict-Webb-Rubin equation of state (mBWR EoS). A complete description of this multi-parameter EoS for pure CO_2 is presented in Appendix E.

Table 5.3. Coefficientes d_{ij} [195].

d_{11}	$4.071119 \cdot 10^{-3}$
d_{21}	$7.198037 \cdot 10^{-5}$
d_{64}	$2.411697 \cdot 10^{-17}$
d_{81}	$2.971072 \cdot 10^{-23}$
d_{82}	$-1.627888 \cdot 10^{-23}$

5.1.2 Results of viscosity modelling

The viscosity of CO_2 systems was calculated using the SUPERTRAPP model with the densities computed from the SAFT-VR Mie EoS. A literature review of the available experimental data on the viscosity of some mixtures of relevance for CCS operations was carried and the results listed in Table 5.4. As can be seen in Table 5.4, experimental data on this property are available in a broad range of temperatures but, in most studies, pressure is limited to either atmospheric pressure or to a maximum pressure of 2.6 MPa. Chapoy et al. [55] is the only work which has considered a wider range of pressure. They have studied the viscosities of a quaternary system at temperatures between 273 and 423 K and pressures up to 150 MPa. The viscosity studies were conducted in the single phase region, *i.e.* Gas (G) phase at low pressures, Liquid (L) above saturation pressure or in the supercritical (SC) region, as described in Table 5.4.

Table 5.4. Literature experimental data for the viscosity of CO_2-mixtures with N_2, O_2, and Ar.

Source	System	Phase	T/K	P/MPa	N	Uncert.
Kestin and Leidenfrost [199]	CO_2/N_2	G	293	0.1-2.17	28	±0.05%
Kestin et al. [200]	CO_2/N_2, CO_2/Ar	G	293-304	0.1-2.6	83	±0.1%
Gururaja et al. [201]	CO_2/N_2, CO_2/O_2	G	298	0.1	17	
Kestin and Ro [202]	CO_2/N_2, CO_2/N_2/Ar, CO_2/Ar,	G	297-773	0.1	64	±0.15%
Kestin et al. [203]	CO_2/O_2	G	298-674	0.1	10	±0.3%
Hobley et al. [204]	CO_2/Ar	G	301-521	0.1	24	<0.7%
Chapoy et al. [55]	$CO_2/N_2/O_2$/Ar	G/L/ SC	273-423	1.5-150	38	
				Total	**264**	

Table 5.5. Average absolute deviation of the viscosity calculations.

System	x_{CO2}	N	T/K	P/MPa	%AAD
CO_2/N_2	0.19-0.90	95	293-773	0.1-2.6	3.12
CO_2/Ar	0.22-0.92	96	293-773	0.1-2.6	1.28
CO_2/O_2	0.19-0.92	19	298-674	0.1	3.25
CO_2/N_2/Ar	0.25-0.53	16	297-673	0.1	1.39
$CO_2/N_2/O_2$/Ar	0.9	38	273-423	1.5-150	5.15
				Total	**2.68%**

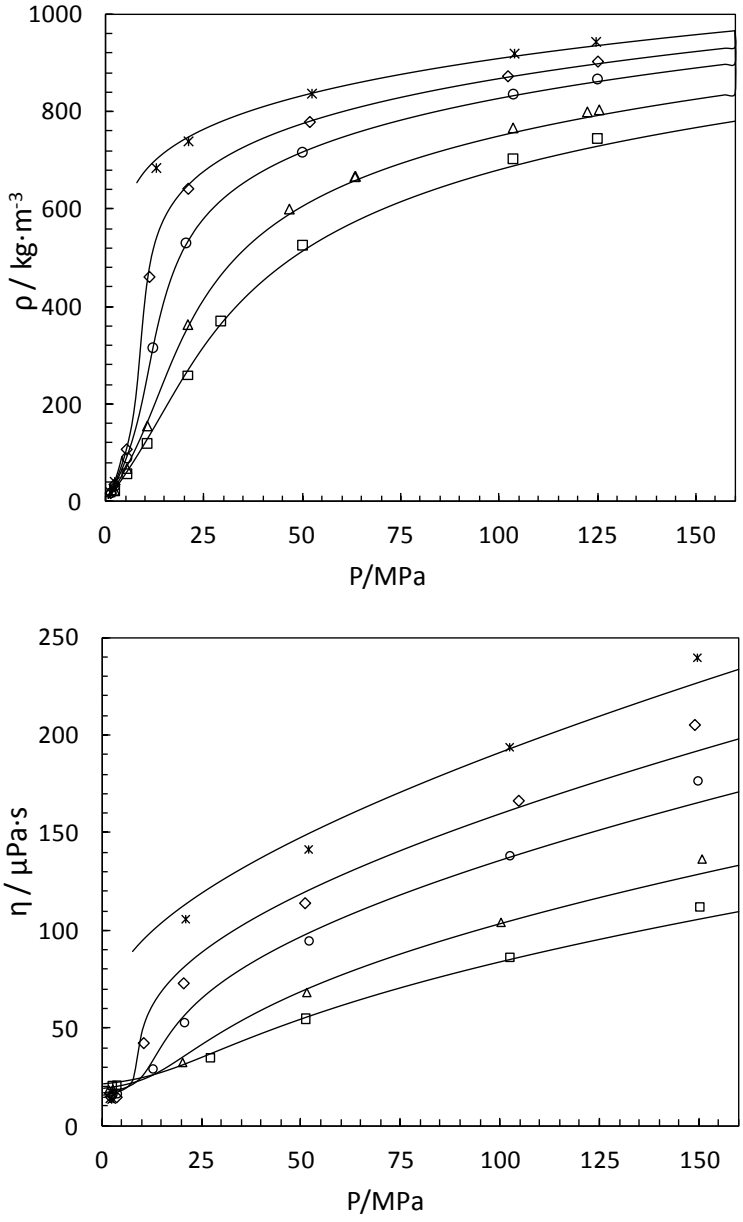

Figure 5.1. Experimental and predicted density and viscosity of CO_2-rich system (90%CO_2, 5%O_2, 2%Ar and 3% N_2). Predictions using the SUPERTRAPP+SAFT-VR Mie EoS. Data at 283 (∗), 298 (◇), 323 (○), 373 (△) and 423K (□) [55].

The modelling results for the viscosity of the CO_2-rich systems are shown in Table 5.5, along with the percentage average absolute deviation (%AAD) between predicted and experimental viscosity values for each studied system. A total of 264 experimental points were considered and an overall %AAD of 2.7 % was calculated for the viscosity values predicted with the SUPERTRAPP+SAFT-VR Mie model. This value represents half of the deviation reported by Huber [205] and Poling et al. [50] and obtained with the SUPERTRAPP model combined with a modified BWR-EoS. Nonetheless, the largest deviations with the TRAPP+SAFT-VR Mie model were obtained at high pressures and low temperatures, as depicted in Figure 5.1, with a maximum deviation of 9.3% for the multicomponent system (90%CO_2, 5%O_2, 2%Ar and 3%N_2).

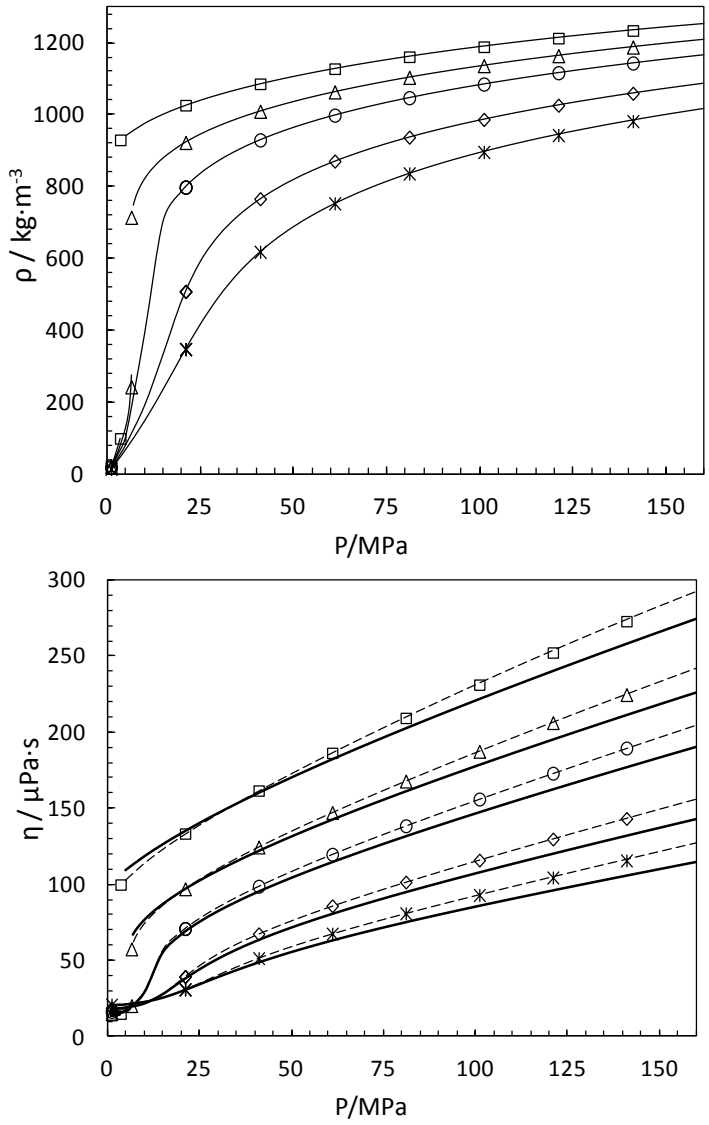

Figure 5.2. Experimental and predicted viscosity of pureCO_2. Predictions using the SAFT-VR Mie EoS and the ST (continuous lines) and CO_2-ST (dashed lines) models. Data at 283 (□), 298 (△), 323 (○), 373 (◇) and 423 K (∗)[42]**.**

The viscosities of pure CO_2 at temperatures between 273 and 423 K and pressures up to 150 MPa have been studied using the SUPERTRAPP and CO_2-SUPERTRAPP models. The density and viscosity predictions are presented in Figure 5.2. The deviation in the density calculations is 0.3%, while the deviations of the viscosity models are 3.8% for the ST and 2.8% for the CO_2-ST. As it can be seen from Figure 5.2, the use of CO_2 as the reference fluid improves the predictions of the TRAPP method.

The viscosity measurements presented in Chapter 2 are included in the project named "Impact of Common Impurities on Carbon Dioxide Capture, Transport and Storage". The system measured was a multicomponent CO_2-rich mixture with 50% of impurities (MIX4). In the framework of this project, the viscosities of other mixtures with 10 and 30% of impurities have been measured. The mixture with 10% of impurities (MIX2) which is included in the work of Chapoy et al. [55] has been studied and presented in Figure 5.1.

The last modelled system is the CO_2-rich mixture with 30% of impurities (MIX3). This multicomponent mixture contains a 70.0% of CO_2, 20.0% of methane, 6.6% ethane, 2.6% propane, 0.4% *n*-butane and 0.4% *i*-butane [24]. The ST and CO_2-ST predictions and the viscosity data from the literature for the MIX3 are plotted in Figure 5.3.

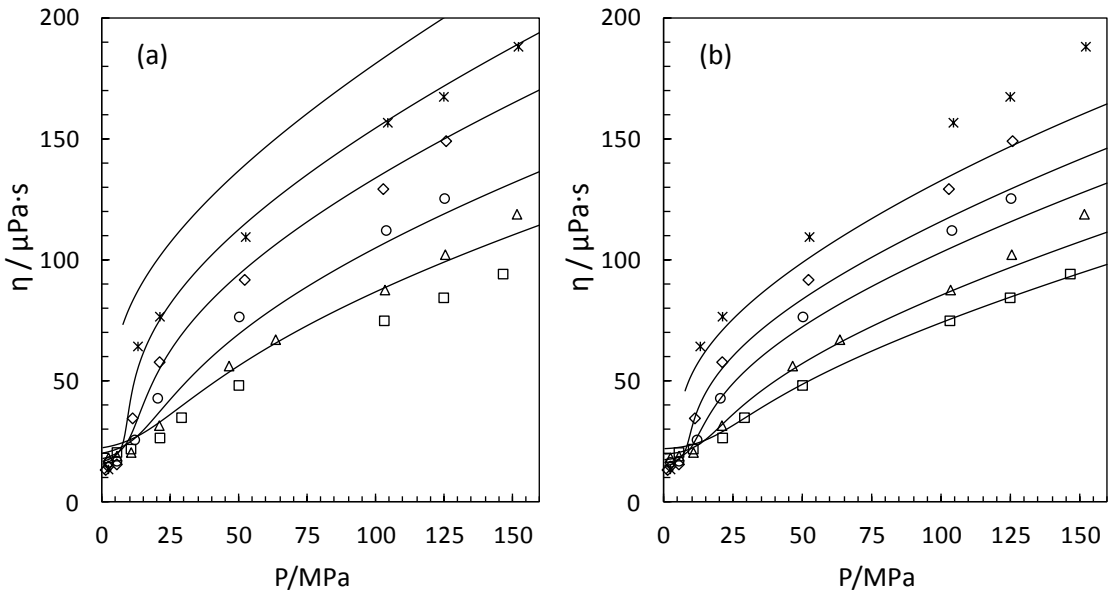

Figure 5.3. Experimental and predicted viscosity of the MIX3. Predictions using the SAFT-VR Mie EoS and the ST (a) CO_2-ST (b). Data at 273 (∗), 298 (◇), 323 (○), 373 (△) and 423 K (□) [24]**.**

In Table 5.6, the average absolute deviations in viscosity predictions of the ST and CO_2-ST models for the pure CO_2, MIX2 and MIX3 are reported. The accuracy of the ST and CO_2-ST models decreases with the increasing amount of impurities. The CO_2-SUPERTRAPP model predicts the viscosity of the studied systems with lower deviation than the ST model. By employing the carbon dioxide as the reference fluid the deviations were reduced around 1.6%. The viscosity predictions are overestimated by the ST model (except for pure CO_2) and underestimated by the CO_2-ST model (Figure 5.3).

Table 5.6. Average absolute deviation of the viscosity calculations.

	SUPERTRAPP	CO_2-SUPERTRAPP
Pure CO_2	3.82	2.77
MIX2 (10% impurities)	5.15	4.02
MIX3 (30% impurities)	10.38	7.64

5.2 Interfacial tension

5.2.1 Density Gradient Theory

The density gradient theory (DGT) has been used to compute the interfacial tension. This model is based on the square gradient of van der Waals [206] and on the reformulation of Cahn and Hilliard [207] to compute interfacial tension values from bulk phase properties such as density and composition. The DGT, when coupled with the appropriate thermodynamic models, has been successfully applied in the prediction of interfacial properties of a wide class of systems and interfaces. The reader is referred to the study of Pereira et al. [208] and references within for more details about coupling the DGT with cubic equations of state. In this work, the SAFT-VR Mie EoS was used to estimate the bulk equilibrium of the investigated systems and the DGT used to predict interfacial properties. The main equations within the DGT framework are given below.

In summary, by applying the minimization criterion of the Helmholtz energy to planar interfaces, the interfacial tension values with respects to the density of a reference component is given by [209, 210]:

$$IFT = \int_{\rho_{ref}^{V}}^{\rho_{ref}^{L}} \sqrt{2\Delta\Omega(\rho)\sum_i \sum_j c_{ij} \frac{d\rho_i}{d\rho_{ref}} \frac{d\rho_j}{d\rho_{ref}}} \, d\rho_{ref} \tag{5.30}$$

where ρ^{L}_{ref} and ρ^{V}_{ref} are the bulk phase densities and the *ref* subscript denotes the reference component of the mixture. $\Delta\Omega$ is the variation of the grand thermodynamic potential which is related to the Helmholtz free energy by the following equation:

$$\Delta\Omega = a_0(\rho) - \sum_i \rho_i \mu_i + p \tag{5.31}$$

where a_0 is the Helmholtz free energy density of the homogeneous fluid at local density, μ_i are the corresponding chemical potentials of each component and p is the pressure at equilibrium. The methodology described by Miqueu et al. [209, 210] was here followed for determining the density distribution of each component across the interface.

In Eq. 5.30, c_{ij} is the cross influence parameter and the mixing rule used based on the geometric mean of the pure component influence parameters [211] and it is given by

$$c_{ij} = (1 + \beta_{ij})\sqrt{c_i c_j} \tag{5.32}$$

where β_{ij} is the binary interaction parameter and c_i and c_j are the pure component influence parameters. In this work, the binary parameter β_{ij} has been fixed to 0, making the calculation of the interfacial tension of the systems investigated fully predictive. The influence parameters c_i and c_j can be derived from theoretical expressions [212]. Nevertheless, the parameters are generally correlated using surface tension data from pure substances, by rewriting Eq. 5.30 for c_i as follows:

$$c_i = \frac{1}{2}\left[\frac{\gamma}{\int_{\rho^V}^{\rho^L} \sqrt{a_0 - \rho\mu + p}\, d\rho}\right]^2 \tag{5.33}$$

There are different approaches for calculating the influence parameters of each pure component [209]. In this work, c_i has been taken as a constant value calculated from surface tension data far from the critical point [213]. Hence, the influence parameters used were adjusted against surface tension data (NIST Database [42]) of the pure components at a reduced temperature T_r= 0.7. The parameters used are reported in

Table 5.7. It is interesting to note that the value of the influence parameter increased with the size of the *n*-alkanes.

Table 5.7. DGT influence parameters.

Substance	c_i / J·m^5·mol^{-2}
CO_2	$2.37 \cdot 10^{-20}$
N_2	$1.53 \cdot 10^{-20}$
Methane	$2.08 \cdot 10^{-20}$
Ethane	$5.36 \cdot 10^{-20}$
Propane	$1.49 \cdot 10^{-19}$
n-butane	$1.68 \cdot 10^{-19}$
n-hexane	$3.77 \cdot 10^{-19}$
n-heptane	$4.85 \cdot 10^{-19}$
n-decane	$9.51 \cdot 10^{-19}$
n-dodecane	$9.73 \cdot 10^{-19}$

Ideal term calculation

In order to calculate the grand thermodynamic potential, it is necessary to determine the total Helmholtz free energy (Equation 5.34) and the total chemical potentials. Only the residual Helmholtz energy and the residual chemical potential are used to describe the equilibrium. In Chapter 4, the equations to calculate the residual contribution with the SAFT-VR Mie EoS are provided.

$$A^{TOTAL} = A^{IDEAL} + A^{RES} \tag{5.34}$$

In the SAFT approach, the Ideal Gas term is calculated by the thermal de Broglie volume [83], which describes the effect of the translational, rotational and vibrational contributions in the kinetic energy of the molecule at a given temperature. However, in this work, a different approach based on the Ideal Gas Gibbs free energy [77] is chosen. In the following equations, the mathematical development followed to calculate the ideal chemical potential and the ideal contribution to the Helmholtz free energy is presented. Therefore, the main equations to calculate the ideal contribution are based on the following IG equations:

$$G^{IDEAL} = \mu^{IDEAL} N \tag{5.35}$$

$$\frac{V}{N} = k\frac{T}{P} \tag{5.36}$$

where G is the Gibbs free energy, μ the chemical potential, N the number of molecules, V the volume, k the Boltzmann constant, T the temperature and P the pressure.

From the general equation of Gibbs, the partial derivative of Gibbs free energy over the pressure is equal to the volume, likewise partial derivative of Gibbs free energy over the number of molecules gives the chemical potential. Therefore, using the Eq. 5.32 and 5.33 and also the results of the partial derivatives commented previously, the chemical potential can be calculated solving the next integral equation:

$$\int d\mu = kT \int \frac{dP}{P} \tag{5.37}$$

The final solution to this equation requires defining boundary conditions. Therefore, a reference pressure and reference chemical potential are considered in order to simplify the calculations, because these reference properties do not affect on the variation of the grand thermodynamic potential $\Delta\Omega$. Hence, the final solution to the integral equation above is:

$$\mu^{IDEAL} = \mu_0 + kT \ln\left(\frac{P}{P_0}\right) \tag{5.38}$$

where μ_0 and P_0 are the reference chemical potential and pressure respectively. The former is assumed as μ_0 =0.

Considering the general equations which define the Gibbs (*G*) and Helmholtz (*A*) free energies, there is a direct thermodynamic relation, *A=G-PV*. Accordingly, combining this relation with the IG equations (Eq. 5.35 and 5.36), the resulting equation to calculate the ideal contribution to the Helmholtz free energy:

$$A^{IDEAL} = \mu^{IDEAL} N - NkT \tag{5.39}$$

Finally, the Eq. 5.38 and 5.39 are rewritten for multicomponent systems. Thus, despite SAFT and DGT follow a statistical mechanics approach, the following equations have been used to calculate the ideal contribution of the chemical potential and Helmholtz free energy density:

$$\mu_i^{IDEAL} = kT \ln\left(\frac{\rho_i kT}{P_0}\right) \tag{5.40}$$

$$a_0^{IDEAL}(\rho) = \frac{A^{IDEAL}}{V} = \sum_i \rho_i \left[kT \ln\left(\frac{\rho_i kT}{P_0}\right) - kT \right] \tag{5.41}$$

5.2.2 Results of IFT modelling

In this section the capability of the DGT coupled with the SAFT-VR Mie EoS to model IFT data from the literature is evaluated. The IFT study has been divided in two parts. In the first part, the interfacial tensions of the CO_2+*n*-C_4 and CO_2+*n*-C_{10} binary systems and the CO_2+*n*-C_4+*n*-C_{10} ternary system have been modelled. The DGT results are presented together with the VLE and saturated densities calculated with the SAFT-VR Mie EoS. The second part is focused on comparing the IFT predictions from DGT+SAFT-VR Mie EoS with experimental data and other IFT calculations from the literature.

The IFT of CO_2 with *n*-butane and *n*-decane have been experimentally studied by Nagarajan et al. [214, 215, 216]. First, binary interaction parameters have been regressed from literature VLE data [214, 215, 217] in the temperature range from 313 to 393 K and optimum k_{ij} parameters are reported in Table 5.8. VLE calculations using the SAFT-VR Mie EoS with the adjusted k_{ij} are presented in the Figure 5.4.

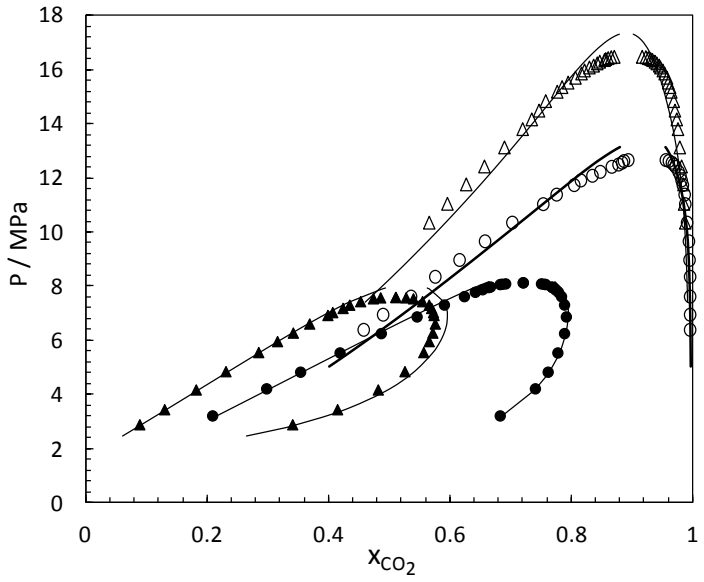

Figure 5.4. Pressure-composition diagram of CO_2+*n*-C_4 (black [214]**) and CO_2+*n*-C_{10} (white** [215]**) systems using the SAFT-VR Mie EoS. Symbols: (●○) T=344.3 and (▲△) T=377.6K.**

Table 5.8. Binary interaction parameters between CO_2, *n*-butane and *n*-decane for the SAFT-VR Mie used in this work.

	CO_2	*n*-C_4	*n*-C_{10}
CO_2	0	0.053	0.057
n-C_4	0.053	0	-0.004
n-C_{10}	0.057	-0.004	0

The saturated densities and IFT of the CO_2+*n*-C_4 and CO_2+*n*-C_{10} binary systems and the CO_2+*n*-C_4+*n*-C_{10} ternary system have been studied with the SAFT-VR Mie EoS and DGT. The modelling results are plotted in Figures 5.5 and 5.6 for the binary systems and Figures 5.7 and 5.8 the ternary. As can be seen in these figures, the DGT+SAFT-VR Mie predictions are in excellent agreement with the measured saturated density and IFT data of the systems considered.

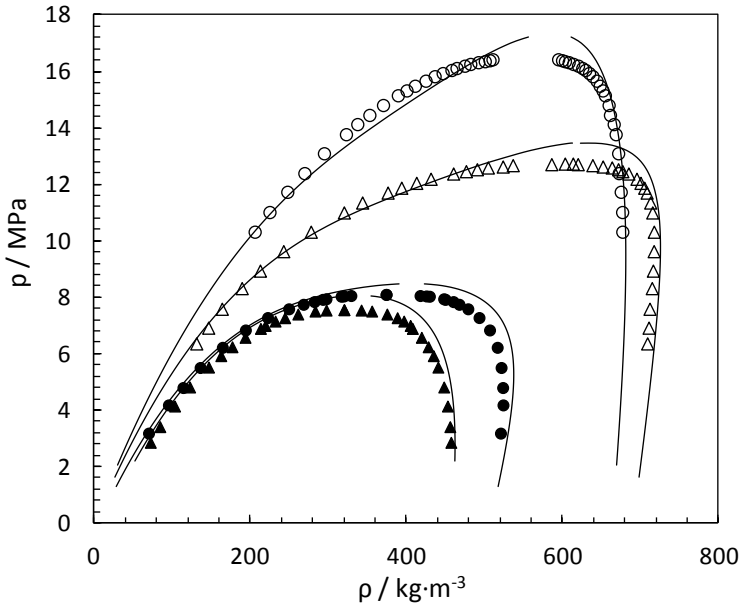

Figure 5.5. Predicted saturated density of CO_2+*n*-C_4 (black) [214] **and CO_2+*n*-C_{10} (white)** [215]**. Symbols: (●○) T=344.3 and (▲△) T=377.6K.**

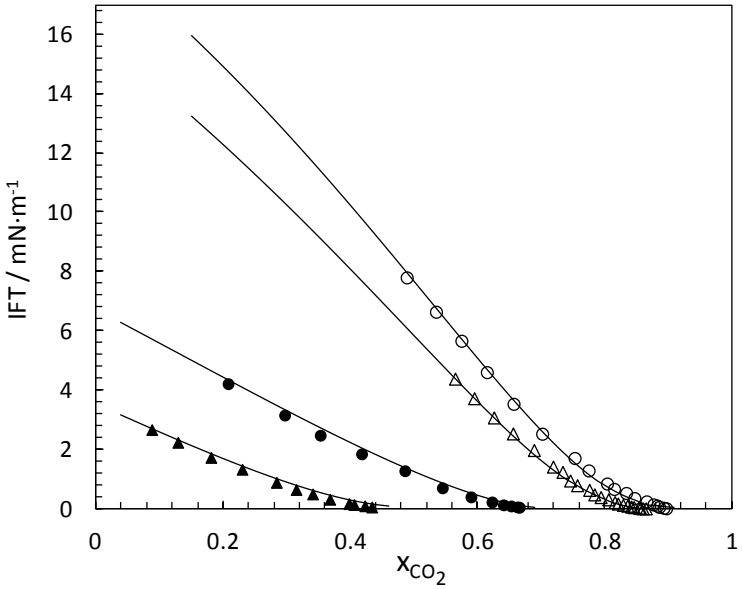

Figure 5.6. Predicted IFT of CO_2+*n*-C_4 (black) [214] **and CO_2+*n*-C_{10} (white)** [215]**. Symbols: (●○) T=344.3 and (▲△) T=377.6K.**

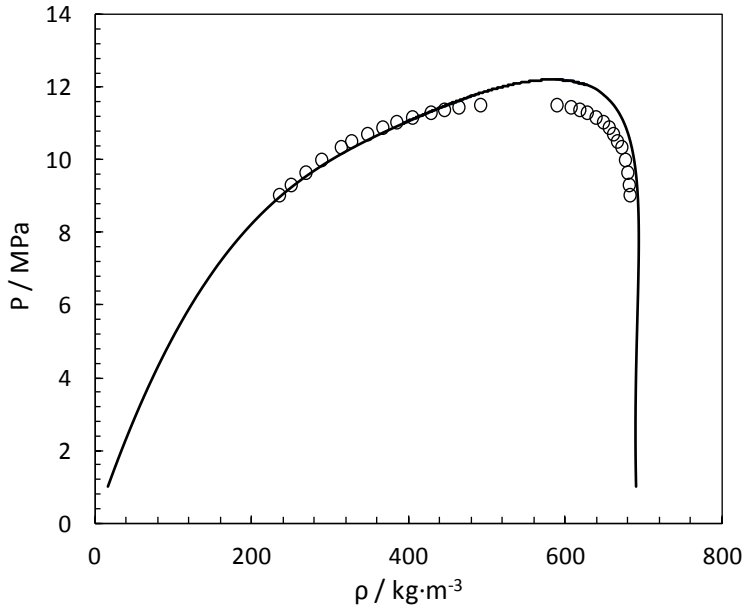

Figure 5.7. Predicted saturated density of CO_2+*n*-C_4+*n*-C_{10} mixture at 344.3K [216]**.**

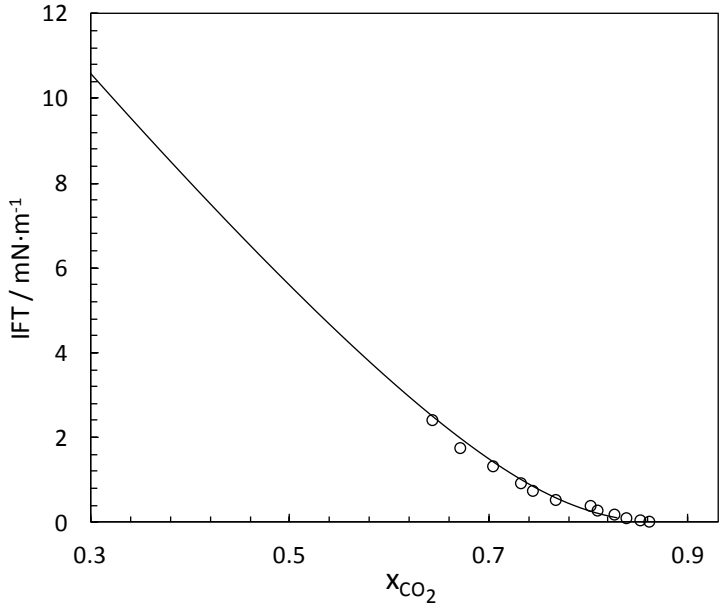

Figure 5.8. Predicted IFT of CO_2+*n*-C_4+*n*-C_{10} mixture at 344.3K [216]**.**

The largest deviations were observed close to the critical point, where the SAFT-VR Mie fails to capture the impact of pressure on the density of the bulk phases. Nonetheless, as can be seen in Figure 5.9, the maximum absolute deviation between predicted and measured IFT data was of 0.26 $mN \cdot m^{-1}$. In general, the IFT values for the CO_2+*n*-C_4 system and the ternary system are slightly overestimated, whereas an inverse behaviour was observed for the CO_2+*n*-C_{10} system.

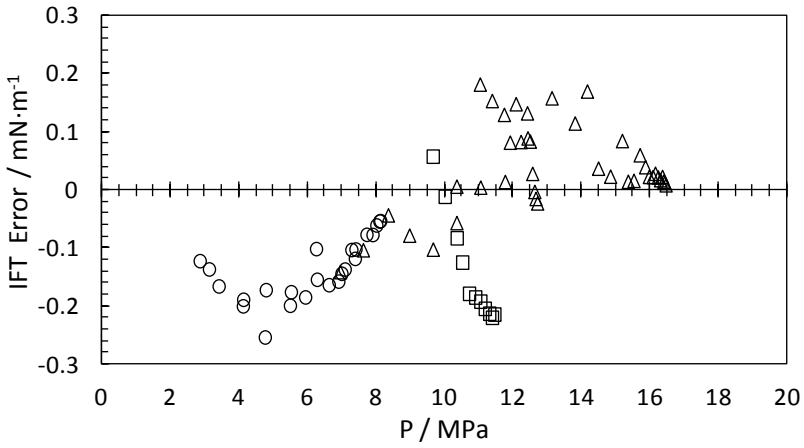

Figure 5.9. Deviation between prediction and experimental IFT data ($IFTerror=IFT^{EXP}-IFT^{CALC}$). Symbols: CO_2+*n*-C_4 (○), CO_2+*n*-C_{10} (△) and CO_2+*n*-C_4+*n*-C_{10} (□) systems.

In addition, the density profiles through the interface were computed with the DGT approach. In Figure 5.10, the density profiles obtained from the flash calculation of a ternary mixture of 90% CO_2, 6% *n*-butane and 4% *n*-decane in mole fraction at 344.3K and 9.31 MPa are plotted. As depicted in Figure 5.10, the density profiles present a local enrichment of the interface with CO_2 molecules as a peak was noticeable in the density profile of carbon dioxide. The location of the peak is closer to the vapour side of the interface suggesting that the adsorption of CO_2 occurred at the surface of the liquid hydrocarbon phase.

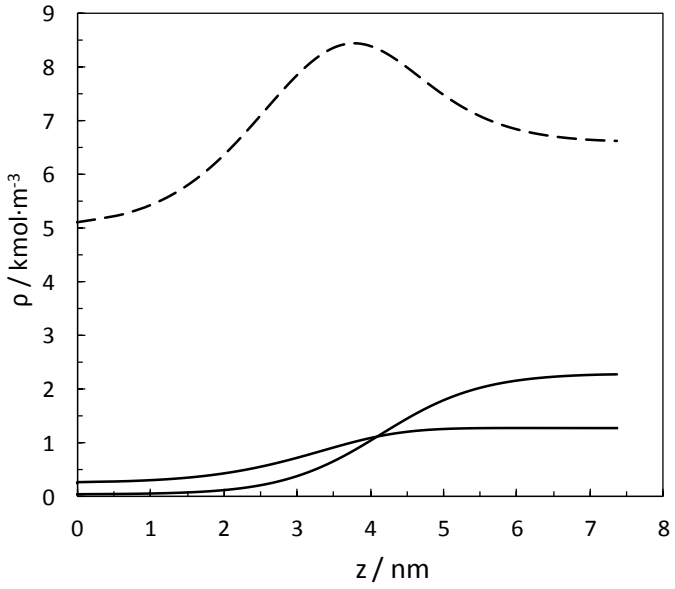

Figure 5.10. Density profiles calculated for each component in the CO_2+*n*-C_4+*n*-C_{10} mixture at 344.3K and 9.31MPa: CO_2 (dashed line), *n*-butane (dotted line) and n-decane (solid line). Total interface length of 7.36 nm.

The density profiles of carbon dioxide for the CO_2+*n*-decane binary systems at 344.3K and 4.6, 6.3 and 8.3 MPa are plotted in Figure 5.11. The results from the DGT+SAFT-VR Mie EoS have compared with the molecular simulation results [218]. The interface of the CO_2+*n*-decane systems also presents enrichment with carbon dioxide. As can be seen in Figure 5.11, the pressure increase leads to an increase of the interface thickness in the binary mixture and to a reduction of the local accumulation on light components, such as CO_2. Comparable results were obtained for the other mixtures and the results are in agreement with those obtained by Miqueu et al. [210].

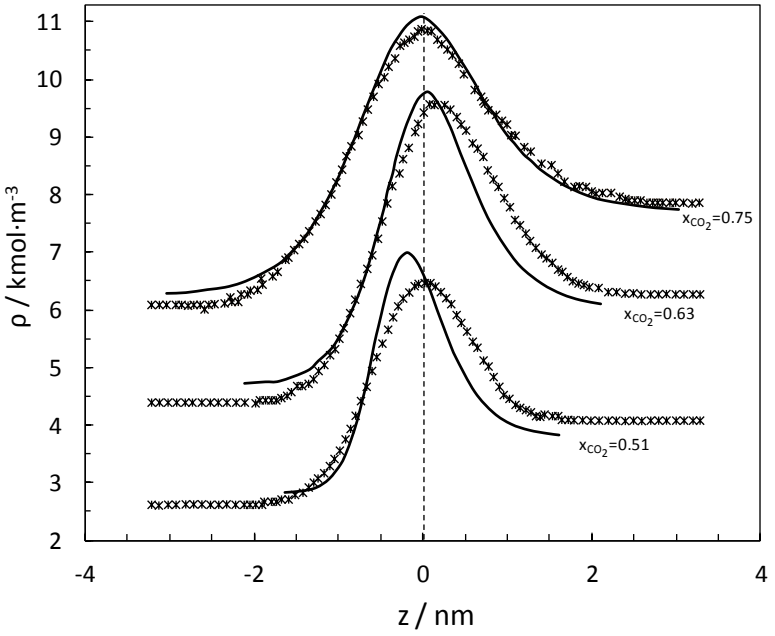

Figure 5.11. Density profiles of carbon dioxide calculated using the DGT+SAFT-VR Mie model for the CO_2+*n*-C_{10} mixture at 344.3K. Symbols: results of molecular simulation (∗) [218]**.**

In the second part of the IFT study, the DGT+SAFT-VR Mie model is compared with the Parachor and DGT models in combination with the VT-PPR78 EoS from the work of Pereira et al. [219]. The Parachor model [220] is the standard method use in the oil industry, based on an empirical correlation [221].

The IFTs of 12 binary systems of CO_2, CH_4 and N_2 with n-alkanes have been studied by comparing the IFT predictions against literature data. The average absolute deviations between the experimental and predicted IFT for the studied systems are reported in Table 5.9. In this table, the AAD in IFT predictions using the DGT+SAFT-VR Mie EoS are presented together with the deviations reported by Pereira et al. [219] using the Parachor+VT-PPR78 and DGT+VT-PPR78 models.

Table 5.9. Average absolute deviations (%AAD) between experimental and predicted IFT using the DGT+SAFT-VR Mie model (this work) and the results from Pereira et al. using the VT-PPR78 with the Parachor and DGT models [219]**.**

					VT-PPR78		SAFT-VR Mie
Comp1	Comp2	ref	T_{range} [K]	N	Parachor	DGT	DGT
Methane	Propane	[220]	258-338	26	26.0	4.8	5.3
	n-Butane	[222]	311-344	4	25.2	4.0	4.5
	n-Hexane	[223]	300-350	9	5.4	8.2	8.4
	n-Heptane	[224]	298-323	18	6.1	10.1	9.8
	n-Decane	[219]	313-442	31	10.0	14.4	12.6
			Overall	88	14.2	9.6	9.1
CO_2	n-Butane	[214]	319-377	14	18.2	10.2	9.7
	n-Heptane	[225]	323-353	10	7.9	5.7	5.8
	n-Decane	[219]	313-442	23	10.0	3.7	4.1
	n-Dodecane	[226]	344	12	7.8	5.9	6.2
			Overall	59	11.1	6.0	6.1
N_2	n-Hexane	[227]	303-333	28	7.2	2.9	3.5
	n-Heptane	[228]	295-373	11	9.8	7.1	7.5
	n-Decane	[219]	313-442	44	21.9	8.5	9.2
			Overall	83	15.3	6.4	7.1

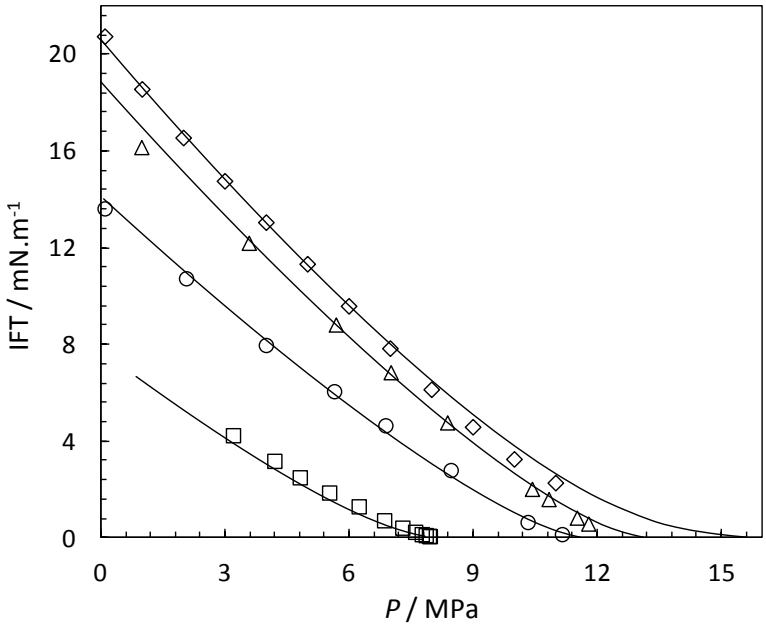

Figure 5.12. Experimental and predicted IFT using the DGT-SAFT VR Mie model for the systems: CO_2+*n*-butane at 338K (□) [214]**, CO_2+*n*-heptane at 353K (○)** [225]**, CO_2+*n*-decane at 343K (△)** [219] **and CO_2+*n*-dodecane at 344K (◇)**[226]**.**

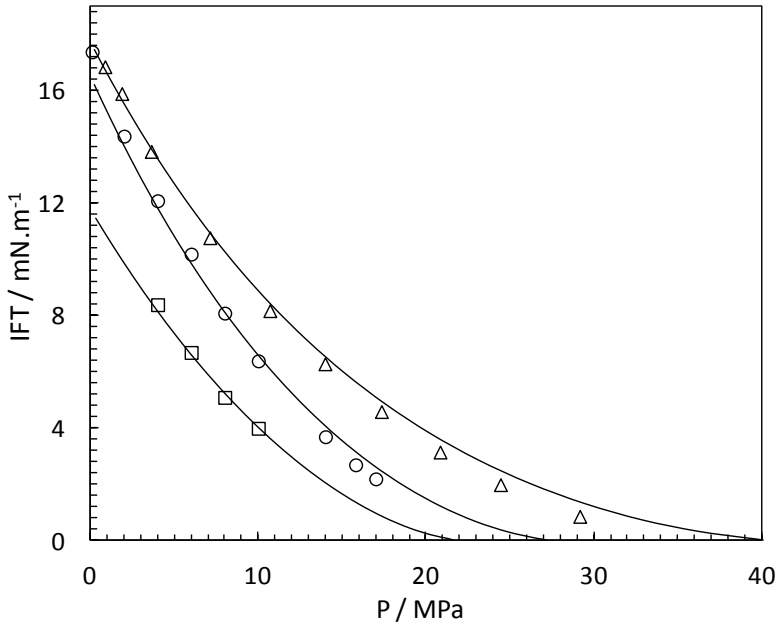

Figure 5.13. Experimental and predicted IFT using the DGT-SAFT VR Mie model for the systems: CH_4+propane at 338K (□) [220]**, CH_4+*n*-hexane at 350K (○)** [223] **and CH_4+*n*-decane at 343K (△)** [219]**.**

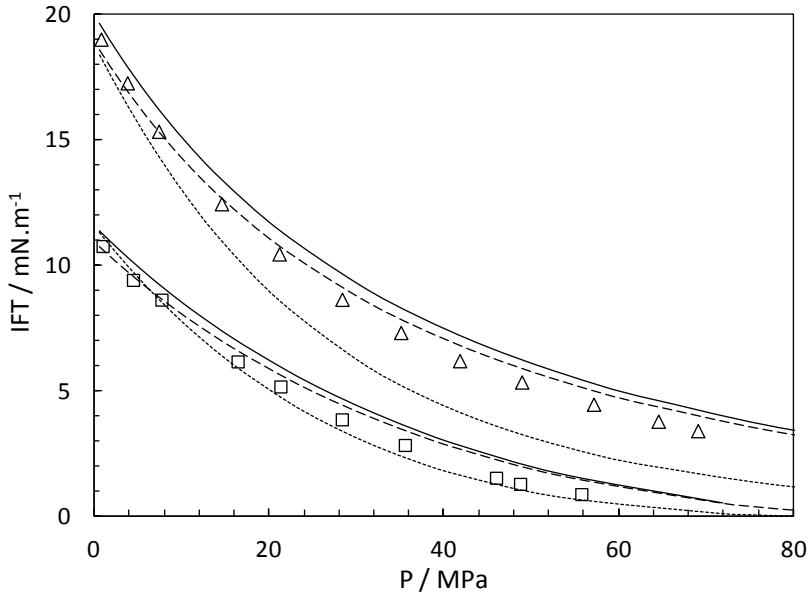

Figure 5.14. Experimental and predicted IFT of N_2+*n*-decane. Solid, dashed and dotted lines represent the predictions using the DGT+SAFT VR Mie, DGT+VT-PPR78 and Parachor+VT-PPR78 models respectively. Symbols: T=343 K (□) and 442 K (△) [219]**.**

As it can be seen in Table 5.9 and Figures 5.12 and 5.13, the DGT+SAFT VR Mie model is in good agreement with the experimental IFT data from the literature. The DGT+SAFT-VR Mie and DGT+VT-PPR78 models present a similar level of accuracy, as depicted in Figure 5.14. However, the DGT+VT-PPR78 model has given the best

predictions of the IFT of the N_2+*n*-alkanes systems and the DGT+SAFT-Mie model has reported the lowest deviation for CH_4+*n*-alkanes systems. The DGT model combined with any of the EoSs has performed the IFT of the studied systems with lower deviation than the Parachor method.

5.3 Conclusions

The TRAPP method and the density gradient theory have been combined with the SAFT-VR Mie EoS to model the viscosity and IFT of CO_2-rich systems.

The viscosities of binary, ternary and quaternary mixtures of CO_2, N_2, O_2 and Ar have been modelled using the SUPERTRAPP model (propane as the reference fluid) with an AAD of 2.68%, with a maximum deviation of 9.3% at the highest pressure of the multicomponent. The capabilities of the SUPERTRAPP and CO_2-SUPERTRAPP (CO_2 as the reference fluid) models have been compared by modelling the viscosity of pure CO_2 and two CO_2-rich mixtures with 10 and 30% of impurities. The comparison has shown that CO_2-ST model is more accurate than ST and the accuracy of both TRAPP models decreases with increasing amount of impurities.

The IFT of several gas+*n*-alkanes mixtures have been studied by coupling the SAFT-VR Mie EoS with the DGT. The DGT + SAFT-VR Mie results are in good agreement with the experimental data from literature and with other DGT study (DGT+VT-PPR78 [219]).

CHAPTER 6: MODELLING AND DISCUSSION OF EXPERIMENTAL MEASUREMENTS

Our measured data presented in Chapter 2 are studied using the thermodynamic models introduced in Chapter 4 and 5. The vapour-liquid equilibria (VLE) data of the Ar+H_2S system are modelled using the SAFT-VR Mie and the PR EoSs. The densities of CH_4 + H_2S, C_2H_6 + H_2S and C_3H_8 + H_2S binary systems and one CO_2 + CH_4 + H_2S ternary mixture are calculated with the SAFT-VR Mie and PR EoSs, as well as with the GERG-2008 EoS, a multiparameter model which will be introduced in the next subsections. Finally, the density and viscosity of the multicomponent CO_2-rich mixture are modelled by coupling the TRAPP model with the SAFT-VR Mie EoS.

6.1 Vapour-liquid equilibrium of H_2S - Ar

The SAFT-VR Mie and PR EoSs have been used to describe the phase equilibrium of the Ar - H_2S at 273.01, 298.00 and 322.96K. Aiming at obtaining a better description close to the critical point, more sophisticated mixing rules have been used for modelling our measured data. Finally, a prediction of the phase diagram has been performed using the PR EoS and extrapolating the binary interaction parameter (BIP) to lower temperatures.

6.1.1 Results

Our VLE data are reported in Table 2.2, together with the uncertainty of the measurements. Unusual VLE behaviour has not been observed during the measurements and the treatment of the data. Due to the pressure limitation of the apparatus, only for the isotherm at 323 K it has been possible to obtain data close to the critical point.

Relative volatility is a property which compares the vapour pressure of each component in a mixture through the composition of the phases (Eq. 6.1) [229]. Unusual behaviour on the trend of relative volatilities may be a sign of inconsistency of measurements. Thus, calculations of relative volatility have been calculated during the measurements as a way of assessing the soundness of the acquired data (Figure 6.1).

$$\alpha_{12} = \frac{(y_1/x_1)}{(y_2/x_2)} \tag{6.1}$$

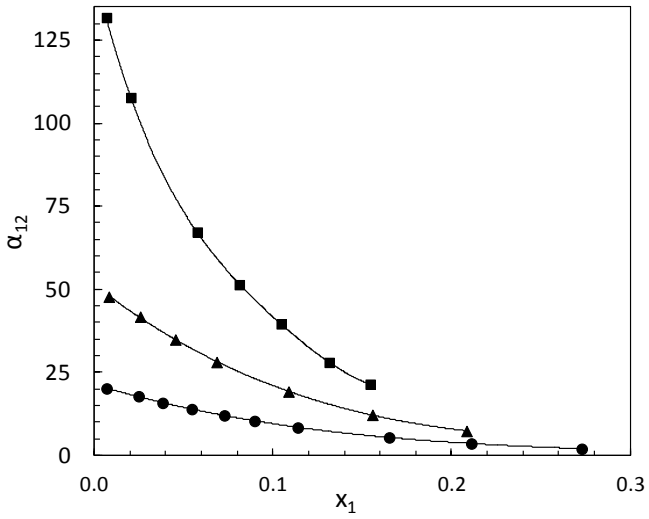

Figure 6.1. Relative volatility, α_{12}, as function of liquid composition of Ar (x_1) at (■) 273 , (▲) 298 and (●) 323 K for the Ar+H_2S system.

Binary interaction parameters for the PR and SAFT-VR Mie EoSs were fitted using the measured VLE data. Two sets of BIPs were regressed for each model. First, a temperature-independent parameter was fitted using the whole range of temperatures, k_{ij}=0.2091 for the PR model and k_{ij}=0.0808 for the SAFT-VR Mie EoS. Second, a BIP was regressed at each temperature (Table 6.1). A depicted in Figure 6.2, the regressed BIPs for the SAFT-VR Mie EoS show a clear linear temperature dependence, whereas the BIPs for the PR EoS seem to be temperature-independent. Following the same approach as in Chapter 4, the BIPs have been regressed by minimizing the objective function given in the following equation which is based on calculated bubble point pressures and measured VLE data.

$$\min\ F = \frac{100}{N}\sum_{1}^{N}\left(\frac{P_{bubble}^{\exp} - P_{bubble}^{cal}}{P_{bubble}^{\exp}}\right) \tag{6.2}$$

Table 6.1. Regressed BIPs for the Ar+H_2S system using the PR and SAFT-VR Mie EoSs.

T [K]	SAFT-VR Mie	PR
273.01	0.0917	0.2108
298.00	0.0781	0.2085
322.96	0.0552	0.2118

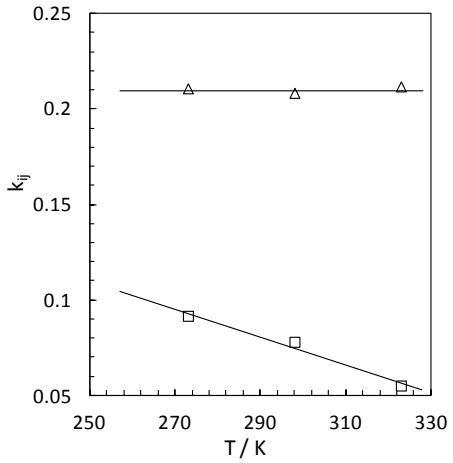

Figure 6.2. Regressed values and trends of the BIPs for the Ar-H_2S system with the (△) PR and (□) SAFT-VR Mie EoSs.

The average absolute deviations in bubble point predictions (k_{ij}=0) and calculations (using the regressed k_{ij}) are reported in Table 6.2. The SAFT-VR Mie EoS is the model which better predicts (k_{ij}=0) the VLE of the present system with an AAD in bubble pressure of 27.9% in comparison with 37.7% reported by the PR EoS. However, using the regressed temperature independent BIP, the PR EoS has reported the lower deviations of the bubble pressures, AAD% of 5.9% for the CEoS and 7.0% for the SAFT-like EoS. The better modelling results of both EoSs have been obtained when fitting one binary interaction parameter at each temperature. Using these fixed temperature BIPs, the SAFT-VR Mie EoS has correlated the VLE of this system with slightly lower deviations, 5.5% and 5.8% in bubble pressure and 3.9% and 4.4% in vapour composition for the SAFT-VR Mie and the PR EoSs respectively.

Table 6.2. Average absolute deviations (%AAD) of bubble pressure (ΔP^{bubble}) and vapour phase composition (Δy_1) of Ar-H_2S system with the PR and SAFT-VR Mie EoS.

T [K]	SAFT-VR Mie			PR		
	k_{ij}	ΔP	Δy_1	k_{ij}	ΔP	Δy_1
273.01	0	42.0	11.9	0	51.6	16.5
	0.0808	9.1	3.8	0.2091	5.8	3.2
	0.0917	5.38	2.7	0.2108	5.6	3.1
298.00	0	27.3	13.9	0	36.9	19.5
	0.0808	5.6	3.6	0.2091	5.9	3.8
	0.0781	5.4	3.7	0.2085	5.8	3.8
322.96	0	14.5	11.9	0	24.69	19.8
	0.0808	6.5	3.9	0.2091	6.0	6.4
	0.0552	5.7	5.5	0.2118	6.0	6.3
Average	0	27.9	12.6	0	37.7	18.6
	0.0808	7.0	3.8	0.2091	5.9	4.5
	$k_{ij,T}$	5.5	3.9	$k_{ij,T}$	5.8	4.4

In Figures 6.2-6.4, the predictions and the calculations of the VLE are presented in pressure-composition diagrams. Each figure contains one isotherm of the Ar-H_2S VLE data and the phase equilibria predicted and calculated using the fixed temperature k_{ij} with both models.

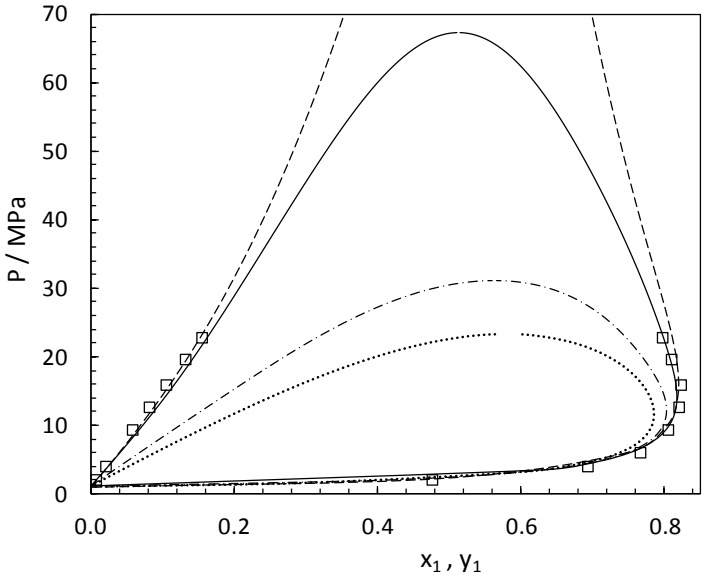

Figure 6.3. Pressure–composition diagram of the Ar (1) + H_2S (2) system at 273.01K. Comparison between measured data (□), the SAFT-VR Mie EoS with k_{ij} = 0 (dot-dashed line) and with k_{ij} = 0.0917 (continuous line) and the PR EoS with k_{ij} =0 (dotted line) and with k_{ij} = 0.2108 (dashed line).

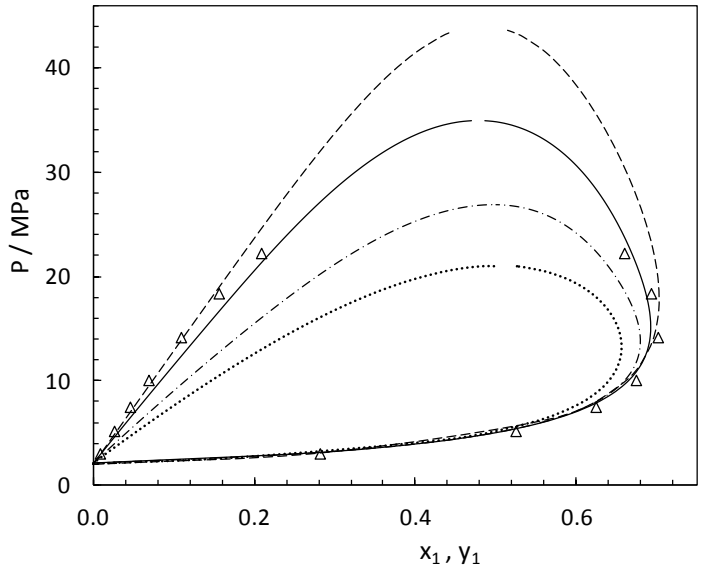

Figure 6.4. Pressure–composition diagram of the Ar (1) + H_2S (2) system at 298K. Comparison between measured data (△), the SAFT-VR Mie EoS with k_{ij} = 0 (dot-dashed line) and with k_{ij} = 0.0781 (continuous line) and the PR EoS with k_{ij} =0 (dotted line) and with k_{ij} = 0.2085 (dashed line).

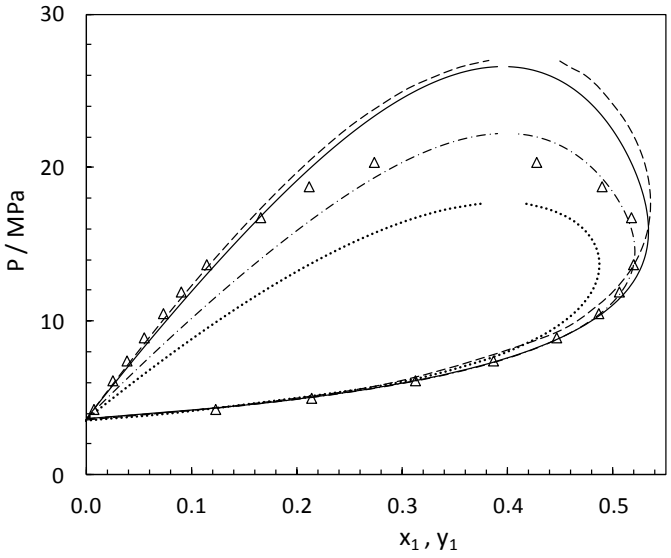

Figure 6.5. Pressure–composition diagram of the Ar (1) + H_2S (2) system at 322.96K. Comparison between measured data (△), the SAFT-VR Mie EoS with k_{ij} = 0 (dot-dashed line) and with k_{ij} = 0.0552 (continuous line) and the PR EoS with k_{ij} =0 (dotted line) and with k_{ij} = 0.2118 (dashed line).

Even though measurements near the critical point were not performed, it can be observed following the trend of the data that the calculations using the fitted parameters seem to overestimate the critical points of the mixture. In order to obtain a more accurate description of the VLE close to the critical point, more sophisticated mixing rules have been used with the PR EoS. The Wong-Sandler (W-S) mixing rules [230] were used (Eqs. 6.3-6.5). The W-S mixing rules are based on the alternative approach proposed by Huron and Vidal (H-V) [231]. The H-V method is founded on the excess Gibbs free energy (g^E) at an infinite pressure reference, where the G^E is calculated from an EoS with an activity coefficient model [230]. The W-S mixing rules are density-independent since they were developed to determinate the *a* and *b* parameters of any CEoS through the excess Helmholtz energy at infinite pressure (Eq.6.3-6.5) [230]. This is the reason why W-S mixing rules improve the results from the H-V approach at high pressure [37].

$$b = \frac{\sum_i \sum_j x_i x_j \left(b - \frac{a}{RT} \right)_{ij}}{1 - \sum_i x_i \left(\frac{a_i}{b_i RT} \right) + \frac{A_\gamma^E (T, P = \infty, x_i)}{CRT}} \tag{6.3}$$

$$b - \frac{a}{RT} = \sum_i \sum_j x_i x_j \left(b - \frac{a}{RT} \right)_{ij} \tag{6.4}$$

$$\left(b-\frac{a}{RT}\right)_{ij}=\frac{1}{2}\left[\left(b-\frac{a}{RT}\right)_{i}+\left(b-\frac{a}{RT}\right)_{j}\right]\left(1-k_{ij}\right) \tag{6.5}$$

where a and b are the PR EoS parameters, $A_{\gamma}^{E}(T,P=\infty, x_i)$ is the excess Helmholtz energy and C a numerical constant (C=-0.6232, for the PR EoS).

To evaluate the excess of Helmholtz energy, Wong and Sandler have assumed that A^E at infinite pressure is approximately equal to the G^E at very low pressure (Eq.6.6). This assumption is based on the thermodynamic relation between the excess Gibbs and Helmholtz energies presented in Equation 6.5. At low pressures, the excess volume (V^E) is usually very small and it can be assumed that $A^E = G^E$. G^E is much more pressure-dependent than A^E, therefore the approximation presented in equation 6.7 is an useful estimation [230].

$$G^E = A^E + PV^E \tag{6.6}$$

$$G^E(T,\bar{x},P\to 0) = A^E(T,\bar{x},P\to 0) \approx A^E(T,\bar{x},P\to\infty) \tag{6.7}$$

Both Huron-Vidal and Wong-Sandler mixing rules are combined with an activity coefficient model. The NRTL local composition model [232] was used to calculate the excess Gibbs energy.

$$\frac{G^E(T,P,x_i)}{RT}=\sum_i x_i \sum_j \frac{x_j \exp\left(-\alpha_{ji}(\tau_{ji}/RT)\right)}{\sum_k x_k \exp\left(-\alpha_{ki}(\tau_{ki}/RT)\right)}\tau_{ji} \tag{6.8}$$

with α_{ii} =0, τ_{ii} =0 and $\alpha_{ji} = \alpha_{ij}$; where α_{ji}, τ_{ij} and τ_{ji} are the adjustable parameters. In this work, the parameters α have been fixed as α_{ij}=0.3. The τ parameters, together with the BIP, have been adjusted to the VLE data.

Minimization of bubble pressure deviations (Eq. 6.2) is the objective function that has been used along this work. However, since three parameters are fitted for this mixing rule, more information is required in order to obtain a good regression. The objective function is based on the results from the flash calculations, *i.e.* composition of the liquid and vapour phases. Therefore, the parameters τ_{ij}, τ_{ji} and k_{ij} are adjusted to the measured data through a modified Simplex algorithm by minimizing the following objective function:

$$\min\ F = \frac{100}{N}\left[\sum_{1}^{N}\left(\frac{x_{\exp}-x_{cal}}{x_{\exp}}\right)^2 + \sum_{1}^{N}\left(\frac{y_{\exp}-y_{cal}}{y_{\exp}}\right)^2\right] \tag{6.9}$$

In Table 6.3 and Figure 6.6, the results of the Ar + H_2S system using the PR EoS with the Wong-Sandler mixing rules are presented. The use of the W-S mixing rules noticeably improves the results of the PR EoS with vdW mixing rules. The AADs in bubble pressures of the PR calculations are reduced on average from 5.8% to 1.2% using these mixing rules. In comparison with Figure 6.5, the description of the region near critical point using the PR EoS with W-S mixing rules is also improved.

Table 6.3. Values of the adjusted binary parameters (τ_{ij} and k_{ij}) and deviation (%AAD) in bubble pressure and vapour composition at each studied temperature using the PR EoS with the W-S mixing rules.

T [K]	τ_{12} [J·mol^{-1}]	τ_{12} [J·mol^{-1}]	k_{ij}	ΔP	Δy_1
273.01	1152	3521	0.5121	1.38	0.34
298.00	372.8	4155	0.5226	0.73	1.07
322.96	-485.0	5384	0.5124	1.27	2.47

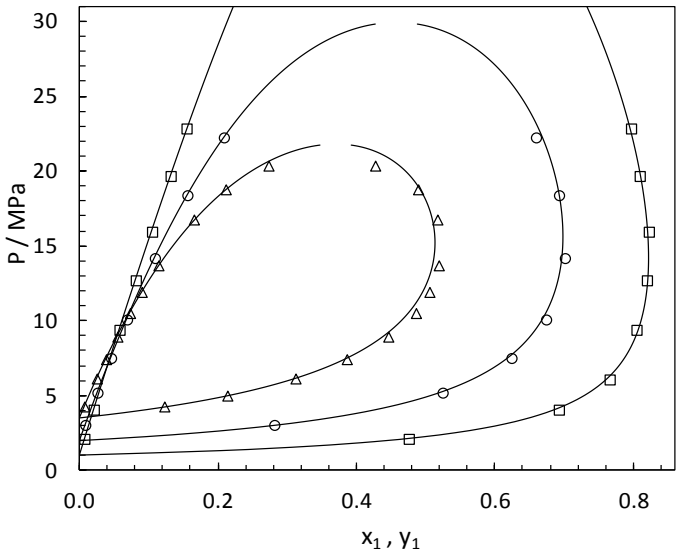

Figure 6.6. Pressure–composition diagram of the Ar + H_2S system using the PR EoS with W-S mixing rules and NRTL activity coefficient model at 273.01, 298.00 and 322.96 K.

The phase diagram of the Ar (1) + H_2S (2) system has been studied using the PR EoS (Figure 6.7). According to the classification proposed by Scott and van Konynenburg [44], the phase diagram of the Ar + H_2S system is classified as type IIIc. Ar + CO_2

[30,233] and CH_4 + *n*-alkanes (heavier than *n*-nonane) [174] binary are other systems which present similar behaviour. Taking into consideration the critical point (CP) of argon, T_c = 150.86 K, and from the phase diagram, our VLE data have been measured at high temperature. Due to the lack of equilibrium data at lowest temperatures, the BIP fitted at 273 K has been extrapolated to lower temperatures. There is no continuous critical line between the critical points of both components and two critical lines have been predicted. The first critical line starts as a vapour-liquid critical (L_2=V) line from the CP of H_2S (T_c = 373.2 K and P_c = 8.94 MPa) and it changes into a liquid-liquid critical (L_1=L_2) line, although it has not been possible to predict the transition point. The second critical line extends from the critical point (CP) of Ar until the upper end point of the first solid-liquid-vapour line (SL_1V). This upper end point is very close to the CP of argon, thus the SL_1V line almost overlaps the saturation line of pure Ar. The second solid-liquid-vapour (SL_2V) starts in the triple point of hydrogen sulphide and, as well as the first critical line, it changes to a L_1L_2V line. Again, it has not been possible to predict at which T-P conditions the SL_2V becomes the SL_1L_2 line. The SL_1V and SL_2V lines do not cross and this is the reason why the Ar- H_2S phase diagram presents no SL_1L_2V quadruple point.

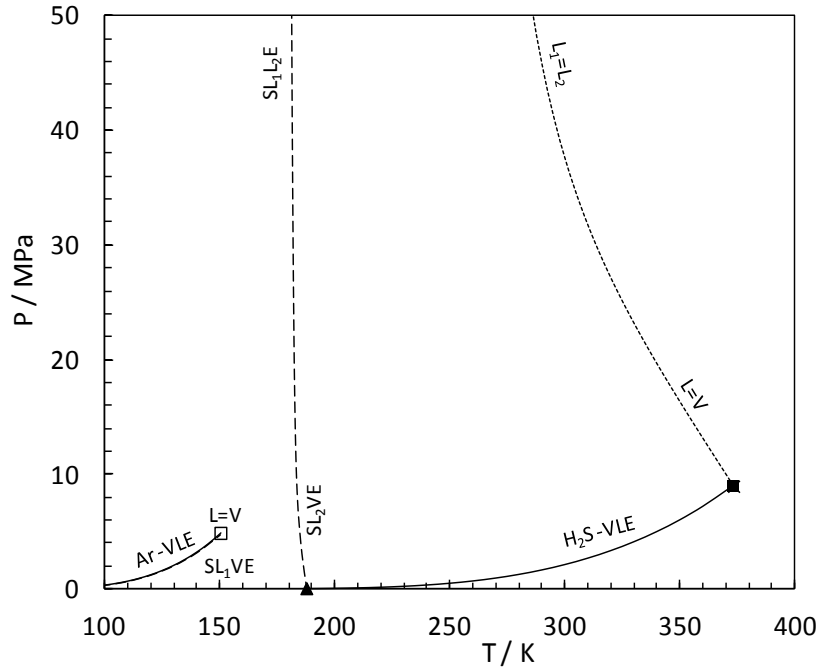

Figure 6.7. P-T diagram of the Ar (1) + H_2S (2) system. Solid lines are the saturations lines of each pure compound [42]**. Doted lines and dashed lines are the critical and solid-fluid equilibrium lines predicted with the PR EoS. Symbols: (□) critical point of Ar, (■) and (▲) critical and triple points of H_2S** [50]

Although solid-fluid equilibrium is slightly out of the scope of this research, the SLV equilibrium has been estimated following the classical approach. Basically, the fugacity (*f*) of a pure compound is related to the enthalpy (*H*), volume (*V*), temperature (*T*) and pressure (*P*) through this basic thermodynamic equation:

$$d\ln f = \frac{dG}{RT} = -\frac{H}{RT^2}dT + \frac{V}{RT}dP \tag{6.10}$$

In order to apply this equation to solid and liquid phases, the Equation 6.10 is integrated between the triple point and the P-T conditions at the SL equilibrium. Thus, the result of the integration is the following equation [165]:

$$\ln\frac{f^{0,L}}{f^{0,S}} = \frac{\Delta H}{RT_t}\left(\frac{T_t}{T}-1\right) - \frac{\Delta c_p}{R}\left(\frac{T_t}{T}-1-\ln\frac{T_t}{T}\right) + \frac{\Delta V(P-P_t)}{RT} \tag{6.11}$$

where ΔH is the latent heat of fusion, Δc_p and ΔV are the variations of heat capacity and volume between the solid and liquid, and P_t and T_t are the pressure and temperature at the triple point.

Regarding the fugacity of the solid phase, two main assumptions must be taking into consideration. First, it has been considered $\Delta c_p = 0$ and $\Delta V = 0$ because the volume and heat capacity can be considered as constant along the melting line [165]. Second, in the case of mixtures, a complete immiscibility in the solid phase is also taken into account, *i.e.* the solid phase is considered pure component.

The SLV equilibrium (SLVE) has been evaluated using the PR EoS with the BIP fitted at the lowest measured temperature (273 K), k_{ij}=0.2108. The equilibrium condition is based on the equality of solid, liquid and vapour fugacities. Thus, the fugacity of the solid phase is calculated by reformulating Equation 6.11 and considering the previous mentioned assumptions ($\Delta c_p = 0$ and $\Delta V = 0$) as follows

$$f_{H_2S}^{S} = f_{H_2S}^{0,L}\left[\exp\left(\frac{\Delta H_{H_2S}}{RT_t}\left(\frac{T_t}{T}-1\right)\right)\right]^{-1} \tag{6.12}$$

where the f^S is the fugacity of the solid H_2S and $f^{0,L}$ the fugacity of pure H_2S at the P-T conditions of the equilibrium. The composition of the solid phase is considered as pure

hydrogen sulphide, z_{H2S}=1, therefore argon is not taken into account in the fugacity of the solid phase.

The algorithm of the SLVE calculation is described in Figure 6.8. At a given temperature, a bubble point calculation is performed. The bubble point routine defines the VLE and ensures the equality of the liquid and vapour fugacities for both compounds. The calculated bubble pressure is used for obtaining the fugacity of the solid phase. Then, if the fugacity of the solid phase is equal to the vapour and liquid fugacities of H_2S, the SLVE will be already defined; in other cases, a new liquid composition will be guessed.

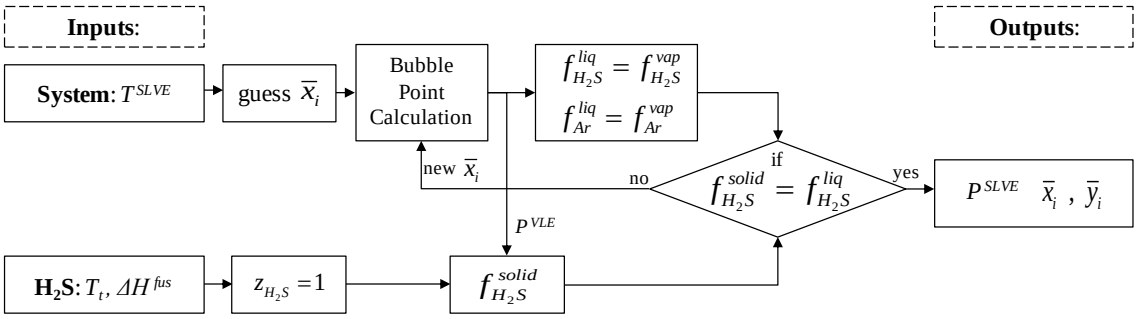

Figure 6.8. Flow chart of the SLVE calculation algorithm.

6.1.2 Conclusions

The VLE of the Ar-H_2S system have been studied using the SAFT-VR Mie and the PR EoS. Better predictions (k_{ij}= 0) of the measured VLE data were obtained with the SAFT-VR Mie EoS. The AAD between measured bubble pressure and calculated using the SAFT-VR Mie EoS with BIPs fitted at each temperature is 5.5% of AAD. The model has better performed the VLE data of this system has been the PR EoS with the Wong-Sandler mixing rules coupled with NRTL activity coefficient model (AAD=1.2%).

Finally, the phase diagram has been studied using the PR EoS. The BIP fitted at 273K has been extrapolated to lower temperature to calculate the critical lines and solid-fluid equilibria lines. According to the modelling results, the phase diagram of the Ar + H_2S can be classified as type IIIc, similar to the phase diagram of Ar + CO_2.

6.2 Density measurements of CH_4 - H_2S systems

The PR, SAFT-VR Mie and GERG-2008 equations of state have been used to model the density of the methane and hydrogen sulphide binary systems with 0.1315, 0.1803 and 0.286 molar fractions of H_2S. The average absolute deviations (%AAD) between the calculations from the models and measured experimental data are presented in following subsections.

6.2.1 Results

In addition to the previously presented models, a multi-parameter EoS, considered the reference model for the prediction of natural gas mixture properties, the GERG-2008 EoS, has been used to model the density of these binary mixtures. The GERG-2008 model is an empirical wide-range equation of state based on pure component EoSs and correlations for the binary systems [234,235]. Like the SAFT-like EoS, the GERG model is expressed in terms of the Helmholtz free energy, as the sum of an ideal gas contribution and a residual part.

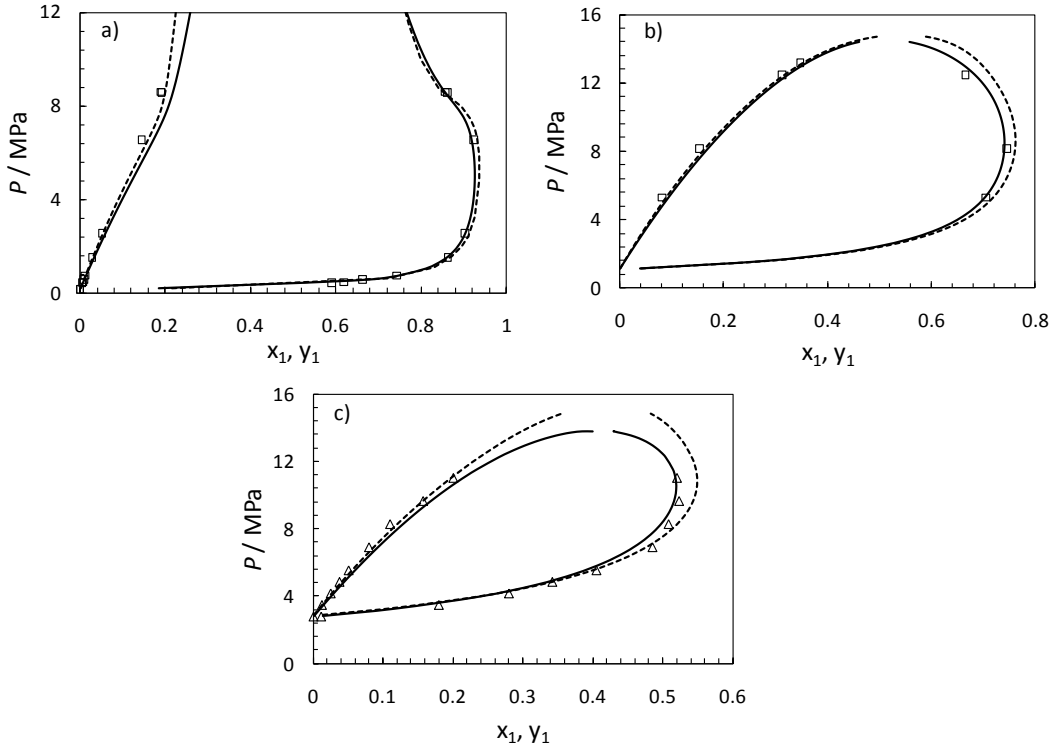

Figure 6.9. P-x diagrams of CH_4 (1) + H_2S (2) system at a) T =223.17K, b) T =273.54K and c) T=310.93. Symbols: (□) Coquelet et al. [45] **and (△) Kohn and Kurata** [43]**. Solid line: calculated bubble and dew lines using PR model with k_{ij} = 0.0807. Dashed line: calculated bubble and dew lines using SAFT-VR Mie EoS with k_{ij} = 0.0314.**

BIPs for the CH_4-H_2S system have been regressed for both the PR EoS (k_{ij}=0.0807) and the SAFT-VR Mie EoS (k_{ij}=0.0314) models using VLE data from the literature [32,43,45] (Figure 6.9). Using these BIPs, the PR EoS is slightly more accurate correlating the phase behaviour of the CH_4-H_2S system than the SAFT-VR Mie EoS, with bubble point pressure AADs of 4.4% and 4.8%, respectively.

The deviations of the PR, SAFT-VR Mie and GERG-2008 models for the three measured systems at each temperature are reported in Table 6.4. Generally, the SAFT-VR Mie EoS shows lower overall deviations (AAD=2.5%) than the other two models, PR EoS (3.0%) and GERG-2008 (3.4%). The experimental densities measured in this work and the predicted densities for the system 0.2860 H_2S molar fraction by using the GERG-2008 and SAFT-VR Mie EoSs are illustrated in Figure 6.10. As the GERG EoS is an empirical model developed for natural gases whose parameters for the CH_4+H_2S binary system have been fitted to experimental data over wide ranges of temperature (189 to 501 K), pressure (0.048 to 68.9 MPa) and methane mol fraction (0.1 to 0.9993) [234], it was unexpected that the GERG-2008 EoS reported the highest deviations for these systems, particularly for the 0.2860 mol fraction of H_2S system (Figure 6.10) with an AAD of 4.9%. However, the GERG-2008 EoS presents better results than SAFT and PR EoSs for the binary mixture with smaller amount of H_2S.

Table 6.4. Average absolute deviations (%AAD) between the studied models and the densities measured in this work.

x_{H2S}	T/K	SAFT-VR Mie	PR	GERG 2008
x=0.1315	253	3.3	4.8	2.1
	273	1.6	1.4	2.0
	293	3.9	2.2	4.3
	Total	3.0	2.9	2.8
x=0.1801	253	1.6	3.4	2.5
	273	1.5	2.0	2.6
	293	2.5	2.0	3.3
	Total	1.9	2.5	2.8
x=0.2860	253	1.8	4.1	4.6
	273	3.2	3.8	5.3
	293	3.1	3.1	4.8
	Total	2.8	3.6	4.9

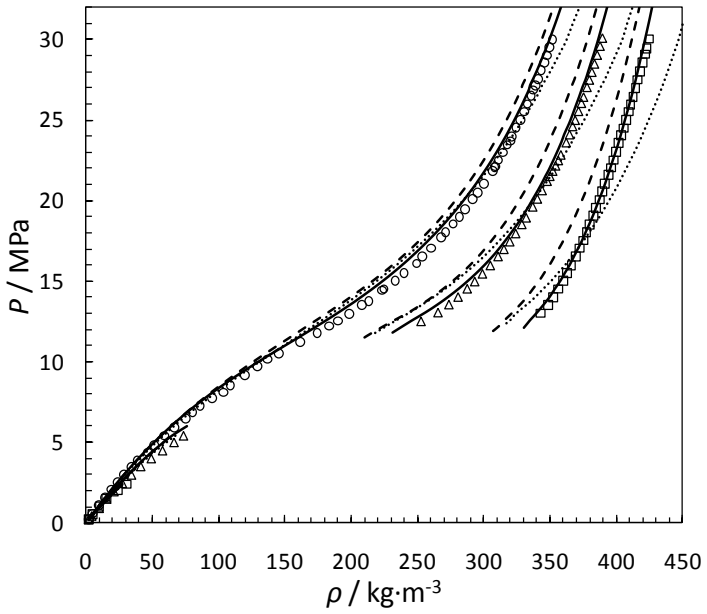

Figure 6.10. Experimental and predicted densities of the 0.714 mole CH_4 + 0.286 mole H_2S system. Experimental results: (□) 253 K, (○) 273 K, (△) 293 K. Lines: Predictions using the SAFT-VR Mie EoS. Dashed lines: Predictions using the GERG-2008 EoS. Dotted lines: Predictions using the PR EoS.

Density data available in the literature (1748 points) and those measured in this work have been modelled with the PR, PR + Peneloux volume correction, SAFT-VR Mie and GERG-2008 equations of state, and the deviations are listed in Table 6.5. As can be observed, the SAFT-VR Mie EoS reports the lower deviation between experimental and calculated densities with an AAD of 4.3%, while GERG-2008 shows similar level of agreement (4.6%). The experimental densities of 50 mol% H_2S + 50 mol% CH_4 and the predicted densities using the PR + Peneloux, GERG-2008 and SAFT-VR Mie EoSs are presented in Figure 6.11, as an example of the modelling result of this system at high pressure (up to 70MPa).

Table 6.5. Average absolute deviation (%AAD) between the available experimental data and the studied models.

Author	No Data	PR	PR+Peneloux	SAFT-VR Mie	GERG 2008
Bailey et al. [33]	80	5.1	3.9	4.6	3.3
Reamer et al. [32]	1140	10.2	5.5	5.0	5.3
This work	526	3.0	5.2	2.5	3.4
Total	1748	7.8	5.4	4.3	4.6

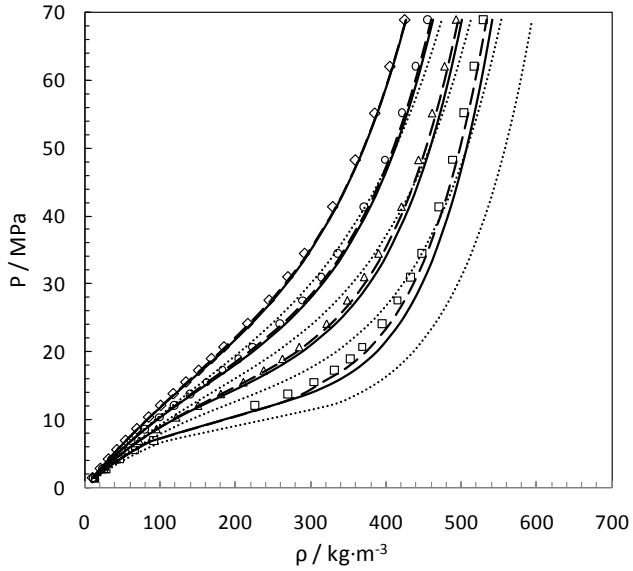

Figure 6.11. Experimental and predicted densities of the 0.5 mole CH_4 + 0.5 mole H_2S system. Experimental results: (□) 311 K, (△) 344 K, (○) 377 K and (◇) 411 K [32]**. Lines: Predictions using the SAFT-VR Mie EoS. Dashed lines: Predictions using the GERG-2008 EoS. Dotted lines: Predictions using the PR+Peneloux EoS.**

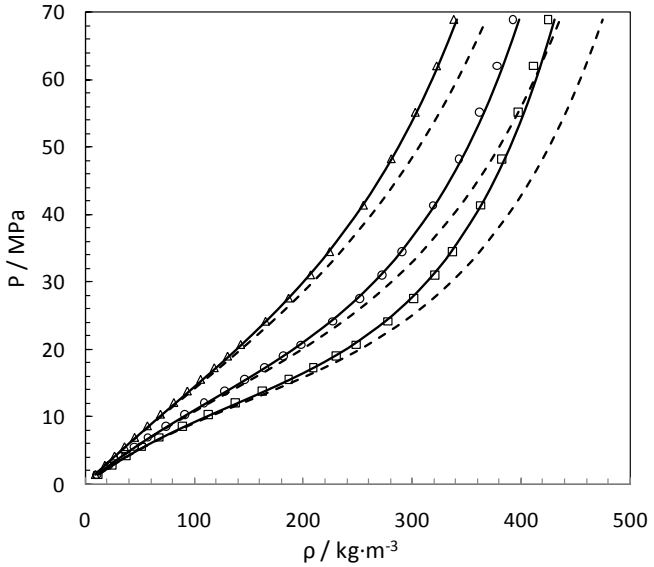

Figure 6.12. Experimental and predicted densities of the 0.7 mole CH_4 + 0.3 mole H_2S system. Comparison of PR+Peneloux (continuous curve), PR (dashes) and literature data at T=311K (□), T=344K (○) and T=411K (△) [32]**.**

The PR-EoS has reported the largest total deviation (AAD=7.8%), especially when PR calculations are compared against Reamer et al. [32] data at pressures above 30 MPa. The results of the PR EoS with volume correction (VC) have not been presented in Table 6.4 because no better density predictions were observed after applying the Peneloux VC to model our measured densities. However, remarkable improvements in

the density calculations with the PR-EoS can be noticed in the results of modelling the full Reamer's data set using the PR-Peneloux, decreasing by half the AAD. The AAD reduces from 7.8% to 5.4% when the complete density data set is modelled using the PR with Peneloux shift model. Figure 6.12 shows the comparison of PR and PR-Peneloux calculations against literature data of the 0.3 mol fraction H_2S system, in order to illustrate the large deviations of the PR EoS at high pressure.

The uncertainties for each measured density were reported together with data in Tables B.1-B.9 (Appendix B). The uncertainties were evaluated as combined standard uncertainty with 95% level of confidence. Despite the low average uncertainty (0.5%), the uncertainty of the density measurements below 0.5MPa is 8.3% with a maximum value of 10.1%. This high uncertainty was expected due to the fact that the vibrating tube densitometer is not the most appropriate technique for the determination of the densities of gases at low pressure (i.e. low mass in the VTD) [54]. The elevated uncertainty of density at low pressure is propagated to compressibility factor calculations (Figure 6.13).

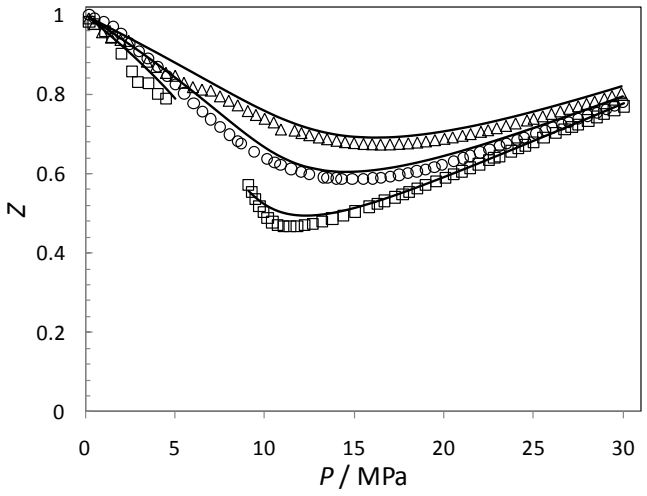

Figure 6.13. Compressibility factor of the 0.8197 mol CH_4 + 0.1803 mol H_2S system. Comparison between the SAFT-VR Mie calculation and experimental data measured in this work: T=253K (□), T=273K (○) and T=293K (△).

Determination of Second virial coefficients

The volumetric behaviour of the CH_4 + H_2S binary mixture at low pressure has been studied with the virial expansion truncated after the second coefficient. A virial equation provides a simple way to describe thermodynamic properties, and the virial coefficients

can be determined by different experimental methods or correlations [236]. The form for our virial expansion is given by:

$$Z = 1 + \rho B(T, x_1) \tag{6.1}$$

where *B* is the second virial coefficient which is calculated as a function of temperature and mol fraction of methane (x_1) as:

$$B(T, x_1) = a + \frac{b}{T} + \frac{c}{T^3} + d x_1 \tag{6.2}$$

where *a*, *b*, *c* and *d* are the parameters reported in Table 6.6. These parameters have been correlated using our density measurements and the low pressure *PTρx* data sets from the literature [32,33]. The correlated virial equation of state has an AAD of 1.5% with a maximum deviation of 5.7% in a wide range of compositions, pressures up to 1.9 MPa and temperatures between 253 and 500 K (Figure 6.14). Several isotherms calculated with our CH_4+H_2S virial equation of state are illustrated in Figure 6.15.

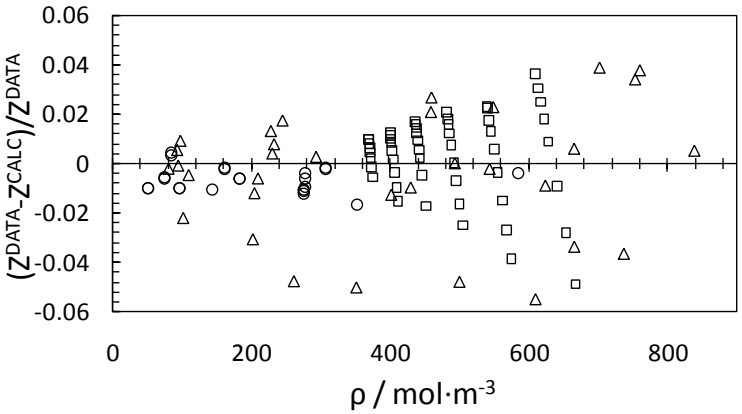

Figure 6.14. Deviations between this work (△), Reamer et al. data (□) [32] **and Bailey et al. data (○)** [33] **and predictions using the low pressure virial EoS.**

Table 6.6. Regressed parameters for the calculation of the second virial coefficient *B*, condition ranges and AAD deviations between the correlation and experimental compressibility factors.

Parameters	**a ($m^3 \cdot mol^{-1}$)**	**b ($m^3 \cdot K \cdot mol^{-1}$)**	**c ($m^3 \cdot K^3 \cdot mol^{-1}$)**	**d ($m^3 \cdot mol^{-1}$)**
	1.5385×10^{-4}	-6.6201×10^{-2}	-1.5017×10^{2}	9.1010×10^{-5}
Range	**CH_4 mole fraction**	**Pressure (MPa)**	**Temperature (K)**	
	0.1 - 0.9	0.17 – 1.88	253 - 500	
Deviation	**%AAD**	**Max.Dev.**		
	1.5%	5.7%		

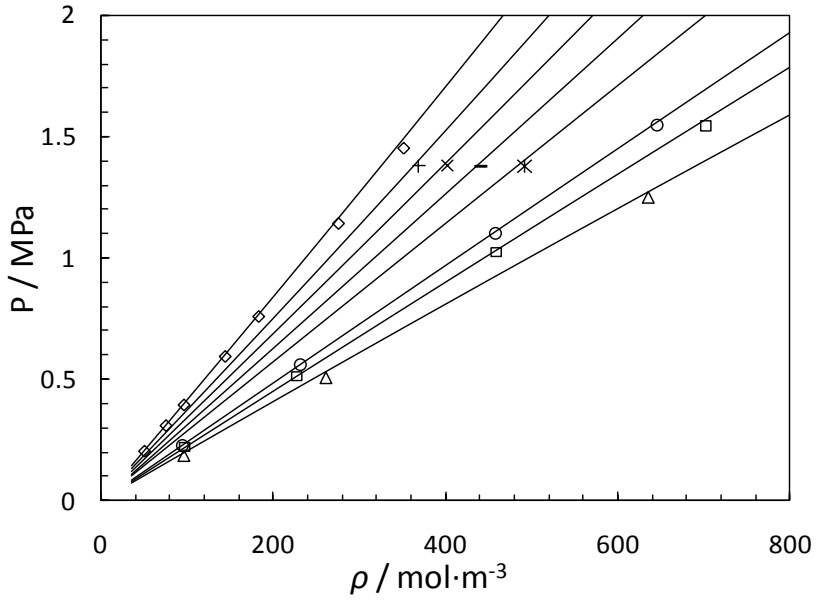

Figure 6.15. P-ρ diagram of several systems of H_2S + CH_4 at 8 isotherms. Comparison of predictions with low pressure virial EoS and experimental data: T=253K and x_{CH4}=0.87 (△), T=273K and x_{CH4}=0.82 (□), T=293K and x_{CH4}=0.71 (○), T=344K and x_{CH4}=0.4 (∗), T=377K and x_{CH4}=0.5 (–), T=411K and x_{CH4}=0.6 (+), T=444K and x_{CH4}=0.8 (×) and T=500K and x_{CH4}=0.5 (◇) [32,33]**.**

6.2.2 Conclusions

Density data measurements for the three binary mixtures of methane with 0.1315, 0.1803 and 0.286 mol fraction of hydrogen sulphide were performed at three temperatures between 253 and 293 K and pressures up to 30 MPa by using a vibrating tube Anton Paar densitometer. The average uncertainty of the measurements at the 95% confidence level is 0.5%, reporting the highest average uncertainty of 8.3% at low pressures (below 0.5 MPa).

The measured experimental data were compared with the densities predicted with the PR, SAFT-VR Mie and GERG-2008 equations of state. For these measurements the SAFT-VR Mie EoS has the lowest average absolute deviation (2.5%) among the three investigated models. The deviations for all models are of the same order (3.4 % for the GERG EoS and for 3.0 % the PR EoS without volume correction 3.0%). However, the GERG-2008 is slightly superior to describe the density of the 0.1315 mol fraction of H_2S system (AAD=2.8%) than the SAFT-VR Mie (AAD=3.0%) and PR (AAD=2.9%) EoSs.

Furthermore, the literature data have been studied with the different models. When compared against the full density dataset, the lowest deviations are observed for the SAFT-VR Mie (4.3 %). The deviations with GERG-2008, PR, PR-Peneloux EoSs were 4.6, 7.8 and 5.4 %, respectively. Significant improvement in density predictions are observed when volume corrections are used with the PR-EoS, due to the overestimated densities predicted by the PR EoS at pressures over 30MPa.

Finally, the measured densities and the *PTρx* data from the literature at low pressure were used to correlate the second virial coefficient as a function of temperature and CH_4 molar fraction. The average absolute deviation of the compressibility factor calculated from our virial EoS in a wide range of compositions and at pressures up to 1.9 MPa and temperatures between 253 and 500 K is 1.5% with a maximum deviation of 5.7%.

6.3 Density measurements of $C_2H_6 + H_2S$ and $C_3H_8 + H_2S$

The densities of the binary systems with 0.661 mole C_2H_6 + 0.339 mole H_2S and 0.867 mole C_3H_8 + 0.133 mole H_2S have been studied using the PR, SAFT-VR Mie and GERG-2008 equations of state. The modelling results are presented by comparing the average deviations (%AAD) between the models and the experimental data.

6.3.1 Results

Before the density calculations, the phase behaviours of the C_2H_6-H_2S and C_3H_8-H_2S binary mixtures have been studied using the PR and SAFT-VR Mie EoSs. Thus, BIPs for these systems have been regressed for both EoSs. The values of BIPs for the system containing ethane are k_{ij}=0.0838 (PR) and k_{ij}=0.0506 (SAFT-VR Mie), and for the system with propane are k_{ij}=0.0819 (PR) and k_{ij}=0.0524 (SAFT-VR Mie). Using the fitted BIPs, the SAFT-VR Mie is slightly more accurate to correlate the VLE of the systems than the PR EoS (Fig 6.16), with bubble point pressure AADs of 4.72 and 3.28% for the SAFT-EoS and 4.76 and 4.55% for the CEoS, respectively for the ethane and the propane systems.

The density deviations between the PR, PR+Peneloux, SAFT-VR Mie and GERG-2008 models and density data measured in this work and from the literature are reported in Table 6.7. Regarding the systems containing ethane, the GERG-2008 model presents a remarkable low deviation (AAD=0.4%), while the SAFT-VR Mie reports has also

reported low deviation (1.1%). Concerning the H_2S+C_3H_8 systems, the SAFT-VR Mie model is the equation of state which presents the lowest AAD (1.9%) and the GERG-2008 EoS has given a slightly higher deviation (2.1%). The PR EoS is the model that has reported the highest deviations 5.3 and 7.0% for the ethane and the propane systems respectively. The use of the Peneloux volume correction improves the density calculations of the PR EoS, reducing the %AAD to 3.58% for the C_2H_6+H_2S and to 3.9% for the H_2S+ C_3H_8 systems.

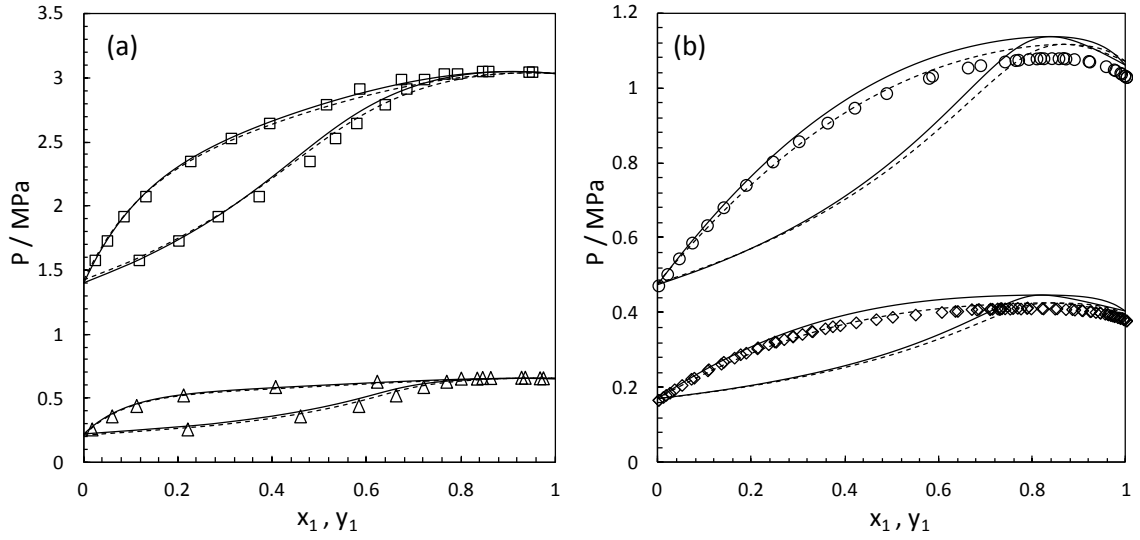

Figure 6.16. P-x diagrams of C_2H_6 (1) + H_2S (2) system (a) at (△) 200 and (□) 253 K [237] **and the H_2S (1) + C_3H_8 (2) system (b) at (◇) 243 and (○) 273 K** [238]**. Solid line: calculated bubble and dew lines using PR model with the adjusted k_{ij}. Dashed line: calculated bubble and dew lines using SAFT-VR Mie EoS with the adjusted k_{ij}.**

Table 6.7. Average absolute deviation (%AAD) between the available experimental data and the studied models.

System	Author	No Data	PR	PR+Peneloux	SAFT-VR Mie	GERG 2008
C_2H_6 + H_2S	Rivollet et al. [20]	346	5.17	3.42	1.14	0.32
	This work	173	5.46	3.90	0.93	0.68
	Total	519	5.27	3.58	1.07	0.44
C_3H_8 + H_2S	Jarne et al. [22]	182	7.49	5.94	3.20	3.27
	This work	170	6.60	1.72	0.45	0.89
	Total	352	7.06	3.90	1.87	2.12

Experimental and predicted densities using the GERG-2008, SAFT-VR Mie and PR EoSs are illustrated in Figures 6.17 and 6.18 at the three measured temperatures. From observing these charts, it is worth noting that the GERG-2008 and SAFT-VR Mie describe similarly the density of both binary mixtures whereas the PR EoS presents significant deviations with increasing pressures.

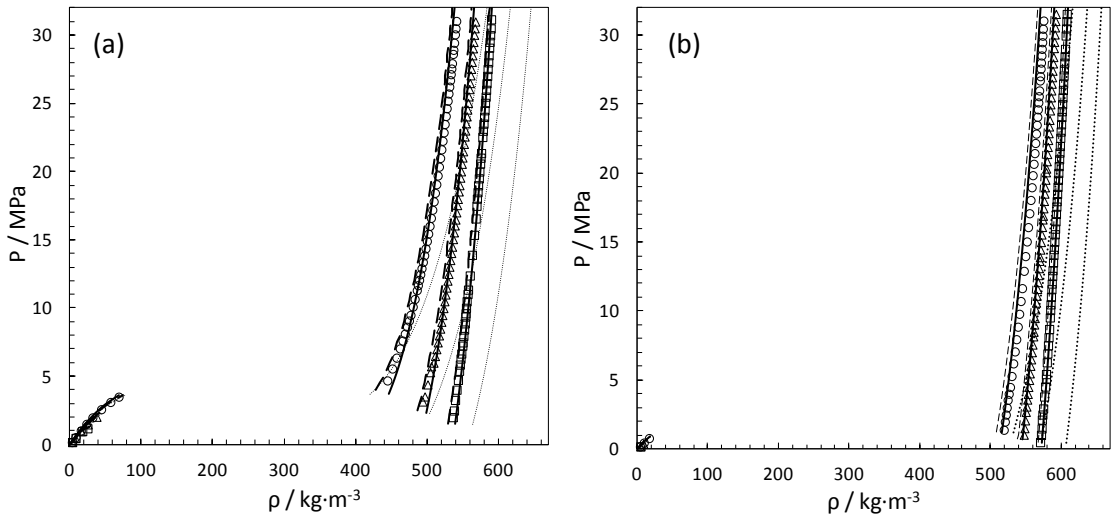

Figure 6.17. Experimental and calculated densities of the systems 0.661 mole C_2H_6 + 0.339 mole H_2S (a) and 0.661 mole C_3H_8 + 0.339 mole H_2S (b). Experimental results: (□) 253 K, (○) 273 K, (△) 293 K. Lines: Predictions using the SAFT-VR Mie EoS. Dashed lines: Predictions using the GERG-2008 EoS. Dotted lines: Predictions using the PR EoS.

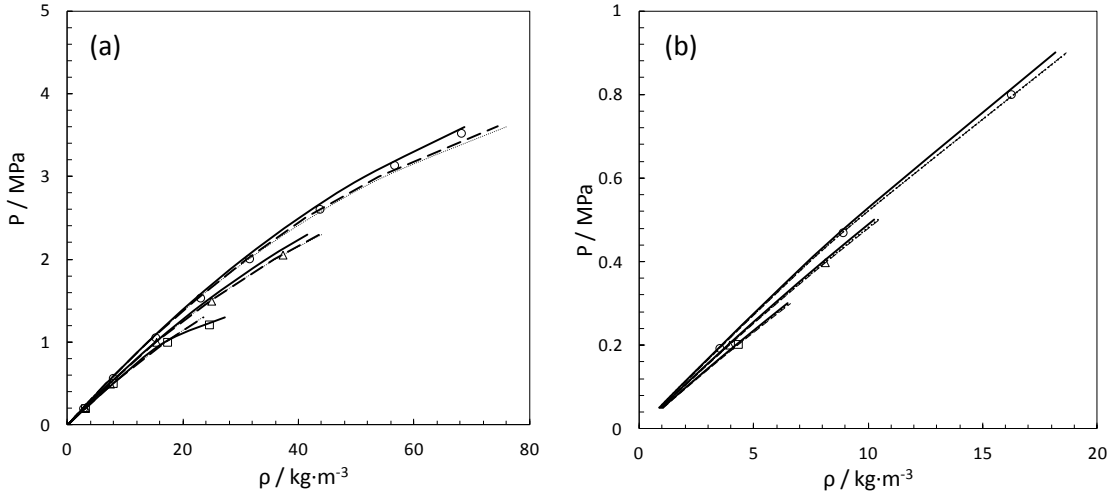

Figure 6.18. Experimental and calculated densities at low pressure of the systems 0.661 mole C_2H_6 + 0.339 mole H2S (a) and 0.661 mole C_3H_8 + 0.339 mole H_2S (b). Experimental results: (□) 253 K, (○) 273 K, (△) 293 K. Lines: Predictions using the SAFT-VR Mie EoS. Dashed lines: Predictions using the GERG-2008 EoS. Dotted lines: Predictions using the PR EoS.

In Tables B.10-B.15, the measured densities are presented together with the uncertainties. The average uncertainty of the measurements is 0.5%, with the uncertainty at low pressure (below 0.5MPa) is 4.8% and the maximum value of 6.9%. The uncertainties of these measurements are lower than the uncertainties reported in the previous section for the CH_4 + H_2S systems. This is because the reference fluid used for the calibration was ethane and there is an important difference between the density of methane and ethane. Nonetheless, the uncertainty at low pressure is much higher than at pressures over 1 MPa and these elevated uncertainties are propagated to the compressibility factor calculations (Figure 6.19) reported also in Tables B.10-B.15.

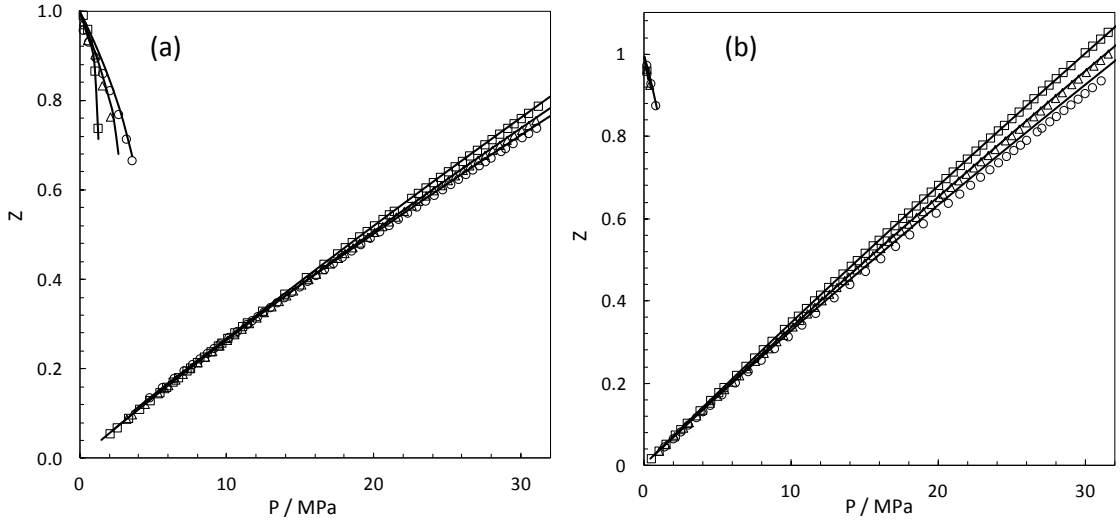

Figure 6.19. Compressibility factor of the systems 0.661 mole C_2H_6 + 0.339 mole H2S (a) and 0.661 mole C_3H_8 + 0.339 mole H_2S (b). Comparison between the SAFT-VR Mie calculation and experimental data measured in this work: T=253K (□), T=273K (○) and T=293K (△).

6.3.2 Conclusions

Density data of the 0.661 mol C_2H_6 + 0.339 mol H_2S and 0.867 mol C_3H_8 + 0.133 mol H_2S binary systems were measured at three temperatures between 253 and 293 K and pressures up to 30 MPa by using a vibrating tube Anton Paar densitometer. The average uncertainty of the measurements is 0.5%, although the uncertainty at low pressures is 4.8% (below 0.5 MPa).

The density data measured in this work and from the literature were compared with the density calculations performed with the PR, PR+Peneloux, SAFT-VR Mie and GERG-2008 equations of state. For the C_2H_6 + H_2S binary systems, the GERG-2008 model is

the EoS which reported the lowest deviations with an AAD=0.4%, while the deviation of the density calculations with the SAFT-VR Mie EoS is 1.1% and the AAD using the PR EoS is 5.3 and 3.6% with and without the Peneloux volume correction respectively. For the studied systems containing C_3H_8, the deviations reported for each model were 1.9% for the SAFT-VR Mie EoS, 2.1% for the GERG-2008 model, 7.1% for the PR and 3.9% for the PR+Peneloux.

6.4 Density measurements of CO_2+CH_4+H_2S ternary system

The PR, SAFT-VR Mie and GERG-2008 EoSs are again the models used for performing the density calculations for the 0.4212 mol CO_2 + 0.4053 mol CH_4 + 0.1735 mol H_2S ternary mixture. The results are presented through the average absolute deviations between the calculations from the models and the measured experimental data.

6.4.1 Results

The P-T envelop of this ternary system has been presented in Chapter 2. The BIPs used for modelling the phase behaviour of the mixture have been regressed during the comparative study in Chapter 4. The density calculations have been performed using the BIPs summarised in Table 6.8.

Table 6.8. Binary interaction parameters between CH_4, CO_2 and H_2S for the PR and SAFT-VR Mie EoSs.

	PR			SAFT-VR Mie		
	CH_4	CO_2	H_2S	CH_4	CO_2	H_2S
CH_4	0	0.0951	0.0807	0	0.0042	0.0314
CO_2	0.0951	0	0.0966	0.0042	0	0.0261
H_2S	0.0807	0.0966	0	0.0314	0.0261	0

The deviations between the measured density data and the calculations from the PR, SAFT-VR Mie and GERG-2008 models are reported in Table 6.9. On average, the SAFT-VR Mie EoS shows the lowest overall deviation (AAD=2.11%). The PR EoS has also performed the density of this mixture with low deviation, 2.24% of AAD, similar to the reported for the SAFT-like EoS. The GERG-2008 model has described the density of this ternary system with the highest overall deviation, 3.99%.

Table 6.9. Average absolute deviations (%AAD) between the studied models and the densities measured in this work.

T [K]	SAFT-VR Mie	PR	GERG 2008
253	1.47	3.36	6.43
273	1.42	3.42	4.74
293	3.01	2.29	2.34
313	2.14	1.77	3.07
333	2.16	2.34	3.72
353	2.48	2.25	3.68
Average	2.11	2.57	3.99

As for the previous presented system 0.714 mol fraction CH_4 + 0.286 mol fraction H_2S (Section 6.2), the GERG-2008 EoS has reported the highest deviations describing the density of the ternary mixtures, particularly at the lowest temperature (Figure 6.20). One has found no reason to explain the weakness of the GERG-2008 model to calculate densities of H_2S-rich systems (around 20%) at low temperature. One expects that after tuning the GERG-2008 parameters taking into account the density data of the CH_4+H_2S binary systems measured in this work, the density calculations of this system will be improved.

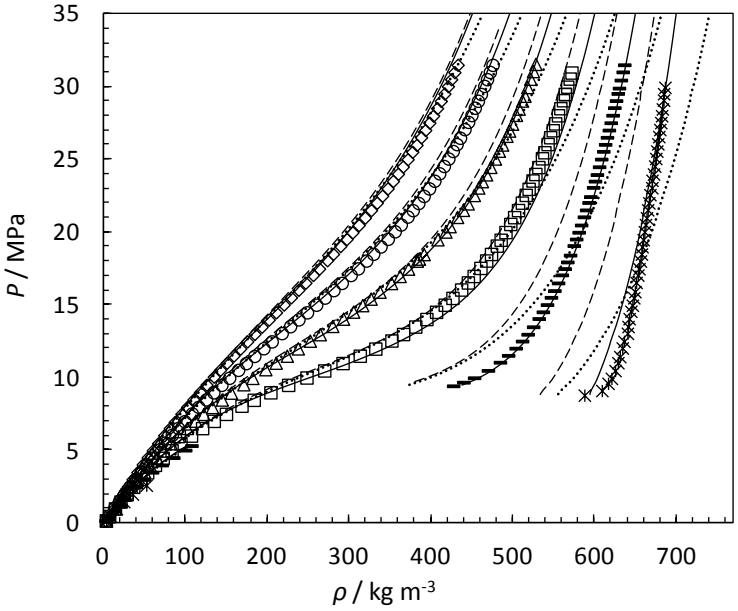

Figure 6.20. Experimental and calculated densities of the CO_2 + CH_4 + H_2S ternary mixture. Continuous lines: calculations using the SAFT-VR Mie EoS. Dashed lines: calculations using the GERG-2008 EoS. Dotted lines: calculations using the PR EoS. Experimental results: (∗) 253 K, (–) 273 K, (□) 293 K, (△) 313, (○) 323 K, and (◇) 353 K.

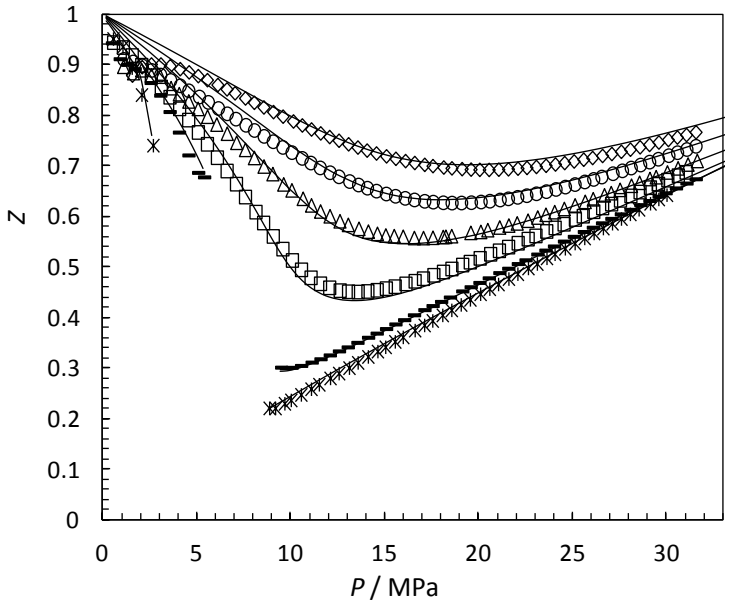

Figure 6.21. Compressibility factor of the CO_2 + CH_4 + H_2S ternary mixture. Comparison between the SAFT-VR Mie calculation and experimental data in this work: (∗) 253 K, (–) 273 K, (□) 293 K, (△) 313, (○) 323 K, and (◇) 353 K.

The results can be divided in two parts: low (253-273K) and high (293-353K) temperature. At the lowest temperatures, the SAFT-VR Mie EoS has performed the density with the lowest deviation, 1.45%. As it can be observed in Figure 6.20, the PR calculations at 253 and 273 K present a totally different behaviour than the measured data, while the GERG-2008 model follows the trend of the data despite the higher AAD. The data at the highest temperatures have been modelled with lower deviation using the PR EoS, 2.2%. Nonetheless, considering the trend of the data and the deviation at the highest pressures of the PR EoS, higher deviations with increasing pressures can be expected.

The higher deviation of the three equations of state is observed at the lowest pressure, with a maximum deviation for all the models around of 19% (Figure 6.22). The high deviation is also related with the high uncertainty of the measurements in the gas state and at low pressures. The average uncertainty of the measurement in the whole range of pressures is 0.4%, while the uncertainty at low pressures (below 0.5 MPa) is 5.8% with a maximum value of 7.9%.

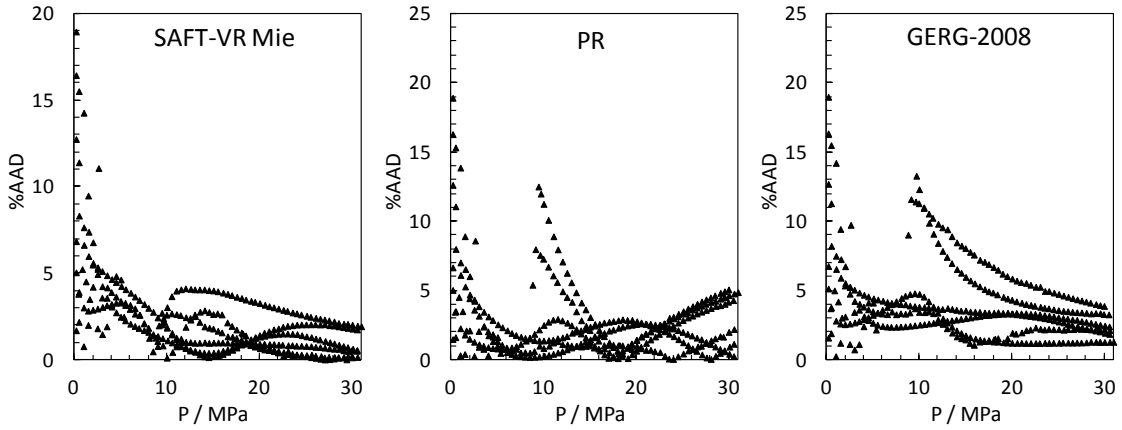

Figure 6.22. Absolute deviations in density calculations of the CO_2 + CH_4 + H_2S ternary mixture at temperatures between 253 and 353K.

6.4.2 Conclusions

The densities of a ternary mixture with 0.4212 mol CO_2 + 0.4053 mol CH_4 + 0.1735 mol H_2S have been measured at 253.10, 273.74, 293.37, 313.82, 333.98 and 353.63K and pressures up to 30MPa using an Anton Paar densitometer. The overall uncertainty of the measurements is 0.4%, with a higher uncertainty of the measurements below 0.5MPa (5.8%).

The SAFT-VR Mie EoS is the model which has reported the lower absolute deviations between our data and the density calculations (AAD=2.1%), particularly at the lowest temperatures. The PR EoS has as well performed the density of this ternary mixture with low deviation (AAD=2.6%). The GERG-2008 model is the EoS that gives the poorest density predictions (AAD=4.0%), especially at the lowest temperatures studied with an average deviation at 253K of 6.4%.

The high deviation reported by the GERG calculations was unexpected as the GERG-2008 EoS is considered the reference model for natural gases. The GERG model reported similar deviations for the 0.714 CH_4 + 0.286 H_2S mixture at 253 K, therefore the GERG-2008 EoS parameters for the CH_4+H_2S binary system can be refitted using our density measurements in order to improve the density predictions presented in this work.

6.5 Density and viscosity measurements of a multicomponent CO_2–rich mixture

The densities of the multicomponent CO_2-rich mixture (MIX4) have been modelled using the PR, PR+Peneloux, SAFT-VR Mie and GERG-2008 equations of state. The viscosity of this mixture has been studied with the TRAPP model using the measured density and the density predictions from the SAFT-VR Mie.

6.5.1 Results

The main components of the studied mixture are carbon dioxide, methane, ethane and nitrogen. The binary interaction parameters used in the density calculations have been regressed during the comparative study in Chapter 4, for the binary systems composed of CO_2, CH_4, C_2H_6 and N_2 and the alkanes. The BIPs between propane, *n*-butane, *i*-butane and *n*-pentane are considered as k_{ij}=0.

The deviations of the PR, PR+Peneloux, SAFT-VR Mie and GERG-2008 EoSs for the measured multicomponent mixture are reported in Table 6.10. The GERG-2008 has reported lowest average deviation (AAD=2.2%). The SAFT-VR Mie EoS presents an AAD slightly higher (2.3%) than the GERG-2008 model. The PR EoS is the model which performs the measured density with higher deviation, 3.0 and 3.3% with and without volume correction.

Table 6.10. Average absolute deviation (%AAD) between the measured density data and the studied models.

	SAFT-VR Mie	PR	PR+Peneloux	GERG-2008
MIX4	2.33	3.32	3.03	2.22

The experimental and modelling results for the density of the MIX4 are plotted in Figure 6.23. The densities calculated using the PR EoS are not presented in order to avoid confusing lines in the chart.

The viscosities of this multicomponent mixture have been studied using the TRAPP model. Under the framework of the TRAPP model the viscosity of the studied mixture is related to the viscosity of the reference fluid. The viscosities of the MIX4 have been predicted using two different reference fluids: propane (SUPERTRAPP) and carbon

dioxide (CO_2-SUPERTRAPP). The density of the mixture, required to compute the viscosity values, have been calculated using the density predictions from the SAFT-VR Mie EoS and the experimental densities measured.

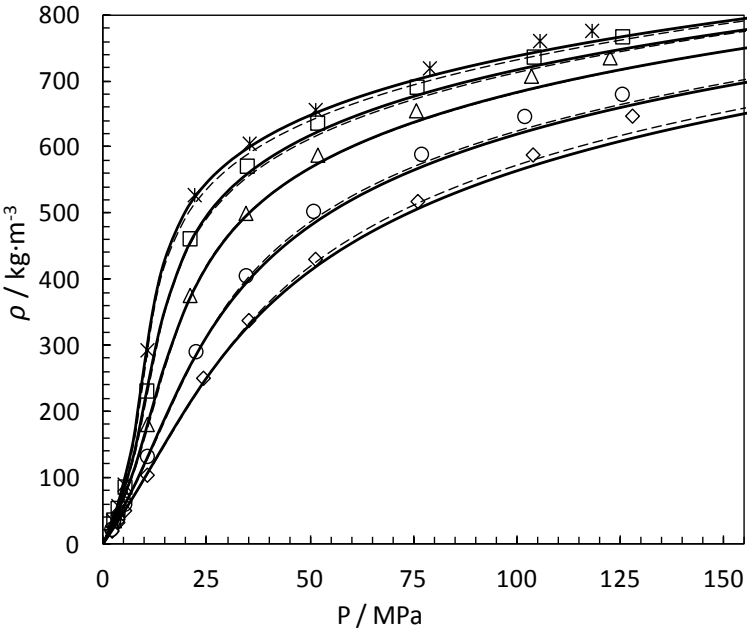

Figure 6.23. *ρ-P* diagram of the MIX4. Comparison of predictions with the SAFT-VR Mie (continuous lines) and GERG-2008 (dashed lines) EoSs and experimental data at 283 (∗), 298 (□), 323 (△), 373 (○) and 423K (◇).

Table 6.11. Average absolute deviation in viscosities calculations with the SUPERTRAPP and CO2-SUPERTRAPP models using predicted and experimental densities.

	SAFT-VR Mie		Experimental density	
	SUPERTRAPP	CO_2-SUPERTRAPP	SUPERTRAPP	CO_2-SUPERTRAPP
MIX4	15.5	16.7	15.3	16.4

In Table 6.11, the average absolute deviations between modelled and experimental viscosities of MIX4 are presented. The SUPPERTRAPP (ST) has reported lower deviation than the CO_2- SUPPERTRAPP (CO_2-ST). As expected, both TRAPP models present better predictions using the measured values of the densities.

In Chapter 5, the viscosities of two CO_2-rich mixtures (MIX2 and MIX3) were calculated using the ST and CO_2-ST models. In that case, the viscosities of these CO_2-rich mixtures with 10 and 30% of impurities were better predicted by the CO_2-ST

model. However, the viscosities of the MIX4 (50% of impurities) have been better performed using the ST model with the propane as reference.

In Figure 6.24, the experimental and modelling results using the ST method coupled with the SAFT-VR Mie EoS are presented. The deviation reported for the ST model at the highest pressure (150 MPa) has been around 20%. The high deviations presented for the ST and CO_2-ST models are the reason why the viscosity calculations have been also performed using the measured densities. However, the use of the experimental density values has not improved remarkably the viscosity predictions. Quantitatively, a correction in the input densities of 2.3% (deviation between experimental and predicted densities) has reduced the deviations in the viscosity calculations around 0.2 and 0.3% for the ST and CO_2-ST models respectively. In Figure 6.25, the viscosity predictions from the ST and CO_2-ST models are presented against the experimental measurements. As depicted in this figure, ST predictions are clearly overestimated, while the CO_2-ST predictions are underestimated.

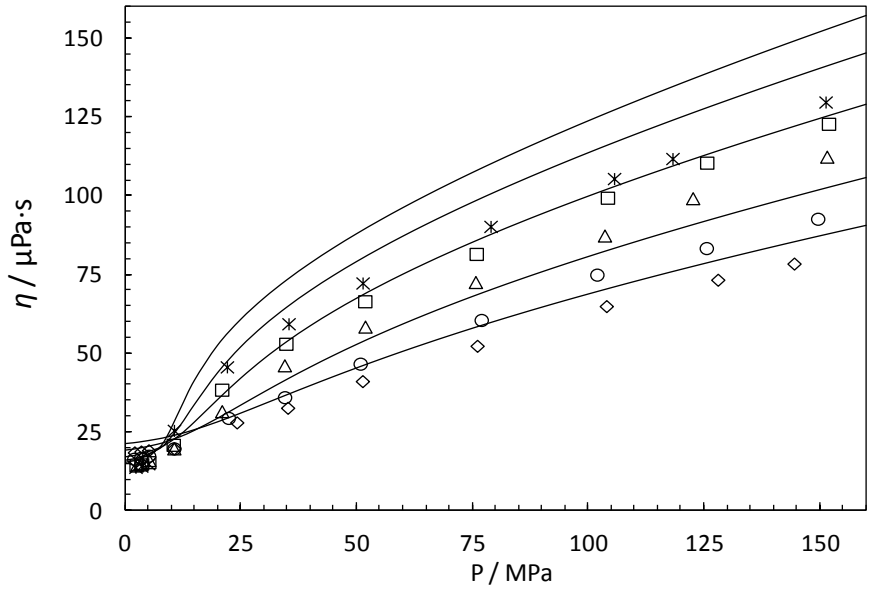

Figure 6.24. Experimental and predicted viscosity of MIX4. Continuous line: predictions using the SUPERTRAPP+SAFT-VR Mie EoS. Data at 283 (∗), 298 (□), 323 (△), 373 (○) and 423K (◇).

In Figure 6.26, the measured viscosities of MIX4 are presented together with the viscosities of pure CO_2 and the two studied multicomponent CO_2-rich mixtures (MIX2 and MIX3) in Chapter 5. It can be observed in this chart that the viscosity of the CO_2-rich mixtures decreases with the increasing amount of impurities.

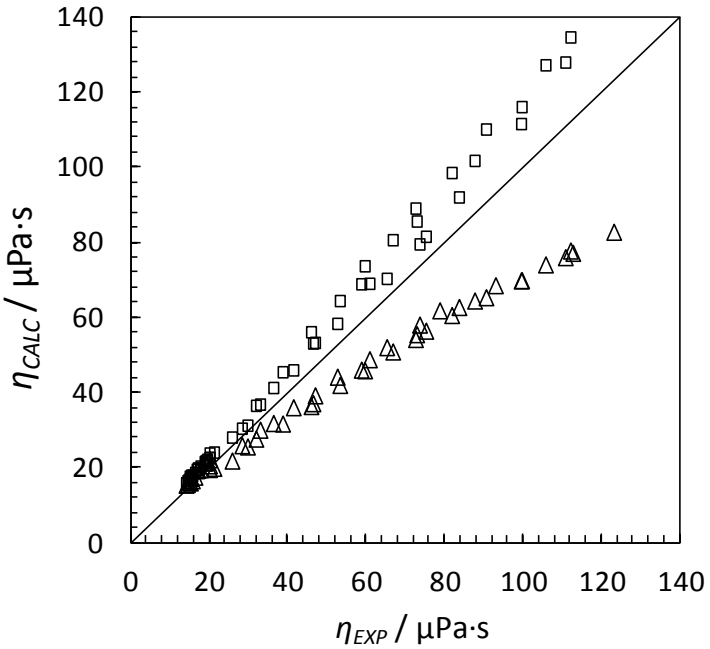

Figure 6.25. Viscosity predictions from ST (□) and CO_2-ST (△) models against experimental measurements.

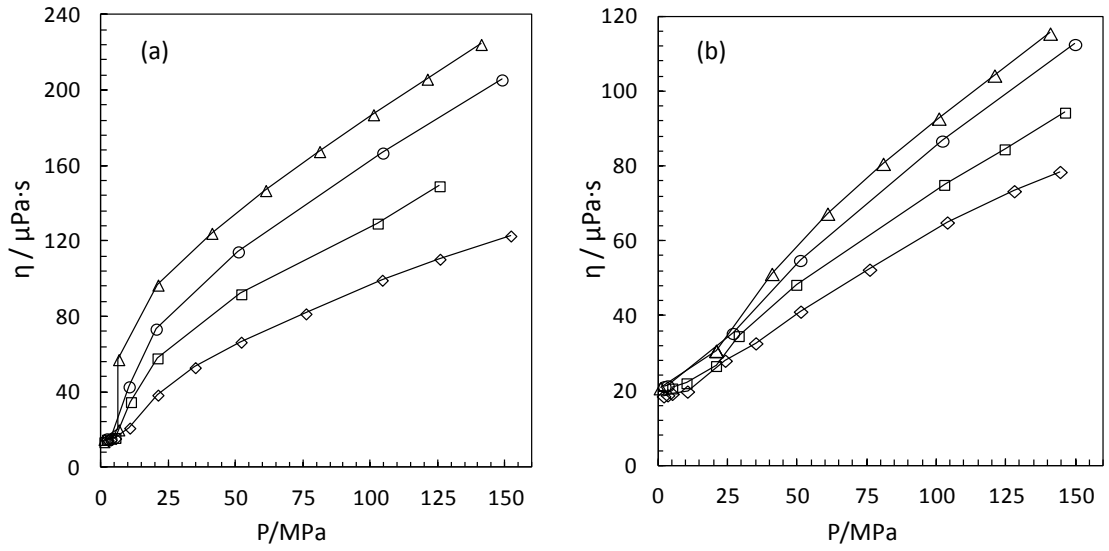

Figure 6.26. Experimental viscosity of pure CO_2 and three multicomponent CO_2-rich mixtures at 298 (a) and 423 (b) K. Data: pure CO_2 (△) [171]**, MIX2(○)** [55]**, MIX3 (□)** [24] **and MIX4 (◇) (this work).**

6.5.2 Conclusions

The densities and the viscosities of a multicomponent CO_2-rich (MIX4) have been measured in an in-house design set-up at 283.3, 298.3, 323.4, 373.5 and 423.4 K and pressures up to 150 MPa.

The GERG-2008 model has reported lower deviation (AAD=2.2%) than the SAFT-VR Mie (2.3%), the PR (3.3%) and PR+Peneloux (3.0%) equations of state.

The viscosities of the MIX4 have been studied using the ST and CO_2-ST models. In contrast with the modelling results reported for the MIX2 and MIX3, the ST+SAFT-VR Mie model has predicted the viscosity of the MIX4 with lower deviation (around 15%) than CO_2-ST model (around 16%). The viscosity predictions of both TRAPP models have slightly improved when using the experimental density measured in this work.

CHAPTER 7: CONCLUSIONS AND FUTURE WORK

In this thesis the phase behaviour and transport properties of mixtures relevant to carbon capture and storage have been investigated. The research covered the experimental and modelling study of thermophysical properties of mixtures containing typical compounds in flue gas streams.

The SAFT-VR Mie EoS has been used for predicting vapour-liquid equilibria and density of mixtures with non-associative compounds. The model was validated with measured and literature data and compared with other equations of state. The SAFT-VR Mie EoS has been coupled with the TRAPP method and the DGT model to predict the viscosity and IFT of CO_2-rich systems, respectively.

The experimental investigations covered VLE, density and viscosity measurements of binary and multicomponent mixtures containing H_2S, CO_2, alkanes, Ar and N_2. The SAFT-VR Mie, PR, PR+Peneloux and GERG-2008 models are the equations of state that have been used for modelling the measured density and VLE data.

7.1 Modelling investigation

Experimental vapour-liquid equilibria and density data for mixtures of CO_2, H_2S, N_2, methane and propane with gases (O_2, Ar, CO, SO_2), alkanes and aromatic compounds have been gathered from the literature. The capabilities of four EoSs for modelling the phase and volumetric behaviour of non-associative compounds have been assessed. Thus, a comparative study has been made between the SRK, PR, PC-SAFT and SAFT-VR Mie EoSs in the scope of CCS. First, the phase behaviours of 108 binary systems of typical components of flue gases and reservoir fluids have been investigated with these EoSs. The SAFT-VR Mie EoS is the model which better predicts (k_{ij}=0) the VLE of these systems with an average deviation in the bubble pressure of 13.3%, although all the models present comparable deviations. Independent temperature binary interaction parameters (BIPs) have been regressed on the VLE data. To correlate the phase equilibria of the investigated systems, all the models lead to similar deviations with slightly lower AAD for the SAFT-VR Mie EoS (4.71%). The PC-SAFT EoS is the

model which reports on average a little higher deviation (5.03%). Secondly, saturated and singles-phase densities of 22 pure components (gases, alkanes and aromatics) have been investigated. Both SAFT-like EoSs are much better than the SRK and PR models in terms of density calculations. The SAFT-VR Mie EoS is the model that better correlates the saturated-densities and $PT\rho$ data for the studied compounds, with AADs of 0.6 and 1.2% respectively. Finally, single-phase fluid densities of 57 binary systems were performed by the evaluated models using the regressed k_{ij} in this work. In this part of the comparative study, the SAFT-VR Mie EoS leads to the lowest deviation in modelling the density of most of binary systems. On average, the deviations in the $PT\rho x$ calculations of binary systems are AAD=2.7% for the SAFT-like EoSs, AAD=3.5% for the CEoS+VC and AAD=6.7% for the CEoS without VC.

The SAFT-VR Mie EoS has been reformulated for the *n*-alkanes series within the framework of the group contribution approach, the SAFT-γ Mie EoS. The model has been first assessed by predicting the saturation properties of pure components, with AADs of 1.57% for the vapour pressure and 0.63% for the saturated liquid density for alkanes between ethane and *n*-C_{12} in the reduced-temperature range of 0.4-0.9. Next, the VLE of the *n*-butane + *n*-decane and ethane + *n*-decane binary systems have been studied with the SAFT-γ Mie EoS. The former system has been predicted with AADs of 3.5% for the bubble pressure and 3% for the vapour composition. However, from the VLE study of the ethane + *n*-decane, it has been concluded that ethane must be considered as an individual species and not as two methyl groups (CH_3- CH_3). Finally, the single-phase densities of 10 binary mixtures *n*-alkanes have been also studied using the SAFT-γ Mie EoS. The calculated densities are in good agreement with the data from the literature (AAD=0.9%).

The viscosities of mixtures of CO_2, N_2, O_2 and Ar have been modelled using the SUPERTRAPP model (propane as the reference fluid) with an AAD of 2.68%, even though most of the modelled data were at low pressure (below 2.6 MPa). The capabilities of the SUPERTRAPP and CO_2-SUPERTRAPP (CO_2 as the reference fluid) models have been compared by modelling the viscosity of pure CO_2 and two CO_2-rich mixtures with 10 and 30% of impurities. For the studied mixtures, CO_2-ST model is more accurate than ST and the accuracy of the studied TRAPP models decreases with increasing amount of impurities. Predicted viscosities using the original SUPERTRAPP

are generally overestimated, while using CO_2-ST model, the predictions are underestimated.

The IFT of several gas+*n*-alkanes mixtures have been studied by coupling the SAFT-VR Mie EoS with the DGT. The DGT + SAFT-VR Mie results are in good agreement with the experimental data from literature and with other DGT studies.

In summary, the main goal of the modelling investigation has been to study the SAFT-VR Mie EoS in order to evaluate its capability to predict the thermophysical properties of mixtures for CCS. Density is the property with more impact in the design of CCS processes and this research has presented the accuracy of the SAFT-VR Mie EoS for predicting this property. Thus, the SAFT-VR Mie EoS can be taken into consideration as an interesting model for designing CCS processes.

7.2 Experimental investigation

The phase behaviour of the H_2S-Ar binary system has been experimentally studied at 273.01, 298.00 and 322.96 K and pressures up to 22 MPa. The PR and SAFT-VR Mie EoS have been selected to investigate the VLE of this system. The SAFT-VR Mie EoS has reported an average absolute deviation (AAD) of 5.5% in bubble pressure using BIPs adjusted for each isotherm. The Peng-Robinson EoS with the Wong-Sandler mixing rules using the NRTL equation is the model which better fits the experimental data of the H_2S-Ar system (AAD=1.2%). With respect to the VLE measurements, the maximum uncertainties on composition have been estimated as $u(x)$= 0.0030 and $u(y)$= 0.0062, for the liquid and vapour phases, respectively.

Densities of three mixtures of the CH_4 + H_2S system with 0.1315, 0.1803 and 0.2860 mole fraction of H_2S have been measured at 253, 273 and 293 K and pressures up to 30 MPa. These measurements have extended the available experimental data of this system to lower temperatures. The literature and the measured density data for the CH_4 + H_2S were studied with the SAFT-VR Mie, PR, PR+Peneloux and GERG-2008 EoSs. The SAFT-VR Mie model has been the EoS which has presented the lowest deviation between the measured data and calculated density (4.3%). The GERG-2008 EoS has presented the highest deviation (5.3%) in the measured system with higher concentration of H_2S.

Densities of the 0.6610 mole C_2H_6 + 0.3390 mole H_2S and 0.8674 mole C_3H_8 + 0.1326 mole H_2S binary systems have also been measured at 253, 273 and 293 K and pressures up to 30 MPa. Measured and literature data concerning these binary systems were modelled with the four EoSs. Amongst the studied models, the PR EoS with and without volume correction presented the highest average deviations. Both GERG-2008 and SAFT-VR Mie EoSs are in good agreement with the measured data; the GERG model reported the lowest deviation for the ethane systems (0.4%) and the SAFT-like EoS for the propane systems (1.9%).

Densities of the 0.4212 mole CO_2 + 0.4053 mole CH_4 + 0.1735 mole H_2S have been measured between 253 and 353 K and pressures up to 31 MPa. The SAFT-VR Mie EoS is the model with the lowest absolute deviations (AAD=2.1%). The PR EoS without volume correction predicts the density of this ternary mixture with higher accuracy than the GERG-2008. The GERG model gives the poorest density calculation (AAD=4.0%), especially at the lowest temperature, showing similar results to those for the CH_4 +H_2S binary system with 0.286 mol fraction of acid gas.

The measured densities have been obtained using a vibrating tube Anton Paar densitometer. The average relative uncertainty of the density measurements is 0.5%, reporting the highest average uncertainty of 8.3% at low pressures (below 0.5 MPa) for the CH_4-H_2S system. Two different calibration methods (the one fluid reference and FPMC methods) have been used for producing the density data. The uncertainty of the measurements at the lowest pressures is very high using both calibration methods. Therefore, these uncertainties are independent of the calibration and the limitation of the apparatus is due to the inertia of the vibrating tube.

Densities and viscosities of a multicomponent CO_2-rich mixture with 40% of CH_4 and 10% of other impurities (MIX4) have been measured between 283 and 423 K and pressures up to 125 MPa for density and up to 150 MPa for viscosity. The uncertainties of the density and viscosity measurements are 0.5 and 2%, respectively. The GERG-2008 model has the lowest deviation in the density calculations of MIX4 (2.2%), while the SAFT-VR Mie EoS has a slightly higher deviation (2.3%). The viscosities of this mixture have been studied with the ST and CO_2-ST models coupled with the SAFT-VR Mie EoS. High deviations are reported for both TRAPP models. The CO_2-ST model shows a higher deviation (16.7%) than the ST model (15.5%) and slightly lower

deviations were obtained by replacing the density prediction with the measured density. Thus, a correction of 2.3% in the density has improved the viscosity predictions in only 0.3%. By comparing the measured viscosities of the MIX4 with the viscosity of pure CO_2, MIX2 and MIX3, it can be concluded that the viscosity of CO_2-rich mixtures decreases with the increasing amount of impurities. Both ST and CO_2-ST models have lower accuracy with higher amount of impurities.

7.3 Future work

The work carried out for this thesis has been focused on the non-associative compounds. Therefore, regarding to the modelling investigation, the comparison of the SAFT-VR Mie EoS with other models could be completed by further studies with associative compounds (*i.e.* water) also related to CCS and other associating models (*e.g.* CPA). In addition to the vapour-liquid equilibrium and density, the comparative study may be extended by considering more thermophysical properties such as heat capacity or speed of sound.

The SUPERTRAPP model has presented limitations in the viscosity prediction of CO_2-rich mixtures with increasing amount of impurities. To overcome this weakness, the ST model can be replaced by the Friction Theory viscosity model which has been coupled with the PC-SAFT EoS with interesting results [239,240].

In this work, the DGT presented an excellent capability for describing the IFT of hydrocarbon systems. In previous studies in the literature, the SAFT-VR Mie EoS has been coupled with DGT for modelling the IFT of aqueous interfaces [241]. Nevertheless, it would be interesting to continue investigating the IFT of aqueous systems, such as CO_2 + brines, with the SAFT-VR Mie + DGT approach.

Concerning the experimental measurements, it would be interesting to extend to lower temperatures the VLE study of the Ar-H_2S system. In addition to the VLE measurements, oxides of nitrogen (NO_x) have not been investigated in this work and there is lack of phase equilibria data of binary systems containing NO_x. [242]. Regarding the density and viscosity measurements, it is recommended to continue measuring the viscosity and density of CO_2-rich mixtures containing different components and concentrations of impurities.

APPENDIX A: UNCERTAINTY OF MEASUREMENTS

Uncertainties of the properties measured have been evaluated as standard uncertainties of type A and type B [243], following the recommendations of NIST (National Institute of Standards and Technology) [244]. Type A of uncertainties is based on the statistical treatment of experimental data. The uncertainty of the composition of the mixtures prepared for density measurements was evaluated as type A and it was calculated as [244]:

$$u(x) = \sqrt{\frac{\sigma^2(x)}{N}} \tag{A.1}$$

where σ^2 is the variance of the values measured and N is the number of measurements.

The uncertainties type B are evaluated by other means (not purely statistical), such as literature, manufacturer information, previous experience or, as in our case, calibrations. Then, uncertainty on temperature and pressure measurements was estimated as type B calculated as [244]:

$$u_{calib}(P,T) = \frac{d}{\sqrt{3}} \tag{A.2}$$

where d is the media of the extreme values from the calibration.

In order to increase the confidence level, the standard uncertainty is expanded by a coverage factor, k [243]. This coverage factor is chosen according to the desired level of confidence, k=2 defines a level of confidence around 95% and k=3 is higher than 99% [244]. The expanded uncertainties are obtained by multiplying the standard uncertainty by the coverage factor:

$$u_{expanded}(\theta) = ku(\theta) \tag{A.3}$$

In this work, the standard uncertainty was expanded by k=2.

Density, compressibility factor, VLE data composition and viscosity have been evaluated as combined standard uncertainty. The combined uncertainty is used when the

measured value is function of several sources of uncertainties ($u_k(\theta)$). In general can be expressed as [245]:

$$u_{comb}\ (\theta) = \sqrt{\sum_{k=1}^{N} u_k^2\ (\theta)} \tag{A.4}$$

However, if there is a mathematical relationship between the measurements, the law of propagation of uncertainty must be applied. This propagation law can be written as [245]:

$$\theta = f(\alpha_1, \alpha_1, \ldots \alpha_N) \tag{A.5}$$

$$u_{comb}(\theta) = \sqrt{\sum_{k=1}^{N} \left(\frac{\partial f}{\partial \alpha_k}\right)^2 u^2(\alpha_k)} \tag{A.6}$$

A.1 Density and compressibility factor uncertainty

Density measurement uncertainty can be expressed through the combination of two sources of expanded standard uncertainty, calibration and densitometer information, due to the mathematical relation used to do the calibration:

$$\rho = a\tau^2 + b \tag{A.7}$$

Therefore, applying the law of propagation of uncertainty [245], density uncertainty was obtained by:

$$u_{calib}(\rho) = \sqrt{\left(\frac{\partial \rho}{\partial \tau}\right)_{a,b}^2 u^2(\tau) + \left(\frac{\partial \rho}{\partial a}\right)_{\tau,b}^2 u^2(a) + \left(\frac{\partial \rho}{\partial b}\right)_{\tau,a}^2 u^2(b)} \tag{A.8}$$

where τ is the time of oscillation and both ‘a’ and ‘b’ are the calibration parameters. Subsequently, the partial derivatives required for calculating $u(\rho)$ are derived from equation B.7 as:

$$\left(\frac{\partial \rho}{\partial \tau}\right)_{a,b} = 2a\tau \qquad \left(\frac{\partial \rho}{\partial a}\right)_{\tau,b} = \tau^2 \qquad \left(\frac{\partial \rho}{\partial b}\right)_{a,\tau} = 1 \tag{A.9}$$

Thus, after replacing the partial derivatives, the combined standard uncertainty on calibration can be calculated by

$$u_{calib}(\rho) = \sqrt{a^2 u^2(\tau) + \tau^2 u^2(a) + u^2(b)} \tag{A.10}$$

where *u(a)* and *u(b)* are the standard deviations calculated after linear regression between reference fluid density values and measured period of vibration at the corresponding temperature of calibration, and *u(τ)* is the standard uncertainty which value is provided by the manufacturer as10^{-8} s.

In addition, the uncertainty on pressure is also taken into consideration and its contribution has been evaluated as:

$$u_P(\rho) = \sqrt{\left(\frac{\partial \rho}{\partial P}\right)^2 u^2(P)} \tag{A.11}$$

where *u(P)* is the expanded uncertainty of the pressure measurements from the calibration and is estimated to be less than 0.003 MPa for low pressure (up to 5 MPa) and 0.005 MPa for higher pressures than 5 MPa (up to 30 MPa).

Finally, the combined standard uncertainty of our density measurements can be expressed by

$$u(\rho) = \sqrt{u_{calib}^2(\rho) + u_P^2(\rho)} \tag{A.12}$$

The calculation of the compressibility factor (*Z*) is function of the 3 properties measured: temperature, pressure and density. The compressibility factor can be formulated as:

$$Z = \frac{P}{\rho R T} \tag{A.13}$$

Consequently, uncertainty in compressibility factor calculation, *u(Z)*, gives an idea of the overall uncertainty of our experimental data due to the consideration of the uncertainties of every measurement. Thus, following the same approach for the propagation of the uncertainty, the uncertainties of the compressibility factors were calculated using the law of propagation as:

$$u(Z)=\sqrt{\left(\frac{\partial Z}{\partial P}\right)_{\rho,T}^{2}u^{2}(P)+\left(\frac{\partial Z}{\partial \rho}\right)_{P,T}^{2}u^{2}(\rho)+\left(\frac{\partial Z}{\partial T}\right)_{P,\rho}^{2}u^{2}(T)} \tag{A.14}$$

where the partial derivatives are obtained from deriving the equation A.13 as follows:

$$\left(\frac{\partial Z}{\partial P}\right)_{\rho,T}=\frac{1}{\rho RT} \qquad \left(\frac{\partial Z}{\partial \rho}\right)_{P,T}=-\frac{P}{\rho^{2}RT} \qquad \left(\frac{\partial Z}{\partial T}\right)_{\rho,P}=-\frac{P}{\rho RT^{2}} \tag{A.15}$$

A.2 VLE data uncertainty

The uncertainty of the vapour and liquid compositions measured in VLE data experiments was calculated as combined uncertainty based on the calibration of the thermal conductivity detector (TCD) and the repeatability of the measurements.

$$u(x,y)=\sqrt{u_{rep}^{2}(x,y)+u_{calib}^{2}(x,y)} \tag{A.16}$$

where $u_{rep}(x,y)$ is the uncertainty based on the repeatability and is calculated as standard uncertainty type A (Eq. A.1) from the standard deviation (σ). u_{calib} is the uncertainty obtained from the calibration of the TCD.

The number of moles of argon (N_{Ar}) and hydrogen sulphide (N_{H2S}) are measured by the gas chromatograph with the TCD. The mol fraction of one of the compounds is calculated as:

$$x_{Ar}=\frac{N_{Ar}}{N_{Ar}+N_{H_2S}} \tag{A.17}$$

Therefore, as a result of there is a mathematical relationship between the measured numbers of moles for both compounds, the calibration uncertainty is evaluated as combined uncertainty applying the law of propagation.

$$u_{calib}(x)=\sqrt{\left(\frac{\partial x}{\partial N_{Ar}}\right)_{N_{H_2S}}^{2}u^{2}(N_{Ar})+\left(\frac{\partial x}{\partial N_{H_2S}}\right)_{N_{Ar}}^{2}u^{2}(N_{H_2S})} \tag{A.18}$$

where $u(N_{Ar})$ and $u(N_{H2S})$ are the standard deviations calculated after linear regression between reference moles injected and the moles measured by TCD for each compound and the partial derivatives are obtained from deriving the equation A.17 as follows:

$$\left(\frac{\partial x}{\partial N_{Ar}}\right)_{N_{H_2S}} = \frac{N_{H_2S}}{(N_{Ar}+N_{H_2S})^2} \qquad \left(\frac{\partial x}{\partial N_{H_2S}}\right)_{N_{H_2S}} = \frac{-N_{Ar}}{(N_{Ar}+N_{H_2S})^2} \tag{A.19}$$

A.3 Viscosity uncertainty

The uncertainty of the viscosity measurements is evaluated as combined uncertainty based on the repeatability (type A) and a series of uncertainties of type B.

$$u(\eta) = \sqrt{u_A^2(\eta) + u_B^2(\eta)} \tag{A.20}$$

where u_A is the uncertainty calculated using the standard deviation (Eq. B.1) of the 9 measurements done per point, and u_B the combined uncertainty based on the calibration and the characteristics of the equipment.

The viscosity is calculated by the Poiseuille equation which can relate the pressure drop across the capillary tube to the viscosity. Reorganising this equation the viscosity is calculated as

$$\eta = \frac{\pi C}{128}\frac{\Delta P\, D^4}{Q\, L} \tag{A.21}$$

where C is a constant, ΔP the pressure drop, D tube diameter, Q the flow rate and L tube length.

Finally, the combined uncertainty u_B is calculated applying the law of propagation of uncertainty and it can be express as

$$u_B(\eta) = \sqrt{\left(\frac{\partial \eta}{\partial \Delta P}\right)^2_{D,Q,L} u^2(\Delta P) + \left(\frac{\partial \eta}{\partial D}\right)^2_{\Delta P,Q,L} u^2(D) + \left(\frac{\partial \eta}{\partial Q}\right)^2_{\Delta P,D,L} u^2(Q) + \left(\frac{\partial \eta}{\partial L}\right)^2_{\Delta P,D,Q} u^2(L)} \tag{A.22}$$

where $u(\Delta P)$, $u(D)$, $u(Q)$ and $u(L)$ are estimated to be ±0.01 psi, ±0.00005 cm, ±0.02 cm^3/h and ±5 cm respectively. The partial derivatives are obtained from deriving Poiseuille equation (B.19):

$$\left(\frac{\partial \eta}{\partial \Delta P}\right)_{D,Q,L} = \frac{\pi C}{128}\frac{D^4}{QL} \tag{A.23}$$

$$\left(\frac{\partial \eta}{\partial D}\right)_{\Delta P,Q,L} = \frac{\pi C}{32}\frac{\Delta P D^3}{QL} \tag{A.24}$$

$$\left(\frac{\partial \eta}{\partial Q}\right)_{\Delta P,D,L} = -\frac{\pi C}{128}\frac{\Delta P D^4}{Q^2 L} \tag{A.25}$$

$$\left(\frac{\partial \eta}{\partial L}\right)_{\Delta P,D,Q} = -\frac{\pi C}{128}\frac{\Delta P D^4}{Q L^2} \tag{A.26}$$

APPENDIX B: EXPERIMENTAL DENSITY DATA

Table B.1. Experimental results of the 0.8685 mol CH_4 + 0.1315 mol H_2S system at 253K, $u(x_{H2S})$=0.0006, u(T)= 0.03 K, u(P)= 0.003 MPa for pressures up to 5 MPa and u(P)= 0.005 MPa for pressures from 5 to 30 MPa.

No	T	P	ρ	u(ρ)		Z	u(Z)	No	T	P	ρ	u(ρ)		Z	u(Z)
	[K]	[MPa]	$\left[\frac{kg}{m^3}\right]$	$\left[\frac{kg}{m^3}\right]$	%		10^{-2}		[K]	[MPa]	$\left[\frac{kg}{m^3}\right]$	$\left[\frac{kg}{m^3}\right]$	%		10^{-2}
1	253.28	0.188	1.76	0.18	10.1	0.93	9.4	37	253.46	12.710	199.55	1.00	0.5	0.56	0.3
2	253.29	0.508	4.80	0.22	4.7	0.92	4.3	38	253.47	13.026	204.72	1.03	0.5	0.56	0.3
3	253.30	1.250	12.25	0.33	2.7	0.89	2.4	39	253.48	13.361	209.99	1.06	0.5	0.56	0.3
4	253.31	1.824	18.07	0.41	2.3	0.88	2.0	40	253.49	13.557	213.18	1.07	0.5	0.56	0.3
5	253.33	2.475	24.75	0.50	2.0	0.87	1.8	41	253.50	13.904	217.77	1.10	0.5	0.56	0.3
6	253.35	3.335	33.57	0.52	1.5	0.87	1.3	42	253.53	14.217	222.31	1.13	0.5	0.56	0.3
7	253.36	4.114	41.57	0.54	1.3	0.87	1.1	43	253.53	14.605	227.86	1.16	0.5	0.56	0.3
8	253.38	4.487	45.79	0.55	1.2	0.86	1.0	44	253.54	15.328	236.23	1.23	0.5	0.57	0.3
9	253.34	4.807	49.57	0.56	1.1	0.85	1.0	45	253.56	16.209	246.09	1.31	0.5	0.58	0.3
10	253.33	5.174	53.92	0.57	1.1	0.84	0.9	46	253.58	16.612	250.04	1.33	0.5	0.58	0.3
11	253.32	5.258	55.98	0.58	1.0	0.82	0.8	47	253.59	17.129	255.23	1.26	0.5	0.59	0.3
12	253.33	5.895	64.88	0.60	0.9	0.79	0.7	48	253.60	17.589	259.35	1.21	0.5	0.59	0.3
13	253.32	6.503	73.25	0.62	0.9	0.78	0.7	49	253.61	18.036	263.28	1.15	0.4	0.60	0.3
14	253.34	6.994	80.75	0.65	0.8	0.76	0.6	50	253.61	18.480	267.15	1.10	0.4	0.60	0.2
15	253.36	7.255	84.54	0.66	0.8	0.75	0.6	51	253.62	18.822	269.80	1.06	0.4	0.61	0.2
16	253.35	7.572	90.00	0.67	0.7	0.74	0.6	52	253.63	19.390	274.47	1.00	0.4	0.62	0.2
17	253.35	7.961	99.59	0.69	0.7	0.70	0.5	53	253.64	19.853	277.53	0.96	0.3	0.63	0.2
18	253.36	8.383	108.50	0.72	0.7	0.68	0.4	54	253.66	21.081	286.30	0.84	0.3	0.64	0.2
19	253.37	8.539	112.16	0.72	0.6	0.67	0.4	55	253.66	21.605	289.87	0.80	0.3	0.65	0.2
20	253.38	8.660	115.11	0.73	0.6	0.66	0.4	56	253.67	22.087	292.82	0.76	0.3	0.66	0.2
21	253.38	8.850	119.77	0.74	0.6	0.65	0.4	57	253.68	22.512	295.31	0.73	0.2	0.67	0.2
22	253.39	9.030	124.20	0.75	0.6	0.64	0.4	58	253.68	22.918	297.52	0.70	0.2	0.67	0.2
23	253.40	9.215	128.92	0.76	0.6	0.63	0.4	59	253.56	23.487	300.68	0.66	0.2	0.68	0.2
24	253.40	9.484	135.48	0.78	0.6	0.61	0.4	60	253.29	24.245	303.67	0.62	0.2	0.70	0.1
25	253.43	9.711	140.67	0.79	0.6	0.60	0.3	61	253.29	24.733	306.89	0.59	0.2	0.70	0.1
26	253.43	9.944	145.46	0.81	0.6	0.60	0.3	62	253.30	25.670	310.08	0.55	0.2	0.72	0.1
27	253.41	10.167	150.17	0.82	0.5	0.59	0.3	63	253.57	26.154	313.25	0.53	0.2	0.73	0.1
28	253.42	10.405	155.11	0.84	0.5	0.59	0.3	64	253.72	26.573	314.90	0.51	0.2	0.74	0.1
29	253.44	10.674	160.71	0.85	0.5	0.58	0.3	65	253.53	27.036	316.40	0.50	0.2	0.75	0.1
30	253.42	10.879	164.94	0.87	0.5	0.58	0.3	66	253.32	27.359	317.71	0.49	0.2	0.75	0.1
31	253.42	11.161	170.62	0.89	0.5	0.57	0.3	67	253.32	27.986	320.59	0.48	0.1	0.76	0.1
32	253.45	11.408	175.60	0.90	0.5	0.57	0.3	68	253.33	28.601	322.89	0.47	0.1	0.77	0.1
33	253.46	11.691	181.06	0.93	0.5	0.56	0.3	69	253.33	29.015	324.42	0.46	0.1	0.78	0.1
34	253.46	11.951	186.09	0.94	0.5	0.56	0.3	70	253.31	29.542	326.32	0.46	0.1	0.79	0.1
35	253.46	12.221	190.99	0.96	0.5	0.56	0.3	71	253.33	30.002	327.17	0.46	0.1	0.80	0.1
36	253.45	12.503	195.90	0.99	0.5	0.56	0.3								

Table B.2. Experimental results of the 0.8685 mol CH_4 + 0.1315 mol H_2S system at 273K, $u(x_{H2S})$=0.0006, u(T)= 0.03 K, u(P)= 0.003 MPa for pressures up to 5 MPa and u(P)=0.005 MPa for pressures from 5 to 30 MPa.

No	T [K]	P [MPa]	ρ $\left[\frac{kg}{m^3}\right]$	u(ρ) $\left[\frac{kg}{m^3}\right]$	u(ρ) %	Z	u(Z) 10^{-2}	No	T [K]	P [MPa]	ρ $\left[\frac{kg}{m^3}\right]$	u(ρ) $\left[\frac{kg}{m^3}\right]$	u(ρ) %	Z	u(Z) 10^{-2}
1	273.21	0.209	1.70	0.17	10.0	0.99	9.6	31	273.26	11.726	146.08	0.69	0.5	0.65	0.3
2	273.21	0.648	5.39	0.22	4.1	0.97	4.0	32	273.26	12.002	150.33	0.70	0.5	0.65	0.3
3	273.24	1.167	10.00	0.26	2.6	0.95	2.5	33	273.26	12.322	155.19	0.72	0.5	0.64	0.3
4	273.24	1.761	15.44	0.30	2.0	0.92	1.8	34	273.26	12.637	159.86	0.74	0.5	0.64	0.3
5	273.25	2.240	19.97	0.34	1.7	0.91	1.5	35	273.26	13.040	165.72	0.76	0.5	0.64	0.3
6	273.26	2.770	25.12	0.37	1.5	0.89	1.3	36	273.27	13.466	171.70	0.78	0.5	0.64	0.3
7	273.27	3.280	30.25	0.40	1.3	0.88	1.1	37	273.27	13.771	175.85	0.80	0.5	0.64	0.3
8	273.25	3.776	35.41	0.42	1.2	0.86	1.0	38	273.30	14.847	189.62	0.87	0.5	0.63	0.3
9	273.27	4.207	40.03	0.44	1.1	0.85	0.9	39	273.31	15.329	195.37	0.90	0.5	0.64	0.3
10	273.27	4.225	40.23	0.44	1.1	0.85	0.9	40	273.32	15.811	200.85	0.93	0.5	0.64	0.3
11	273.26	4.666	45.13	0.45	1.0	0.84	0.8	41	273.32	16.120	204.24	0.96	0.5	0.64	0.3
12	273.26	5.086	49.93	0.47	0.9	0.83	0.8	42	273.32	16.817	211.55	1.00	0.5	0.64	0.3
13	273.28	5.512	54.98	0.48	0.9	0.81	0.7	43	273.33	17.352	216.85	1.04	0.5	0.65	0.3
14	273.28	5.933	60.12	0.48	0.8	0.80	0.6	44	273.34	17.978	222.75	1.09	0.5	0.65	0.3
15	273.30	6.333	65.17	0.49	0.8	0.79	0.6	45	273.34	18.233	225.06	1.11	0.5	0.66	0.3
16	273.31	6.712	70.10	0.51	0.7	0.78	0.6	46	273.35	18.773	229.81	1.05	0.5	0.66	0.3
17	273.31	7.200	76.68	0.52	0.7	0.76	0.5	47	273.35	19.531	236.12	0.97	0.4	0.67	0.3
18	273.31	7.483	80.60	0.52	0.6	0.75	0.5	48	273.37	20.048	240.23	0.83	0.3	0.68	0.2
19	273.31	7.817	85.33	0.53	0.6	0.74	0.5	49	273.36	20.692	245.12	0.68	0.3	0.68	0.2
20	273.29	8.136	89.96	0.54	0.6	0.73	0.4	50	273.33	21.405	250.29	0.54	0.2	0.69	0.1
21	273.28	8.496	95.31	0.55	0.6	0.72	0.4	51	273.31	22.905	260.37	0.36	0.1	0.71	0.1
22	273.29	8.809	100.05	0.56	0.6	0.71	0.4	52	273.29	23.690	265.29	0.34	0.1	0.72	0.1
23	273.27	9.149	105.29	0.57	0.5	0.70	0.4	53	273.27	24.569	270.52	0.31	0.1	0.74	0.1
24	273.28	9.596	112.28	0.59	0.5	0.69	0.4	54	273.27	25.361	275.02	0.29	0.1	0.75	0.1
25	273.27	9.851	116.33	0.60	0.5	0.69	0.4	55	273.27	26.319	280.21	0.26	0.1	0.76	0.1
26	273.28	10.137	120.88	0.61	0.5	0.68	0.3	56	273.26	27.255	285.03	0.24	0.1	0.77	0.1
27	273.29	10.446	125.82	0.63	0.5	0.67	0.3	57	273.26	28.276	290.05	0.23	0.1	0.79	0.1
28	273.29	10.749	130.66	0.64	0.5	0.67	0.3	58	273.26	29.372	295.19	0.21	0.1	0.81	0.1
29	273.26	11.062	135.65	0.65	0.5	0.66	0.3	59	273.25	30.481	300.13	0.21	0.1	0.82	0.1
30	273.25	11.361	140.37	0.67	0.5	0.66	0.3								

Table B.3. Experimental results of the 0.8685 mol CH_4 + 0.1315 mol H_2S system at 293K, $u(x_{H2S})$=0.0006, u(T)= 0.03 K, u(P)= 0.003 MPa for pressures up to 5 MPa and u(P)= 0.005 MPa for pressures from 5 to 30 MPa.

No	T [K]	P [MPa]	ρ $\left[\frac{kg}{m^3}\right]$	u(ρ) $\left[\frac{kg}{m^3}\right]$	u(ρ) %	Z	u(Z) 10^{-2}	No	T [K]	P [MPa]	ρ $\left[\frac{kg}{m^3}\right]$	u(ρ) $\left[\frac{kg}{m^3}\right]$	u(ρ) %	Z	u(Z) 10^{-2}
1	293.18	0.239	1.86	0.18	9.5	0.97	9.2	31	293.19	13.230	140.02	0.71	0.5	0.71	0.4
2	293.18	0.469	3.71	0.19	5.3	0.96	5.0	32	293.18	13.726	145.96	0.74	0.5	0.71	0.4
3	293.19	0.792	6.46	0.22	3.4	0.93	3.2	33	293.20	14.242	152.42	0.76	0.5	0.71	0.4
4	293.21	1.117	9.20	0.24	2.7	0.92	2.4	34	293.20	14.579	156.48	0.78	0.5	0.70	0.4
5	293.19	1.341	11.22	0.26	2.3	0.90	2.1	35	293.20	14.924	160.62	0.81	0.5	0.70	0.4
6	293.20	1.820	15.41	0.29	1.9	0.89	1.7	36	293.20	15.365	165.51	0.83	0.5	0.70	0.4
7	293.19	2.300	20.14	0.32	1.6	0.86	1.4	37	293.20	15.806	170.31	0.86	0.5	0.70	0.4
8	293.18	2.890	25.81	0.36	1.4	0.85	1.2	38	293.19	16.228	174.96	0.89	0.5	0.70	0.4
9	293.19	3.396	30.35	0.38	1.3	0.85	1.1	39	293.19	16.699	180.07	0.92	0.5	0.70	0.4
10	293.19	3.988	35.82	0.41	1.1	0.84	1.0	40	293.20	17.183	185.14	0.95	0.5	0.70	0.4
11	293.19	4.428	40.25	0.42	1.0	0.83	0.9	41	293.19	17.682	190.29	0.98	0.5	0.70	0.4
12	293.20	4.887	44.78	0.44	1.0	0.82	0.8	42	293.20	18.163	195.16	1.01	0.5	0.70	0.4
13	293.20	5.494	50.99	0.45	0.9	0.81	0.7	43	293.23	18.686	200.27	0.99	0.5	0.71	0.3
14	293.20	5.964	55.59	0.46	0.8	0.81	0.7	44	293.29	19.219	205.31	0.87	0.4	0.71	0.3
15	293.20	6.411	60.21	0.46	0.8	0.80	0.6	45	293.23	19.770	210.30	0.73	0.3	0.71	0.2
16	293.19	6.909	65.40	0.47	0.7	0.80	0.6	46	293.22	20.355	215.54	0.58	0.3	0.71	0.2
17	293.19	7.335	70.05	0.48	0.7	0.79	0.5	47	293.20	20.932	220.42	0.43	0.2	0.72	0.1
18	293.19	7.786	74.96	0.49	0.7	0.79	0.5	48	293.20	21.495	224.99	0.39	0.2	0.72	0.1
19	293.18	8.263	79.99	0.50	0.6	0.78	0.5	49	293.23	22.173	230.34	0.37	0.2	0.73	0.1
20	293.18	8.722	85.68	0.51	0.6	0.77	0.5	50	293.23	22.860	235.56	0.34	0.1	0.73	0.1
21	293.19	9.097	90.09	0.53	0.6	0.76	0.4	51	293.21	23.505	240.20	0.32	0.1	0.74	0.1
22	293.19	9.534	95.16	0.54	0.6	0.76	0.4	52	293.22	24.254	245.19	0.30	0.1	0.75	0.1
23	293.18	9.972	100.39	0.56	0.6	0.75	0.4	53	293.22	25.052	250.52	0.28	0.1	0.76	0.1
24	293.19	10.368	105.20	0.57	0.5	0.74	0.4	54	293.21	25.865	255.77	0.26	0.1	0.76	0.1
25	293.19	10.794	110.28	0.59	0.5	0.74	0.4	55	293.21	26.669	260.49	0.24	0.1	0.77	0.1
26	293.19	11.183	115.06	0.61	0.5	0.73	0.4	56	293.20	27.629	265.96	0.22	0.1	0.79	0.1
27	293.19	11.608	120.16	0.63	0.5	0.73	0.4	57	293.20	28.496	270.59	0.21	0.1	0.80	0.1
28	293.18	12.003	124.94	0.65	0.5	0.73	0.4	58	293.21	29.415	275.27	0.20	0.1	0.81	0.1
29	293.18	12.415	130.08	0.67	0.5	0.72	0.4	59	293.21	29.995	278.16	0.20	0.1	0.81	0.1
30	293.18	12.830	135.13	0.69	0.5	0.72	0.4	60	293.21	30.419	280.17	0.19	0.1	0.82	0.1

Table B.4. Experimental results of 0.8197 mol CH_4 + 0.1803 mol H_2S system at 253K, $u(x_{H2S})$=0.0008, u(T)= 0.03 K, u(P)= 0.003 MPa for pressures up to 5 MPa and u(P)= 0.005 MPa for pressures from 5 to 30 MPa.

No	T	P	ρ	u(ρ)		Z	u(Z)	No	T	P	ρ	u(ρ)		Z	u(Z)
	[K]	[MPa]	$\left[\frac{kg}{m^3}\right]$	$\left[\frac{kg}{m^3}\right]$	%		10^{-2}		[K]	[MPa]	$\left[\frac{kg}{m^3}\right]$	$\left[\frac{kg}{m^3}\right]$	%		10^{-2}
1	253.03	0.225	2.10	0.18	8.7	0.98	8.6	31	252.98	16.314	285.18	1.32	0.5	0.53	0.2
2	253.05	0.472	4.43	0.22	4.9	0.97	4.8	32	252.99	16.702	288.37	1.32	0.5	0.53	0.2
3	253.07	1.105	10.58	0.31	2.9	0.96	2.8	33	253.01	17.275	293.02	1.24	0.4	0.54	0.2
4	253.08	1.496	14.53	0.36	2.5	0.94	2.4	34	253.02	17.701	296.11	1.19	0.4	0.55	0.2
5	253.08	2.006	20.39	0.43	2.1	0.90	1.9	35	253.03	18.070	299.00	1.15	0.4	0.55	0.2
6	253.25	2.607	28.21	0.50	1.8	0.85	1.5	36	253.02	18.537	302.29	1.10	0.4	0.56	0.2
7	253.21	2.947	32.50	0.51	1.6	0.83	1.3	37	253.02	19.009	305.49	1.04	0.3	0.57	0.2
8	253.16	3.517	38.95	0.52	1.3	0.83	1.1	38	253.02	19.564	309.06	0.99	0.3	0.58	0.2
9	253.19	4.054	46.42	0.54	1.2	0.80	0.9	39	253.01	20.084	312.27	0.93	0.3	0.59	0.2
10	253.18	4.507	52.31	0.55	1.1	0.79	0.8	40	253.01	20.574	315.19	0.89	0.3	0.60	0.2
11	253.12	4.809	59.33	0.56	0.9	0.74	0.7	41	253.00	21.010	317.91	0.85	0.3	0.61	0.2
12	253.13	5.304	67.27	0.58	0.9	0.72	0.6	42	253.00	21.473	320.52	0.81	0.3	0.61	0.2
13	252.91	9.089	146.00	0.75	0.5	0.57	0.3	43	253.00	21.973	323.20	0.77	0.2	0.62	0.1
14	252.91	9.296	153.90	0.77	0.5	0.55	0.3	44	253.00	22.531	326.01	0.73	0.2	0.63	0.1
15	252.91	9.508	162.60	0.78	0.5	0.54	0.3	45	253.00	22.822	327.46	0.71	0.2	0.64	0.1
16	252.91	9.727	172.12	0.79	0.5	0.52	0.2	46	253.00	23.125	329.05	0.69	0.2	0.64	0.1
17	252.90	9.948	181.75	0.81	0.4	0.50	0.2	47	253.01	23.774	332.07	0.64	0.2	0.66	0.1
18	252.90	10.181	191.68	0.82	0.4	0.49	0.2	48	253.01	24.145	333.77	0.62	0.2	0.66	0.1
19	252.90	10.440	200.58	0.84	0.4	0.48	0.2	49	253.02	24.553	335.64	0.60	0.2	0.67	0.1
20	252.89	10.727	209.51	0.86	0.4	0.47	0.2	50	253.02	25.031	337.77	0.58	0.2	0.68	0.1
21	252.89	11.063	217.25	0.88	0.4	0.47	0.2	51	253.03	25.582	340.15	0.55	0.2	0.69	0.1
22	252.89	11.429	224.63	0.91	0.4	0.47	0.2	52	253.04	26.249	342.94	0.52	0.2	0.70	0.1
23	252.90	11.825	231.88	0.93	0.4	0.47	0.2	53	253.07	26.760	345.19	0.51	0.1	0.71	0.1
24	252.90	12.251	239.02	0.97	0.4	0.47	0.2	54	253.07	27.152	346.63	0.50	0.1	0.72	0.1
25	252.91	12.717	246.10	1.00	0.4	0.47	0.2	55	253.06	27.510	348.27	0.49	0.1	0.72	0.1
26	252.92	13.223	253.09	1.04	0.4	0.48	0.2	56	253.07	28.062	350.41	0.48	0.1	0.73	0.1
27	252.92	13.782	260.02	1.09	0.4	0.49	0.2	57	253.08	28.543	352.25	0.47	0.1	0.74	0.1
28	252.94	14.392	266.89	1.14	0.4	0.50	0.2	58	253.08	28.966	353.85	0.46	0.1	0.75	0.1
29	252.95	15.070	273.89	1.20	0.4	0.51	0.2	59	253.08	29.496	355.79	0.46	0.1	0.76	0.1
30	252.97	15.829	280.91	1.28	0.5	0.52	0.2	60	253.08	30.039	357.73	0.46	0.1	0.77	0.1

Table B.5. Experimental results of the 0.8197 mol CH_4 + 0.1803 mol H_2S system at 273K, $u(x_{H2S})$=0.0008, u(T)= 0.03 K, u(P)= 0.003 MPa for pressures up to 5 MPa and u(P)=0.005 MPa for pressures from 5 to 30 MPa.

No	T	P	ρ	u(ρ)		Z	u(Z)	No	T	P	ρ	u(ρ)		Z	u(Z)
	[K]	[MPa]	$\left[\frac{kg}{m^3}\right]$	$\left[\frac{kg}{m^3}\right]$	%		10^{-2}		[K]	[MPa]	$\left[\frac{kg}{m^3}\right]$	$\left[\frac{kg}{m^3}\right]$	%		10^{-2}
1	273.04	0.220	1.87	0.18	9.6	1.00	9.5	32	273.13	15.510	224.73	0.91	0.4	0.59	0.2
2	273.05	0.512	4.39	0.21	4.8	0.99	4.6	33	273.13	16.041	231.85	0.95	0.4	0.59	0.2
3	273.06	1.024	8.86	0.25	2.8	0.98	2.3	34	273.13	16.504	237.74	0.98	0.4	0.59	0.2
4	273.06	1.546	13.54	0.29	2.1	0.97	2.0	35	273.11	17.004	243.74	1.02	0.4	0.59	0.2
5	273.06	1.998	17.83	0.32	1.8	0.95	1.7	36	273.08	17.522	249.57	1.06	0.4	0.60	0.2
6	273.07	2.472	22.64	0.35	1.5	0.93	1.4	37	273.10	18.017	254.80	1.09	0.4	0.60	0.2
7	273.08	3.006	28.12	0.38	1.4	0.91	1.2	38	273.08	18.504	259.61	1.13	0.4	0.61	0.2
8	273.08	3.496	33.34	0.41	1.2	0.89	1.1	39	273.07	19.004	264.22	1.12	0.4	0.61	0.2
9	273.07	4.037	39.48	0.43	1.1	0.87	0.9	40	273.05	19.490	268.43	0.98	0.4	0.62	0.2
10	273.06	4.568	45.89	0.45	1.0	0.85	0.8	41	273.06	19.898	271.74	0.87	0.3	0.62	0.1
11	273.02	5.020	51.69	0.46	0.9	0.83	0.7	42	273.05	20.545	276.64	0.71	0.3	0.63	0.1
12	273.04	5.526	58.55	0.48	0.8	0.80	0.7	43	273.07	21.088	280.47	0.60	0.2	0.64	0.1
13	273.05	6.060	66.20	0.49	0.7	0.78	0.6	44	273.08	21.490	283.16	0.52	0.2	0.64	0.1
14	273.05	6.535	73.36	0.49	0.7	0.76	0.5	45	273.07	22.026	286.58	0.44	0.2	0.65	0.1
15	273.06	7.007	80.78	0.51	0.6	0.74	0.5	46	273.10	22.561	289.86	0.37	0.1	0.66	0.1
16	273.06	7.503	88.86	0.52	0.6	0.72	0.4	47	273.11	23.102	293.06	0.36	0.1	0.67	0.1
17	273.08	8.037	97.86	0.54	0.5	0.70	0.4	48	273.12	23.507	295.40	0.34	0.1	0.68	0.1
18	273.09	8.509	106.04	0.55	0.5	0.68	0.4	49	273.13	24.081	298.69	0.32	0.1	0.69	0.1
19	273.09	8.697	109.34	0.56	0.5	0.68	0.3	50	273.14	24.511	301.13	0.31	0.1	0.69	0.1
20	273.11	9.417	122.17	0.58	0.5	0.66	0.3	51	273.15	25.182	304.96	0.29	0.1	0.70	0.1
21	273.11	10.159	135.60	0.61	0.5	0.64	0.3	52	273.15	25.661	307.41	0.28	0.1	0.71	0.1
22	273.14	10.580	143.25	0.63	0.4	0.63	0.3	53	273.14	26.076	309.49	0.27	0.1	0.72	0.1
23	273.13	10.896	148.97	0.65	0.4	0.62	0.3	54	273.14	26.577	312.08	0.26	0.1	0.72	0.1
24	273.13	11.490	159.68	0.68	0.4	0.61	0.3	55	273.14	26.982	314.11	0.25	0.1	0.73	0.1
25	273.13	12.024	169.16	0.70	0.4	0.60	0.3	56	273.13	27.492	316.71	0.24	0.1	0.74	0.1
26	273.17	12.519	177.81	0.73	0.4	0.60	0.2	57	273.13	28.026	319.37	0.23	0.1	0.75	0.1
27	273.16	13.305	191.11	0.77	0.4	0.59	0.2	58	273.13	28.568	321.92	0.22	0.1	0.75	0.1
28	273.13	13.513	194.52	0.79	0.4	0.59	0.2	59	273.13	29.088	324.13	0.22	0.1	0.76	0.1
29	273.13	14.007	202.45	0.82	0.4	0.59	0.2	60	273.13	29.546	325.75	0.21	0.1	0.77	0.1
30	273.11	14.299	207.01	0.83	0.4	0.59	0.2	61	273.13	29.999	327.01	0.21	0.1	0.78	0.1
31	273.13	14.904	216.11	0.87	0.4	0.59	0.2								

Table B.6. Experimental results of the 0.8197 mol CH_4 + 0.1803 mol H_2S system at 293K, $u(x_{H2S})$=0.0008, u(T)= 0.03 K, u(P)= 0.003 MPa for pressures up to 5 MPa and u(P)= 0.005 MPa for pressures from 5 to 30 MPa.

No	T	P	ρ	u(ρ)		Z	u(Z)	No	T	P	ρ	u(ρ)		Z	u(Z)
	[K]	[MPa]	$\left[\frac{kg}{m^3}\right]$	$\left[\frac{kg}{m^3}\right]$	%		10^{-2}		[K]	[MPa]	$\left[\frac{kg}{m^3}\right]$	$\left[\frac{kg}{m^3}\right]$	%		10^{-2}
1	293.27	0.193	1.54	0.15	9.7	0.99	9.5	32	293.45	15.532	182.32	0.84	0.5	0.67	0.3
2	293.27	0.498	4.03	0.21	5.2	0.98	5.1	33	293.41	16.017	188.26	0.87	0.5	0.67	0.3
3	293.35	0.936	7.74	0.23	3.0	0.96	2.9	34	293.45	16.485	193.92	0.90	0.5	0.67	0.2
4	293.33	1.434	12.03	0.27	2.2	0.94	2.1	35	293.40	17.009	200.00	0.94	0.5	0.67	0.2
5	293.36	1.962	16.56	0.30	1.8	0.94	1.6	36	293.41	17.526	205.67	0.97	0.5	0.67	0.2
6	293.35	2.422	20.50	0.33	1.6	0.93	1.4	37	293.42	18.033	211.20	1.01	0.5	0.68	0.2
7	293.38	2.915	26.63	0.36	1.4	0.87	1.1	38	293.42	18.536	216.41	1.02	0.5	0.68	0.2
8	293.33	3.440	30.85	0.38	1.2	0.88	1.0	39	293.41	19.019	221.14	0.92	0.4	0.68	0.2
9	293.42	3.941	35.88	0.40	1.1	0.87	1.0	40	293.41	19.519	225.91	0.79	0.4	0.68	0.2
10	293.35	4.502	41.72	0.43	1.0	0.85	0.9	41	293.41	20.054	230.93	0.65	0.3	0.69	0.1
11	293.32	5.019	46.91	0.44	0.9	0.85	0.8	42	293.42	20.511	234.95	0.54	0.2	0.69	0.1
12	293.32	5.508	52.59	0.45	0.9	0.83	0.8	43	293.41	21.059	239.83	0.40	0.2	0.69	0.1
13	293.34	6.006	58.11	0.46	0.8	0.82	0.6	44	293.35	21.512	243.53	0.39	0.2	0.70	0.1
14	293.31	6.513	63.51	0.46	0.7	0.81	0.5	45	293.34	22.090	248.06	0.37	0.1	0.70	0.1
15	293.32	7.004	68.50	0.47	0.7	0.81	0.5	46	293.37	22.488	251.05	0.36	0.1	0.71	0.1
16	293.32	7.520	74.89	0.48	0.6	0.79	0.4	47	293.39	22.971	254.58	0.34	0.1	0.71	0.1
17	293.33	8.008	80.89	0.49	0.6	0.78	0.4	48	293.41	23.490	258.21	0.32	0.1	0.72	0.1
18	293.32	8.507	87.23	0.51	0.6	0.77	0.4	49	293.39	24.024	261.83	0.31	0.1	0.73	0.1
19	293.33	9.072	94.80	0.53	0.6	0.76	0.4	50	293.39	24.659	266.01	0.29	0.1	0.73	0.1
20	293.32	9.526	100.87	0.54	0.5	0.75	0.3	51	293.42	25.034	268.44	0.28	0.1	0.74	0.1
21	293.37	10.013	107.38	0.56	0.5	0.74	0.3	52	293.41	25.538	271.56	0.27	0.1	0.74	0.1
22	293.32	10.518	114.24	0.58	0.5	0.73	0.3	53	293.37	26.028	274.53	0.26	0.1	0.75	0.1
23	293.33	10.922	121.63	0.60	0.5	0.71	0.3	54	293.42	26.523	277.36	0.25	0.1	0.76	0.1
24	293.35	11.685	130.63	0.63	0.5	0.71	0.3	55	293.41	27.022	280.18	0.24	0.1	0.76	0.1
25	293.36	12.068	136.11	0.65	0.5	0.70	0.3	56	293.37	27.520	283.00	0.23	0.1	0.77	0.1
26	293.36	12.506	142.15	0.67	0.5	0.70	0.3	57	293.38	27.986	285.56	0.22	0.1	0.78	0.1
27	293.36	13.036	149.41	0.70	0.5	0.69	0.3	58	293.38	28.437	287.96	0.21	0.1	0.78	0.1
28	293.36	13.500	155.72	0.72	0.5	0.69	0.3	59	293.38	28.979	290.66	0.21	0.1	0.79	0.1
29	293.34	14.027	162.75	0.75	0.5	0.68	0.3	60	293.37	29.405	292.65	0.20	0.1	0.80	0.1
30	293.34	14.501	169.12	0.78	0.5	0.68	0.3	61	293.37	29.932	295.13	0.20	0.1	0.80	0.1
31	293.37	15.006	175.59	0.81	0.5	0.68	0.3								

Table B.7. Experimental results of the 0.714 mol CH_4 + 0.286 mol H_2S system at 253K, $u(x_{H2S})$=0.0011, u(T)= 0.03 K, u(P)= 0.003 MPa for pressures up to 5 MPa and u(P)= 0.005 MPa for pressures from 5 to 30 MPa.

No	T	P	ρ	u(ρ)		Z	u(Z)	No	T	P	ρ	u(ρ)		Z	u(Z)
	[K]	[MPa]	$\left[\frac{kg}{m^3}\right]$	$\left[\frac{kg}{m^3}\right]$	%		10^{-2}		[K]	[MPa]	$\left[\frac{kg}{m^3}\right]$	$\left[\frac{kg}{m^3}\right]$	%		10^{-2}
1	252.96	0.508	5.18	0.23	4.4	0.99	4.3	21	253.11	20.550	389.58	0.89	0.2	0.53	0.1
2	252.94	1.010	10.45	0.30	2.9	0.97	2.7	22	253.10	21.049	391.70	0.85	0.2	0.54	0.1
3	252.95	1.513	16.11	0.37	2.3	0.95	2.2	23	253.15	21.583	393.97	0.80	0.2	0.55	0.1
4	253.00	2.008	22.87	0.43	1.9	0.88	1.7	24	253.17	22.039	395.89	0.76	0.2	0.56	0.1
5	253.02	2.407	28.16	0.48	1.7	0.86	1.5	25	253.15	22.523	397.90	0.73	0.2	0.57	0.1
6	253.27	13.000	342.99	1.03	0.3	0.38	0.2	26	253.09	23.043	399.91	0.69	0.2	0.58	0.1
7	253.23	13.535	348.43	1.07	0.3	0.39	0.2	27	253.07	23.585	402.01	0.66	0.2	0.59	0.1
8	253.17	14.005	352.44	1.11	0.3	0.40	0.2	28	253.09	24.033	403.73	0.63	0.2	0.60	0.1
9	253.25	14.514	356.43	1.15	0.3	0.41	0.2	29	253.12	24.495	405.58	0.60	0.1	0.61	0.1
10	253.16	15.038	360.04	1.20	0.3	0.42	0.2	30	253.14	25.004	407.49	0.58	0.1	0.62	0.1
11	253.22	15.498	363.19	1.25	0.3	0.43	0.2	31	253.11	25.528	409.34	0.55	0.1	0.63	0.1
12	253.14	16.004	366.38	1.29	0.4	0.44	0.3	32	253.09	25.963	410.91	0.54	0.1	0.64	0.1
13	253.21	16.513	369.43	1.34	0.4	0.45	0.3	33	253.06	26.459	412.74	0.52	0.1	0.65	0.1
14	253.18	17.054	372.46	1.27	0.3	0.46	0.2	34	253.05	26.980	414.51	0.50	0.1	0.66	0.1
15	253.13	17.511	374.95	1.22	0.3	0.47	0.2	35	253.07	27.494	416.29	0.49	0.1	0.67	0.1
16	253.19	18.047	377.75	1.15	0.3	0.48	0.2	36	253.10	28.034	418.14	0.48	0.1	0.68	0.1
17	253.16	18.491	380.05	1.10	0.3	0.49	0.2	37	253.13	28.568	420.00	0.47	0.1	0.69	0.1
18	253.12	19.058	382.70	1.04	0.3	0.50	0.2	38	253.16	29.087	421.82	0.46	0.1	0.69	0.1
19	253.15	19.521	384.91	0.99	0.3	0.51	0.2	39	253.16	29.450	423.08	0.46	0.1	0.70	0.1
20	253.16	20.070	387.42	0.94	0.2	0.52	0.1	40	253.16	30.025	425.02	0.46	0.1	0.71	0.1

Table B.8. Experimental results of the 0.714 mol CH_4 + 0.286 mol H_2S system at 273K, $u(x_{H2S})$=0.0011, u(T)= 0.03 K, u(P)= 0.003 MPa for pressures up to 5 MPa and u(P)= 0.005 MPa for pressures from 5 to 30 MPa.

No	T	P	ρ	u(ρ)		Z	u(Z)	No	T	P	ρ	u(ρ)		Z	u(Z)
	[K]	[MPa]	$\left[\frac{kg}{m^3}\right]$	$\left[\frac{kg}{m^3}\right]$	%		10^{-2}		[K]	[MPa]	$\left[\frac{kg}{m^3}\right]$	$\left[\frac{kg}{m^3}\right]$	%		10^{-2}
1	272.97	0.448	4.32	0.22	5.1	0.97	5.0	25	273.10	18.931	331.97	1.16	0.3	0.53	0.2
2	272.98	0.925	9.10	0.25	2.7	0.95	2.5	26	273.16	19.608	336.94	0.94	0.3	0.54	0.2
3	272.99	1.499	15.62	0.29	1.8	0.89	1.6	27	273.23	20.100	340.42	0.81	0.2	0.55	0.1
4	272.98	1.959	21.08	0.32	1.5	0.86	1.4	28	273.20	20.623	344.02	0.69	0.2	0.56	0.1
5	272.99	2.470	27.39	0.35	1.3	0.84	1.2	29	273.19	21.199	347.78	0.57	0.2	0.57	0.1
6	273.07	2.991	34.29	0.38	1.1	0.81	1.0	30	273.21	21.506	349.84	0.52	0.1	0.57	0.1
7	273.06	3.515	41.26	0.41	1.0	0.80	0.9	31	273.14	21.825	351.99	0.47	0.1	0.58	0.1
8	273.02	4.006	49.21	0.43	0.9	0.76	0.7	32	273.16	22.152	354.18	0.42	0.1	0.58	0.1
9	273.02	4.495	57.70	0.45	0.8	0.73	0.6	33	273.16	22.483	356.27	0.38	0.1	0.59	0.1
10	273.00	5.009	66.37	0.46	0.7	0.71	0.6	34	273.18	22.828	358.14	0.37	0.1	0.60	0.1
11	273.03	5.418	73.50	0.47	0.6	0.69	0.5	35	273.20	23.590	362.19	0.34	0.1	0.61	0.1
12	273.01	12.511	252.68	0.73	0.3	0.46	0.2	36	273.37	24.085	364.70	0.32	0.1	0.62	0.1
13	273.00	13.055	265.48	0.76	0.3	0.46	0.2	37	273.25	24.591	367.01	0.31	0.1	0.63	0.1
14	273.00	13.551	273.70	0.79	0.3	0.46	0.2	38	273.19	24.981	368.95	0.30	0.1	0.63	0.1
15	273.00	14.019	280.64	0.82	0.3	0.47	0.2	39	273.23	25.533	371.48	0.28	0.1	0.64	0.1
16	273.00	14.532	287.50	0.85	0.3	0.47	0.2	40	273.25	26.031	373.67	0.27	0.1	0.65	0.1
17	273.01	14.977	293.17	0.88	0.3	0.48	0.2	41	273.22	26.410	375.25	0.26	0.1	0.66	0.1
18	273.00	15.457	298.99	0.91	0.3	0.48	0.2	42	273.24	27.020	377.85	0.25	0.1	0.67	0.1
19	272.99	15.974	304.94	0.95	0.3	0.49	0.2	43	273.05	27.474	379.67	0.24	0.1	0.68	0.1
20	272.99	16.531	310.78	0.98	0.3	0.50	0.2	44	273.06	27.956	381.54	0.23	0.1	0.68	0.1
21	273.03	16.977	315.19	1.02	0.3	0.50	0.2	45	273.10	28.471	383.53	0.23	0.1	0.69	0.1
22	273.08	17.450	319.61	1.05	0.3	0.51	0.2	46	273.05	29.015	385.58	0.22	0.1	0.70	0.1
23	273.11	17.956	324.07	1.09	0.3	0.52	0.2	47	273.03	29.571	387.72	0.21	0.1	0.71	0.1
24	273.09	18.521	328.70	1.13	0.3	0.53	0.2	48	273.03	30.070	389.49	0.21	0.1	0.72	0.1

Table B.9. Experimental results of the 0.714 mol CH_4 + 0.286 mol H_2S system at 293K, $u(x_{H2S})$=0.0011, u(T)= 0.03 K, u(P)= 0.003 MPa for pressures up to 5 MPa and u(P)= 0.005 MPa for pressures from 5 to 30 MPa.

No	T	P	ρ	u(ρ)		Z	u(Z)	No	T	P	ρ	u(ρ)		Z	u(Z)
	[K]	[MPa]	$\left[\frac{kg}{m^3}\right]$	$\left[\frac{kg}{m^3}\right]$	%		10^{-2}		[K]	[MPa]	$\left[\frac{kg}{m^3}\right]$	$\left[\frac{kg}{m^3}\right]$	%		10^{-2}
1	293.27	0.227	1.99	0.19	9.5	0.99	9.3	34	293.30	15.503	239.94	0.84	0.4	0.56	0.3
2	293.27	0.560	4.92	0.21	4.3	0.99	4.2	35	293.31	16.108	249.28	0.88	0.4	0.56	0.3
3	293.28	1.101	9.72	0.25	2.6	0.98	2.5	36	293.34	16.524	253.44	0.91	0.4	0.57	0.3
4	293.28	1.547	14.1	0.29	2.1	0.95	2.0	37	293.34	17.035	260.09	0.94	0.4	0.57	0.3
5	293.28	2.065	19.16	0.31	1.6	0.94	1.5	38	293.35	17.740	267.95	0.99	0.4	0.57	0.3
6	293.30	2.511	23.63	0.34	1.4	0.92	1.2	39	293.33	18.012	271.26	1.00	0.4	0.58	0.3
7	293.29	2.976	28.53	0.37	1.3	0.91	1.1	40	293.33	18.543	276.99	1.02	0.4	0.58	0.3
8	293.29	3.489	33.95	0.40	1.2	0.89	1.0	41	293.33	19.012	281.75	0.92	0.3	0.59	0.2
9	293.42	3.851	38.01	0.41	1.1	0.88	1.0	42	293.33	19.476	286.23	0.80	0.3	0.59	0.2
10	293.43	4.386	46.59	0.42	0.9	0.82	0.8	43	293.34	20.081	291.58	0.65	0.2	0.60	0.1
11	293.44	4.823	51.27	0.43	0.8	0.82	0.7	44	293.34	20.504	295.67	0.54	0.2	0.60	0.1
12	293.39	5.407	58.83	0.45	0.8	0.80	0.7	45	293.31	21.026	300.53	0.41	0.1	0.61	0.1
13	293.32	5.943	66.82	0.46	0.7	0.77	0.6	46	293.33	21.863	306.80	0.38	0.1	0.62	0.1
14	293.33	6.464	75.29	0.46	0.6	0.75	0.4	47	293.32	22.053	308.34	0.37	0.1	0.62	0.1
15	293.31	6.885	80.49	0.47	0.6	0.74	0.4	48	293.31	22.118	308.67	0.37	0.1	0.62	0.1
16	293.27	7.261	85.92	0.48	0.6	0.74	0.4	49	293.31	22.512	311.24	0.36	0.1	0.63	0.1
17	293.27	7.749	94.83	0.49	0.5	0.71	0.4	50	293.30	22.979	314.55	0.34	0.1	0.64	0.1
18	293.28	8.092	103.64	0.50	0.5	0.68	0.4	51	293.30	23.460	317.83	0.32	0.1	0.64	0.1
19	293.29	8.523	108.80	0.51	0.5	0.68	0.4	52	293.31	23.712	319.93	0.32	0.1	0.64	0.1
20	293.30	9.149	119.96	0.53	0.4	0.66	0.3	53	293.29	23.988	321.16	0.31	0.1	0.65	0.1
21	293.30	9.741	129.36	0.55	0.4	0.66	0.3	54	293.30	24.512	324.48	0.29	0.1	0.66	0.1
22	293.33	10.169	136.99	0.57	0.4	0.65	0.3	55	293.29	25.012	327.50	0.28	0.1	0.66	0.1
23	293.29	10.516	145.41	0.58	0.4	0.63	0.3	56	293.30	25.515	330.43	0.27	0.1	0.67	0.1
24	293.29	11.236	161.66	0.61	0.4	0.60	0.3	57	293.30	25.988	333.07	0.26	0.1	0.68	0.1
25	293.30	11.789	174.33	0.64	0.4	0.59	0.3	58	293.31	26.506	335.86	0.24	0.1	0.69	0.1
26	293.32	12.220	183.56	0.66	0.4	0.58	0.3	59	293.33	26.879	337.31	0.24	0.1	0.69	0.1
27	293.32	12.521	189.88	0.67	0.4	0.57	0.3	60	293.64	27.145	339.08	0.23	0.1	0.70	0.1
28	293.31	12.964	198.31	0.69	0.4	0.57	0.3	61	293.53	27.520	340.85	0.23	0.1	0.70	0.1
29	293.30	13.528	208.17	0.72	0.3	0.57	0.2	62	293.43	28.085	343.33	0.22	0.1	0.71	0.1
30	293.29	13.780	213.21	0.74	0.3	0.56	0.2	63	293.42	28.586	345.52	0.21	0.1	0.72	0.1
31	293.30	14.426	223.09	0.78	0.3	0.56	0.2	64	293.40	29.019	347.54	0.21	0.1	0.73	0.1
32	293.31	14.523	224.65	0.78	0.3	0.56	0.2	65	293.33	29.517	349.82	0.20	0.1	0.73	0.1
33	293.30	15.049	233.30	0.81	0.3	0.56	0.2	66	293.33	29.998	352.02	0.20	0.1	0.74	0.1

Table B.10. Experimental results of the 0.661 mol C_2H_6 + 0.339 mol H_2S system at 253K, $u(x_{H2S})$=0.0013, u(T)= 0.03 K, u(P)= 0.003 MPa for pressures up to 5 MPa and u(P)= 0.005 MPa for pressures from 5 to 30 MPa.

No	T [K]	P [MPa]	ρ $\left[\frac{kg}{m^3}\right]$	u(ρ) $\left[\frac{kg}{m^3}\right]$	u(ρ) %	Z	u(Z) 10^{-2}	No	T [K]	P [MPa]	ρ $\left[\frac{kg}{m^3}\right]$	u(ρ) $\left[\frac{kg}{m^3}\right]$	u(ρ) %	Z	u(Z) 10^{-2}
1	253.15	0.201	3.03	0.19	6.2	0.99	6.0	29	253.56	17.510	569.80	0.83	0.1	0.46	0.1
2	253.20	0.504	7.84	0.21	2.6	0.96	2.4	30	253.28	18.031	570.38	0.87	0.2	0.47	0.1
3	253.26	1.001	17.25	0.25	1.4	0.87	1.3	31	253.42	18.507	571.29	0.90	0.2	0.48	0.1
4	253.21	1.212	24.50	0.29	1.2	0.74	1.1	32	253.25	19.012	572.01	0.98	0.2	0.50	0.1
5	254.94	2.029	536.64	0.31	0.1	0.06	0.1	33	253.53	19.520	573.08	0.99	0.2	0.51	0.1
6	254.68	2.514	538.24	0.34	0.1	0.07	0.1	34	253.26	20.020	573.83	1.01	0.2	0.52	0.1
7	254.55	3.289	539.75	0.37	0.1	0.09	0.1	35	253.27	20.599	574.87	0.91	0.2	0.53	0.1
8	254.49	4.039	541.84	0.40	0.1	0.11	0.1	36	253.26	21.031	575.55	0.79	0.1	0.55	0.1
9	254.42	4.758	543.81	0.41	0.1	0.13	0.1	37	253.36	21.367	576.23	0.64	0.1	0.55	0.1
10	254.36	5.423	545.37	0.41	0.1	0.15	0.1	38	253.35	22.551	578.00	0.53	0.1	0.58	0.1
11	254.32	5.878	546.50	0.42	0.1	0.16	0.1	39	253.32	23.006	578.75	0.41	0.1	0.59	0.1
12	254.25	6.319	547.42	0.44	0.1	0.17	0.1	40	253.41	23.525	579.60	0.38	0.1	0.61	0.1
13	254.16	6.687	548.47	0.45	0.1	0.18	0.1	41	253.45	24.024	580.44	0.37	0.1	0.62	0.1
14	254.09	7.265	549.92	0.45	0.1	0.20	0.1	42	253.46	24.508	581.12	0.37	0.1	0.63	0.1
15	254.06	7.505	550.39	0.46	0.1	0.20	0.1	43	253.67	25.048	581.76	0.36	0.1	0.64	0.1
16	253.99	7.973	551.40	0.47	0.1	0.22	0.1	44	253.51	25.504	582.65	0.34	0.1	0.65	0.1
17	254.25	8.447	552.45	0.48	0.1	0.23	0.1	45	253.48	26.002	583.31	0.32	0.1	0.66	0.1
18	254.07	8.899	553.44	0.49	0.1	0.24	0.1	46	253.33	26.491	583.92	0.32	0.1	0.68	0.1
19	254.01	9.395	554.19	0.50	0.1	0.25	0.1	47	253.30	27.022	584.83	0.31	0.1	0.69	0.1
20	253.95	9.635	554.51	0.52	0.1	0.26	0.1	48	253.27	27.529	585.42	0.29	0.1	0.70	0.1
21	253.79	10.036	555.10	0.54	0.1	0.27	0.1	49	253.25	28.017	586.22	0.28	0.1	0.71	0.1
22	253.87	10.516	556.00	0.56	0.1	0.28	0.1	50	253.35	28.538	586.77	0.27	0.1	0.73	0.1
23	253.57	11.049	557.27	0.57	0.1	0.30	0.1	51	253.38	29.088	587.57	0.26	0.1	0.74	0.1
24	253.54	11.370	557.93	0.60	0.1	0.30	0.1	52	253.31	29.517	588.21	0.24	0.1	0.75	0.1
25	253.59	12.403	560.38	0.63	0.1	0.33	0.1	53	253.28	30.003	588.90	0.24	0.1	0.76	0.1
26	253.69	13.915	563.40	0.65	0.1	0.37	0.1	54	253.25	30.502	589.70	0.23	0.1	0.77	0.1
27	253.55	15.381	566.27	0.66	0.1	0.40	0.1	55	253.29	31.166	590.21	0.23	0.1	0.79	0.1
28	253.55	16.580	568.66	0.68	0.1	0.43	0.1								

Table B.11. Experimental results of the 0.661 mol C_2H_6 + 0.339 mol H_2S system at 253K, $u(x_{H2S})$=0.0013, u(T)= 0.03 K, u(P)= 0.003 MPa for pressures up to 5 MPa and u(P)= 0.005 MPa for pressures from 5 to 30 MPa.

No	T [K]	P [MPa]	ρ $\left[\frac{kg}{m^3}\right]$	u(ρ) $\left[\frac{kg}{m^3}\right]$	u(ρ) %	Z	u(Z) 10^{-2}	No	T [K]	P [MPa]	ρ $\left[\frac{kg}{m^3}\right]$	u(ρ) $\left[\frac{kg}{m^3}\right]$	u(ρ) %	Z	u(Z) 10^{-2}
1	272.97	0.212	3.01	0.17	5.7	0.98	5.6	32	273.01	16.504	540.35	0.70	0.1	0.42	0.1
2	272.98	0.497	7.36	0.22	3.0	0.93	2.8	33	273.00	17.030	541.54	0.72	0.1	0.44	0.1
3	272.99	1.001	15.36	0.26	1.7	0.90	1.5	34	273.00	17.563	542.76	0.74	0.1	0.45	0.1
4	273.00	1.498	24.88	0.30	1.2	0.83	1.1	35	273.00	18.014	543.63	0.76	0.1	0.46	0.1
5	273.00	2.055	37.25	0.34	0.9	0.76	0.7	36	273.00	18.562	544.96	0.78	0.1	0.47	0.1
6	273.89	3.174	494.07	0.37	0.1	0.09	0.1	37	273.00	19.020	545.99	0.80	0.1	0.48	0.1
7	273.85	3.543	497.09	0.40	0.1	0.10	0.1	38	273.00	19.571	547.11	0.87	0.2	0.50	0.1
8	273.82	4.425	501.16	0.42	0.1	0.12	0.1	39	273.00	20.034	548.10	0.90	0.2	0.51	0.1
9	273.79	5.321	504.77	0.44	0.1	0.15	0.1	40	273.00	20.587	549.23	0.93	0.2	0.52	0.1
10	273.68	5.756	506.16	0.44	0.1	0.16	0.1	41	273.01	21.047	550.19	0.96	0.2	0.53	0.1
11	272.99	6.021	509.59	0.45	0.1	0.16	0.1	42	273.01	21.503	551.08	1.00	0.2	0.54	0.1
12	272.99	6.508	511.60	0.47	0.1	0.18	0.1	43	273.01	22.046	552.15	1.04	0.2	0.55	0.1
13	272.98	7.008	513.56	0.48	0.1	0.19	0.1	44	273.00	22.584	553.21	1.09	0.2	0.57	0.1
14	272.99	7.506	515.43	0.48	0.1	0.20	0.1	45	273.00	23.024	554.08	1.11	0.2	0.58	0.1
15	272.99	8.017	517.26	0.49	0.1	0.21	0.1	46	273.00	23.546	555.04	1.05	0.2	0.59	0.1
16	273.01	8.515	518.95	0.51	0.1	0.23	0.1	47	273.00	24.060	556.05	0.97	0.2	0.60	0.1
17	273.01	9.014	520.53	0.52	0.1	0.24	0.1	48	273.01	24.560	557.00	0.83	0.1	0.61	0.1
18	273.01	9.508	521.97	0.52	0.1	0.25	0.1	49	273.01	25.048	557.87	0.68	0.1	0.62	0.1
19	273.01	10.019	523.50	0.53	0.1	0.26	0.1	50	273.01	25.523	558.70	0.54	0.1	0.63	0.1
20	273.00	10.520	524.91	0.54	0.1	0.28	0.1	51	273.02	26.058	559.73	0.36	0.1	0.64	0.1
21	273.01	11.014	526.35	0.55	0.1	0.29	0.1	52	273.01	26.500	560.45	0.34	0.1	0.65	0.1
22	273.02	11.522	527.75	0.56	0.1	0.30	0.1	53	273.01	27.067	561.43	0.31	0.1	0.67	0.1
23	273.00	12.030	529.14	0.57	0.1	0.31	0.1	54	273.02	27.540	562.30	0.29	0.1	0.68	0.1
24	273.00	12.522	530.51	0.59	0.1	0.33	0.1	55	273.01	28.052	563.22	0.26	0.1	0.69	0.1
25	273.00	13.049	531.85	0.60	0.1	0.34	0.1	56	273.00	28.535	564.05	0.24	0.1	0.70	0.1
26	273.01	13.539	533.12	0.61	0.1	0.35	0.1	57	273.00	29.042	564.85	0.23	0.1	0.71	0.1
27	273.00	14.054	534.45	0.63	0.1	0.36	0.1	58	273.00	29.512	565.62	0.21	0.1	0.72	0.1
28	273.00	14.514	535.57	0.64	0.1	0.38	0.1	59	273.00	30.037	566.50	0.21	0.1	0.73	0.1
29	273.00	15.071	536.94	0.65	0.1	0.39	0.1	60	273.00	30.511	567.30	0.20	0.1	0.74	0.1
30	273.00	15.565	538.15	0.67	0.1	0.40	0.1	61	273.00	31.005	568.07	0.20	0.1	0.76	0.1
31	273.00	16.072	539.33	0.69	0.1	0.41	0.1								

Table B.12. Experimental results of the 0.661 mol C_2H_6 + 0.339 mol H_2S system at 293K, $u(x_{H2S})$=0.0013, u(T)= 0.03 K, u(P)= 0.003 MPa for pressures up to 5 MPa and u(P)= 0.005 MPa for pressures from 5 to 30 MPa.

No	T	P	ρ	u(ρ)		Z	u(Z)	No	T	P	ρ	u(ρ)		Z	u(Z)
	[K]	[MPa]	$\left[\frac{kg}{m^3}\right]$	$\left[\frac{kg}{m^3}\right]$	%		10^{-2}		[K]	[MPa]	$\left[\frac{kg}{m^3}\right]$	$\left[\frac{kg}{m^3}\right]$	%		10^{-2}
1	293.47	0.201	2.70	0.19	6.9	0.96	6.8	30	293.53	16.036	504.02	0.72	0.1	0.41	0.1
2	293.47	0.567	7.84	0.20	2.5	0.93	2.4	31	293.52	16.620	505.90	0.74	0.1	0.42	0.1
3	293.44	1.057	15.20	0.23	1.5	0.90	1.3	32	293.53	17.219	507.86	0.77	0.2	0.44	0.1
4	293.45	1.535	22.98	0.25	1.1	0.86	1.0	33	293.55	17.831	509.79	0.79	0.2	0.45	0.1
5	293.45	2.009	31.45	0.27	0.9	0.82	0.7	34	293.53	18.456	511.55	0.81	0.2	0.46	0.1
6	293.46	2.608	43.66	0.30	0.7	0.77	0.6	35	293.55	19.088	513.49	0.84	0.2	0.48	0.1
7	293.47	3.138	56.58	0.33	0.6	0.71	0.6	36	293.53	19.728	515.36	0.86	0.2	0.49	0.1
8	293.48	3.526	68.15	0.37	0.6	0.67	0.5	37	293.52	20.375	517.16	0.90	0.2	0.51	0.1
9	293.64	4.715	444.72	0.40	0.1	0.14	0.1	38	293.54	21.010	518.84	0.93	0.2	0.52	0.1
10	293.65	5.590	451.51	0.43	0.1	0.16	0.1	39	293.54	21.642	520.56	0.96	0.2	0.54	0.1
11	293.65	6.386	457.50	0.44	0.1	0.18	0.1	40	293.55	22.270	522.22	0.99	0.2	0.55	0.1
12	293.64	7.060	462.33	0.46	0.1	0.20	0.1	41	293.56	22.889	523.75	1.02	0.2	0.56	0.1
13	293.66	7.636	466.11	0.47	0.1	0.21	0.1	42	293.57	23.496	525.20	1.05	0.2	0.58	0.1
14	293.65	8.142	469.33	0.48	0.1	0.22	0.1	43	293.53	24.084	526.73	1.03	0.2	0.59	0.1
15	293.65	8.646	472.44	0.48	0.1	0.24	0.1	44	293.54	24.655	527.99	0.91	0.2	0.60	0.1
16	293.65	9.099	475.09	0.49	0.1	0.25	0.1	45	293.53	25.204	529.38	0.76	0.1	0.61	0.1
17	293.52	9.518	477.28	0.50	0.1	0.26	0.1	46	293.56	25.734	530.52	0.60	0.1	0.62	0.1
18	293.53	10.125	480.41	0.51	0.1	0.27	0.1	47	293.55	26.234	531.63	0.45	0.1	0.64	0.1
19	293.49	10.681	483.12	0.52	0.1	0.28	0.1	48	293.53	26.704	532.76	0.41	0.1	0.65	0.1
20	293.50	11.330	486.10	0.53	0.1	0.30	0.1	49	293.53	27.148	533.70	0.39	0.1	0.66	0.1
21	293.50	11.693	487.62	0.55	0.1	0.31	0.1	50	293.53	27.563	534.55	0.35	0.1	0.66	0.1
22	293.51	12.083	489.36	0.56	0.1	0.32	0.1	51	293.54	27.951	535.47	0.33	0.1	0.67	0.1
23	293.53	12.494	490.97	0.58	0.1	0.33	0.1	52	293.54	28.632	536.83	0.31	0.1	0.69	0.1
24	293.51	12.931	492.74	0.59	0.1	0.34	0.1	53	293.51	28.931	537.39	0.29	0.1	0.69	0.1
25	293.50	13.395	494.62	0.61	0.1	0.35	0.1	54	293.51	29.452	538.43	0.27	0.1	0.70	0.1
26	293.51	13.880	496.50	0.64	0.1	0.36	0.1	55	293.48	30.064	539.55	0.25	0.1	0.72	0.1
27	293.51	14.390	498.32	0.66	0.1	0.37	0.1	56	293.49	30.508	540.43	0.23	0.1	0.73	0.1
28	293.52	14.926	500.24	0.68	0.1	0.38	0.1	57	293.48	31.049	541.38	0.22	0.1	0.74	0.1
29	293.52	15.468	502.11	0.70	0.1	0.40	0.1								

Table B.13. Experimental results of the 0.8674 mol C_3H_8 + 0.1326 mol H_2S system at 253K, $u(x_{H2S})$=0.0010, u(T)= 0.03 K, u(P)= 0.003 MPa for pressures up to 5 MPa and u(P)= 0.005 MPa for pressures from 5 to 30 MPa.

No	T [K]	P [MPa]	ρ $\left[\frac{kg}{m^3}\right]$	u(ρ) $\left[\frac{kg}{m^3}\right]$	u(ρ) %	Z	u(Z) 10^{-2}	No	T [K]	P [MPa]	ρ $\left[\frac{kg}{m^3}\right]$	u(ρ) $\left[\frac{kg}{m^3}\right]$	u(ρ) %	Z	u(Z) 10^{-2}
1	253.45	0.203	4.29	0.20	4.7	0.96	4.5	31	253.42	16.530	591.85	0.96	0.2	0.57	0.1
2	253.48	0.506	569.99	0.22	0.1	0.02	0.1	32	253.44	17.060	592.50	1.04	0.2	0.58	0.1
3	254.32	1.032	571.31	0.26	0.1	0.04	0.1	33	253.43	17.589	593.09	1.05	0.2	0.60	0.1
4	254.31	1.502	572.14	0.31	0.1	0.05	0.1	34	253.42	17.987	593.57	1.08	0.2	0.62	0.1
5	254.30	2.134	572.54	0.33	0.1	0.08	0.1	35	253.43	18.510	594.13	0.97	0.2	0.63	0.1
6	253.51	2.505	573.29	0.36	0.1	0.09	0.1	36	253.43	19.023	594.73	0.84	0.1	0.65	0.1
7	253.49	2.947	574.34	0.39	0.1	0.10	0.1	37	253.43	19.531	595.32	0.69	0.1	0.67	0.1
8	253.52	3.815	575.72	0.42	0.1	0.13	0.1	38	253.44	20.030	595.85	0.57	0.1	0.68	0.1
9	253.54	4.538	577.20	0.43	0.1	0.16	0.1	39	253.43	20.531	596.38	0.43	0.1	0.70	0.1
10	253.55	5.089	578.38	0.44	0.1	0.18	0.1	40	253.42	21.024	597.01	0.40	0.1	0.71	0.1
11	253.50	5.442	578.38	0.45	0.1	0.19	0.1	41	253.44	21.509	597.48	0.39	0.1	0.73	0.1
12	253.49	6.297	579.54	0.47	0.1	0.22	0.1	42	253.45	21.988	598.03	0.39	0.1	0.75	0.1
13	253.49	6.936	580.36	0.48	0.1	0.24	0.1	43	253.44	22.579	598.60	0.38	0.1	0.77	0.1
14	253.50	7.527	581.21	0.48	0.1	0.26	0.1	44	253.41	23.037	599.17	0.36	0.1	0.78	0.1
15	253.50	8.113	581.99	0.50	0.1	0.28	0.1	45	253.42	23.562	599.72	0.34	0.1	0.80	0.1
16	253.49	8.710	582.83	0.51	0.1	0.30	0.1	46	253.42	24.094	600.28	0.34	0.1	0.81	0.1
17	253.48	9.553	583.79	0.52	0.1	0.33	0.1	47	253.44	24.510	600.76	0.33	0.1	0.83	0.1
18	253.45	10.091	584.35	0.53	0.1	0.35	0.1	48	253.43	25.018	601.27	0.31	0.1	0.84	0.1
19	253.45	10.501	584.81	0.54	0.1	0.36	0.1	49	253.40	25.506	601.74	0.30	0.1	0.86	0.1
20	253.46	11.048	585.40	0.56	0.1	0.38	0.1	50	253.44	26.055	602.33	0.28	0.1	0.88	0.1
21	253.45	11.598	586.10	0.58	0.1	0.40	0.1	51	253.43	26.513	602.69	0.27	0.1	0.89	0.1
22	253.46	12.010	586.55	0.60	0.1	0.42	0.1	52	253.41	27.093	603.31	0.25	0.1	0.91	0.1
23	253.45	12.562	587.22	0.61	0.1	0.43	0.1	53	253.42	27.546	603.77	0.25	0.1	0.93	0.1
24	253.45	12.979	587.69	0.64	0.1	0.45	0.1	54	253.40	28.028	604.28	0.24	0.1	0.94	0.1
25	253.44	13.535	588.39	0.67	0.1	0.47	0.1	55	253.38	28.498	604.77	0.23	0.1	0.96	0.1
26	253.44	14.093	588.97	0.70	0.1	0.49	0.1	56	253.41	29.029	605.34	0.23	0.1	0.97	0.1
27	253.44	14.505	589.56	0.71	0.1	0.50	0.1	57	253.40	30.001	606.23	0.22	0.1	1.00	0.1
28	253.45	15.043	590.21	0.73	0.1	0.52	0.1	58	253.40	30.510	606.77	0.22	0.1	1.02	0.1
29	253.44	15.585	590.82	0.89	0.1	0.54	0.1	59	253.43	31.050	607.30	0.21	0.1	1.04	0.1
30	253.45	15.990	591.30	0.93	0.2	0.55	0.1	60	253.39	31.562	607.75	0.21	0.1	1.05	0.1

Table B.14. Experimental results of the 0.8674 mol C_3H_8 + 0.1326 mol H_2S system at 273K, $u(x_{H2S})$=0.0010, u(T)= 0.03 K, u(P)= 0.003 MPa for pressures up to 5 MPa and u(P)= 0.005 MPa for pressures from 5 to 30 MPa.

No	T	P	ρ	u(ρ)		Z	u(Z)	No	T	P	ρ	u(ρ)		Z	u(Z)
	[K]	[MPa]	$\left[\frac{kg}{m^3}\right]$	$\left[\frac{kg}{m^3}\right]$	%		10^{-2}		[K]	[MPa]	$\left[\frac{kg}{m^3}\right]$	$\left[\frac{kg}{m^3}\right]$	%		10^{-2}
1	273.72	0.201	3.92	0.18	4.6	0.96	4.5	33	273.67	16.114	572.85	0.76	0.1	0.53	0.1
2	273.66	0.398	8.09	0.23	2.9	0.93	2.7	34	273.68	16.659	573.61	0.78	0.1	0.55	0.1
3	273.76	1.047	546.94	0.27	0.1	0.04	0.1	35	273.68	16.930	574.03	0.80	0.1	0.55	0.1
4	273.80	1.519	547.89	0.32	0.1	0.05	0.1	36	273.67	17.469	574.79	0.82	0.1	0.57	0.1
5	273.84	2.086	548.84	0.36	0.1	0.07	0.1	37	273.67	18.004	575.55	0.84	0.1	0.59	0.1
6	273.85	2.703	549.79	0.39	0.1	0.09	0.1	38	273.68	18.533	576.26	0.92	0.2	0.60	0.1
7	273.82	3.088	550.74	0.42	0.1	0.11	0.1	39	273.68	18.991	576.92	0.95	0.2	0.62	0.1
8	273.82	3.594	551.83	0.44	0.1	0.12	0.1	40	273.67	19.542	577.62	0.98	0.2	0.64	0.1
9	273.82	4.005	552.54	0.46	0.1	0.14	0.1	41	273.67	20.083	578.39	1.01	0.2	0.65	0.1
10	273.82	4.510	553.48	0.46	0.1	0.15	0.1	42	273.65	20.352	578.70	1.05	0.2	0.66	0.1
11	273.82	5.018	554.61	0.47	0.1	0.17	0.1	43	273.66	20.882	579.50	1.10	0.2	0.68	0.1
12	273.82	5.495	555.46	0.50	0.1	0.19	0.1	44	273.67	21.406	580.16	1.15	0.2	0.69	0.1
13	273.82	6.041	556.29	0.51	0.1	0.20	0.1	45	273.66	21.920	580.85	1.17	0.2	0.71	0.1
14	273.82	6.512	557.37	0.51	0.1	0.22	0.1	46	273.66	22.423	581.50	1.11	0.2	0.72	0.1
15	273.82	7.031	558.39	0.52	0.1	0.24	0.1	47	273.66	22.917	582.16	1.02	0.2	0.74	0.1
16	273.82	7.586	559.31	0.54	0.1	0.25	0.1	48	273.66	23.404	582.75	0.87	0.2	0.75	0.1
17	273.79	8.180	560.40	0.55	0.1	0.27	0.1	49	273.65	23.879	583.39	0.72	0.1	0.77	0.1
18	273.70	8.513	560.88	0.55	0.1	0.29	0.1	50	273.65	24.569	584.13	0.57	0.1	0.79	0.1
19	273.70	9.042	561.71	0.56	0.1	0.30	0.1	51	273.95	25.011	584.71	0.38	0.1	0.80	0.1
20	273.70	9.510	562.45	0.57	0.1	0.32	0.1	52	273.82	25.516	585.31	0.36	0.1	0.82	0.1
21	273.68	10.141	563.44	0.58	0.1	0.34	0.1	53	273.78	26.019	585.92	0.33	0.1	0.83	0.1
22	273.69	10.627	564.33	0.59	0.1	0.35	0.1	54	273.77	26.506	586.52	0.31	0.1	0.85	0.1
23	273.68	11.122	565.14	0.60	0.1	0.37	0.1	55	273.77	26.976	587.10	0.27	0.1	0.86	0.1
24	273.69	11.619	565.97	0.62	0.1	0.39	0.1	56	273.78	27.450	587.64	0.25	0.1	0.88	0.1
25	273.68	12.118	566.75	0.63	0.1	0.40	0.1	57	273.78	27.978	588.27	0.24	0.1	0.89	0.1
26	273.68	12.619	567.54	0.64	0.1	0.42	0.1	58	273.77	28.442	588.80	0.22	0.1	0.91	0.1
27	273.68	13.126	568.32	0.66	0.1	0.43	0.1	59	273.73	29.091	589.54	0.22	0.1	0.93	0.1
28	273.68	13.655	569.15	0.67	0.1	0.45	0.1	60	273.73	29.541	590.04	0.21	0.1	0.94	0.1
29	273.68	13.924	569.59	0.69	0.1	0.46	0.1	61	273.79	30.078	590.66	0.21	0.1	0.96	0.1
30	273.68	14.474	570.40	0.71	0.1	0.48	0.1	62	273.77	30.592	591.25	0.20	0.1	0.97	0.1
31	273.68	15.021	571.26	0.73	0.1	0.49	0.1	63	273.79	31.056	591.75	0.20	0.1	0.99	0.1
32	273.67	15.568	572.04	0.74	0.1	0.51	0.1	64	273.71	31.570	592.34	0.20	0.1	1.00	0.1

Table B.15. Experimental results of the 0.8674 mol C_3H_8 + 0.1326 mol H_2S system at 293K, $u(x_{H2S})$=0.0010, u(T)= 0.03 K, u(P)= 0.003 MPa for pressures up to 5 MPa and u(P)= 0.005 MPa for pressures from 5 to 30 MPa.

No	T [K]	P [MPa]	ρ $\left[\frac{kg}{m^3}\right]$	u(ρ) $\left[\frac{kg}{m^3}\right]$	u(ρ) %	Z	u(Z) 10^{-2}	No	T [K]	P [MPa]	ρ $\left[\frac{kg}{m^3}\right]$	u(ρ) $\left[\frac{kg}{m^3}\right]$	u(ρ) %	Z	u(Z) 10^{-2}
1	293.39	0.194	3.48	0.19	5.4	0.97	5.3	24	293.47	18.072	556.51	0.60	0.1	0.56	0.1
2	293.39	0.470	8.87	0.20	2.3	0.93	2.2	25	293.47	18.994	558.11	0.62	0.1	0.59	0.1
3	293.43	0.801	16.22	0.23	1.4	0.88	1.3	26	293.45	19.869	559.49	0.64	0.1	0.61	0.1
4	293.42	1.401	518.57	0.25	0.0	0.05	0.1	27	293.46	20.694	560.85	0.66	0.1	0.64	0.1
5	293.40	1.995	520.13	0.27	0.1	0.07	0.1	28	293.45	21.471	562.13	0.69	0.1	0.66	0.1
6	293.41	2.505	521.47	0.31	0.1	0.08	0.1	29	293.45	22.205	563.19	0.71	0.1	0.68	0.1
7	293.41	3.015	522.80	0.34	0.1	0.10	0.1	30	293.45	22.885	564.25	0.73	0.1	0.70	0.1
8	293.41	3.569	524.08	0.38	0.1	0.12	0.1	31	293.44	23.521	565.29	0.75	0.1	0.72	0.1
9	293.41	4.015	525.61	0.40	0.1	0.13	0.1	32	293.45	24.107	566.06	0.78	0.1	0.74	0.1
10	293.42	4.503	527.43	0.43	0.1	0.15	0.1	33	293.44	24.646	566.85	0.67	0.1	0.75	0.1
11	293.39	5.302	529.64	0.44	0.1	0.17	0.1	34	293.44	25.145	567.51	0.57	0.1	0.77	0.1
12	293.40	6.217	531.97	0.46	0.1	0.20	0.1	35	293.44	25.599	568.18	0.38	0.1	0.78	0.1
13	293.40	7.085	534.16	0.47	0.1	0.23	0.1	36	293.43	26.016	568.72	0.36	0.1	0.79	0.1
14	293.41	7.972	536.27	0.48	0.1	0.26	0.1	37	293.43	26.738	569.66	0.33	0.1	0.81	0.1
15	293.41	8.877	538.44	0.48	0.1	0.29	0.1	38	293.43	27.051	570.13	0.31	0.1	0.82	0.1
16	293.42	9.813	540.44	0.50	0.1	0.31	0.1	39	293.42	27.595	570.79	0.27	0.1	0.84	0.1
17	293.42	10.741	542.48	0.51	0.1	0.34	0.1	40	293.42	28.038	571.26	0.25	0.1	0.85	0.1
18	293.42	11.676	544.45	0.52	0.1	0.37	0.1	41	293.43	28.554	571.91	0.24	0.1	0.86	0.1
19	293.63	12.932	546.99	0.53	0.1	0.41	0.1	42	293.42	29.031	572.41	0.22	0.1	0.88	0.1
20	293.49	14.000	549.06	0.54	0.1	0.44	0.1	43	293.40	29.515	573.02	0.22	0.1	0.89	0.1
21	293.47	15.062	551.16	0.56	0.1	0.47	0.1	44	293.39	29.989	573.41	0.21	0.1	0.91	0.1
22	293.47	16.103	552.99	0.57	0.1	0.50	0.1	45	293.39	30.491	573.95	0.21	0.1	0.92	0.1
23	293.46	17.109	554.81	0.59	0.1	0.53	0.1	46	293.40	31.086	574.74	0.20	0.1	0.94	0.1

Table B.16. Experimental results of the 0.4213 mol CO_2 + 0.4053 CH_4 + 0.1735 mol H_2S system at 253K, u(x_{CO2})= 0.0010, u(x_{CH4})= 0.0011, u(x_{H2S})= 0.0008, u(T)= 0.03 K, u(P)= 0.003 MPa for pressures up to 5 MPa and u(P)= 0.005 MPa for pressures from 5 to 30 MPa.

No	T	P	ρ	u(ρ)		Z	u(Z)	No	T	P	ρ	u(ρ)		Z	u(Z)
	[K]	[MPa]	$\left[\frac{kg}{m^3}\right]$	$\left[\frac{kg}{m^3}\right]$	%		10^{-2}		[K]	[MPa]	$\left[\frac{kg}{m^3}\right]$	$\left[\frac{kg}{m^3}\right]$	%		10^{-2}
1	252.87	0.502	7.77	0.26	3.3	0.95	3.2	26	253.00	18.514	657.39	0.45	0.1	0.41	0.1
2	253.02	1.007	15.84	0.27	1.7	0.94	1.3	27	252.98	19.016	658.15	0.42	0.1	0.43	0.1
3	253.09	1.500	24.69	0.27	1.1	0.89	1.0	28	252.98	19.505	659.53	0.40	0.1	0.44	0.1
4	252.91	2.017	35.34	0.28	0.8	0.84	0.7	29	252.98	20.048	661.02	0.38	0.1	0.45	0.1
5	252.92	2.627	52.23	0.32	0.6	0.74	0.5	30	252.99	20.538	662.35	0.35	0.1	0.46	0.1
6	253.24	8.815	587.61	0.43	0.1	0.22	0.1	31	253.07	21.003	663.60	0.33	0.1	0.47	0.1
7	253.38	9.133	609.00	0.41	0.1	0.22	0.1	32	253.30	21.554	665.05	0.31	0.1	0.48	0.1
8	253.18	9.628	616.58	0.38	0.1	0.23	0.1	33	253.25	22.033	666.45	0.30	0.1	0.49	0.1
9	253.14	9.969	620.68	0.42	0.1	0.24	0.1	34	253.31	22.594	667.75	0.28	0.1	0.50	0.1
10	253.14	10.505	625.10	0.46	0.1	0.25	0.1	35	253.21	23.070	670.10	0.27	0.1	0.51	0.1
11	253.13	11.043	628.59	0.53	0.1	0.26	0.1	36	253.18	23.582	670.25	0.26	0.1	0.52	0.1
12	253.14	11.462	630.95	0.57	0.1	0.27	0.1	37	253.12	24.012	672.17	0.26	0.1	0.53	0.1
13	253.14	12.057	633.95	0.65	0.1	0.28	0.1	38	253.11	24.559	673.60	0.25	0.1	0.54	0.1
14	253.23	12.517	636.06	0.70	0.1	0.29	0.1	39	253.12	25.081	674.94	0.25	0.1	0.55	0.1
15	253.17	13.065	640.22	0.75	0.1	0.30	0.1	40	253.10	25.592	676.17	0.24	0.1	0.56	0.1
16	253.08	13.529	641.03	0.81	0.1	0.31	0.1	41	253.11	26.092	677.41	0.24	0.1	0.57	0.1
17	253.05	14.071	642.36	0.84	0.1	0.32	0.1	42	253.09	26.585	678.61	0.24	0.1	0.58	0.1
18	253.07	14.580	644.46	0.76	0.1	0.33	0.1	43	253.06	27.071	679.84	0.22	0.1	0.59	0.1
19	253.06	14.996	646.27	0.69	0.1	0.34	0.1	44	253.03	27.548	681.04	0.22	0.1	0.60	0.1
20	253.03	15.506	648.04	0.65	0.1	0.35	0.1	45	253.09	28.022	682.03	0.22	0.1	0.60	0.1
21	253.05	15.930	649.39	0.60	0.1	0.36	0.1	46	253.12	28.486	682.96	0.22	0.1	0.61	0.1
22	253.05	16.564	650.86	0.56	0.1	0.37	0.1	47	253.10	29.093	684.39	0.21	0.1	0.63	0.1
23	253.04	17.068	653.00	0.52	0.1	0.38	0.1	48	253.44	29.536	684.46	0.21	0.1	0.63	0.1
24	253.04	17.501	654.43	0.49	0.1	0.39	0.1	49	253.19	29.971	686.09	0.21	0.1	0.64	0.1
25	252.99	18.033	656.15	0.47	0.1	0.40	0.1								

Table B.17. Experimental results of the 0.4213 mol CO_2 + 0.4053 CH_4 + 0.1735 mol H_2S system at 273K, u(x_{CO2})= 0.0010, u(x_{CH4})= 0.0011, u(x_{H2S})= 0.0008, u(T)= 0.03 K, u(P)= 0.003 MPa for pressures up to 5 MPa and u(P)= 0.005 MPa for pressures from 5 to 30 MPa.

No	T	P	ρ	u(ρ)		Z	u(Z)	No	T	P	ρ	u(ρ)		Z	u(Z)
	[K]	[MPa]	$\left[\frac{kg}{m^3}\right]$	$\left[\frac{kg}{m^3}\right]$	%		10^{-2}		[K]	[MPa]	$\left[\frac{kg}{m^3}\right]$	$\left[\frac{kg}{m^3}\right]$	%		10^{-2}
1	273.79	0.202	2.82	0.22	7.9	0.97	7.7	30	273.71	17.518	563.42	0.39	0.1	0.42	0.1
2	273.74	0.449	6.47	0.24	3.8	0.94	3.7	31	273.79	17.971	566.80	0.36	0.1	0.43	0.1
3	273.74	0.863	12.88	0.26	2.0	0.91	1.8	32	273.79	18.442	570.18	0.34	0.1	0.44	0.1
4	273.82	1.261	19.04	0.28	1.5	0.90	1.3	33	273.78	19.099	574.70	0.33	0.1	0.45	0.1
5	273.71	1.657	25.28	0.30	1.2	0.89	1.0	34	273.76	19.546	577.65	0.31	0.1	0.46	0.1
6	273.72	2.511	39.52	0.33	0.8	0.86	0.7	35	273.78	20.013	580.63	0.30	0.1	0.47	0.1
7	273.73	3.021	48.96	0.36	0.7	0.84	6.0	36	273.76	20.510	583.72	0.29	0.1	0.48	0.1
8	273.71	3.518	59.31	0.38	0.6	0.81	0.5	37	273.77	21.074	587.10	0.29	0.1	0.49	0.1
9	273.72	4.016	71.29	0.43	0.6	0.77	0.4	38	273.75	21.548	589.86	0.28	0.1	0.50	0.1
10	273.71	4.521	85.30	0.47	0.5	0.72	0.3	39	273.78	22.058	592.74	0.28	0.1	0.51	0.1
11	273.71	5.038	99.83	0.54	0.5	0.69	0.3	40	273.77	22.467	595.00	0.26	0.1	0.51	0.1
12	273.70	5.354	107.49	0.58	0.5	0.68	0.2	41	273.79	23.096	598.38	0.26	0.1	0.52	0.1
13	273.72	9.458	427.26	0.71	0.2	0.30	0.1	42	273.76	23.526	600.64	0.26	0.1	0.53	0.1
14	273.72	9.705	439.90	0.76	0.2	0.30	0.1	43	273.79	23.982	602.97	0.24	0.1	0.54	0.1
15	273.70	10.012	452.88	0.82	0.2	0.30	0.1	44	273.75	24.515	605.65	0.24	0.1	0.55	0.1
16	273.70	10.517	469.80	0.88	0.2	0.30	0.1	45	273.74	25.041	608.23	0.24	0.1	0.56	0.1
17	273.72	11.080	484.46	0.92	0.2	0.31	0.1	46	273.72	25.573	610.79	0.24	0.1	0.57	0.1
18	273.71	11.550	494.51	0.83	0.2	0.32	0.1	47	273.75	26.052	613.04	0.23	0.1	0.58	0.1
19	273.72	12.045	503.64	0.75	0.1	0.33	0.1	48	273.73	26.540	615.30	0.23	0.1	0.59	0.1
20	273.71	12.533	511.51	0.71	0.1	0.33	0.1	49	273.75	27.037	617.55	0.23	0.1	0.60	0.1
21	273.73	13.001	518.30	0.65	0.1	0.34	0.1	50	273.77	27.542	619.81	0.23	0.1	0.60	0.1
22	273.72	13.517	525.07	0.62	0.1	0.35	0.1	51	273.77	28.056	622.07	0.22	0.1	0.61	0.1
23	273.70	14.084	531.84	0.57	0.1	0.36	0.1	52	273.72	28.578	624.32	0.22	0.1	0.62	0.1
24	273.73	14.543	536.87	0.54	0.1	0.37	0.1	53	273.84	29.062	626.38	0.22	0.1	0.63	0.1
25	273.71	15.040	541.99	0.52	0.1	0.38	0.1	54	273.86	29.553	628.43	0.22	0.1	0.64	0.1
26	273.71	15.539	546.78	0.50	0.1	0.39	0.1	55	273.72	29.922	629.96	0.21	0.1	0.65	0.1
27	273.71	16.004	551.01	0.46	0.1	0.40	0.1	56	273.71	30.474	632.22	0.21	0.1	0.66	0.1
28	273.72	16.529	555.52	0.44	0.1	0.40	0.1	57	273.72	31.034	634.47	0.21	0.1	0.67	0.1
29	273.72	17.083	560.03	0.42	0.1	0.41	0.1	58	273.72	31.527	636.43	0.21	0.1	0.67	0.1

Table B.18. Experimental results of the 0.4213 mol CO_2 + 0.4053 CH_4 + 0.1735 mol H_2S system at 293K, u(x_{CO2})= 0.0010, u(x_{CH4})= 0.0011, u(x_{H2S})= 0.0008, u(T)= 0.03 K, u(P)= 0.003 MPa for pressures up to 5 MPa and u(P)= 0.005 MPa for pressures from 5 to 30 MPa.

No	T	P	ρ	u(ρ)		Z	u(Z)	No	T	P	ρ	u(ρ)		Z	u(Z)
	[K]	[MPa]	$\left[\frac{kg}{m^3}\right]$	$\left[\frac{kg}{m^3}\right]$	%		10^{-2}		[K]	[MPa]	$\left[\frac{kg}{m^3}\right]$	$\left[\frac{kg}{m^3}\right]$	%		10^{-2}
1	293.35	0.507	6.82	0.24	3.6	0.94	3.5	33	293.36	16.560	445.27	0.34	0.1	0.47	0.1
2	293.33	1.027	13.95	0.26	1.9	0.93	1.7	34	293.37	17.005	452.34	0.33	0.1	0.48	0.1
3	293.33	1.501	20.74	0.28	1.4	0.92	1.3	35	293.38	17.560	460.59	0.32	0.1	0.48	0.1
4	293.33	2.005	28.30	0.30	1.1	0.90	0.9	36	293.37	18.070	467.66	0.32	0.1	0.49	0.1
5	293.34	2.516	36.34	0.33	0.9	0.88	0.8	37	293.39	18.520	473.55	0.31	0.1	0.50	0.1
6	293.33	3.047	45.16	0.36	0.8	0.86	0.6	38	293.37	19.093	480.62	0.31	0.1	0.50	0.1
7	293.33	3.511	53.30	0.38	0.7	0.84	0.5	39	293.36	19.495	485.34	0.30	0.1	0.51	0.1
8	293.35	4.024	62.80	0.43	0.7	0.81	0.5	40	293.35	20.024	491.23	0.30	0.1	0.52	0.1
9	293.34	4.505	72.30	0.47	0.6	0.79	0.5	41	293.36	20.581	497.12	0.30	0.1	0.53	0.1
10	293.35	5.022	83.15	0.54	0.6	0.77	0.4	42	293.37	21.049	501.83	0.28	0.1	0.53	0.1
11	293.34	5.503	94.01	0.58	0.6	0.74	0.4	43	293.36	21.538	506.55	0.28	0.1	0.54	0.1
12	293.35	6.035	106.90	0.71	0.7	0.72	0.5	44	293.36	22.048	511.26	0.28	0.1	0.55	0.1
13	293.35	6.550	120.47	0.77	0.6	0.69	0.5	45	293.36	22.580	515.98	0.28	0.1	0.56	0.1
14	293.34	7.049	134.71	0.83	0.6	0.66	0.4	46	293.36	22.995	519.51	0.28	0.1	0.56	0.1
15	293.35	7.530	149.64	0.90	0.6	0.64	0.4	47	293.38	23.569	524.22	0.28	0.1	0.57	0.1
16	293.35	8.089	168.64	0.94	0.6	0.61	0.3	48	293.37	24.016	527.76	0.28	0.1	0.58	0.1
17	293.36	8.494	183.56	0.85	0.5	0.59	0.3	49	293.38	24.491	531.40	0.28	0.1	0.58	0.1
18	293.34	9.009	203.92	0.77	0.4	0.56	0.2	50	293.38	25.093	535.84	0.27	0.1	0.59	0.1
19	293.34	9.522	225.63	0.73	0.3	0.54	0.2	51	293.40	25.511	538.82	0.27	0.1	0.60	0.1
20	293.35	10.028	248.02	0.68	0.3	0.51	0.1	52	293.39	26.073	542.71	0.27	0.1	0.61	0.1
21	293.35	10.512	269.73	0.65	0.2	0.49	0.1	53	293.38	26.543	545.86	0.27	0.1	0.62	0.1
22	293.35	11.021	292.11	0.60	0.2	0.48	0.1	54	293.39	27.022	548.97	0.26	0.1	0.62	0.1
23	293.36	11.524	313.15	0.57	0.2	0.47	0.1	55	293.38	27.494	551.96	0.26	0.1	0.63	0.1
24	293.34	12.013	332.14	0.55	0.2	0.46	0.1	56	293.40	28.049	555.38	0.26	0.1	0.64	0.1
25	293.35	12.570	351.82	0.53	0.1	0.45	0.1	57	293.47	28.537	558.30	0.26	0.1	0.65	0.1
26	293.36	13.015	366.07	0.49	0.1	0.45	0.1	58	293.46	29.086	561.49	0.26	0.1	0.66	0.1
27	293.36	13.529	380.99	0.47	0.1	0.45	0.1	59	293.43	29.505	563.87	0.25	0.1	0.66	0.1
28	293.35	14.046	394.56	0.45	0.1	0.45	0.1	60	293.42	29.521	563.96	0.25	0.1	0.66	0.1
29	293.36	14.542	406.38	0.42	0.1	0.45	0.1	61	293.42	30.015	566.70	0.25	0.1	0.67	0.1
30	293.35	15.029	416.99	0.39	0.1	0.46	0.1	62	293.43	30.573	569.71	0.25	0.1	0.68	0.1
31	293.35	15.499	426.41	0.37	0.1	0.46	0.1	63	293.43	30.988	571.90	0.24	0.1	0.69	0.1
32	293.36	16.075	437.02	0.36	0.1	0.47	0.1								

Table B.19. Experimental results of the 0.4213 mol CO_2 + 0.4053 CH_4 + 0.1735 mol H_2S system at 313K, u(x_{CO2})= 0.0010, u(x_{CH4})= 0.0011, u(x_{H2S})= 0.0008, u(T)= 0.03 K, u(P)= 0.003 MPa for pressures up to 5 MPa and u(P)= 0.005 MPa for pressures from 5 to 30 MPa.

No	T	P	ρ	u(ρ)		Z	u(Z)	No	T	P	ρ	u(ρ)		Z	u(Z)
	[K]	[MPa]	$\left[\frac{kg}{m^3}\right]$	$\left[\frac{kg}{m^3}\right]$	%		10^{-2}		[K]	[MPa]	$\left[\frac{kg}{m^3}\right]$	$\left[\frac{kg}{m^3}\right]$	%		10^{-2}
1	313.77	1.038	13.75	0.25	1.8	0.90	1.7	32	313.87	16.521	351.49	0.32	0.1	0.56	0.1
2	313.75	1.567	21.04	0.27	1.3	0.88	1.1	33	313.87	17.007	361.88	0.31	0.1	0.56	0.1
3	313.75	1.996	26.62	0.29	1.1	0.89	1.0	34	313.87	17.512	372.22	0.30	0.1	0.56	0.1
4	313.74	2.521	34.03	0.32	0.9	0.88	0.8	35	313.83	18.058	382.85	0.30	0.1	0.56	0.1
5	313.74	3.001	40.61	0.35	0.9	0.88	0.7	36	313.83	18.510	391.24	0.29	0.1	0.56	0.1
6	313.75	3.567	49.57	0.37	0.7	0.85	0.6	37	313.84	18.198	385.49	0.29	0.1	0.56	0.1
7	313.75	4.004	56.42	0.41	0.7	0.84	0.6	38	313.80	19.528	408.07	0.28	0.1	0.57	0.1
8	313.74	4.510	64.65	0.45	0.7	0.83	0.6	39	313.79	20.060	417.84	0.28	0.1	0.57	0.1
9	313.74	5.010	73.12	0.51	0.7	0.81	0.6	40	313.79	20.431	422.95	0.29	0.1	0.57	0.1
10	313.74	5.511	81.99	0.56	0.7	0.80	0.6	41	313.78	21.066	432.12	0.27	0.1	0.58	0.1
11	313.74	6.003	91.09	0.68	0.7	0.78	0.5	42	313.79	21.552	439.18	0.27	0.1	0.58	0.1
12	313.73	6.559	101.88	0.74	0.7	0.76	0.5	43	313.78	21.996	445.01	0.26	0.1	0.59	0.1
13	313.74	7.060	112.31	0.80	0.7	0.75	0.5	44	313.77	22.574	452.57	0.27	0.1	0.59	0.1
14	313.73	7.526	122.01	0.86	0.7	0.73	0.5	45	313.77	23.088	458.00	0.27	0.1	0.60	0.1
15	313.80	8.002	132.60	0.90	0.7	0.72	0.5	46	313.80	23.526	462.46	0.27	0.1	0.60	0.1
16	313.74	8.515	144.54	0.82	0.6	0.70	0.4	47	313.78	23.992	467.63	0.27	0.1	0.61	0.1
17	313.97	8.988	155.81	0.74	0.5	0.68	0.4	48	313.77	24.505	472.75	0.27	0.1	0.62	0.1
18	313.95	9.564	170.89	0.70	0.4	0.66	0.3	49	313.77	25.079	478.32	0.26	0.1	0.62	0.1
19	313.93	10.002	181.96	0.65	0.4	0.65	0.3	50	313.76	25.618	483.17	0.26	0.1	0.63	0.1
20	314.11	10.599	197.77	0.62	0.3	0.64	0.2	51	313.77	26.043	487.19	0.26	0.1	0.63	0.1
21	314.05	11.044	210.44	0.58	0.3	0.62	0.1	52	313.76	26.643	492.40	0.26	0.1	0.64	0.1
22	314.03	11.527	223.99	0.55	0.2	0.61	0.1	53	313.76	27.002	495.74	0.25	0.1	0.65	0.1
23	314.02	12.030	237.46	0.53	0.2	0.60	0.1	54	313.76	27.476	499.37	0.25	0.1	0.65	0.1
24	313.99	12.561	252.13	0.50	0.2	0.59	0.1	55	313.76	28.082	504.09	0.25	0.1	0.66	0.1
25	313.93	13.005	264.28	0.47	0.2	0.58	0.1	56	313.75	28.512	507.35	0.25	0.1	0.67	0.1
26	313.91	13.573	279.59	0.45	0.2	0.58	0.1	57	313.75	29.063	511.46	0.25	0.1	0.67	0.1
27	313.87	14.074	292.75	0.43	0.1	0.57	0.1	58	313.76	29.394	514.50	0.24	0.1	0.68	0.1
28	313.90	14.556	305.11	0.40	0.1	0.57	0.1	59	313.76	29.995	517.84	0.24	0.1	0.69	0.1
29	313.92	15.003	316.23	0.38	0.1	0.56	0.1	60	313.76	30.562	521.48	0.24	0.1	0.70	0.1
30	313.92	15.449	326.44	0.36	0.1	0.56	0.1	61	313.77	31.092	524.78	0.24	0.1	0.70	0.1
31	313.91	15.928	337.30	0.35	0.1	0.56	0.1	62	313.77	31.584	527.84	0.23	0.1	0.71	0.1

Table B.20. Experimental results of the 0.4213 mol CO_2 + 0.4053 CH_4 + 0.1735 mol H_2S system at 333K, u(x_{CO2})= 0.0010, u(x_{CH4})= 0.0011, u(x_{H2S})= 0.0008, u(T)= 0.03 K, u(P)= 0.003 MPa for pressures up to 5 MPa and u(P)= 0.005 MPa for pressures from 5 to 30 MPa.

No	T	P	ρ	u(ρ)		Z	u(Z)	No	T	P	ρ	u(ρ)		Z	u(Z)
	[K]	[MPa]	$\left[\frac{kg}{m^3}\right]$	$\left[\frac{kg}{m^3}\right]$	%		10^{-2}		[K]	[MPa]	$\left[\frac{kg}{m^3}\right]$	$\left[\frac{kg}{m^3}\right]$	%		10^{-2}
1	333.97	1.052	12.88	0.24	1.9	0.91	4.1	32	333.98	16.529	291.14	0.31	0.1	0.63	35.1
2	333.96	1.547	19.04	0.26	1.4	0.91	5.1	33	333.95	17.074	302.04	0.30	0.1	0.63	36.1
3	333.95	2.037	25.28	0.28	1.1	0.90	6.1	34	333.95	17.529	310.90	0.29	0.1	0.63	37.1
4	334.01	2.538	31.82	0.30	1.0	0.89	7.1	35	333.97	18.066	321.07	0.29	0.1	0.63	38.1
5	334.01	3.014	38.18	0.33	0.9	0.88	8.1	36	334.03	18.529	329.55	0.28	0.1	0.63	39.1
6	333.97	3.547	45.49	0.35	0.8	0.87	9.1	37	333.99	19.035	338.52	0.28	0.1	0.63	40.1
7	333.96	4.058	52.69	0.39	0.7	0.86	10.1	38	334.04	19.558	347.43	0.27	0.1	0.63	41.1
8	333.98	4.513	59.27	0.43	0.7	0.85	11.1	39	333.99	20.075	355.90	0.27	0.1	0.63	42.1
9	333.96	5.080	67.70	0.49	0.7	0.84	12.1	40	333.97	20.544	363.29	0.27	0.1	0.63	43.1
10	333.98	5.554	74.96	0.53	0.7	0.83	13.1	41	333.98	21.089	371.52	0.26	0.1	0.63	44.1
11	333.99	6.091	83.43	0.65	0.8	0.81	14.1	42	333.97	21.528	377.87	0.26	0.1	0.64	45.1
12	333.95	6.561	91.06	0.71	0.8	0.80	15.1	43	333.98	22.022	384.75	0.25	0.1	0.64	46.1
13	333.95	7.024	98.78	0.76	0.8	0.79	16.1	44	333.99	22.509	391.25	0.25	0.1	0.64	47.1
14	333.98	7.557	107.93	0.83	0.8	0.78	17.1	45	334.00	23.023	397.83	0.26	0.1	0.65	48.1
15	333.99	8.010	115.91	0.86	0.7	0.77	18.1	46	334.01	23.551	404.30	0.26	0.1	0.65	49.1
16	334.04	8.522	125.20	0.78	0.6	0.76	19.1	47	334.03	24.062	410.28	0.26	0.1	0.65	50.1
17	333.96	9.007	134.23	0.71	0.5	0.75	20.1	48	334.00	24.563	415.90	0.26	0.1	0.66	51.1
18	333.96	9.522	144.06	0.67	0.5	0.74	21.1	49	333.98	25.077	421.44	0.25	0.1	0.66	52.1
19	333.95	10.007	153.57	0.62	0.4	0.73	22.1	50	334.00	25.596	426.80	0.25	0.1	0.67	53.1
20	333.97	10.554	164.53	0.59	0.4	0.72	23.1	51	333.96	26.069	431.50	0.25	0.1	0.67	54.1
21	333.96	11.014	173.95	0.55	0.3	0.71	24.1	52	333.96	26.504	435.67	0.25	0.1	0.68	55.1
22	334.00	11.512	184.30	0.52	0.3	0.70	25.1	53	333.96	27.098	441.15	0.24	0.1	0.68	56.1
23	333.96	12.038	195.42	0.50	0.3	0.69	26.1	54	333.96	27.599	445.58	0.24	0.1	0.69	0.1
24	333.96	12.509	205.49	0.48	0.2	0.68	27.1	55	333.96	28.067	449.58	0.24	0.1	0.70	0.1
25	334.09	13.077	217.74	0.45	0.2	0.67	28.1	56	333.96	28.567	453.70	0.24	0.1	0.70	0.1
26	334.05	13.552	228.01	0.43	0.2	0.66	29.1	57	333.96	29.048	457.54	0.24	0.1	0.71	0.1
27	334.01	14.023	238.22	0.41	0.2	0.66	30.1	58	333.98	29.514	461.14	0.23	0.1	0.71	0.1
28	333.98	14.507	248.68	0.38	0.2	0.65	31.1	59	333.96	30.071	465.30	0.23	0.1	0.72	0.1
29	334.02	15.029	259.87	0.36	0.1	0.64	32.1	60	333.96	30.533	468.64	0.23	0.1	0.73	0.1
30	333.97	15.520	270.28	0.34	0.1	0.64	33.1	61	333.97	31.029	472.12	0.23	0.1	0.73	0.1
31	333.98	16.035	281.02	0.33	0.1	0.64	34.1	62	333.95	31.516	475.42	0.22	0.1	0.74	0.1

Table B.21. Experimental results of the 0.4213 mol CO_2 + 0.4053 CH_4 + 0.1735 mol H_2S system at 353K, u(x_{CO2})= 0.0010, u(x_{CH4})= 0.0011, u(x_{H2S})= 0.0008, u(T)= 0.03 K, u(P)= 0.003 MPa for pressures up to 5 MPa and u(P)= 0.005 MPa for pressures from 5 to 30 MPa.

No	T	P	ρ	u(ρ)		Z	u(Z)	No	T	P	ρ	u(ρ)		Z	u(Z)
	[K]	[MPa]	$\left[\frac{kg}{m^3}\right]$	$\left[\frac{kg}{m^3}\right]$	%		10^{-2}		[K]	[MPa]	$\left[\frac{kg}{m^3}\right]$	$\left[\frac{kg}{m^3}\right]$	%		10^{-2}
1	353.65	2.031	23.88	0.32	1.3	0.90	1.2	30	353.59	16.543	246.73	0.28	0.1	0.71	0.1
2	353.66	2.524	29.49	0.34	1.1	0.90	1.0	31	353.62	17.074	255.96	0.28	0.1	0.70	0.1
3	353.64	3.030	35.41	0.37	1.1	0.90	0.9	32	353.58	17.511	263.48	0.27	0.1	0.70	0.1
4	353.68	3.526	41.36	0.41	1.0	0.90	0.8	33	353.58	18.089	273.25	0.27	0.1	0.70	0.1
5	353.67	4.057	47.90	0.47	1.0	0.89	0.8	34	353.58	18.522	280.47	0.26	0.1	0.70	0.1
6	353.66	4.531	53.88	0.51	0.9	0.89	0.8	35	353.58	19.065	289.34	0.26	0.1	0.69	0.1
7	353.66	5.018	60.18	0.63	1.0	0.88	0.8	36	353.58	19.541	296.95	0.26	0.1	0.69	0.1
8	353.64	5.505	66.63	0.68	1.0	0.87	0.9	37	353.60	20.004	304.18	0.25	0.1	0.69	0.1
9	353.64	6.060	74.16	0.73	1.0	0.86	0.9	38	353.64	20.505	311.84	0.25	0.1	0.69	0.1
10	353.64	6.547	80.94	0.79	1.0	0.85	0.8	39	353.61	21.017	319.45	0.24	0.1	0.69	0.1
11	353.64	6.976	87.03	0.83	0.9	0.84	0.8	40	353.64	21.532	326.87	0.24	0.1	0.69	0.1
12	353.64	7.530	95.09	0.75	0.8	0.83	0.7	41	353.61	22.039	333.98	0.24	0.1	0.69	0.1
13	353.64	8.003	102.13	0.68	0.7	0.83	0.5	42	353.65	22.519	340.52	0.25	0.1	0.70	0.1
14	353.63	8.511	109.82	0.64	0.6	0.82	0.5	43	353.65	23.021	347.15	0.25	0.1	0.70	0.1
15	353.64	9.022	117.74	0.60	0.5	0.81	0.4	44	353.64	23.535	353.72	0.25	0.1	0.70	0.1
16	353.63	9.533	125.82	0.57	0.5	0.80	0.3	45	353.65	24.034	359.90	0.24	0.1	0.70	0.1
17	353.63	10.085	134.71	0.53	0.4	0.79	0.2	46	353.64	24.525	365.79	0.24	0.1	0.71	0.1
18	353.62	10.557	142.45	0.50	0.4	0.78	0.2	47	353.63	25.029	371.64	0.24	0.1	0.71	0.1
19	353.62	11.047	150.60	0.48	0.3	0.77	0.2	48	353.63	25.538	377.37	0.24	0.1	0.71	0.1
20	353.62	11.537	158.88	0.46	0.3	0.76	0.2	49	353.65	26.012	382.54	0.23	0.1	0.72	0.1
21	353.61	12.014	167.02	0.43	0.3	0.76	0.1	50	353.65	26.542	388.13	0.23	0.1	0.72	0.1
22	353.62	12.512	175.63	0.42	0.2	0.75	0.1	51	353.71	27.036	393.18	0.23	0.1	0.72	0.1
23	353.62	13.022	184.52	0.40	0.2	0.74	0.1	52	353.66	27.542	398.19	0.23	0.1	0.73	0.1
24	353.59	13.517	193.23	0.37	0.2	0.74	0.1	53	353.68	28.026	402.85	0.23	0.1	0.73	0.1
25	353.59	14.006	201.88	0.35	0.2	0.73	0.1	54	353.66	28.539	407.64	0.22	0.1	0.74	0.1
26	353.59	14.506	210.75	0.33	0.2	0.72	0.1	55	353.65	29.043	412.20	0.22	0.1	0.74	0.1
27	353.58	15.040	220.23	0.32	0.1	0.72	0.1	56	353.65	29.540	416.57	0.22	0.1	0.75	0.1
28	353.58	15.538	229.05	0.30	0.1	0.71	0.1	57	353.65	30.047	420.90	0.22	0.1	0.75	0.1
29	353.60	16.054	238.15	0.29	0.1	0.71	0.1	58	353.65	30.526	424.88	0.21	0.1	0.76	0.1

APPENDIX C: CUBIC EQUATIONS OF STATE

C.1 SRK EoS

The main expression of the Soave-Redlich-Kwong (SRK) [88] equation of state is

$$P = \frac{RT}{v-b} - \frac{a\alpha(T)}{v(v+b)} \tag{C.1}$$

The α-function proposed by Soave is given by

$$\alpha(T) = \left[1 + m\left(1 - \sqrt{\frac{T}{T_c}}\right)\right]^2 \tag{C.2}$$

with

$$m = 0.480 + 1.574\omega - 0.176\omega^2 \tag{C.3}$$

The a and b parameters are calculated from critical conditions as

$$a = 0.42748\frac{R^2T_c^2}{P_c^2} \tag{C.4}$$

$$b = 0.08664\frac{RT_c}{P_c} \tag{C.5}$$

The critical properties and acentric factor values for the studied compounds are presented in Table C.1.

C.2 PR EoS

Peng and Robinson (PR) [89] proposed the following equation of state

$$P = \frac{RT}{v-b} - \frac{a\alpha(T)}{v^2 + 2vb - b^2} \tag{C.6}$$

The α-function is given by

$$\alpha(T) = \left[1 + m\left(1 - \sqrt{\frac{T}{T_c}}\right)\right]^2 \tag{C.7}$$

with

$$m = 0.37464 + 1.54226\omega - 0.26992\omega^2 \qquad \text{for } \omega < 0.49 \qquad \text{(C.8)}$$

$$m = 0.3796 + 1.485\omega - 0.1644\omega^2 + 0.01667\omega^3 \qquad \text{for } \omega \geq 0.49 \qquad \text{(C.9)}$$

The *a* and *b* parameters are calculated from critical conditions as

$$a = 0.45724 \frac{R^2 T_c^2}{P_c^2} \qquad \text{(C.4)}$$

$$b = 0.07780 \frac{RT_c}{P_c} \qquad \text{(C.5)}$$

Table C.1. Critical properties, acentric factors and volume correction parameters used for the cubic EoS [50]**.**

Compound	T_c/K	P_c/MPa	ω	V^C_i/ $m^3 \cdot m^{-1}$	
				SRK	PR
CO_2	304.20	7.376	0.2276	3.37	-1.82
Methane	190.58	4.604	0.0108	0.68	-5.02
Ethane	305.42	4.880	0.0990	2.69	-5.63
Propane	369.82	4.250	0.1518	5.13	-6.20
i-Butane	408.14	3.649	0.1770	7.45	-6.96
n-Butane	425.18	3.797	0.1931	8.00	-6.32
i-Pentane	460.43	3.381	0.2275	11.14	-6.02
n-Pentane	469.70	3.370	0.2515	12.41	-4.97
n-Hexane	507.60	3.025	0.3013	17.46	-3.02
n-Heptane	540.20	2.740	0.3495	23.37	-0.16
n-Octane	568.70	2.490	0.3996	30.53	3.89
n-Nonane	594.60	2.290	0.4435	38.14	8.47
n-Decane	617.70	2.110	0.4923	47.31	14.64
n-Dodecane	658.00	1.820	0.5764	67.59	28.90
n-C_{14}	692.40	1.621	0.6617	90.82	47.10
n-C_{15}	708.00	1.480	0.6863	105.28	56.95
n-C_{16}	723.00	1.400	0.7174	118.49	67.19
n-C_{18}	747.00	1.270	0.8114	151.61	96.21
n-C_{20}	768.00	1.160	0.9069	189.72	130.80
n-C_{24}	799.80	0.903	1.0853	301.43	231.22
n-C_{32}	853.20	0.618	1.4422	618.84	536.20
N_2	126.05	3.394	0.0403	0.94	-4.12
H_2S	373.20	8.940	0.0810	1.57	-4.02
O_2	154.58	5.043	0.0218	0.61	-3.60
CO	132.92	3.499	0.0663	1.26	-3.86
SO_2	430.75	7.884	0.2451	4.76	-2.07
Argon	150.86	4.898	-0.0040	0.41	-3.90
Benzene	562.20	4.890	0.2120	8.87	-5.72
Toluene	591.80	4.160	0.2621	13.12	-4.54

APPENDIX D: PC-SAFT EQUATION OF STATE

In this Appendix, a summary of the necessary equations for calculating the residual Helmholtz free energy and the compressibility factor with the PC-SAFT equation of state [69] is provided.

- Residual Helmholtz free energy:

$$a^{res} = \frac{A^{res}}{NkT} \tag{D.1}$$

$$a^{res} = a^{hc} + a^{disp} + a^{assoc} \tag{D.2}$$

- Hard-Chain reference Contribution:

$$a^{hc} = \overline{m}\, a^{hs} - \sum_i x_i (m_i - 1) \ln g_{ii}^{hs}\left(\sigma_{ii}\right) \tag{D.3}$$

where,

$$\overline{m} = \sum_i x_i m_i \tag{D.4}$$

$$a^{hs} = \frac{1}{\zeta_0}\left[\frac{3\zeta_1\zeta_2}{\left(1-\zeta_3\right)} + \frac{{\zeta_2}^3}{\zeta_3\left(1-\zeta_3\right)^2} + \left(\frac{{\zeta_2}^3}{{\zeta_3}^2} - \zeta_0\right)\ln\left(1-\zeta_3\right)\right] \tag{D.5}$$

$$g_{ij}^{hs} = \frac{1}{\left(1-\zeta_3\right)} + \left(\frac{d_i d_j}{d_i + d_j}\right)\frac{3\zeta_2}{\left(1-\zeta_3\right)^2} + \left(\frac{d_i d_j}{d_i + d_j}\right)^2 \frac{2{\zeta_2}^2}{\zeta_0\left(1-\zeta_3\right)^3} \tag{D.6}$$

where ζ_n is defined as

$$\zeta_n = \frac{\pi}{6}\rho\sum_i x_i m_i {d_i}^n \qquad n \in \{0,1,2,3\} \tag{D.7}$$

- Temperature-dependent segment diameter:

$$d_i(T) = \int_0^{\sigma}\left[1 - \exp\left(-\frac{u(r)}{kT}\right)\right]dr = \sigma_i\left[1 - 0.12\exp\left(-\frac{3\varepsilon_i}{kT}\right)\right] \tag{D.8}$$

- Dispersion contribution:

$$a^{disp} = -2\pi\rho I_1(\eta,\bar{m})\overline{m^2\varepsilon\sigma^3} - \pi\rho\bar{m}C_1 I_2(\eta,\bar{m})\overline{m^2\varepsilon^2\sigma^3} \tag{D.9}$$

where,

$$C_1 = \left(1+\bar{m}\frac{8\eta-2\eta^2}{(1-\eta)^4}+(1-\bar{m})\frac{20\eta-27\eta^2+12\eta^3-2\eta^4}{\left[(1-\eta)(2-\eta)\right]^2}\right)^{-1} \tag{D.10}$$

$$\overline{m^2\varepsilon\sigma^3} = \sum_i\sum_j x_i x_j m_i m_j \left(\frac{\varepsilon_{ij}}{kT}\right)\sigma_{ij}^{\ 3} \tag{D.11}$$

$$\overline{m^2\varepsilon^2\sigma^3} = \sum_i\sum_j x_i x_j m_i m_j \left(\frac{\varepsilon_{ij}}{kT}\right)^2\sigma_{ij}^{\ 3} \tag{D.12}$$

$$I_1(\eta,\bar{m}) = \sum_{i=0}^{6} a_i(\bar{m})\eta^i \tag{D.13}$$

$$I_2(\eta,\bar{m}) = \sum_{i=0}^{6} b_i(\bar{m})\eta^i \tag{D.14}$$

where the coefficients a_i and b_i depend on the chain length according to:

$$a_i(\bar{m}) = a_{0i} + \frac{\bar{m}-1}{\bar{m}}a_{1i} + \frac{\bar{m}-1}{\bar{m}}\frac{\bar{m}-2}{\bar{m}}a_{2i} \tag{D.15}$$

$$b_i(\bar{m}) = b_{0i} + \frac{\bar{m}-1}{\bar{m}}b_{1i} + \frac{\bar{m}-1}{\bar{m}}\frac{\bar{m}-2}{\bar{m}}b_{2i} \tag{D.16}$$

and the parameters a_{ij} and b_{ij} are reported in Table D.1.

- Association contribution:

$$a^{ASSOC} = \sum_{i=1}^{n} x_i \sum_{a=1}^{s_i} n_{ai}\left[\ln X_i^{\ A} - \frac{X_i^{\ A}}{2} + \frac{1}{2}\right] \tag{D.17}$$

$$X_i^{\ A} = \frac{1}{1+\rho\sum_{j=1}^{n} x_j \sum_{b=1}^{s_j} n_{b,j} X_j^{\ B}\Delta^{A_i B_j}} \tag{D.18}$$

$$\Delta^{A_iB_j} = d_{ij}^3 g_{ij}(d_{ij}) K^{A_iB_j} \left[\exp\left(\varepsilon^{A_iB_j} / kT \right) - 1 \right] \tag{D.19}$$

- Compressibility factor:

$$Z = 1 + \eta \left(\frac{\partial \tilde{a}^{res}}{\partial \eta} \right)_{T, x_i} \tag{D.20}$$

$$Z = Z^{id} + Z^{hc} + Z^{disp} + Z^{assoc} \tag{D.21}$$

- Hard-chain contribution to the compressibility factor:

$$Z^{hc} = \bar{m} Z^{hs} - \sum_i x_i (m_i - 1) \left(g_{ii}^{hs} \right)^{-1} \rho \frac{\partial g_{ii}^{hs}}{\partial \rho} \tag{D.22}$$

where,

$$Z^{hs} = \frac{\zeta_3}{(1-\zeta_3)} + \frac{3\zeta_1\zeta_2}{\zeta_0 (1-\zeta_3)^2} + \frac{3\zeta_2^{\,3} - \zeta_3\zeta_2^{\,3}}{\zeta_0 (1-\zeta_3)^3} \tag{D.23}$$

$$\rho \frac{\partial g_{ii}^{hs}}{\partial \rho} = \frac{\zeta_3}{(1-\zeta_3)^2} + \left(\frac{d_i d_j}{d_i + d_j} \right) \left(\frac{3\zeta_2}{(1-\zeta_3)^2} + \frac{6\zeta_2\zeta_3}{(1-\zeta_3)^3} \right) + \left(\frac{d_i d_j}{d_i + d_j} \right)^2 \left(\frac{4\zeta_2^{\,2}}{(1-\zeta_3)^3} + \frac{6\zeta_2^{\,2}\zeta_3}{(1-\zeta_3)^4} \right) \tag{D.24}$$

- Dispersion contribution to the compressibility factor:

$$Z^{disp} = -2\pi\rho \frac{\partial(\eta I_1)}{\partial \eta} \overline{m^2 \varepsilon \sigma^3} - \pi\rho\bar{m} \left[C_1 \frac{\partial(\eta I_2)}{\partial \eta} + C_2 \eta I_2 \right] \overline{m^2 \varepsilon^2 \sigma^3} \tag{D.25}$$

where,

$$C_2 = \frac{\partial C_1}{\partial \eta} = -C_1^{\,2} \left(\bar{m} \frac{8 + 20\eta - 4\eta^2}{(1-\eta)^5} + (1-\bar{m}) \frac{40 - 48\eta + 12\eta^2 + 2\eta^3}{\left[(1-\eta)(2-\eta) \right]^3} \right) \tag{D.26}$$

$$\frac{\partial(\eta I_1)}{\partial \eta} = \sum_{j=0}^{6} a_j(\bar{m})(j+1)\eta^j \tag{D.27}$$

$$\frac{\partial(\eta I_2)}{\partial \eta} = \sum_{j=0}^{6} b_j(\bar{m})(j+1)\eta^j \tag{D.28}$$

Table D.1. Universal Model Constants for equations Eq.D.15 and D.16.

i	a_{0i}	a_{1i}	a_{2i}	b_{0i}	b_{1i}	b_{2i}
0	0.910563	-0.3084	-0.09061	0.724095	-0.57555	0.097688
1	0.636128	0.186053	0.452784	2.238279	0.69951	-0.25576
2	2.686135	-2.503	0.59627	-4.00258	3.892567	-9.15586
3	-26.5474	21.41979	-1.72418	-21.0036	-17.2155	20.64208
4	97.75921	-65.2559	-4.13021	26.85564	192.6723	-38.8044
5	-159.592	83.31868	13.77663	206.5513	-161.826	93.62677
6	91.29777	-33.7469	-8.67285	-355.602	-165.208	-29.6669

Table D.2. PC-SAFT pure-component parameters from the literature used in this work.

	PC-SAFT [69,70]		
Compound	m	σ [Å]	ε/k_B [K]
CO_2	2.073	2.785	169.21
Methane	1.000	3.704	150.03
Ethane	1.607	3.521	191.42
Propane	2.002	3.618	208.11
i-Butane	2.262	3.757	216.53
n-Butane	2.332	3.709	222.88
i-Pentane	2.562	3.830	230.75
n-Pentane	2.690	3.773	231.20
n-Hexane	3.058	3.798	236.77
n-Heptane	3.483	3.805	238.40
n-Octane	3.818	3.837	242.78
n-Nonane	4.208	3.845	244.51
n-Decane	4.663	3.838	243.87
n-Dodecane	5.306	3.896	249.21
n-Tetradecane	5.900	3.939	254.21
n-Pentadecane	6.285	3.953	254.14
n-Hexadecane	6.649	3.955	254.70
n-Octadecane	7.327	3.966	256.20
n-Eicosane	7.985	3.987	257.75
n-C_{24}	9.357	4.035	265.04
n-C_{32}	12.066	4.121	276.17
N_2	1.205	3.313	90.96
H_2S	1.716	3.009	224.96
O_2	1.146	3.171	113.98
CO	1.310	3.251	92.15
SO_2	2.861	2.683	205.35
Argon	0.929	3.478	122.23
Benzene	2.465	3.648	287.35
Toluene	2.815	3.717	285.69

APPENDIX E: MBWR EQUATION OF STATE

Younglove and Ely [197] have correlated the carbon dioxide density with high accuracy in a wide range of temperatures and pressures using the modified Benedict-Webb-Rubin equation of state (mBWR). The mBWR EoS is expressed as

$$\begin{aligned}
P = \rho RT &+ \rho^2\left[G(1)T + G(2)T^{1/2} + G(3) + G(4)T^{-1} + G(5)T^{-2}\right] + \\
&+ \rho^3\left[G(6)T + G(7) + G(8)T^{-1} + G(9)T^{-2}\right] + \\
&+ \rho^4\left[G(10)T + G(11) + G(12)T^{-1}\right] + \rho^5\left[G(13)T^{-1}\right] + \\
&+ \rho^6\left[G(14)T^{-1} + G(15)T^{-2}\right] + \rho^7\left[G(16)T^{-1}\right] + \\
&+ \rho^8\left[G(17)T^{-1} + G(18)T^{-2}\right] + \rho^9\left[G(19)T^{-2}\right] + \\
&+ \rho^3\left[G(20)T^{-2} + G(21)T^{-3}\right]\exp\left(\gamma\rho^2\right) + \\
&+ \rho^5\left[G(22)T^{-2} + G(23)T^{-4}\right]\exp\left(\gamma\rho^2\right) + \\
&+ \rho^7\left[G(24)T^{-2} + G(25)T^{-3}\right]\exp\left(\gamma\rho^2\right) + \\
&+ \rho^9\left[G(26)T^{-2} + G(27)T^{-4}\right]\exp\left(\gamma\rho^2\right) + \\
&+ \rho^{11}\left[G(28)T^{-2} + G(29)T^{-3}\right]\exp\left(\gamma\rho^2\right) + \\
&+ \rho^{13}\left[G(30)T^{-2} + G(31)T^{-3} + G(32)T^{-4}\right]\exp\left(\gamma\rho^2\right)
\end{aligned} \tag{E.1}$$

where γ is a nonlinear parameter defined as $\gamma=1/\rho_c^2$ and the *G(i)* are the parameters reported in Table E.1.

Table E.1. CO_2 coefficients for the mBWR EoS [197]**.**

G	Values
G(1)	$-9.81851066\cdot10^{-4}$
G(2)	$9.95062267\cdot10^{-2}$
G(3)	-2.2838016
G(4)	$2.81827635\cdot10^{2}$
G(5)	$-3.47001263\cdot10^{4}$
G(6)	$3.94706709\cdot10^{3}$
G(7)	$-3.25550001\cdot10^{-2}$
G(8)	4.84320083
G(9)	$-3.52181543\cdot10^{4}$
G(10)	$-3.24053603\cdot10^{-6}$
G(11)	$4.68596685\cdot10^{-1}$
G(12)	$-7.54547012\cdot10^{-1}$
G(13)	$-3.81894354\cdot10^{-6}$
G(14)	$-4.42192934\cdot10^{-3}$
G(15)	5.16925168
G(16)	$2.12450985\cdot10^{-4}$
G(17)	$-2.61009475\cdot10^{-6}$
G(18)	$-8.88533389\cdot10^{-3}$
G(19)	$1.55226179\cdot10^{-4}$
G(20)	$4.15091005\cdot10^{4}$
G(21)	$-1.10173967\cdot10^{6}$
G(22)	$2.91990583\cdot10^{2}$
G(23)	$1.43254607\cdot10^{6}$
G(24)	1.08574208
G(25)	$-2.47799657\cdot10^{1}$
G(26)	$1.99293591\cdot10^{-3}$
G(27)	$1.02749908\cdot10^{1}$
G(28)	$3.77618865\cdot10^{-6}$
G(29)	$-3.32276512\cdot10^{-4}$
G(30)	$1.79196707\cdot10^{-9}$
G(31)	$9.45076628\cdot10^{-7}$
G(32)	$-1.23400943\cdot10^{-4}$

APPENDIX F: EXECUTIVE SUMMARY

Executive Summary

" Experimental and modelling studies of the phase behaviour and transport properties of mixtures related to carbon capture and storage "

Alfonso Gonzalez Perez, PhD student

Supervised by Antonin Chapoy (IPE, Heriot-Watt University),
Christophe Coquelet (CTP, Mines-ParisTech)
and Patrice Paricaud (UCP, ENSTA-ParisTech).

SCOPE

It is now widely accepted that anthropogenic CO_2 emissions produced from the burning of fossil fuels are responsible for the apparent rapid rise in global temperatures recorded over the past century. Worldwide concerns over the threat of global warming have provoked the majority of industrialised countries into working to reduce carbon emissions. To meet these goals, nations must increase investment in 'clean' renewable sources of energy and develop solutions for reducing CO_2 emissions. CO_2 storage in depleted reservoirs and its application in Enhanced Oil/Gas Recovery (EOR) are among techniques being suggested for reducing the emission of this greenhouse gas. The industry has a long experience with injection of CO_2 for EOR processes. However, the main source of CO_2 is now industrial plants (i.e. power plants, chemical processes etc.) and these CO_2 sources contain different impurities (e.g. N_2, CO, H_2 etc.). Challenging fluid behaviour can occur, close to the critical point of CO_2, such as multiphase behaviour. This may alter the conditions of CO_2 transport or EOR operations in the exploitation of hydrocarbons. The objective here is to develop a model for investigating the effect of CO_2 (and impurities) on the phase behaviour and physical properties (density, viscosity, IFT, etc.) of CO_2-oil systems.

EQUATIONS OF STATE

The main aim of this research is to develop an accurate equation of state (EoS) for mixtures of CO_2, hydrocarbons and other gases as N_2, O_2, Ar, etc. An EoS is a thermodynamic model which describes the state of pure fluids and mixtures under a given set of physical conditions (pressure, temperature, and composition). Many equations of state have been proposed since 1834 when Clapeyron [1] proposed the Ideal Gas (IG) law. The next milestone in the history of EoS was the van der Waals (vdW) equation of state (1873) that is the base of cubic equations of state (CEoS). Although the vdW equation of state was the first EoS that considered a pairwise attractive inter-molecular force, there was no significant improvement of CEoS until 1949 when Redlich and Kwong revised the van der Waals EoS.

In the 1970's, Soave proposed a modification known as Soave-Redlich-Kwong (SRK) EoS [2]. Peng and Robinson (PR) later developed an EoS [3]. The simplicity and reasonable accuracy, giving good results for mixture of nonpolar fluids; this is why SRK and PR had rapidly gained acceptance by the hydrocarbon industry. Then, the cubic family of EoS are based on a cubic dependence on the volume with two or more adjustable parameters which are fitted to experimental data:

$$SRK: \quad P = \frac{RT}{v-b} - \frac{\alpha(T)}{v(v-b)} \qquad (1)$$

$$PR: \quad P = \frac{RT}{v-b} - \frac{\alpha(T)}{v^2 + 2bv - b^2} \qquad (2)$$

where P is the pressure, v the molar volume and T the temperature. $\alpha(T)$ is a function of temperature, acentric factor and critical temperature (T_c) and pressure (P_c), and b (co-volume parameter) is a parameter independent of temperature calculated using T_c and P_c.

Cubic EoS have been widely employed in the thermodynamic community [4] and, many modifications have been proposed. For the purpose of improving cubic EoS, different functional terms or additional parameters were proposed, such as the use of Peneloux volume translation [5] which provides better predictions of liquid densities [6].

However, the accuracy of these equations decreases when predicting the behaviour of molecules that creates hydrogen bonding, such as water and alcohols. This can be explained by the fact that cubic EoS

were developed by assuming only the presence of dispersion interactions between molecules [7]. In order to improve the CEoS for associative fluids it was necessary to add some contributions in the perturbation expansion of the free energy according to the thermodynamic perturbation theory (TPT) of Wertheim. Besides, the Cubic Plus Association EoS (CPA) [8] was developed by combining the simplicity of a cubic equation of state (SRK) and the TPT theory employed for the association part, By applying Wertheim's TPT and extending it to mixtures, Chapman et al. [9] derived the Statistical Associating Fluid Theory (SAFT) equation of state. Many modifications of the SAFT EoS were suggested over the years, such as CK-SAFT [10], LJ-SAFT [11], SAFT-VR [12], soft-SAFT [13] and PC-SAFT [14]. When perturbation theory is applied the Helmholtz free energy can be expressed as a sum of different contributions. The versions of the SAFT EoS differ from the type of intermolecular potential used for the dispersion forces (square-well, Leonard-Jones, Mie, etc).

Leaving aside the SAFT EoS, another EoS based on perturbation theories have been developed in the last 25 years, as a result of advances in thermodynamic statistical mechanics and computer power, Among these equations are the perturbed hard chain theory (PHCT) [15], [16] and its derivatives : the perturbed soft chain theory (PSCT) [17], [18], the perturbed anisotropic chain theory (PACT) [19], [20] or the and associated perturbed anisotropic chain theory (APACT) [21], [22].

EXPERIMENTAL MEASUREMENTS

In parallel to the modelling study, some experimental work was done in order to extend the available literature data. Isothermal vapour-liquid equilibrium of the H_2S-Ar binary system was determined experimentally at three temperatures from 258 to 288 K, using a two pneumatic capillary samplers system developed in our laboratory [23]. Densities of five H_2S binary systems (three CH_4-H_2S systems with 13, 18 and 28% of acid gas, ethane-30%H_2S and propane-10%H_2S) were measured continuously at 3 temperatures (253, 273 and 293K) and at pressures up to 30MPa, using a HTHP Vibrating Tube densitometer, Anton Paar DMA 512. Following the same technique, the density of the ternary system 42%CO_2, 40%CH_4 and 18%H_2S was measured at pressures ranging from 0.2 to 31.5MPa and at 6 temperatures (253, 273, 293, 313, 333 and 353K).

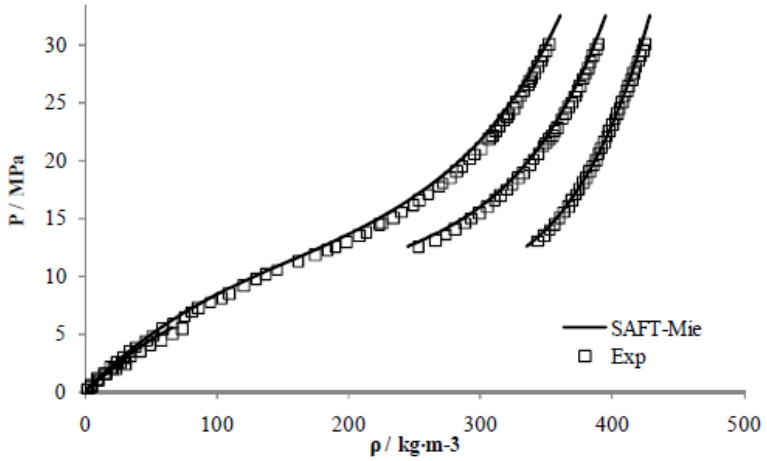

Fig. 1: Density of binary system CH_4 - 28.6%H_2S at 253, 273 and 293K. Continuous line is the predicted density by SAFT-VR Mie and symbols are experimental data (this work).

The densities and viscosities of a multicomponent mixture of 50% CO_2, 40% CH_4 and 10% of other impurities were measured at 5 temperatures (283, 298, 323, 373 and 423K) and at 2.5-150MPa pressure

range, using an Anton Paar densitometer and the capillary tube technique for viscosity measurements at the Heriot Watt University, Scotland. These experimental data continued studying the impact of impurities on the viscosity and density of CO_2-rich systems.

THERMODYNAMIC MODEL

The SAFT-VR Mie EoS proposed by Lafitte et al. [24] is one of the latest versions of the SAFT equations of state. The SAFT-VR Mie is characterized by the use of the Mie potential to describe the attractive and repulsive interactions between the segments which build the molecules. The Mie potential is defined as:

$$u^{Mie}(r) = \frac{\lambda_r}{\lambda_r - \lambda_a}\left(\frac{\lambda_r}{\lambda_a}\right)^{\frac{\lambda_r}{\lambda_r-\lambda_a}} \varepsilon\left(\left(\frac{\sigma}{r}\right)^{\lambda_r} - \left(\frac{\sigma}{r}\right)^{\lambda_a}\right) \tag{3}$$

where r is radial distance, σ the temperature-independent segment diameter, ε the potential depth; λ_r and λ_a are the repulsive and attractive ranges, respectively.

The SAFT-VR Mie EoS can be expressed in terms of the reduced Helmholtz energy as the summation of several contributions:

$$a = \frac{A}{NkT} = a^{IDEAL} + a^{MONO} + a^{CHAIN} + a^{ASSOC} \tag{4}$$

where a^{IDEAL} is the ideal gas contribution, a^{MONO} the monomer contribution, a^{CHAIN} the contribution due to chain formation and a^{ASSOC} the association contribution.

Several EoS have been compared in this work. The equations of state selected for the comparative study are the two original classical CEoS, PR and SRK, the well known PC-SAFT and SAFT-VR Mie. Besides these models, a group contribution approach of SAFT-VR Mie (SAFT-γ Mie) is used and all models are compared on their ability to predict the densities of mixtures. This comparative analysis has included an enormous amount of experimental data collected from the literature, as well as our own measurements. The PVT data collected were the densities of gases and liquids, supercritical single phases, and the densities of binary mixtures along the vapour-liquid equilibria (VLE). The studied systems consist of 22 pure components and around 120 binary systems which are the combination of 5 small molecules (CO_2, H_2S, N_2, CH_4 and C_2H_6) with n-alkanes, aromatics (benzene and toluene) and some gases (O_2, Ar, CO and SO_2).

The comparative study is divided into two parts. On the one hand, the phase equilibrium of the systems presented previously was studied in two ways. Firstly, bubble point pressure and vapour phase composition are predicted with zero binary interaction parameters (k_{ij}=0) and the absolute average deviations are calculated by comparing the data from the literature and the predictions of the models. The different deviations of PR, SRK, PC-SAFT and SAFT-VR Mie can be compared in this ways. Since the optimal k_{ij} values are not zero, binary parameters had to be regressed on VLE data. In order to do a fair comparison between EoS, the regression was done treating the k_{ij}'s as temperature independent. Subsequently, the deviations of each model were determinate from the bubble point calculations with the regressed k_{ij}'s. An example of the result of this comparison is presented in the Table 1.

Table 1. Deviations in bubble point pressures and vapour phase compositions calculated by SRK, PR, PC-SAFT and SAFT-VR Mie with zero and regressed k_{ij}'s. The binary systems presented are CO_2+Comp2.

		SRK			PR			PC-SAFT			SAFT-VR Mie		
Comp2	T_{range}	k_{ij}	%ΔP	%Δy_1	k_{ij}	%ΔP	%Δy_1	k_{ij}	%ΔP	%Δy_1	k_{ij}	%ΔP	%Δy_1
O_2	218K 298K	0	21.70	11.06	0	22.81	12.10	0	20.80	11.09	0	19.21	10.02
		0.1072	5.46	4.01	0.1188	6.29	3.68	0.0475	7.63	6.47	-0.0291	5.01	3.68
Ar	233K 299K	0	22.95	7.82	0	17.52	7.87	0	15.80	8.06	0	14.17	8.12
		0.1230	4.74	4.29	0.1211	6.85	2.92	0.0213	5.51	3.96	-0.0163	6.25	2.66
SO_2	313K 403K	0	11.90	-	0	12.86	-	0	21.00	-	0	6.19	-
		0.0676	5.38	-	0.0671	5.54	-	0.0424	7.85	-	0.0038	5.83	-
CO	223K 283K	0	12.21	3.88	0	10.27	2.83	0	9.65	5.59	0	8.03	4.95
		-0.0710	5.42	5.02	-0.0573	5.69	4.37	-0.0103	6.89	4.85	-0.0078	6.18	5.49

On the other hand, the predictions of densities of gas, liquid and supercritical phases were compared against the compiled density data from the literature. In order to improve density calculations, especially for liquid phases, a volume transition has been used with both CEoS. Firstly, maximum and absolute average deviation in the calculated saturated liquid density of pure component was compared for the different equations of state. Afterwards, pure component densities of single phases were calculated at temperatures ranging from 253 to 553K and at pressures up to 200MPa (Table 2). Secondly, the comparative study continued with density calculations of binary systems and the comparison with the literature data collected.

Table 2. Density deviations of some pure components calculated by SRK, PR, PC-SAFT and SAFT-VR Mie.

EoS	V_{correc}		N_2	O_2	Ar	CO_2	CO	SO_2	CH_4	C_2H_6	Total
SRK	No	%AAD	1.96	1.19	1.35	0.36	2.05	8.01	1.23	2.61	2.35
		max Dev %	3.45	3.83	3.34	2.17	3.93	21.27	6.08	15.90	-
	Yes	%AAD	1.00	1.16	0.91	0.36	1.01	3.76	1.16	1.96	1.42
		max Dev %	3.40	3.91	4.05	2.17	4.82	37.05	6.17	42.49	-
PR	No	%AAD	7.46	5.67	6.69	0.24	7.27	3.63	7.09	7.82	5.73
		max Dev %	12.91	12.15	12.78	1.78	13.21	13.53	11.90	11.60	-
	Yes	%AAD	1.03	0.86	0.72	0.24	0.99	2.62	0.62	2.54	1.20
		max Dev %	1.95	2.36	1.48	1.78	1.90	20.65	3.79	21.72	-
PCSAFT		%AAD	2.64	1.55	1.05	0.73	1.90	1.99	1.45	2.15	1.68
		max Dev %	4.95	3.24	2.01	16.04	4.30	20.81	2.48	4.05	-
SAFT-Mie		%AAD	0.41	0.30	1.84	2.44	0.84	1.71	0.95	0.41	1.11
		max Dev %	1.16	1.19	3.39	5.11	1.77	8.60	1.94	6.26	-

The SAFT-VR Mie EoS provides very good density predictions for pure component and binary systems according to the comparative study carried out. Since most models for transport properties are functions of temperatures and density, these models can be combined with the SAFT-Mie EoS for an accurate

prediction of the transport properties of mixtures. In this work, three transport properties were modelled with SAFT-VR Mie and two models based on density predictions from the EoS. Thus, density, viscosity and interfacial tension (IFT) of CO_2-rich systems were calculated by using SAFT-Mie, TraPP model (viscosity) and DGT (IFT), respectively, for mixtures related to carbon capture storage.

Density

The CO_2 captured from power plants and other industrial sources contain impurities which have effects on the thermophysical properties. Different kinds and concentrations of impurities depend on the type of capture process, but generally the impurities are N_2, O_2, Ar, CO, H_2, CO, CH_4, SO_2, NO_x, H_2S and the lighter alkanes.

The densities of 6 multicomponent CO_2-rich systems were calculated with the SAFT-VR Mie EoS. The studied systems were CO_2 mixtures with 5%, 10% and 30% of impurities, using experimental data from the literature over wide ranges of temperatures and pressures.

Viscosity

TRAPP (TRAnsport Properties Prediction) is a predictive model based on the extended corresponding states theory (ECS) [25], [26], and used to estimate the viscosity and thermal conductivity of pure fluids and their mixtures over the entire fluid phase region. In the original TRAPP, methane was employed as the reference fluid [27], although several reference fluids can be selected [28]. Accordingly, the residual viscosity of the mixture at a corresponding state point (T_0 and ρ_0) is given by:

$$\Delta\eta(\rho,T) = \eta_m - \eta_m^0 = F_{\eta m}[\eta_R - \eta_R^0] + \Delta\eta^{ENSKOG} \quad (5)$$

where $\eta_m{}^0$ is the viscosity of the mixture at low pressure evaluated by Herning and Zipperer [29] approximation. The term $\Delta\eta^{ENSKOG}$ accounts for size differences based on a hard sphere assumption. The term η_R-$\eta_R{}^0$ is the residual viscosity of the reference fluid which is calculated as [30]:

$$\eta_R - \eta_R^0 = G_1 \exp[\rho_0^{0.1} G_2 + \rho_0^{0.5}(\rho_{r,R} - 1)G_3] - G_1 \quad (6)$$

where η_R is the real viscosity at T_0 and ρ_0 of the reference fluid, $\eta_R{}^0$ is the viscosity at low pressure and T_0, and $\rho_{r,R}$ is the reduced density calculated as $\rho_{r,R} = \rho_0/\rho_{c,R}$. The corresponding state (T_0 and ρ_0) is calculated as $T_0 = T/f_m$ and $\rho_0 = \rho h_m$. G_1, G_2 and G_3 are parameters that can be calculated by equations with correlated parameters for a reference fluid (propane).

The viscosities of CO_2-rich systems have been investigated. A literature review of viscosity data was carried out, with a particularly attention to systems of interest for CCS. The viscosity of binary systems of CO_2 with any of the impurities presented in the CCS chain was calculated by coupling the SAFT-VR Mie and TraPP models. Thereby, the viscosity of 4 multicomponent CO_2-rich mixtures with 5, 10, 30 and 50% of impurities has been modelled as well with TraPP.

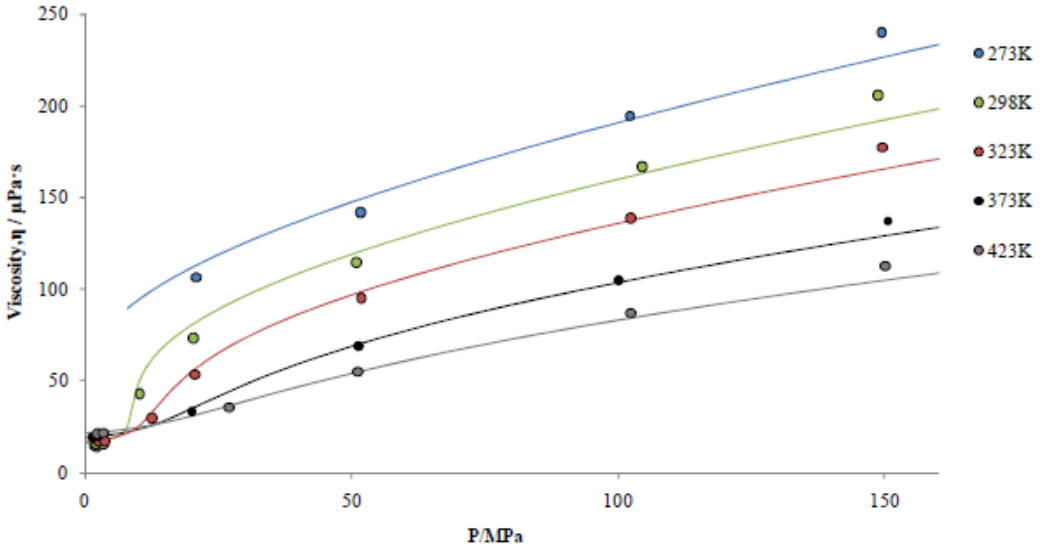

Fig. 2: Experimental [31] and predicted viscosity of a CO_2-rich system (90%CO_2, 5%O_2, 2%Ar and 3%N_2).

Interfacial Tension

The density gradient theory (DGT) has been used to compute the interfacial tension. This model is based on the square gradient of van der Waals [32] and on the reformulation of Cahn and Hilliard [33] to compute interfacial tension values from bulk phase properties such as density and composition. The DGT, when coupled with appropriate thermodynamic models, has been successfully applied in the prediction of interfacial properties of a wide class of systems and interfaces. In this work, the SAFT-VR Mie EoS was used to estimate the bulk equilibrium of the investigated systems and DGT used to predict interfacial properties. The main equations within the DGT framework are given below.

In summary, by applying the minimization criterion of the Helmholtz energy to planar interfaces, the interfacial tension values with respects to the density of a reference component is given by Miqueu et al. [34], [35] as

$$IFT = \int_{\rho_{ref}^{V}}^{\rho_{ref}^{L}} \sqrt{2\Delta\Omega(\rho)\sum_i\sum_j c_{ij}\frac{d\rho_i}{d\rho_{ref}}\frac{d\rho_j}{d\rho_{ref}}}\,d\rho_{ref} \tag{7}$$

where ρ^{L}_{ref} and ρ^{V}_{ref} are the bulk phase densities and the *ref* subscript denotes the reference component of the mixture. $\Delta\Omega$ is the variation of the grand thermodynamic potential which is related to the Helmholtz free energy by the following equation:

$$\Delta\Omega = f_0(\rho) - \sum_i \rho_i\mu_i + p \tag{8}$$

where f_0 is the Helmholtz free energy density of the homogeneous fluid at local density, μ_i are the chemical potential of each component and p is the pressure at equilibrium. The methodology described by Miqueu et al. was here followed for determining the density distribution of each component across the interface.

The saturated densities and IFT of CO_2 systems were modelled by coupling the DGT with the SAFT-VR Mie EoS (Figure 3). In addition, other systems, such as N_2 and CH_4 with n-alkanes, have been studied with this model.

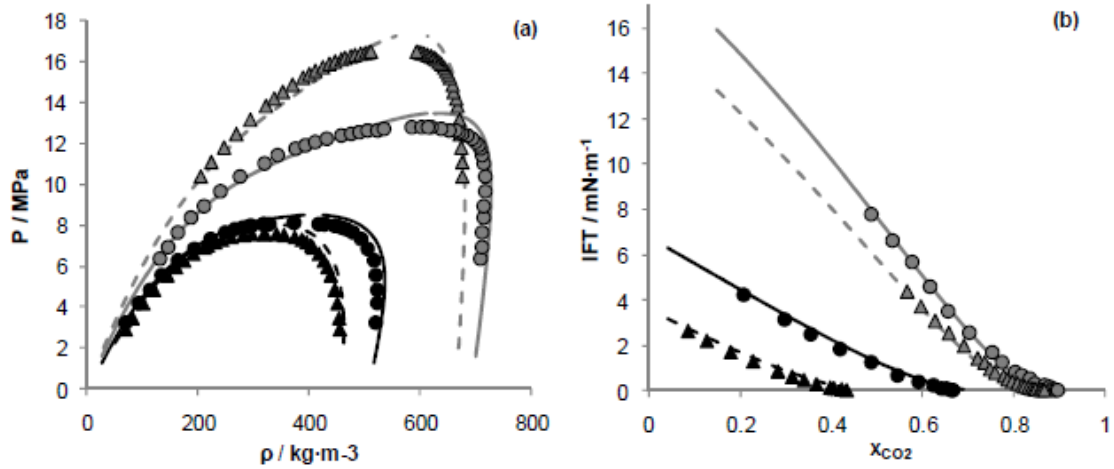

Fig. 3: Predicted densities (a) and IFT (b) of CO_2-nC_4 (black) [36] and CO_2-nC_{10} (grey) [37] mixtures. Symbols: (●) T=344.3 and (▲) T=377.6K.

CONCLUSIONS

The main objective of the research was to assess the capabilities of the SAFT-VR Mie EoS for describing the thermophysical properties of mixtures in the contest of CCS. This work focuses on non-associative compounds, and aims at analysing if SAFT-Mie can lead to a big improvement in the prediction of VLE and densities of these components in comparison with classical approaches (cubic EoS and PC-SAFT). Therefore, we compare the most sophisticated EoS with classical CEoS which have reported very good results. As result of the comparative study of EoS, the SAFT-VR Mie EoS reported slight lower deviations than SRK, PR or PC-SAFT in the description of VLE. Thereby, SAFT-VR Mie showed better results than the others EoS for the density calculation.

As was expected, SAFT-VR Mie is an accurate equation of state in density description. Therefore, it has been used to describe the density of CO_2-rich systems with different amounts of impurities relevant to the transport of CO_2 in CCS chain. Furthermore, by using the computed bulk phase properties, the TRAPP and DGT models were able to predict the viscosity and IFT of CO_2-rich mixture with relative low deviations to experimental data, endorsing the capability of the methods for estimating key transport properties of fluids in CCS streams. Nevertheless, it is noteworthy that TraPP model provides worse viscosity predictions as the amount of impurities increases.

REFERENCES

[1] É. Clapeyron, "Puissance motrice de la chaleur," *J. l' ' Ec. Polytech.*, vol. 14, no. 153, 1834.

[2] G. Soave, "Equilibrium constants from a modified Redlkh-Kwong equation of state," *J. Chem. Eng. Sci.*, vol. 27, no. 6, pp. 1197–1203, 1972.

[3] D.-Y. Peng and D. B. Robinson, "A New Two-Constant Equation of State," *Ind. Eng. Chem. Fundam.*, vol. 15, no. 1, pp. 59–64, Feb. 1976.

[4] A. Maghari and L. Hosseinzadeh-Shahri, "Evaluation of the performance of cubic equations of state in predicting the regularities in dense fluids," *Fluid Phase Equilib.*, vol. 206, no. 1–2, pp. 287–311, Apr. 2003.

[5] A. Péneloux, E. Rauzy, and R. Fréze, "A consistent correction for Redlich-Kwong-Soave volumes," *Fluid Phase Equilib.*, vol. 8, no. 1, 1982.

[6] K. Pedersen, P. Christensen, and J. Shaikh, *Phase behavior of petroleum reservoir fluids*, CRC Press. Boca Raton, FL, 2007.

[7] C. Tsonopoulos and J. L. Heidman, "From Redlich-Kwong to the present," *Fluid Phase Equilib.*, vol. 24, no. 1–2, pp. 1–23, Jan. 1985.

[8] G. M. Kontogeorgis, E. C. Voutsas, I. V. Yakoumis, and D. P. Tassios, "An Equation of State for Associating Fluids," *Ind. Eng. Chem. Res.*, vol. 35, no. 11, pp. 4310–4318, Jan. 1996.

[9] W. G. Chapman, K. E. Gubbins, G. Jackson, and M. Radosz, "SAFT: Equation-of-state solution model for associating fluids," *Fluid Phase Equilib.*, vol. 52, pp. 31–38, Dec. 1989.

[10] S. H. Huang and M. Radosz, "Equation of state for small, large, polydisperse, and associating molecules," *Ind. Eng. Chem. Res.*, vol. 29, no. 11, pp. 2284–2294, Nov. 1990.

[11] T. Kraska and K. E. Gubbins, "Phase Equilibria Calculations with a Modified SAFT Equation of State. 2. Binary Mixtures of n - Alkanes, 1-Alkanols, and Water," *Ind. Eng. Chem. Res.*, vol. 35, no. 12, pp. 4738–4746, Jan. 1996.

[12] A. Gil-Villegas, A. Galindo, P. J. Whitehead, S. J. Mills, G. Jackson, and A. N. Burgess, "Statistical associating fluid theory for chain molecules with attractive potentials of variable range," *J. Chem. Phys.*, vol. 106, no. 10, p. 4168, 1997.

[13] F. J. Blas and L. F. Vega, "Associating Fluid Theory (SAFT) Equation of State," vol. 5885, no. 1996, pp. 660–674, 1998.

[14] J. Gross and G. Sadowski, "Perturbed-Chain SAFT: An Equation of State Based on a Perturbation Theory for Chain Molecules," *Ind. Eng. Chem. Res.*, vol. 40, no. 4, pp. 1244–1260, Feb. 2001.

[15] S. Beret and J. M. Prausnitz, "Perturbed hard-chain theory. Equation of state for fluids containing small or large molecules," *AIChE J.*, vol. 21, no. 6, 1975.

[16] M. D. Donohue and J. M. Prausnitz, "Perturbed hard chain theory for fluid mixtures: thermodynamic properties for mixtures in natural gas and petroleum technology," *AIChE J.*, vol. 24, no. 5, 1978.

[17] K. E. Gubbins and C. H. Twu, "Thermodynamics of polyatomic fluid mixtures—I theory," *Chem. Eng. Sci.*, vol. 33, no. 7, pp. 863–878, Jan. 1978.

[18] C. H. Twu and K. E. Gubbins, "Thermodynamics of polyatomic fluid mixtures—II," *Chem. Eng. Sci.*, vol. 33, no. 7, pp. 879–887, Jan. 1978.

[19] P. Vimalchand and M. D. Donohue, "Thermodynamics of quadrupolar molecules: the perturbed-anisotropic-chain theory," *Ind. Eng. Chem. Fundam.*, vol. 24, no. 2, pp. 246–257, May 1985.

[20] P. Vimalchand, I. Celmins, and M. D. Donohue, "VLE calculations for mixtures containing multipolar compounds using the perturbed anisotropic chain theory," *AIChE J.*, vol. 32, no. 10, pp. 1735–1738, Oct. 1986.

[21] G. D. Ikonomou and M. D. Donohue, "Extension of the Associated Perturbed Anisotropic Chain Theory to Mixtures with More Than One Associating Component," *Fluid Phase Equilib.*, vol. 39, no. 129, 1988.

[22] I. G. Economou and M. D. Donohue, "Thermodynamic Inconsistencies in and Accuracy of Chemical-Equations of State for Associating Fluids," *Ind. Eng. Chem. Res.*, vol. 31, no. 1203, 1992.

[23] C. Coquelet, A. Valtz, P. Stringari, M. Popovic, D. Richon, and P. Mougin, "Phase equilibrium data for the hydrogen sulphide+methane system at temperatures from 186 to 313K and pressures up to about 14MPa," *Fluid Phase Equilib.*, vol. 383, pp. 94–99, Dec. 2014.

[24] T. Lafitte, A. Apostolakou, C. Avendaño, A. Galindo, C. S. Adjiman, E. a Müller, and G. Jackson, "Accurate statistical associating fluid theory for chain molecules formed from Mie segments.," *J. Chem. Phys.*, vol. 139, no. 15, p. 154504, Oct. 2013.

[25] H. J. M. Hanley and E. G. D. Cohen, "Analysis of the transport coefficients for simple dense fluids: The diffusion and bulk viscosity coefficients," *Physica A: Statistical Mechanics and its Applications*, vol. 83, no. 2. pp. 215–232, 1976.

[26] K. C. Mo and K. E. Gubbins, "Conformal solution theory for viscosity and thermal conductivity of mixtures," *Molecular Physics*, vol. 31, no. 3. pp. 825–847, 1976.

[27] J. F. Ely and H. J. M. Hanley, "Prediction of transport properties. 2. Thermal conductivity of pure fluids and mixtures," *Ind. Eng. Chem. Fundam.*, vol. 22, no. 1, pp. 90–97, 1983.

[28] M. L. Huber, D. G. Friend, and J. F. Ely, "Prediction of the thermal conductivity of refrigerants and refrigerant mixtures," *Fluid Phase Equilibria*, vol. 80. pp. 249–261, 1992.

[29] F. Herning and L. Zipperer, "Calculations of the Viscosity of Technical Gas Mixtures from the Viscosity of individual gases," *Gas. Wasserfach*, vol. 79, pp. 49–69, 1936.

[30] B. A. Younglove and J. F. Ely, "Thermophysical properties of fluids II. Methane, ethane, propane, isobutane and normal butane.," *J. Phys. Chem. Ref. Data*, vol. 16, p. 577, 1987.

[31] A. Chapoy, M. Nazeri, M. Kapateh, R. Burgass, C. Coquelet, and B. Tohidi, "Effect of impurities on thermophysical properties and phase behaviour of a CO2-rich system in CCS," *Int. J. Greenh. Gas Control*, vol. 19, pp. 92–100, 2013.

[32] J. S. Rowlinson, "Translation of J. D. van der Waals' 'The thermodynamik theory of capillarity under the hypothesis of a continuous variation of density,'" *J. Stat. Phys.*, vol. 20, no. 2, pp. 197–200, 1979.

[33] J. W. H. Cahn John E., "Free Energy of a Nonuniform System. I. Interfacial Free Energy," *J. Chem. Phys.*, vol. 28, no. 2, pp. 258–267, 1958.

[34] C. Miqueu, B. Mendiboure, C. Graciaa, and J. Lachaise, "Modelling of the surface tension of binary and ternary mixtures with the gradient theory of fluid interfaces," *Fluid Phase Equilib.*, vol. 218, no. 2, pp. 189–203, 2004.

[35] C. Miqueu, B. Mendiboure, A. Graciaa, and J. Lachaise, "Modeling of the surface tension of multicomponent mixtures with the gradient theory of fluid interfaces," *Ind. Eng. Chem. Res.*, vol. 44, no. 9, pp. 3321–3329, 2005.

[36] J. R.L., J.-C. Hsu, and N. Nagarajan, "Equilibrium Phase Compositions, Phase Densities, and Interfacial Tensions for CO2+Hydrocarbon System. 1. CO2+n-Butane," *J. Chem. Eng. Data*, pp. 485–491, 1985.

[37] N. Nagarajan and R. L. Robinson, "Equilibrium phase compositions, phase densities, and interfacial tensions for carbon dioxide + hydrocarbon systems. 2. Carbon dioxide + n-decane," *J. Chem. Eng. Data*, vol. 31, no. 2, pp. 168–171, 1986.

APPENDIX G: PPEPPD CONFERENCE POSTER

Vapour-liquid equilibria and density modelling of CO2-rich systems with PC-SAFT and SAFT-VR Mie

Alfonso González Pérez[a,b], Patrice Paricaud[c], Antonin Chapoy[b], Christophe Coquelet[a]

[a] Mines ParisTech PSL Research University, CTP-Centre of Thermodynamics of Processes, France
[b] Institute of Petroleum Engineering, Heriot Watt University, United Kingdom
[c] Laboratoire Chimie et Procédé, UCP-ENSTA ParisTech, Université Paris-Saclay, France

alfonso.gonzalez_perez@mines-paristech.fr

Introduction

Carbon Capture and Storage (CCS) has been proposed as a potential method to mitigate climate change. Carbon storage may allow continuing to burn fossil fuels in power stations preventing CO_2 emissions to the atmosphere and covering the electricity demand in conjunction with other zero-emissions technologies (renewable resources and nuclear power plants) [1]. However, power stations are not the only source of CO_2 which can be fitted with carbon capture technologies; many other industrial processes also produce large amounts of CO_2, such as cement manufacturing or natural gas treatment. CCS refers to a large number of technologies and processes, such as combustion methods, transport pipelines or injection systems. The development of accurate thermodynamic models to predict thermophysical properties (such as density, phase diagram, enthalpy or specific heat capacity) is required for a safe, optimum and worthwhile transport and storage of CO_2-rich steams.

Modelling

Several thermodynamic models have been used in the literature to predict the phase behaviour and densities of CO_2-rich systems. This work compares the well-known PC-SAFT [2] and the recently updated SAFT-VR Mie [3]. These models have been applied for the description of VLE and densities of CO_2-rich systems.

PC-SAFT

$$a^{RESIDUAL} = a^{HARD-CHAIN} + a^{DISPERSION}$$

$$u(r) = \begin{cases} \infty & r < (\sigma - s_1) \\ 3\varepsilon & (\sigma - s_1) \le r < \sigma \\ -\varepsilon & \sigma \le r < \alpha\sigma \\ 0 & r \ge \alpha\sigma \end{cases}$$

$$\varepsilon_{ij} = (1 - k_{ij})\sqrt{\varepsilon_i \varepsilon_j}$$

SAFT-VR Mie

$$a^{RESIDUAL} = a^{MONOMER} + a^{CHAIN}$$

$$u(r) = \frac{\lambda_r}{\lambda_r - \lambda_a}\left(\frac{\lambda_r}{\lambda_a}\right)^{\frac{\lambda_a}{\lambda_r - \lambda_a}} \varepsilon \left[\left(\frac{\sigma}{r}\right)^{\lambda_r} - \left(\frac{\sigma}{r}\right)^{\lambda_a}\right]$$

$$\varepsilon_{ij} = (1 - k_{ij})\frac{\sqrt{\sigma_i^3 \sigma_j^3}}{\sigma_{ij}^3}\sqrt{\varepsilon_i \varepsilon_j}$$

Vapour-Liquid Equilia

The VLE of 10 binary systems combination of carbon dioxide with 6 n-alkanes and 4 gases (N_2, O_2, Ar and H_2S) were modelled with PC-SAFT and SAFT-VR Mie. Bubble pressures and vapour phase compositions are predicted with and without binary interaction parameter (BIP). BIPs were regressed on literature VLE data. In order to do a fair comparison between both EoS, the regressions were done treating the k_{ij}'s as temperature independent BIP. In the following table are presented the fitted BIP and the results of VLE calculations for the 10 binary systems studied.

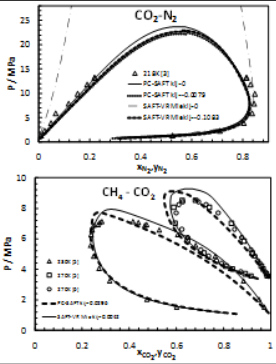

		PC-SAFT			SAFT-VR Mie		
Comp 2	T_{RANGE} [K]	k_{ij}	ΔP^{bubble} (%)	Δy_1 (%)	k_{ij}	ΔP^{bubble} (%)	Δy_1 (%)
Methane	153 - 293	0.0296	4.1	1.4	0.0042	3.4	1.4
Ethane	207 - 293	0.0650	2.9	2.7	0.0537	2.1	2.3
Propane	210 - 363	0.0724	3.1	0.6	0.0674	2.3	0.6
n-butane	228 - 418	0.0646	3.3	1.0	0.0531	1.8	0.9
n-hexane	213 - 293	0.0711	3.7	0.8	0.0670	3.9	0.9
n-decane	277 - 594	0.0631	4.3	0.9	0.0568	2.1	1.1
Nitrogen	218 - 301	-0.0079	4.9	1.9	-0.1083	6.3	2.9
Oxygen	218 - 298	0.0475	7.6	5.7	-0.0291	5.0	3.7
Argon	233 - 299	0.0213	5.5	4.0	-0.0163	6.2	2.7
H2S	225 - 366	0.0618	1.7	1.0	0.0621	1.1	1.9
Overall			3.4	1.8		4.1	2.0

Density

Single phase density (ρ-PTx) of pure CO_2 and 10 binary CO_2 systems was modelled with the SAFT-VR Mie and PC-SAFT EoSs. These binary systems are identical to those presented in the VLE section. Therefore, the regressed BIP have been used in order to avoid wrong calculations of the two phase region during ρ-PTx calculations. The AAD of density calculations using the studied SAFT models are reported in the above table.

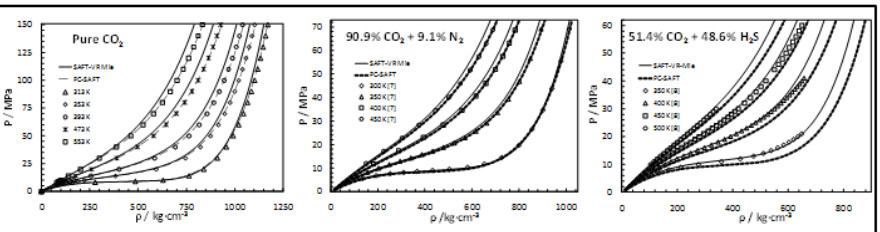

%AAD density	Pure CO_2	Binary mixture of CO_2 and component 2:										
		Methane	Ethane	Propane	n-butane	n-hexane	n-decane	Nitrogen	Oxygen	Argon	H_2S	Total
PC-SAFT	0.9	4.2	6.4	4.3	2.9	3.2	1.0	3.5	3.1	6.0	4.5	4.7
SAFT-VR Mie	1.8	3.1	5.6	3.2	2.2	2.8	0.7	3.0	2.3	5.7	3.9	3.9

Conclusions

The PC-SAFT EoS can predict (no BIP) the phase equilibria of CO_2 binary systems with lower AAD than SAFT-VR Mie, when k_{ij} is fixed to zero. Nevertheless, the VLE of most of the studied systems were better predicted using the SAFT-VR Mie EoS, leaving aside the CO_2-N_2 system which bubble pressure deviation was 22.4%. Binary interaction parameters were fitted for each binary system. Using the regressed BIP, SAFT-VR Mie model reports lower deviations (3.4% in ΔP^{bubble} and 1.8% in Δy_1) in phase equilibrium calculations than by the PC-SAFT model (4.1% in ΔP^{bubble} and 2.0% in Δy_1).

The PC-SAFT EoS reports better results for CO_2 density calculations in a wide temperature and pressure range, particularly lower deviations at supercritical state densities (0.54%). Despite the PC-SAFT EoS performed with higher accuracy pure CO_2 density, the SAFT-VR Mie EoS is better in term of density predictions of the CO_2 binary systems. SAFT-VR Mie EoS gives an AAD of 3.9%, while PC-SAFT EoS reports 4.7%.

Reference

[1] M. E. Boot-Handford et al., *Energy Environ. Sci.*, vol.7, no.1, pp.130-189, 2014.
[2] J. Gross and G. Sadowski, *Ind. Eng. Chem. Res.*, vol.40, no.4, pp.1244-1260, 2001.
[3] T. Lafitte et al., *J. Chem. Phys.*, vol.139, no.5, p.154504, 2013.
[4] M. Yorizane et al., J. Chem. Eng., vol.4, pp.10–16, 1971.
[5] J. Davalos et al., J.Chem.Eng.Data, 21(1), p81-84, 1976.
[6] T. A. Al-Sahhaf et al., Ind. Eng. Chem., Fundam. 22, 372-380, 1983.
[7] H. B. Brugge et al., J. Chem. Eng. Data, vol.42, no.5, pp.903–907, 1997.
[8] C. Liu, PhD thesis, Texas A&M University, 1985.[8] M. Yorizane et al., J. Chem. Eng., vol.4,

REFERENCES

[1] J. G. J. Olivier, M. Muntean, and J. A. H. W. Peters, "Trends in global CO_2 emissions: 2015 report," *PBL Netherlands Environ. Assess. Agency Eur. Comm. Jt. Res. Cent.*, pp. 1–78, 2015.

[2] L. M. Bert Metz, Ogunlade Davidson, Heleen de Coninck, Manuela Loos, *IPCC Special Report on Carbon Dioxide Capture and Storage. Working Group III of the Intergovernmental Panel on Climate Change*. Cambridge, UK: Cambridge University Press, 2005.

[3] IPCC, "Summary for Policymakers," *Spec. Rep. Renew. Energy Sources*, no. May, 2011.

[4] M. E. Boot-Handford, J. C. Abanades, E. J. Anthony, M. J. Blunt, S. Brandani, N. Mac Dowell, and J. R. Fernandez, "Carbon capture and storage update," *Energy Environ. Sci.*, vol. 7, pp. 130–189, 2014.

[5] U. S. DOE and NETL, "Advanced Carbon Dioxide Capture R&D Program : Technology Update," no. May, 2013.

[6] R. Zevenhoven and P. Kilpinen, "Flue gases and fuel gases," in *Control of Pollutants in Flue Gases and Fuel Gases*, 2001, p. 2.1-2.12.

[7] M. Wallace, L. Goudarzi, K. Callahan, and R. Wallace, "A Review of the CO2 Pipeline Infrastructure in the U.S.," *Doe/Netl-2014/1681*, 2015.

[8] P. Noothout, F. Wiersma, O. Hurtado, P. Roelofsen, and D. Macdonald, "CO2 Pipeline Infrastructure. Report 2013-2018," *Glob. CCS Inst.*, no. January, 2014.

[9] H. Li, "Thermodynamic properties of CO2 mixtures and their applications in advanced power cycles with CO2 capture processes," Royal Institute of technology (Stockholm), 2008.

[10] Y. Suehiro, M. Nakajima, K. Yamada, and M. Uematsu, "Critical parameters of $\{xCO_2 + (1-x)CHF_3\}$ forx= (1.0000, 0.7496, 0.5013, and 0.2522)," *J. Chem. Thermodyn.*, vol. 28, pp. 1153–1164, 1996.

[11] Project DYNAMIS, "Towards Hydrogen and Electricity Production with Carbon Dioxide Capture and Storage," 2007.

[12] P. N. Seevam, J. M. Race, and M. J. Downie, "Carbon dioxide pipelines for sequestration in the UK: an engineering gap analysis," *J. pipeline Eng.*, vol. 6, 2007.

[13] C. Coquelet, A. Valtz, and P. Arpentinier, "Thermodynamic study of binary and ternary systems containing CO_2+impurities in the context of CO_2 transportation," *Fluid Phase Equilib.*, vol. 382, pp. 205–211, 2014.

[14] L. . S. Melzer, "Carbon Dioxide Enhanced Oil Recovery (CO_2 EOR): Factors Involved in Adding Carbon Capture , Utilization and Storage (CCUS) to Enhanced Oil Recovery.," Mindland, TX, USA, 2012.

[15] M. Blunt, "Carbon dioxide storage," *Grantham Inst. Clim. Chang. Brief. Pap.*, vol. 4, 2010.

[16] N. I. Diamantonis, G. C. Boulougouris, E. Mansoor, D. M. Tsangaris, and I. G. Economou, "Evaluation of Cubic, SAFT, and PC-SAFT Equations of State for the Vapor–Liquid Equilibrium Modeling of CO_2 Mixtures with Other Gases," *Ind. Eng. Chem. Res.*, vol. 52, pp. 3933–3942, 2013.

[17] Z. X. Zhang, G. X. Wang, P. Massarotto, and V. Rudolph, "Optimization of pipeline transport for CO2 sequestration," *Energy Convers. Manag.*, vol. 47, pp. 702–715, 2006.

[18] A. Meisen and X. Shuai, "Research and development issues in CO_2 capture," *Energ Convers Manag.*, vol. 38, pp. 37–42, 1997.

[19] E. Hendriks, G. M. Kontogeorgis, R. Dohrn, J. De Hemptinne, and V. Vesovic, "Industrial Requirements for Thermodynamics and Transport Properties," pp. 11131–11141, 2010.

[20] F. Rivollet, C. Jarne, and D. Richon, "PρT and VLE for Ethane + Hydrogen Sulfide from (254 . 05 to 363 . 21) K at Pressures up to 20 MPa," *J. Chem. Eng. Data*, vol. 48, pp. 1883–1890, 2005.

[21] F. Rivollet, "Etude des proprietes volumetriques (PVT) d'hydrocarbures legers (C1-C4), du dioxyde de carbone et de l'hydrogene sulfure," Ecole des Mines de Paris, 2005.

[22] C. Jarne, F. Rivollet, and D. Richon, "P ρ T data for hydrogen sulfide + propane from (263 to 363) K at pressures up to 40 MPa," *J. Chem. Eng. Data*, vol. 56, pp. 84–88, 2011.

[23] A. Chapoy, M. Nazeri, M. Kapateh, R. Burgass, B. Tohidi, and C. Coquelet, "'Impact of Common Impurities on CO2 Capture, Tr ansport and Storage 2011 – 2014 Final Report,'" 2014.

[24] M. Nazeri, "Impact of impurities on thermo-physical properties of CO2-rich systems: Experimental and modelling," IPE Heriot Watt University, 2015.

[25] Energy.ihs.com, "EDIN database, fields and reservoir information," 2009.

[26] W. F. J. Burgers, P. S. Northrop, H. S. Kheshgi, and J. A. Valencia, "Worldwide development potential for sour gas," *Energy Procedia*, vol. 4, pp. 2178–2184, 2011.

[27] A. Chapoy, C. Coquelet, H. Liu, A. Valtz, and B. Tohidi, "Vapour-liquid equilibrium data for the hydrogen sulphide (H2S)+carbon dioxide (CO2) system at temperatures from 258 to 313K," *Fluid Phase Equilib.*, vol. 356, pp. 223–228, 2013.

[28] S. Laugier and D. Richon, "New apparatus to perform fast determinations of mixture vapor–liquid equilibria up to 10 MPa and 423 K," *Rev. Sci. Instrum.*, vol. 57, p. 469, 1986.

[29] A. Chapoy, A. H. Mohammadi, B. Tohidi, and D. Richon, "Estimation of Water Content for Methane + Water and Methane + Ethane + n- Butane + Water Systems Using a New Sampling Device," *J. Chem. Eng. Data*, vol. 50, pp. 1157–1161, 2005.

[30] C. Coquelet, A. Valtz, F. Dieu, D. Richon, P. Arpentinier, and F. Lockwood, "Isothermal P, x, y data for the argon + carbon dioxide system at six temperatures from 233.32 to 299.21 K and pressures up to 14 MPa," *Fluid Phase Equilib.*, vol. 273, pp. 38–43, 2008.

[31] N. W. Chakroun and A. F. Ghoniem, "High-efficiency low LCOE combined cycles for sour gas oxy-combustion with CO2 capture," *Int. J. Greenh. Gas Control*, vol. 41, pp. 1–11, 2015.

[32] H. H. Reamer, B. H. Sage, and W. N. Lacey, "Phase Equilibria in Hydrocarbon Systems - Volumetric and Phase Behavior of the Methane-Hydrogen Sulfide System," *Ind. Eng. Chem.*, vol. 43, pp. 976–981, 1951.

[33] D. M. Bailey, C. H. Liu, J. C. Holste, and K. R. Hall, "Gas Processors Assoc. Research Report 107, Tulsa, Oklahoma," 1987.

[34] R. L. Robinson Jr. and R. H. Jacoby, "Better compressibility factors," *Hydrocarb. Process. Pet. Refin.*, vol. 44, pp. 141–145, 1965.

[35] G. M. Rambosek, "Liquid-vapor equilibrium composition relationships in the propane-hydrogen sulfide systems," Ohio State University, 1950.

[36] N. Sakoda and M. Uematsu, "A Thermodynamic Property Model for the Binary Mixture of Methane and Hydrogen Sulfide," *Int. J. Thermophys.*, vol. 26, pp. 1303–1325, 2005.

[37] C. Coquelet and D. Richon, “Experimental determination of phase diagram and modeling : Application to refrigerant mixtures ´ termination expe ´ rimentale des diagrammes de phases et De ´ lisations : Application aux me ´ langes de fluides leurs mode ` nes frigorige,” *Int. J. Refrig.*, vol. 32, no. 7, pp. 1604–1614, 2009.

[38] C. Bouchot and D. Richon, “An enhanced method to calibrate vibrating tube densimeters,” *Fluid Phase Equilib.*, vol. 191, pp. 189–208, 2001.

[39] C. Coquelet, D. Ramjugernath, H. Madani, A. Valtz, P. Naidoo, and A. H. Meniai, “Experimental measurement of vapor pressures and densities of pure hexafluoropropylene,” *J. Chem. Eng. Data*, vol. 55, pp. 2093–2099, 2010.

[40] M. Nazeri, A. Chapoy, A. Valtz, C. Coquelet, and B. Tohidi, “Densities and derived thermophysical properties of the 0.9505 CO2+0.0495 H2S mixture from 273 K to 353 K and pressures up to 41 MPa,” *Fluid Phase Equilib.*, vol. 423, pp. 156–171, 2016.

[41] A. Vale, “Hydrogen sulphide,” *Med. (Baltimore).*, vol. 40, no. 3, p. 127, 2012.

[42] V. Diky, C. D. Muzny, E. W. Lemmon, R. D. Chirico, and M. Frenkel, “NIST Standard Reference Database 103a: NIST ThermoData Engine: Version 2.7 - Pure Compounds,” 2007.

[43] J. P. Kohn and F. Kurata, “Heterogeneous phase equilibria of the methane—hydrogen sulfide system,” *AIChE J.*, vol. 4, pp. 211–217, 1958.

[44] P. H. V. Konynenburg and R. L. Scott, “Critical Lines and Phase Equilibria in Binary Van Der Waals Mixtures,” *Philos. Trans. R. Soc. A Math. Phys. Eng. Sci.*, vol. 298, pp. 495–540, 1980.

[45] C. Coquelet, A. Valtz, P. Stringari, M. Popovic, D. Richon, and P. Mougin, “Phase equilibrium data for the hydrogen sulphide+methane system at temperatures from 186 to 313K and pressures up to about 14MPa,” *Fluid Phase Equilib.*, vol. 383, pp. 94–99, 2014.

[46] R. A. Heidemann and A. M. Khalil, “The calculation of critical points,” *AIChE J.*, vol. 26, pp. 769–779, 1980.

[47] S. Langè, M. Campestrini, and P. Stringari, “Phase behavior of system methane + hydrogen sulfide,” *AIChE J.*, vol. 7, pp. 405–410, 2016.

[48] W. B. Kay and B. Brice, “Liquid-Vapor Equilibrium Relations in Ethane-Hydrogen Sulfide System,” *J. Ind. Eng. Chem.*, vol. 45, pp. 615–618, 1953.

[49] J. Brewer, N. Rodewald, and F. Kurata, “Phase equilibria of the propane-hydrogen sulfide system from the cricondontherm to the solid-liquid-vapor region,” *AIChE J.*, vol. 7, pp. 13–16, 1961.

[50] B. E. Poling, J. M. Prausnitz, and J. P. O’Connell, *The Properties of Gases and Liquids*, Fifth Edit. McGraw-Hill, 2001.

[51] D. B. Robinson and J. A. Bailey, “The Carbon Dioxide-Hydrogen Sulphide-Methane System: Part I. Phase Behavior at 100F,” *Can. J. Chem. Eng.*, vol. 34, p. 151, 1957.

[52] D. B. Robinson, A. P. Lorenzo, and C. A. Macrygeorgos, “The Carbon Dioxide-Hydrogen Sulphide-Methane System: Part II. Pahse Behavior at 40F and 160F,” *Can. J. Chem. Eng.*, vol. 37, pp. 212–217, 1959.

[53] H. T. Kennedy and D. R. Wieland, “Equilibrium in the Methane-Carbon Dioxide-Hydrogen Sulfide-Sulfur System,” *Pet. Trans. AIME*, vol. 219, pp. 166–169, 1960.

[54] M. Dicko, G. Belaribi-Boukais, C. Coquelet, A. Valtz, F. Brahim Belaribi, P. Naidoo, and D. Ramjugernath, “Reply to ‘Comments on “Experimental measurement of vapor pressures and densities at saturation of pure hexafluoropropylene oxide: Modeling using a crossover equation of state,”’” *Ind. Eng. Chem. Res.*, vol. 50, pp. 4761–4768, 2011.

[55] A. Chapoy, M. Nazeri, M. Kapateh, R. Burgass, C. Coquelet, and B. Tohidi, "Effect of impurities on thermophysical properties and phase behaviour of a CO2-rich system in CCS," *Int. J. Greenh. Gas Control*, vol. 19, pp. 92–100, 2013.
[56] B. Tohidi, R. W. Burgass, A. Danesh, and A. C. Todd, "Viscosity and density of methane + methylcyclohexane from (323 to 423) K and pressures to 140 MPa," *J. Chem. Eng. Data*, vol. 46, pp. 385–390, 2001.
[57] H. J. M. Hanley and E. G. D. Cohen, "Analysis of the transport coefficients for simple dense fluids: The diffusion and bulk viscosity coefficients," *Physica A: Statistical Mechanics and its Applications*, vol. 83, pp. 215–232, 1976.
[58] J. N. Israelachvili, *Intermolecular and Surface Forces*. Elsevier, 2011.
[59] J. N. Israelachvili, "Historical Perspective 1.1," in *Intermolecular and Surface Forces*, 2011, pp. 3–22.
[60] A. J. Stone, *The Theory of Intermolecular Forces, International Series of Monographs on Chemistry*. Oxford: Clarendon Press, 1996.
[61] W. Sutherland, "LII. The viscosity of gases and molecular force," *Philos. Mag. Ser. 5*, vol. 36, pp. 507–531, 1893.
[62] W. Sutherland, "XI. The law of attraction amongst the molecules of a gas," *Philos. Mag. Ser. 5*, vol. 22, pp. 81–95, 1886.
[63] W. Sutherland, "XXXVI. On the law of molecular force," *Philos. Mag. Ser. 5*, vol. 27, pp. 305–321, 1889.
[64] H. Yukawa, "On the interaction of elementary particles.," *Proc. Phys. Math. Soc. Japan.*, vol. 17, 1935.
[65] J. E. Jones, "On the Determination of Molecular Fields. I. From the Variation of the Viscosity of a Gas with Temperature," *Proc. R. Soc. A Math. Phys. Eng. Sci.*, vol. 106, pp. 441–462, 1924.
[66] J. E. Jones, "On the Determination of Molecular Fields. II. From the Equation of State of a Gas," *Proc. R. Soc. A Math. Phys. Eng. Sci.*, vol. 106, pp. 463–477, 1924.
[67] J. E. Lennard-Jones, "Cohesion," *Proc. Phys. Soc.*, vol. 43, pp. 461–482, 1931.
[68] S. Dufal, "Development and application of advanced thermodynamic molecular description for complex reservoir fluids containing carbon dioxide and brines by," Imperial College London, 2013.
[69] J. Gross and G. Sadowski, "Perturbed-Chain SAFT: An Equation of State Based on a Perturbation Theory for Chain Molecules," *Ind. Eng. Chem. Res.*, vol. 40, pp. 1244–1260, 2001.
[70] F. Tumakaka and G. Sadowski, "Application of the Perturbed-Chain SAFT equation of state to polar systems," *Fluid Phase Equilib.*, vol. 217, pp. 233–239, 2004.
[71] S. S. Chen and A. Kreglewski, "Applications of the Augmented van der Waals Theory of Fluids.: I. Pure Fluids," *Berichte der Bunsengesellschaft für Phys. Chemie*, vol. 81, pp. 1048–1052, 1977.
[72] T. Lafitte, A. Apostolakou, C. Avendaño, A. Galindo, C. S. Adjiman, E. a Müller, and G. Jackson, "Accurate statistical associating fluid theory for chain molecules formed from Mie segments.," *J. Chem. Phys.*, vol. 139, no. 15, p. 154504, 2013.
[73] G. Mie, "Zur kinetischen Theorie der einatomigen Körper," *Ann. Phys.*, vol. 316, pp. 657–697, 1903.
[74] T. Lafitte, D. Bessieres, M. M. Piñeiro, and J.-L. Daridon, "Simultaneous estimation of phase behavior and second-derivative properties using the statistical associating fluid theory with variable range approach.," *J. Chem. Phys.*, vol. 124,

p. 24509, 2006.
[75] S. Dufal, "Development and application of advanced thermodynamic molecular description for complex reservoir fluids containing carbon dioxide and brines," 2013.
[76] F. Jahn, M. Cook, and M. Graham, *Hydrocarbon Exploration and production*. Aberdeen, UK, 1998.
[77] M. L. Michelsen and J. Mollerup, *Thermodynamic Models: Fundamentals and Computational Aspects*, Second edi. Tie-Line Publications, 2007.
[78] P. A. Rock, *Chemical Thermodynamics*. Oxford: Oxford University Press, 1983.
[79] H. Orbey and S. I. Sandler, *Modeling Vapor-Liquid Equilibria. Cubic Equations of State and their Mixing Rules*. 1998.
[80] P. W. Atkins, *Physical Chemistry*. Oxford: Oxford University Press, 1982.
[81] A. Maghari and M. Hamzehloo, "Second-order thermodynamic derivative properties of binary mixtures of n-alkanes through the SAFT-CP equation of state," *Fluid Phase Equilib.*, vol. 302, pp. 195–201, 2011.
[82] É. Clapeyron, "Puissance motrice de la chaleur," *J. l' Ec. Polytech.*, vol. 14, 1834.
[83] L. L. Lee, *Molecular Thermodynamics of Nonideal Fluids*. Butterworth, Boston, 1988.
[84] J. D. van der Waals, "van der Waals, J.D., 1873. Over de continuiteit van den Gas- en vloestoftoestand (Über die Kontinuittät des Gas- und Flüssigkeitszustands)," *Diss. Univ. Leiden, Niederlande, Dtsch. Übersetzung, Leipzig*, 1873.
[85] O. Redlich and J. N. S. Kwong, "On the Thermodynamics of Solutions. V. An Equation of State. Fugacities of Gaseous Solutions.," *Chem. Rev.*, vol. 44, pp. 233–244, 1949.
[86] N. F. Carnahan and K. E. Starling, "Equation of State for Nonattracting Rigid Spheres," *J. Chem. Phys.*, vol. 51, p. 635, 1969.
[87] N. F. Carnahan and K. E. Starling, "Intermolecular repulsions and the equation of state for fluids," *AlChE J.*, vol. 18, pp. 1184–1189, 1972.
[88] G. Soave, "Equilibrium constants from a modified Redkh-Kwong equation of state," *J. Chem. Eng. Sci.*, vol. 27, pp. 1197–1203, 1972.
[89] D. Y. Peng and D. B. Robinson, "A New Two-Constant Equation of State," *Ind. Eng. Chem. Fundam.*, vol. 15, pp. 59–64, 1976.
[90] S. Dufal, T. Lafitte, A. Galindo, G. Jackson, and A. J. Haslam, "Developing intermolecular-potential models for use with the SAFT-VRMie equation of state," *AIChE J.*, vol. 61, pp. 2891–2912, 2015.
[91] A. Maghari and L. Hosseinzadeh-Shahri, "Evaluation of the performance of cubic equations of state in predicting the regularities in dense fluids," *Fluid Phase Equilib.*, vol. 206, pp. 287–311, 2003.
[92] A. Péneloux, E. Rauzy, and R. Fréze, "A consistent correction for Redlich-Kwong-Soave volumes," *Fluid Phase Equilib.*, vol. 8, p. 237, 1982.
[93] K. Pedersen, P. Christensen, and J. Shaikh, *Phase behavior of petroleum reservoir fluids*, CRC Press. Boca Raton, FL, 2007.
[94] C. Tsonopoulos and J. L. Heidman, "From Redlich-Kwong to the present," *Fluid Phase Equilib.*, vol. 24, pp. 1–23, 1985.
[95] E. A. Muller and K. E. Gubbins, "Molecular-Based Equations of State for Associating Fluids : A Review of SAFT and Related Approaches," *Ind. Eng. Chem. Res.*, vol. 78, pp. 2193–2211, 2001.
[96] M. S. Wertheim, "Fluids with highly directional attractive forces. I. Statistical thermodynamics," *J. Stat. Phys.*, vol. 35, pp. 19–34, 1984.

[97] M. S. Wertheim, "Fluids with highly directional attractive forces. II. Thermodynamic perturbation theory and integral equations," *J. Stat. Phys.*, vol. 35, pp. 35–47, 1984.
[98] M. S. Wertheim, "Fluids with highly directional attractive forces. III. Multiple attraction sites," *J. Stat. Phys.*, vol. 42, pp. 459–476, 1986.
[99] M. S. Wertheim, "Fluids with highly directional attractive forces. IV. Equilibrium polymerization," *J. Stat. Phys.*, vol. 42, pp. 477–492, 1986.
[100] G. M. Kontogeorgis, E. C. Voutsas, I. V. Yakoumis, and D. P. Tassios, "An Equation of State for Associating Fluids," *Ind. Eng. Chem. Res.*, vol. 35, pp. 4310–4318, 1996.
[101] W. G. Chapman, K. E. Gubbins, G. Jackson, and M. Radosz, "SAFT: Equation-of-state solution model for associating fluids," *Fluid Phase Equilib.*, vol. 52, pp. 31–38, 1989.
[102] S. H. Huang and M. Radosz, "Equation of state for small, large, polydisperse, and associating molecules," *Ind. Eng. Chem. Res.*, vol. 29, pp. 2284–2294, 1990.
[103] T. Kraska and K. E. Gubbins, "Phase Equilibria Calculations with a Modified SAFT Equation of State. 2. Binary Mixtures of n -Alkanes, 1-Alkanols, and Water," *Ind. Eng. Chem. Res.*, vol. 35, pp. 4738–4746, 1996.
[104] A. Gil-Villegas, A. Galindo, P. J. Whitehead, S. J. Mills, G. Jackson, and A. N. Burgess, "Statistical associating fluid theory for chain molecules with attractive potentials of variable range," *J. Chem. Phys.*, vol. 106, no. 10, p. 4168, 1997.
[105] F. J. Blas and L. F. Vega, "Prediction of Binary and Ternary Diagrams Using the Statistical Associating Fluid Theory (SAFT) Equation of State," *Ind. Eng. Chem. Res.*, vol. 5885, no. 1996, pp. 660–674, 1998.
[106] J. Gross and G. Sadowski, "Application of the Perturbed-Chain SAFT Equation of State to Associating Systems," *Ind. Eng. Chem. Res.*,vol. 41, pp. 5510–5515, 2002.
[107] S. Beret and J. M. Prausnitz, "Perturbed hard-chain theory. Equation of state for fluids containing small or large molecules," *AIChE J.*, vol. 21, no. 6, 1975.
[108] M. D. Donohue and J. M. Prausnitz, "Perturbed hard chain theory for fluid mixtures: thermodynamic properties for mixtures in natural gas and petroleum technology," *AIChE J.*, vol. 24, p. 78, 1978.
[109] K. E. Gubbins and C. H. Twu, "Thermodynamics of polyatomic fluid mixtures I theory," *Chem. Eng. Sci.*, vol. 33, pp. 863–878, 1978.
[110] C. H. Twu and K. E. Gubbins, "Thermodynamics of polyatomic fluid mixtures II," *Chem. Eng. Sci.*, vol. 33, pp. 879–887, 1978.
[111] P. Vimalchand and M. D. Donohue, "Thermodynamics of quadrupolar molecules: the perturbed-anisotropic-chain theory," *Ind. Eng. Chem. Fundam.*, vol. 24, pp. 246–257, 1985.
[112] P. Vimalchand, I. Celmins, and M. D. Donohue, "VLE calculations for mixtures containing multipolar compounds using the perturbed anisotropic chain theory," *AIChE J.*, vol. 32, pp. 1735–1738, 1986.
[113] G. D. Ikonomou and M. D. Donohue, "Extension of the Associated Perturbed Anisotropic Chain Theory to Mixtures with More Than One Associating Component," *Fluid Phase Equilib.*, vol. 39, p. 129, 1988.
[114] I. G. Economou and M. D. Donohue, "Thermodynamic Inconsistencies in and Accuracy of Chemical-Equations of State for Associating Fluids," *Ind. Eng. Chem. Res.*, vol. 31, p. 1203, 1992.
[115] W. G. Chapman, G. Jackson, and K. E. Gubbins, "Phase equilibria of associating fluids ‐ Chain molecules with multiple bonding sites," *Molec. Phys.*, vol. 65, pp. 1057–1079, 1988.

[116] George Jackson, W. G. Chapman, and K. E. Gubbins, "Phase equilibria of associating fluids ‐ Spherical molecules with multiple bonding sites," *Molec. Phys.*, vol. 65, pp. 1–31, 1988.
[117] S. H. Huang and M. Radosz, "Equation of state for small, large, polydisperse, and associating molecules: extension to fluid mixtures," *Ind. Eng. Chem. Res.*, vol. 30, pp. 1994–2005, 1991.
[118] Y.-H. Fu and S. I. Sandler, "A Simplified SAFT Equation of State for Associating Compounds and Mixtures," *Ind. Eng. Chem. Res.*, vol. 34, pp. 1897–1909, 1995.
[119] G. Kontogeorgis and G. Folas, *Thermodynamic Models for Industrial Applications From Classical and Advanced Mixing Rules to Association Theories*, 1st ed. Chippenham, Wiltshire: CPI Antony Rowe Ltd, 2010.
[120] M. C. dos Ramos, H. Docherty, F. J. Blas, and A. Galindo, "Application of the generalised SAFT-VR approach for long-ranged square-well potentials to model the phase behaviour of real fluids," *Fluid Phase Equilib.*, vol. 276, pp. 116–126, 2009.
[121] W. G. Chapman, K. E. Gubbins, G. Jackson, and M. Radosd, "New Reference Equation of State for Associating Liquids," *Ind. Eng. Chem. Res.*, vol. 29, pp. 1709–1721, 1990.
[122] D. A. McQuarrie, *Statistical Mechanics*. Sausalito, CA: Universtiy Science Books, 2000.
[123] A. R. Leach, *Molecular Modelling: Principles and Application.*, 2 edition. 2001.
[124] A. Khan, "Radial Distribution Functions of Fluid Argon," *Phys. Rev.*, vol. 134, pp. A367–A384, 1964.
[125] T. Kraska and K. E. Gubbins, "Phase Equilibria Calculations with a Modified SAFT Equation of State. 1. Pure Alkanes, Alkanols, and Water," *Ind. Eng. Chem. Res.*, vol. 35, pp. 4727–4737, 1996.
[126] C. Mccabe, A. Gil-villegas, and G. Jackson, "Gibbs ensemble computer simulation and SAFT-VR theory of non-conformal square-well monomer–dimer mixtures," no. April, pp. 27–36, 1999.
[127] N. Von Solms, M. L. Michelsen, and G. M. Kontogeorgis, "Equation of State for Highly Asymmetric and Associating Mixtures," *Ind. Eng. Chem. Res.*, vol. 42, pp. 1098–1105, 2003.
[128] A. Tihic, G. M. Kontogeorgis, N. von Solms, and M. L. Michelsen, "Applications of the simplified perturbed-chain SAFT equation of state using an extended parameter table," *Fluid Phase Equilib.*, vol. 248, pp. 29–43, 2006.
[129] J. A. Barker and D. Henderson, "Perturbation Theory and Equation of State for Fluids: The Square-Well Potential," *J. Chem. Phys.*, vol. 47, no. 8, p. 2856, 1967.
[130] J. A. Barker and D. Henderson, "Perturbation Theory and Equation of State for Fluids. II. A Successful Theory of Liquids," *J. Chem. Phys.*, vol. 47, p. 4714, 1967.
[131] T. Boublik, "Hard-sphere equation of state," *J. Chem. Phys.*, vol. 53, p. 471, 1970.
[132] G. A. Mansoori, N. F. Carnahan, K. E. Starling, and T. W. Leland Jr, "Equilibrium Thermodynamic Properties of the Mixture of Hard Spheres," *J. Chem. Phys.*, vol. 54, p. 1523, 1971.
[133] Y. C. Chiew, "Percus-Yevick integral equation theory for athermal hard-sphere chains. II. Average intermolecular correlation functions.," *Mol. Phys.*, vol. 73, p. 359, 1991.
[134] I. Senol, "Perturbed-Chain Statistical Association Fluid Theory (PC-SAFT) Parameters for Propane , Ethylene , and Hydrogen under Supercritical

Conditions," *World Acad. Sci. Eng. Technol.*, vol. 59, pp. 1395–1403, 2011.
[135] H. Liu and Y. Hu, "Molecuar thermodynamic theory for polymer systems. II. Equation of state for chain fluids.," *Fluid Phase Equilib*, vol. 122, no. 75, 1996.
[136] R. W. Zwanzig, "High-Temperature Equation of State by a Perturbation Method. I. Nonpolar Gases.," *J. Chem. Phys.*, vol. 22, p. 1420, 1954.
[137] L. A. Davies, "Describing the Properties of Chains of Segments Interacting Via Soft-Core Potentials of Variable Range with the SAFT-VR Approach 1," *Ind. Eng. Chem. Res*, vol. 19, pp. 675–686, 1998.
[138] T. M. Reed and K. E. Gubbins, *Discusses the relation between the pair potential and the polarization of the electronic clouds surrounding the atoms*. Tokyo: McGraw-Hill, 1973.
[139] B. H. Patel, H. Docherty, S. Varga, a. Galindo *, and G. C. Maitland, "Generalized equation of state for square-well potentials of variable range," *Mol. Phys.*, vol. 103, pp. 129–139, 2005.
[140] S. Gupta and J. D. Olson, "Industrial Needs in Physical Properties," *Ind. Eng. Chem. Res.*, vol. 42, pp. 6359–6374, 2003.
[141] V. Papaioannou, T. Lafitte, C. Avendaño, C. S. Adjiman, G. Jackson, E. a Müller, and A. Galindo, "Group contribution methodology based on the statistical associating fluid theory for heteronuclear molecules formed from Mie segments.," *J. Chem. Phys.*, vol. 140, p. 54107, 2014.
[142] A. L. Lydersen, "Estimation of critical properties of organic compounds. Eng. Exp. Stn. Rep. 3.," Madison, WI, 1955.
[143] J. Gmehling, "Group contribution methods for the estimation of activity coefficients," *Fluid Phase Equilib.*, vol. 30, pp. 119–134, 1986.
[144] T. Holderbaum and J. Gmehling, "PSRK: A Group Contribution Equation of State Based on UNIFAC," *Fluid Phase Equilib.*, vol. 70, pp. 251–265, 1991.
[145] J.-N. Jaubert and F. Mutelet, "VLE predictions with the Peng–Robinson equation of state and temperature dependent kij calculated through a group contribution method," *Fluid Phase Equilib.*, vol. 224, pp. 285–304, 2004.
[146] J. D. Pults, R. A. Greenkorn, and K.-C. Chao, "Chain-of-rotators group contribution equation of state," *Chem. Eng. Sci.*, vol. 44, pp. 2553–2564, 1989.
[147] M. Hajiw, A. Chapoy, and C. Coquelet, "Hydrocarbons - water phase equilibria using the CPA equation of state with a group contribution method," *Can. J. Chem. Eng.*, vol. 93, pp. 432–442, 2015.
[148] S. Tamouza, J.-P. Passarello, P. Tobaly, and J.-C. de Hemptinne, "Group contribution method with SAFT EOS applied to vapor liquid equilibria of various hydrocarbon series," *Fluid Phase Equilib.*, vol. 222–223, pp. 67–76, 2004.
[149] S. Tamouza, J.-P. Passarello, P. Tobaly, and J.-C. de Hemptinne, "Application to binary mixtures of a group contribution SAFT EOS (GC-SAFT)," *Fluid Phase Equilib.*, vol. 228–229, pp. 409–419, 2005.
[150] T. X. Nguyen Thi, S. Tamouza, P. Tobaly, J.-P. Passarello, and J.-C. de Hemptinne, "Application of group contribution SAFT equation of state (GC-SAFT) to model phase behaviour of light and heavy esters," *Fluid Phase Equilib.*, vol. 238, pp. 254–261, 2005.
[151] F. S. Emami, A. Vahid, J. R. Elliott, and F. Feyzi, "Group Contribution Prediction of Vapor Pressure with Statistical Associating Fluid Theory , Perturbed-Chain Statistical Associating Fluid Theory , and Elliott - Suresh - Donohue Equations of State," pp. 8401–8411, 2008.
[152] C. Le Thi, S. Tamouza, J. Passarello, P. Tobaly, J. De Hemptinne, and R. Cedex, "Modeling Phase Equilibrium of H 2 + n -Alkane and CO 2 + n -Alkane Binary Mixtures Using a Group Contribution Statistical Association Fluid Theory

Equation of State (GC - SAFT - EOS) with a k," pp. 6803–6810, 2006.
[153] D. N. Huynh, M. Benamira, J.-P. Passarello, P. Tobaly, and J.-C. de Hemptinne, "Application of GC-SAFT EOS to polycyclic aromatic hydrocarbons," *Fluid Phase Equilib.*, vol. 254, pp. 60–66, 2007.
[154] A. Tihic, G. M. Kontogeorgis, N. Von Solms, and M. L. Michelsen, "A Predictive Group-Contribution Simplified PC-SAFT Equation of State : Application to Polymer Systems," pp. 5092–5101, 2008.
[155] A. Lymperiadis, C. S. Adjiman, A. Galindo, and G. Jackson, "A group contribution method for associating chain molecules based on the statistical associating fluid theory (SAFT-gamma).," *J. Chem. Phys.*, vol. 127, 2007.
[156] A. Fredenslund and P. Rasmussen, "From UNIFAC to SUPERFAC - and back?," *Fluid Phase Equilib.*, vol. 24, pp. 115–150, Jan. 1985.
[157] V. Papaioannou, "A molecular-based group contribution equation of state for the description of fluid phase behaviour and thermodynamic derivative properties of mixtures (SAFT- γ Mie)," Imperial College London, 2012.
[158] F. Herning and L. Zipperer, "Calculations of the Viscosity of Technical Gas Mixtures from the Viscosity of individual gases," *Gas. Wasserfach*, vol. 79, pp. 49–69, 1936.
[159] M. L. Michelsen and B. Equations, "Robust and Efficient Solution Procedures for Association Models," pp. 8449–8453, 2006.
[160] H. Tahani and P. Engineering, "Determination of the Velocity of Sound in Reservoir Fluids Using an Equation of State By Hoda Tahani Submitted for the degree of Doctor of Philosophy in Petroleum Engineering Institute of Petroleum Engineering," no. November, 2011.
[161] P. Paricaud, "A general perturbation approach for equation of state development: Applications to simple fluids, ab initio potentials, and fullerenes," *J. Chem. Phys.*, vol. 124, 2006.
[162] E. Ziegel, W. Press, B. Flannery, S. Teukolsky, and W. Vetterling, *Numerical Recipes in Fortran*, vol. 140. 1992.
[163] S. Dufal, T. Lafitte, A. J. Haslam, A. Galindo, G. N. I. Clark, C. Vega, and G. Jackson, "The A in SAFT: developing the contribution of association to the Helmholtz free energy within a Wertheim TPT1 treatment of generic Mie fluids," *Mol. Phys.*, vol. 113, pp. 948–984, 2015.
[164] K. Schou Pedersen and C. Hasdbjerg, "PC-SAFT Equation of State Applied to Petroleum Reservoir Fluids," *SPE Annu. Tech. Conf. Exhib.*, vol. 1, pp. 1–10, 2007.
[165] J. M. Prausnitz, R. N. Lichtenthaler, and E. G. de Azevedo, *Molecular Thermodynamics of Fluid- Phase Equilibria*, 3rd ed. New Jersey, 1999.
[166] J. L. Daridon, H. Saint-Guirons, B. La Courette, P. Xans, and C. Leibovici, "A generalized process for phase equilibrium calculation with cubic equations of state," *Int. J. Thermophys.*, vol. 14, pp. 1101–1108, 1993.
[167] D. Peng and D. Robinson, "The characterization of the heptanes and heavier fractions for the GPA Peng-Robinson programs," *Gas Process. Assoc.*, vol. RR-28, 1978.
[168] J. O. Valderrama and M. Alfaro, "Liquid volumes from generalized cubic equations of state: Take it with care," *Oil Gas Sci. Technol.*, vol. 55, pp. 523–531, 2000.
[169] J.-N. Jaubert, R. Privat, Y. L. E. Guennec, and L. Coniglio, "Note on the properties altered by application of a Péneloux–type volume translation to an equation of state," *Fluid Phase Equilib.*, vol. 419, pp. 88–95, 2016.
[170] T. Lafitte, A. Apostolakou, C. Avendaño, A. Galindo, C. S. Adjiman, E. a.

Müller, and G. Jackson, "Accurate statistical associating fluid theory for chain molecules formed from Mie segments," *J. Chem. Phys.*, vol. 139, 2013.

[171] M. M. Lemmon and M. Huber, "NIST Standard Reference Database 23: Reference Fluid Thermodynamic and Transport Properties Database (REFPROP): Version 9.1." Gaithersburg: National Institute of Standards and Technology, Standard Reference Data Program, 2012.

[172] N. K. Muirbrook and J. M. Prausnitz, "Multicomponent vapor-liquid equilibria at high pressures: Part I. Experimental study of the nitrogen-oxygen-carbon dioxide system at 0°C," *AIChE J.*, vol. 11, pp. 1092–1096, 1965.

[173] A. A. Kukarni, B. Y. Zarah, K. D. Luks, and J. P. Kohn, "Phase-equilbriums behavior of system carbon dioxide-n-decane at low temperatures," *J. Chem. Eng. Data*, vol. 19, pp. 92–94, 1974.

[174] J. van der Steen, T. W. de Loos, and J. de Swaan Arons, "The volumetric analysis and prediction of liquid-liquid-vapor equilibria in certain carbon dioxide + n-alkane systems," *Fluid Phase Equilib.*, vol. 51, pp. 353–367, 1989.

[175] A. J. Davenport and J. S. Rowlinson, "The solubility of hydrocarbons in liquid methane.," *Trans. Faraday Soc.*, vol. 59, p. 78, 1963.

[176] M. Yorizane, S. Yoshimura, H. Masuoka, and M. Nakamura, "Prediction of high pressure vapor-liquid equilibria for multicomponent systems by the bwr equation of state," *J. Chem. Eng.*, vol. 4, pp. 10–16, 1971.

[177] F. A. Somait and A. J. Kidnay, "Liquid-vapor equilibriums at 270.00 K for systems containing nitrogen, methane, and carbon dioxide," *J. Chem. Eng. Data*, vol. 23, pp. 301–305, 1978.

[178] I. M. Elshayal and B. C. Lu, "Vapour—liquid equilibria in the argon—ethane and argon—methane—ethane systems at 155 K," *Cryogenics (Guildf).*, vol. 11, pp. 285–289, 1971.

[179] G. J. Besserer and D. B. Robinson, "Equilibrium-phase properties of nitrogen-hydrogen sulfide system," *J. Chem. Eng. Data*, vol. 20, pp. 157–161, 1975.

[180] W. Yan, F. Varzandeh, and E. H. Stenby, "PVT modeling of reservoir fluids using PC-SAFT EoS and Soave-BWR EoS," *Fluid Phase Equilib.*, vol. 386, pp. 96–124, 2015.

[181] R. Span and W. Wagner, "A New Equation of State for Carbon Dioxide Covering the Fluid Region from the Triple-Point Temperature to 1100 K at Pressures up to 800 MPa," *J. Phys. Chem. Ref. Data*, vol. 25, p. 1509, 1996.

[182] C. Liu, "Experimental Densities, Entropies, and Energies for Pure H2S and Equimolar Mixtures of H_2S/CH_4 and H_2S/CO_2 between 300 and 500 K," Texas A&M University, 1985.

[183] H. B. Brugge, J. C. Holste, K. R. Hall, B. E. Gammon, and K. N. Marsh, "Densities of Carbon Dioxide + Nitrogen from 225 K to 450 K at Pressures up to 70 MPa," *J. Chem. Eng. Data*, vol. 42, pp. 903–907, 1997.

[184] M. Jaeschke and H. M. Hinze, "Determination of the Real Gas Behaviour of Methane and Nitrogen and Their Mixtures in the Temperature Range from 270 K to 353 K and at Pressures Up To 30 MPa," *Fortschr.-Ber. VDI, R. 6, nr, 262*, 1991.

[185] V. Papaioannou, C. S. Adjiman, G. Jackson, and A. Galindo, "Simultaneous prediction of vapour-liquid and liquid-liquid equilibria (VLE and LLE) of aqueous mixtures with the SAFT-?? group contribution approach," *Fluid Phase Equilib.*, vol. 306, pp. 82–96, 2011.

[186] S. Dufal, V. Papaioannou, M. Sadeqzadeh, T. Pogiatzis, A. Chremos, C. S. Adjiman, G. Jackson, and A. Galindo, "Prediction of Thermodynamic Properties and Phase Behavior of Fluids and Mixtures with the SAFT-γ Mie Group-

Contribution Equation of State," *J. Chem. Eng. Data*, vol. 59, pp. 3272–3288, 2014.

[187] H. H. Reamer and B. H. Sage, "Phase Equilibria in Hydrocarbon Systems. Volumetric and Phase Behavior of the Ethane-n-Decane System.," *J. Chem. Eng. Data*, vol. 7, pp. 161–168, 1962.

[188] B. A. Bufkin, R. L. Robinson, S. S. Estrera, and K. D. Luks, "Solubility of ethane in n-decane at pressures to 8.2 MPa and temperatures from 278 to 411 K," *J. Chem. Eng. Data*, vol. 31, pp. 421–423, 1986.

[189] H. H. Reamer and B. H. Sage, "Phase Equilibria in Hydrocarbon Systems. Phase Behavior in the n-Butane-n-Decane System.," *J. Chem. Eng. Data*, vol. 9, pp. 24–28, 1964.

[190] H. H. Reamer, B. H. Sage, and W. N. Lacey, "Phase Equilibria in Hydrocarbon Systems: n-butane - decane system in the condensed region," *Ind. Eng. Chem.*, vol. 38, pp. 986–989, 1946.

[191] A. Dejoz, V. González-Alfaro, P. J. Miguel, and M. I. Vázquez, "Isobaric Vapor−Liquid Equilibria for Binary Systems Composed of Octane, Decane, and Dodecane at 20 kPa," *J. Chem. Eng. Data*, vol. 41, no. 1, pp. 93–96, Jan. 1996.

[192] K. C. Mo and K. E. Gubbins, "Conformal solution theory for viscosity and thermal conductivity of mixtures," *Molecular Physics*, vol. 31, pp. 825–847, 1976.

[193] J. F. Ely and H. J. M. Hanley, "Prediction of transport properties. 2. Thermal conductivity of pure fluids and mixtures," *Ind. Eng. Chem. Fundam.*, vol. 22, pp. 90–97, 1983.

[194] M. L. Huber, "NIST Thermophysical Properties of Hydrocarbon Mixtures Database (SUPERTRAPP)," 2007.

[195] A. Fenghour, W. A. Wakeham, and V. Vesovic, "The Viscosity of Carbon Dioxide," *J. Phys. Chem. Ref. Data*, vol. 27, no. 1, p. 31, 1998.

[196] M. L. Huber, D. G. Friend, and J. F. Ely, "Prediction of the thermal conductivity of refrigerants and refrigerant mixtures," *Fluid Phase Equilib.*, vol. 80, pp. 249–261, 1992.

[197] B. A. Younglove and J. F. Ely, "Thermophysical properties of fluids II. Methane, ethane, propane, isobutane and normal butane.," *J. Phys. Chem. Ref. Data*, vol. 16, p. 577, 1987.

[198] K. E. Gubbins and C. G. Gray, "Perturbation theory for the angular pair correlation function in molecular fluids," *Molecular Physics*, vol. 23, pp. 187–191, 1972.

[199] J. Kestin and W. Leidenfrost, "The effect of pressure on the viscosity of N2CO2 mixtures," *Physica*, vol. 25, pp. 525–536, 1959.

[200] J. Kestin, Y. Kobayashi, and R. T. Wood, "The viscosity of four binary, gaseous mixtures at 20° and 30°C," *Physica*, vol. 32, pp. 1065–1089, 1966.

[201] G. J. Gururaja, M. a. Tirunarayanan, and A. Ramachandran, "Dynamic viscosity of gas mixtures," *J. Chem. Eng. Data*, vol. 12, pp. 562–567, 1967.

[202] J. Kestin and S. T. Ro, "The Viscosity of Nine Binary and Two Ternary Mixtures of Gases at Low Density," *Berichte der Bunsengesellschaft für Phys. Chemie*, vol. 78, pp. 20–24, 1974.

[203] J. Kestin, H. E. Khalifa, S. T. Ro, and W. A. Wakeham, "The viscosity and diffusion coefficients of eighteen binary gaseous systems," *Phys. A Stat. Mech. its Appl.*, vol. 88, pp. 242–260, Aug. 1977.

[204] A. Hobley, G. P. Matthews, and A. Townsend, "The use of a novel capillary flow viscometer for the study of the argon/carbon dioxide system," *Int. J. Thermophys.*, vol. 10, pp. 1165–1179, 1989.

[205] M. L. Huber, *Transport Properties of Fluids, Their Correlation, Prediction and Estimation.* Cambridge, UK: Cambridge Univ. Press, 1996.
[206] J. S. Rowlinson, "Translation of J. D. van der Waals' 'The thermodynamik theory of capillarity under the hypothesis of a continuous variation of density,'" *J. Stat. Phys.*, vol. 20, pp. 197–200, 1979.
[207] J. E. Cahn and J. W. Hilliard, "Free Energy of a Nonuniform System. I. Interfacial Free Energy," *J. Chem. Phys.*, vol. 28, pp. 258–267, 1958.
[208] L. M. C. Pereira, A. Chapoy, R. Burgass, M. B. Oliveira, J. a. P. Coutinho, and B. Tohidi, "Study of the impact of high temperatures and pressures on the equilibrium densities and interfacial tension of the carbon dioxide/water system," *J. Chem. Thermodyn.*, vol. 93, pp. 404–415, 2016.
[209] C. Miqueu, B. Mendiboure, C. Graciaa, and J. Lachaise, "Modelling of the surface tension of binary and ternary mixtures with the gradient theory of fluid interfaces," *Fluid Phase Equilib.*, vol. 218, pp. 189–203, 2004.
[210] C. Miqueu, B. Mendiboure, A. Graciaa, and J. Lachaise, "Modeling of the surface tension of multicomponent mixtures with the gradient theory of fluid interfaces," *Ind. Eng. Chem. Res.*, vol. 44, pp. 3321–3329, 2005.
[211] B. S. Carey, "The gradient theory of fluid interfaces.," University of Minnesota, 1979.
[212] K. S. C. Freeman and I. R. McDonald, "Molecular theory of surface tension," *Molecular Physics*, vol. 26, pp. 529–537, 1973.
[213] T. Lafitte, B. Mendiboure, M. M. Piñeiro, D. Bessières, and C. Miqueu, "Interfacial properties of water/CO2: A comprehensive description through a gradient theory-SAFT-VR mie approach," *J. Phys. Chem. B*, vol. 114, pp. 11110–11116, 2010.
[214] J. R.L., J.-C. Hsu, and N. Nagarajan, "Equilibrium Phase Compositions, Phase Densities, and Interfacial Tensions for CO_2+Hydrocarbon System. 1. CO2+n-Butane," *J. Chem. Eng. Data*, pp. 485–491, 1985.
[215] N. Nagarajan and R. L. Robinson, "Equilibrium phase compositions, phase densities, and interfacial tensions for carbon dioxide + hydrocarbon systems. 2. Carbon dioxide + n-decane," *J. Chem. Eng. Data*, vol. 31, pp. 168–171, 1986.
[216] N. Nagarajan, K. a. M. Gasem, and R. L. Robinson, "Equilibrium phase compositions, phase densities, and interfacial tensions for carbon dioxide + hydrocarbon systems. 6. Carbon dioxide + n-butane + n-decane," *J. Chem. Eng. Data*, vol. 35, pp. 228–231, 1990.
[217] A. Shariati, L. J. Florusse, and C. J. Peters, "Phase behavior of the butane + decane binary system," *J. Chem. Eng. Data*, vol. 56, pp. 920–922, 2011.
[218] E. a Müller and A. Mejía, "Interfacial properties of selected binary mixtures containing n-alkanes," *Fluid Phase Equilib.*, vol. 282, pp. 68–81, 2009.
[219] L. M. C. Pereira, A. Chapoy, R. Burgass, and B. Tohidi, "Measurement and modelling of high pressure density and interfacial tension of (gas + n-alkane) binary mixtures," *J. Chem. Thermodyn.*, vol. 97, pp. 55–69, 2016.
[220] C. F. Weinaug and D. L. Katz, "Surface Tensions of Methane-Propane Mixtures," *Ind. Eng. Chem.*, vol. 35, pp. 239–246, 1943.
[221] R. P. Sutton, "General engineering," in *Pet. Eng. Handb. Vol. 1*, J. R. Fanchi and L. W. Lake, Eds. Society of Petroleum Engineers, 2006, pp. 257–331.
[222] B. F. Pennington and E. W. Hough, "Interfacial tension of the methane-normal butane system," *Prod. Mon.*, vol. 7, 1965.
[223] O. G. Nino-Amezquita, S. Enders, P. T. Jaeger, and R. Eggers, "Measurement and Prediction of Interfacial Tension of Binary Mixtures," *Ind. Eng. Chem. Res.*, vol. 49, pp. 592–601, 2010.

[224] P. T. Jaeger and R. Eggers, "Interfacial properties at elevated pressures in reservoir systems containing compressed or supercritical carbon dioxide," *J. Supercrit. Fluids*, vol. 66, pp. 80–85, 2012.
[225] P. T. Jaeger, M. B. Alotaibi, and H. A. Nasr-El-Din, "Influence of Compressed Carbon Dioxide on the Capillarity of the Gas−Crude Oil−Reservoir Water System," *J. Chem. Eng. Data*, vol. 55, no. 11, pp. 5246–5251, Nov. 2010.
[226] C. Cumicheo, M. Cartes, H. Segura, E. A. Müller, and A. Mejía, "High-pressure densities and interfacial tensions of binary systems containing carbon dioxide+n-alkanes: (n-Dodecane, n-tridecane, n-tetradecane)," *Fluid Phase Equilib.*, vol. 380, pp. 82–92, 2014.
[227] T. Jianhua, J. Satherley, and D. J. Schiffrin, "Density and intefacial tension of nitrogen-hydrocarbon systems at elevated pressures," *Chin. J. Chem. Eng.*, vol. 1, pp. 223–231, 1993.
[228] O. G. Niño Amézquita, S. Enders, P. T. Jaeger, and R. Eggers, "Interfacial properties of mixtures containing supercritical gases," *J. Supercrit. Fluids*, vol. 55, pp. 724–734, 2010.
[229] C. F. Poole, *Encyclopedia of Separation Science*. Cambridge, Massachusetts: Academic Press, 2000.
[230] D. S. H. Wong and S. I. Sandler, "A theoretically correct mixing rule for cubic equations of state," *AIChE J.*, vol. 38, pp. 671–680, 1992.
[231] M.-J. Huron and J. Vidal, "New mixing rules in simple equations of state for representing vapour-liquid equilibria of strongly non-ideal mixtures," *Fluid Phase Equilib.*, vol. 3, pp. 255–271, 1979.
[232] H. Renon and J. M. Prausnitz, "Local compositions in thermodynamic excess functions for liquid mixtures," *AIChE J.*, vol. 14, pp. 135–144, 1968.
[233] M. Campestrini, "Thermodynamic study of solid-liquid-vapour equilibrium: application to cryogenics and air separation unit," Mines-ParisTech University, 2014.
[234] O. Kunz and W. Wagner, "The GERG-2008 wide-range equation of state for natural gases and other mixtures: An expansion of GERG-2004," *J. Chem. Eng. Data*, vol. 57, pp. 3032–3091, 2012.
[235] O. Kunz, R. Klimeck, W. Wagner, and M. Jaeschke, *The GERG-2004 Wide-Range Equation of State for Natural Gases and Other Mixtures*. 2007.
[236] D. J. Naresh and J. K. Singh, "Virial coefficients of hard-core attractive Yukawa fluids," *Fluid Phase Equilib.*, vol. 285, pp. 36–43, 2009.
[237] H. Kalra, D. B. Robinson, and T. R. Krishnan, "The equilibrium phase properties of the ethane-hydrogen sulfide system at subambient temperatures," *J. Chem. Eng. Data*, vol. 22, pp. 85–88, 1977.
[238] M. Dicko, C. Coquelet, P. Theveneau, and P. Mougin, "Phase Equilibria of H 2 S-Hydrocarbons (Propane, n -Butane, and n -Pentane) Binary Systems at Low Temperatures," *J. Chem. Eng. Data*, vol. 57, pp. 1534–1543, 2012.
[239] S. E. Quiñones-Cisneros, C. K. Zéberg-Mikkelsen, J. Fernández, and J. García, "General friction theory viscosity model for the PC-SAFT equation of state," *AIChE J.*, vol. 52, pp. 1600–1610, 2006.
[240] S. P. Tan, H. Adidharma, B. F. Towler, and M. Radosz, "Friction Theory and Free-Volume Theory Coupled with Statistical Associating Fluid Theory for Estimating the Viscosity of Pure n -Alkanes," *Ind. Eng. Chem. Res.*, vol. 44, pp. 8409–8418, 2005.
[241] Y. T. F. Chow, D. K. Eriksen, A. Galindo, A. J. Haslam, G. Jackson, G. C. Maitland, and J. P. M. Trusler, "Interfacial tensions of systems comprising water, carbon dioxide and diluent gases at high pressures: Experimental measurements

and modelling with SAFT-VR Mie and square-gradient theory," *Fluid Phase Equilib.*, vol. 407, pp. 159–176, 2015.

[242] C. Coquelet, P. Stringari, M. Hajiw, A. Gonzalez, L. Pereira, M. Nazeri, R. Burgass, and A. Chapoy, "Transport of CO2: Presentation of New Thermophysical Property Measurements and Phase Diagrams," in *13th International Conference on Greenhouse Gas Control Technologies, GHGT-13, Lausanne, Switzerland*, 2016.

[243] "JCGM 200: 2012 International vocabulary of metrology – Basic and general concepts and associated terms (VIM)," no. Vim, 2012.

[244] B. N. T. and C. E. Kuyatt, "NIST Technical Note 1297. Edition Guidelines for Evaluating and Expressing the Uncertainty of NIST Measurement Results," 1994.

[245] H. H. Ku, "Notes on the use of propagation of error formulas," *J. Res. Natl. Bur. Stand. Sect. C Eng. Instrum.*, vol. 70C, p. 263, 1966.

Résumé

L'objectif principal de ce travail est le développement d'une équation d'état précise pour la détermination des propriétés thermodynamique de mélange de gaz riche en gaz acides (CO_2, H_2S) contenant des hydrocarbures et autres gaz (impuretés) comme N_2, O_2, Ar, etc présente lors du stockage du CO_2 (CCS). Après comparaisons avec des données expérimentales, nous avons retenu le modèle SAFT-VR Mie qui prédit de manière satisfaisante les masses volumiques pour les composés purs et les équilibres entre phases. Trois types de propriétés de transport ont également été prédites avec le modèle thermodynamique SAFT-VR Mie associé avec deux autres modèles de prédiction des propriétés de transport (TRAPP et DGT). La prédiction de ces propriétés de transport (viscosité et tension superficielle) repose sur une estimation la plus précise possible des masses volumiques.

Pour compléter les banques données expérimentales, les équilibres liquide-vapeur concernant le système binaire H_2S-Ar ont été déterminés à l'aide d'un dispositif de mesure dont la méthode technique repose sur la méthode « statique analytique » avec échantillonnage des phases (échantillonneur capillaire ROLI™). De plus, à l'aide d'un densimètre à tube vibrant, les masses volumiques de cinq systèmes binaires (H_2S – hydrocarbures (méthane, éthane et propane) ont été mesurées. Les masses volumiques d'un système ternaire (CO_2/CH_4/H_2S) et les masses volumiques et les viscosités d'un mélange multi-constituant riche en CO_2 ont aussi été mesurées. Les données sont parfaitement représentées par les modèles développés au cours de cette thèse.

Mots Clés

CCS, SAFT, CO_2, Équilibre de phase, Densité, Propriétés de transport.

Abstract

The main aim of this research is to develop a thermodynamic model from an accurate equation of state (EoS) for CO_2, hydrocarbons and other gases as N_2, O_2, Ar, etc. The SAFT-VR Mie EoS was selected to study the phase behaviour and transport properties of mixtures related to carbon capture and storage (CCS). In order to asses this new version of SAFT, several equations of state have been compared (PR, SRK and PC-SAFT).

SAFT-VR Mie EoS provides very good density predictions for pure component and binary systems according to the comparative study carried out. Therefore, three transport properties were modelled with SAFT-VR Mie and two models based on density predictions from the EoS. Thus, density, viscosity and interfacial tension (IFT) of CO2-rich systems were calculated by this SAFT-EoS (density), TraPP model (viscosity) and DGT (IFT), in the framework of CCS.

Some experimental work was done, in order to extend the available literature data. Isothermal vapour-liquid equilibrium of H_2S-Ar binary system was determined at three temperatures from 258 to 288 K. Densities of five binary systems of H_2S with methane, ethane and propane were measured continuously at 3 temperatures (253, 273 and 293K) and at pressures up to 30MPa, Following the same technique, the density of the ternary system 42%CO_2, 40%CH_4 and 18%H_2S was measured at pressures ranging from 0.2 to 31.5MPa and at 6 temperatures between 253 and 353K. Densities and viscosities of a multicomponent CO_2-rich with 50% of impurities were measured at 5 temperatures between 283 and 423 K and at pressures up to 150 MPa.

Keywords

CCS, SAFT, CO_2, Phase Equilibria, Density, Transport Properties.